DEVELOPMENT OF ALBUMIN BASED NANOPARTICLES FOR BIOMEDICAL APPLICATIONS

Ph.D. THESIS

by

BHARAT BHUSHAN

CENTRE OF NANOTECHNOLOGY
INDIAN INSTITUTE OF TECHNOLOGY ROORKEE
ROORKEE-247667 (INDIA)
OCTOBER, 2015

DEVELOPMENT OF ALBUMIN BASED NANOPARTICLES FOR BIOMEDICAL APPLICATIONS

A THESIS

Submitted in partial fulfilment of the requirements for the award of the degree

of

DOCTOR OF PHILOSOPHY

by

BHARAT BHUSHAN

CENTRE OF NANOTECHNOLOGY
INDIAN INSTITUTE OF TECHNOLOGY ROORKEE
ROORKEE-247667 (INDIA)
OCTOBER, 2015

INDIAN INSTITUTE OF TECHNOLOGY ROORKEE
ROORKEE

CANDIDATE'S DECLARATION

I hereby certify that the work which is being presented in this thesis entitled **"DEVELOPMENT OF ALBUMIN BASED NANOPARTICLES FOR BIOMEDICAL APPLICATIONS"** in partial fulfilment of the requirements for the award of the Degree of Doctor of Philosophy and submitted in the Centre of Nanotechnology of the Indian Institute of Technology Roorkee is an authentic record of my own work carried out during a period from July, 2011 to October, 2015 under the supervision of Dr. P. Gopinath, Assistant Professor, Department of Biotechnology, Indian Institute of Technology Roorkee.

The matter presented in this thesis has not been submitted by me for the award of any other degree of this or any other Institute.

Signature of the Candidate

This is to certify that the above statement made by the candidate is correct to the best of my knowledge.

Date: _____ **Signature of Supervisor**

The Ph. D. Viva-Voce Examination of **Mr. Bharat Bhushan**, Research Scholar, has been held on .....

Chairman, SRC **Signature of External Examiner**

This is to certify that the student has made all the corrections in the thesis.

Signature of Supervisor **Head of the Department**

Dated:_____

Dedicated

to my Beloved Parents

ACKNOWLEDGEMENTS

As I reflect upon the years gone by, I deeply feel the need to acknowledge my gratitude to many wonderful people who have helped me to reach this delightful day.

First and foremost**,** I would like to convey my heartfelt thanks to my supervisor, Dr. P. Gopinath for his continuous guidance, support and motivation. It was his cordial behaviour, constructive criticism and invaluable support due to which I could complete this challenging work. I am obliged for the ample freedom he provided me in conducting my work.

I offer my venerable thanks to the former and present Heads of the Centre Prof. S. K. Nath, Prof. Vijaya Agarwala and Prof. R. Jayaganthan, respectively for their insight and support. I extend my sincere thanks to research committee members of my thesis, Prof. R. P. Singh (Chairman DRC), Prof. S. K. Nath (Internal Expert) and Dr. M. Sankar (External Expert) for their fruitful criticism and precious suggestions.

My sincere thanks to the Head, Institute Instrumentation Centre, Department of Chemistry and Department of Chemical Engineering for providing me the necessary facilities. I also thanks to all office staff members for their continuous support and helping nature. I owe delectably my personal respect towards Dr. R. Rajesh Kannan and S. Nandha Gopal (Scientific Assistant), Centre for Nanoscience and Nanotechnology, Sathyabama University for their help in zebrafish experiments.

My heartfelt thanks to my colleagues and friends especially Dr. S. Chockalingam, Vijayesh, Uday and Deepa for assisting in the numerous laboratory investigations, scientific discussions, data interpretation, invaluable suggestions and encouragement in the progress of this research work. Their wonderful sense of humor helped me to see positive aspects of even the most difficult moments of research and life. I also extend my sincere gratitude to my other labmates Poornima, Abhay, Ishita, Deepika, Rajkumar and Shanid who extended their helping hands and valuable advice indeed. I am indebted to them for their jovial company, homely atmosphere, motivation and encouragement for the completion of my research work. I will always cherish my friendship with Deepa, Nikhil, Poornima, Uday, Danish and Akash, who has been a pillar of support during the stressful times and has always been available for me.

I bow to my adorable parents for their support and encouragement, not only to go complete this gigantic task but to have a pride to succeed in every walk of life. I acknowledge your sacrifices and love showered on me throughout my life. Emotions of my heart should find new boundaries to contain my love for my brother and sister for being everything to me all through my career.

The financial assistance provided by Department of Biotechnology (DBT) from July, 2011 to August, 2012 and Ministry of Human Resource Development (MHRD) from September 2012 to October, 2015 that made my research work very smooth and prompt, is gratefully acknowledged.

Last but not the least I feel privileged for my stay at IIT Roorkee and providing a great work culture and a wonderful ambience. I take an oath to serve for the mankind of my nation and the whole world with whatever the knowledge and wisdom I possess and will acquire in future by virtue of furtherance of my research work and results thereof.

(Bharat Bhushan)

ABSTRACT

The last two decades have witnessed an unprecedented growth in the field of biomedical nanotechnology. A vast variety of nanomaterials are inspected so far in this campaign but among them only few have succeeded in their clinical trials. However, major drawbacks are associated with these nanoparticles which impede their future implications. In this regard, albumin based nanoparticles have emerged as a promising nano-platform due to their high drug holding capacity, ability to protect entrapped cargo molecules from degradation, improved solubility and bioavailability of drug, enhanced cellular uptake, biocompatible and non immunogenic nature due to its biological origin. Moreover, the presence of functionally charged groups offers albumin with various possibilities for surface modifications and interactions with various nanoparticles and drug molecules. Thus, the current thesis focuses on the development of albumin based nanoparticles and proposes their employment in anticancer and antioxidant applications.

In Anticancer applications, albumin nanoparticles based water soluble nanoformulation of highly hydrophobic anticancer drug niclosamide (i.e. BSA-Nic NPs) has been prepared, which overcomes the drawbacks associated with niclosamide such as poor water solubility and limited systemic bioavailability of the drug. Successful synthesis of spherical, highly monodispersed nanoparticles was confirmed by various physicochemical characterization techniques. The therapeutic efficacy of prepared nanoparticles was examined against cancer cells by cell viability assay and morphological analyses. The gene expression analysis confirms the successful induction of apoptosis by these nanoparticles. Another major hurdle in cancer therapy is generalized distribution of therapeutic molecules which results in the implications of higher drug dose that cause severe side effects. In order to address the problems associated with non-specific distribution, cytotoxicity and genotoxicity at higher dose of silver nanoparticles (Ag NPs), a folate conjugated albumin stabilized silver nanoparticles (FA-BSA-Ag NPs) was prepared. The therapeutic potential and cellular uptake was determined on human breast cancer cells, MCF-7 (FR-positive cells) having abundant folate receptor (FR) on its surface and human lung cancer cells, A549 (FR-negative cells). Moreover, the successful induction of apoptosis was confirmed by reactive oxygen species (ROS), cell cycle, morphological and nuclear analysis, followed by apoptotic signalling gene expression analysis.

ROS induced oxidative stress is one of the major factors responsible for various diseases and disorders including cancer. In case of excessive oxidative stress the antioxidant enzymes

defence system of the body gets impaired, which in turn disturb the oxidative balance and cellular homeostasis. Nanoceria (CNPs) has emerged as potential nano-agent in antioxidant therapy because of its exceptional antioxidative activity. In antioxidant applications, a highly biocompatible nanoceria encapsulated albumin nanoparticles (BCNPs) was synthesized, which overcomes the various drawbacks associated with nanoceria such as poor cellular uptake and short residence time in body. Such artificial antioxidant nanozyme protects the cells against actively generating ROS by providing a desired steady state level of therapeutic dose over a period of time as examined *in vitro*. Furthermore, the gene expression analysis confirms the preservation of antioxidant defence system of the cell and their protection from oxidant-mediated apoptosis. Finally, other problems accompanied with nanoceria such as poor solubility and use of harmful chemicals during preparation was addressed by synthesizing albumin coated nanoceria (ANC) by alkaline based precipitation method without altering their antioxidative property. These nanoparticles were highly biocompatible and provided protection against oxidative stress as examined on both *in vitro* and *in vivo* models.

In summary, the present study demonstrated the potential of albumin based nanoparticles in anticancer and antioxidant applications. Such nanoparticles open up a new avenue for the development of improved nano-drug therapies for future clinical trials.

Keywords

Albumin nanoparticles, niclosamide, cancer therapy, antioxidant therapy, apoptosis, silver nanoparticles, nanoceria, nanozyme

LIST OF PUBLICATIONS

I. In Refereed Journals

1. **B. Bhushan** and P. Gopinath. Antioxidant nanozyme: A facile synthesis and evaluation of reactive oxygen species scavenging potential of nanoceria encapsulated albumin nanoparticles. *Journal of Material Chemistry B*, 3, 4843-4852 (2015).
2. **B. Bhushan**, P. Dubey, S. Uday Kumar, A. Sachdev, I. Matai and P. Gopinath. Bionanotherapeutics: Niclosamide Encapsulated Albumin Nanoparticles as a Novel Drug Delivery System for Cancer Therapy. *RSC Advances*, 5, 12078-12086 (2015).
3. **B. Bhushan** and P. Gopinath. Tumor-targeted folate-decorated albumin stabilised silver nanoparticle induce apoptosis at low concentration in human breast cancer cells. *RSC Advances*, 5, 86242-86253 (2015).
4. P. Dubey, **B. Bhushan**, A. Sachdev, I. Matai, S. Uday Kumar and P. Gopinath. Silver nanoparticles incorporated composite nanofiber for potential wound dressing applications. *Journal of Applied polymer Science*, 132, 42473 (2015).
5. P. Dubey, I. Matai, S Uday Kumar, A. Sachdev, **B. Bhushan**, and P. Gopinath. Perturbation of cellular mechanistic system by silver nanoparticles toxicity: cytotoxic, genotoxic and epigenetic potential. *Advances in Colloid and Interface Science*, 221, 4-21 (2015).
6. **B. Bhushan**, S. Uday Kumar, I. Matai, A. Sachdev, P. Dubey and P. Gopinath. Ferritin Nanocages: A novel platform for biomedical applications. *Journal of Biomedical Nanotechnology*, 10, 2950-2976 (2014).
7. S. Uday Kumar, I. Matai, P. Dubey, **B. Bhushan,** A. Sachdev and P. Gopinath. Differentially cross-linkable core-shell nanofibers for tunable delivery of anticancer drugs: synthesis, characterization and its anticancer efficacy. *RSC Advances*, 4, 38263 - 38272 (2014).
8. I. Matai, A. Sachdev, P. Dubey, S. Uday Kumar, **B. Bhushan** and P. Gopinath, Antibacterial activity and mechanism of Ag-ZnO nanocomposite on S.aureus and GFP-

expressing antibiotic resistant E.coli. *Colloids and Surfaces B:Biointerfaces*, 115, 359-367 (2014).

9. S. Uday Kumar, **B. Bhushan***, P. Dubey, I. Matai, A. Sachdev and P. Gopinath. Emerging Applications of Nanoparticles for Lung Cancer Diagnosis and Therapy. *International Nano Letters***,** 3, 45 (2013). (*Equal contribution).
10. A. Sachdev, I. Matai, S. Uday Kumar, **B. Bhushan**, P. Dubey and P. Gopinath, A novel one-step synthesis of PEG passivated multicolour fluorescent carbon dots for potential biolabeling application. *RSC Advances*, 3, 16958-16961 **(**2013).
11. S. Nayak, **B. Bhushan**, R. Jayaganthan, P. Gopinath, R. D. Agarwal, D. Lahiri, Strengthening of Mg Based Alloy through Grain Refinement for Orthopedic Application. *Journal of Mechanical Behavior of Biomedical Materials*, 59, 57-70 (2016).
12. R. M. Kumar, K. K. Kuntal, S. Singh, P. Gupta, **B. Bhushan**, P. Gopinath and D. Lahiri. Electrophoretic Deposition of Hydroxyapatite Coating on Mg-3Zn Substrate for Orthopaedic Application. *Surface and Coatings Technology*, 287, 82-92 (2016).
13. **B. Bhushan**, S. Nandhagopal, R. Rajesh Kannan and P. Gopinath. Bio mimetic nanomaterials: A facile synthesis and evaluation of antioxidant potential of albumin coated nanoceria on human lung epithelial cells and zebrafish. (*Submitted*)
14. **B. Bhushan**, S. Nandhagopal, R. Rajesh Kannan and P. Gopinath. Therapeutic Nanozymes: Antioxidative and cytoprotective effects of nanoceria against the hydrogen peroxide induced oxidative stress in fibroblast cells and in zebrafish. (*Submitted*)
15. Bulbul Tirkey, **B. Bhushan**, S. Uday Kumar and P. Gopinath. Suicide gene therapy: Prodrug Loaded Albumin Nanoparticles as a Novel Therapeutic Approach for Cancer Therapy. (*Submitted*)

II. Book and Book Chapters

1. P. Gopinath, S Uday Kumar, I. Matai, **B. Bhushan**, D. Malwal, A. Sachdev, P. Dubey. Cancer Nanotheranostics. *Springer briefs in applied science and technology*, pp. 1–93 (2015).
2. I. Matai, A. Sachdev, S. Uday Kumar, P. Dubey, **B. Bhushan** and P. Gopinath* 'Dendrimer: A promising nanocarrier for cancer therapy' in book titled "Nanotechnology: Recent Trends, Emerging Issues and Future Directions" *Nova publishers*, 127-155 (2014).

3. A. Sachdev, S. Uday Kumar, I. Matai, G. Bhargavi, P. Dubey, **B. Bhushan** and P. Gopinath, "Polymers as nanocarrier for cancer theranostic applications" in book titled "Recent Developments in Carbohydrates Polymer Research" *Research Signpost Publishers,* 45-55**,** ISBN: 978-81-308-0534-4, **(**2014).

III. In Conferences

1. **B. Bhushan** and P.Gopinath. Imapct of albumin on translational research- A journey from laboratory to market. *New Horizons in Translational Medicine*. *January 2016. Page No. 17.*
2. **B. Bhushan** and P. Gopinath. "Fabrication, Characterization, and Anticancer Potential of Niclosamide Encapsulated Albumin Nanoparticles", RBF 7th International Symposium on "Advances in New Drug Discovery Technologies and Translational Research" Feb 2-4, 2015. *P-33.*
3. A. Sachdev, I. Matai, S. Uday Kumar, P. Dubey, **B. Bhushan**, and P. Gopinath. Chitosan-based fluorescent non-viral vector for simultaneous delivery of gene and imaging agents. *Asian Chitin Journal, Volume 9 No.1June 2013. Page No.17.*
4. S. Uday Kumar, A. Sachdev, P. Dubey, **B. Bhushan**, I. Matai and P. Gopinath. Curcumin loaded chitosan-PEO nanofibers for wound healing. *Asian Chitin Journal, Volume 9 No.1June 2013. Page No.17.*
5. I. Matai, A. Sachdev, S. Uday Kumar, P. Dubey, **B. Bhushan**, and P. Gopinath. Enhanced Antibacterial activity of Chitosan-drug conjugates against *S.aureus* and antibiotic resistant GFP expressing *E.coli. Asian Chitin Journal, Volume 9 No.1June 2013. Page No.18.*
6. I. Matai, G.Bhargavi, A. Sachdev, S. Uday Kumar, P. Dubey, **B. Bhushan**, and P. Gopinath. Chitosan Nanoparticles: Synthesis, Characterization and Antibacterial activity. *Asian Chitin Journal, Volume 9 No.1June 2013. Page No.18.*

CONTENTS

LIST OF FIGURES

LIST OF TABLES

ABBREVIATIONS

% …….....	Percent
µg ……...	Microgram
µL	Microliter
µM …….....	Micromolar
µS……	Micro Siemens
4T1	Mouse Breast Cancer Cells
5-FU	5-Fluorouracil
Å ……...	Angstrom
a.u.	Arbitrary Unit
A549	Human Lung Adenocarcinoma Epithelial Cells
ACS ……...	American Cancer Society
AFM …….....	Atomic Force Microscope
Ag NPs	Silver Nanoparticles
$AgNO_3$	Silver Nitrate
AML	Acute Myeloid Leukemia
ANC	BSA Coated Cerium Oxide Nanoparticles
AO …….....	Acridine Orange
ATP	Adenosine Triphosphate
ATV	Atorvastatin
BAD	Bcl-2-Associated Death Promoter
BAX	Bcl-2-Associated X Protein
BCL2	B-cell Lymphoma 2
BCL2L1	Basal Cell Lymphoma-Extra Large
BCNPs	Nanoceria Encapsulated BSA Nanoparticles
BHK-21	Baby Hamster Kidney cells
BNPs	BSA Nanoparticles
BSA …….....	Bovine Serum Albumin
BSA-Ag NPs	BSA Stabilized Silver Nanoparticles
BSA-Nic NPs	Niclosamide Encapsulated BSA Nanoparticles
CAGR …..…….....	Compound Annual Growth Rate
Caspases …….....	Cysteine-aspartic acid proteases
CCMV	Cowpea Chlorotic Mottle Virus

cDNA …….....	Complementary Deoxyribonucleic Acid
C-dots	Carbon Dots
Ce	Cerium
cm …….....	Centimeter
CNPs	Cerium Oxide Nanoparticles
CO_2	Carbon Dioxide
CPCs	Cardiac Progenitor Cells
CPMV	Cowpea Mosaic Virus
CSFs	Colony-Stimulating Factor
Cu	Copper
Cur	Curcumin
DCFH-DA	2',7'- dichlorfluorescein diacetate
DEX	Dextran
DLS	Dynamic Light Scattering
DMEM	Dulbecco's Modified Eagle's Medium
DMSO	Dimethyl Sulfoxide
DOX	Doxorubicin
dpf	Days Post Fertilization
dsDNA …….....	Double Stranded DNA
E.coli	Escherichia coli
EA …….....	Early Apoptosis
EB …….....	Ethidium Bromide
EDC	1-ethyl-3-(3-dimethylaminopropyl)-carbodiimide hydrochloride
EDS ……...	Energy Dispersive Spectra
EDX …….....	Energy Dispersive X-ray detector
EE …….....	Encapsulation Efficiency
EGCG	Epigallocatechin Gallate
EPR …….....	Enhanced Permeability and Retention Effect
FA …….....	Folic Acid
FA-BSA-Ag NPs	Folic Acid Conjugated BSA Stabilized Silver Nanoparticles
FBP	Folate Binding Protein
FDA ...…….....	Food and Drug Administration
Fe_3O_4	Magnetite
FE-SEM	Field Emission Scanning Electron Microscopy

$FeSO_4.7H_2O$	Iron (II) Sulfate Heptahydrate
FITC …….....	Fluorescein Isothiocyanate
FR …….....	Folate Receptor
FTIR	Fourier Transform Infrared Spectroscopy
GAPDH …….....	Glyceraldehyde-3-phosphate dehydrogenase
GFP …….....	Green Fluorescent Protein
GPX	Glutathione Peroxidases
GSH	Glutathione
GST	Glutathione S-Transferases
h	Hour
H_2O	Water
H_2O_2	Hydrogen Peroxide
HCT 116	Human Colon Carcinoma Cells
hpf	Hours Post Fertilization
Hsp	Heat Shock Protein
HT29 …….....	Human Colon Adenocarcinoma Cells
IC_{50}	Half Maximal Inhibitory Concentration
ICP-MS	Inductively Coupled Plasma Mass Spectrometry
IL-2 …….....	Interleukin-2
INF-α …….....	Interferon-alfa
JCPDS ……...	Joint Committee on Powder Diffraction Standards
JNKs	c-Jun N-terminal Kinases
K562	Human Chronic Myelogenous Leukemia
KB	Human Nasopharyngeal Carcinoma Cells
KBr	Potassium Bromide
kDa …….....	Kilo Dalton
keV …….....	Kilo Electron Volt
L-132	Human Lung Epithelial Cells
LA …….....	Late Apoptosis
LTB	Heat-Labile Enterotoxin Subunit B
M ……...	Molar
mbar …….....	Millibar
MCF 10A	Human Mammary Epithelial Cells
MCF-7	Human Breast Adenocarcinoma Cells

mg	Milligram
MGC803 …….....	Gastric Cancer Cells
min	Minute
mL	Milliliter
mM	Millimolar
MOMP …….....	Membrane Permeabilization
MRI	Magnetic Resonance Imaging
mRNA	Messenger RNA
MTT	3-[4,5-dimethylthiozol- 2-yl]-2,5 diphenyltetrazolium bromide
MV	Methyl Violet
mV	Milli Volt
MVBs	Multivesicular Bodies
$NaBH_4$ …….....	Sodium Borohydride
nab™ …….....	Nanometer Albumin-Bound Technology
NaCl …….....	Sodium Chloride
NaOH	Sodium Hydroxide
ng	Nanogram
NHS	N-hydroxy succinimide
Nic ..…….....	Niclosamide
nm	Nanometer
NPs ……...	Nanoparticles
NS	Not specify
^oC	Degree Celsius
OD …….....	Optical Density
PAMAM	Poly(amidoamine)
PBS…….....	Phosphate Buffered Saline
PCL	Polycaprolactone
PCR ……...	Polymerase Chain Reaction
PDT	Photodynamic Therapy
PEG ……...	Polyethylene Glycol
PEI	Poly(ethylenimine)
PEO	Poly(ethylene oxide)
pH	Potential of Hydrogen
PI	Propidium Iodide

PLA	Poly(lactid acid)
PLGA	Poly(lactic-coglycolic acid
PTX	Paclitaxel
QDs	Quantum Dots
rGFP	Recombinant Green Fluorescent Proteins
Rho B	Rhodamine B
RNA	Ribonucleic Acid
RNase ……...	Ribonuclease
ROS ..…….....	Reactive Oxygen Species
rpm	Revolutions per minute
RT-PCR …….....	Reverse Transcriptase-Polymerase Chain Reaction
s	Second
SAED …….....	Selected Area Electron Diffraction
siRNA	Short Interfering RNA
SKOV3 …….....	Human Ovarian Cancer cells
SLP	Solid Lipid Nanoparticles
SOD …….....	Super Oxide Dismutase
STATs	Signal Transducers and Activators of Transcription
TEM	Transmission Electron Microscope
TG/DTA ……...	Thermo gravimetric/ Differential Thermal Analyzer
Tris-HCl	Tris (hydroxymethyl) aminomethane hydrochloride
Trp	Tryptophan
UPRT	Uracil Phosphoribosyl Transferase
UV	Ultra Violet
VBLS	Vinblastine Sulfate
wt%	Weight percent
XRD	X-Ray Diffraction
Zn	Zinc
ZnO	Zinc Oxide

CHAPTER 1

INTRODUCTION

This chapter gives a brief introduction on the potential of nanotechnology for biomedical applications. This chapter also includes the objectives, experimental approaches, significance and salient features of the present study.

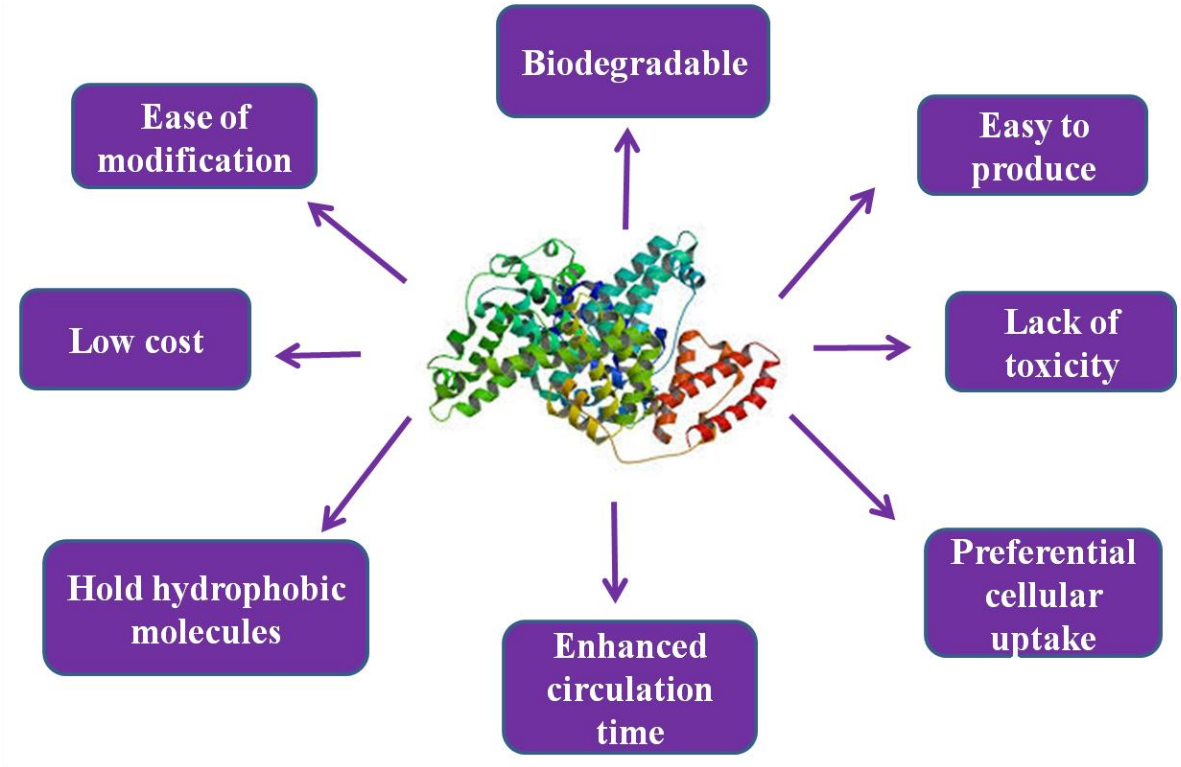

CHAPTER 1

INTRODUCTION

Cancer, once considered as disease of western world, developing country like India is now on the edge of major cancer epidemic with more than one million cases reported per year, which is expected to be get doubled in next 2 decades. According to the world cancer report 2014, cancer is amongst the leading cause of mortality and morbidity worldwide and is responsible for approximately 8.2 million deaths. Around 14 million total new cases have been indentified, of which 700,000 in India were recorded in 2012, which is expected to rise by about 70 % in next two decades (Torre et al, 2015). Moreover, more than 60 % of these new cases and 70 % of total cancer deaths occur in Asia, Africa, South and Central America. Lung and breast cancers are among the most commonly diagnosed cancer in men and women respectively. The lung cancer is a leading cause of cancer deaths in male worldwide, while breast cancer is leading cause of cancer deaths in females in less developed countries. Tobacco use is one of the major factors responsible for around 20 % global cancer deaths and 70 % of lung cancer deaths. Presently, the conventional therapies including surgery, irradiation and chemotherapy employed for the cancer treatment suffer severe drawbacks such as non specific accumulation of the therapeutic molecules which results in reduced therapeutic efficacy, higher toxicity to neighbour tissues and limits the maximum dose availability. In cancer therapy, due to the heterogeneity and diverse cause associated with cancer, personalized medication and treatment are the ultimate goals for their treatment. A major challenge among the researchers is to develop a delivery system that has high accuracy, therapeutic efficacy and biocompatible.

Free radicals also emerged as a major pathologic factor responsible for various diseases and disorders including cancer (Kumar et al., 2008, Emiret et al., 2004, Misra et al., 2009, Finkel et al., 2000), affecting various organs of the body including lungs. Lungs have been under continuous exposure to both exogenous free radical sources including photochemical air pollution, tobacco smoke, electromagnetic or particulate radiation, drugs etc. and endogenous free radical sources including activated phagocytes, enzymatic activity e.g. xanthine oxidase, mitochondrial electron transport etc. Oxidative stress arises due to the incomplete removal of these toxic free radicals and by impaired balance between the oxidants and antioxidants in the

body leading to various respiratory diseases such as adult respiratory distress syndrome, cystic fibrosis, and idiopathic pulmonary fibrosis. Numerous approaches have been implied and tested so far to protect the cells from oxidative stress and restore physiological antioxidants activities. This provokes a need to develop an artificial antioxidant system that is safe and effective (Schunemann et al., 1997, Bargagli et al., 2009, Park et al., 2009).

In past decades, the tremendous impact of nanotechnology in cancer therapy is in the realm of drug delivery. By programming various properties of nanoparticles such as chemical and physical, we can modulate their biological properties including immunogenicity, circulation half life and toxicity necessary for the development of drug delivery system. The emerging trend is to exploit the shape, size and surface chemistry of nanoparticles which are responsible for their cellular uptake, half life in blood, immune response and renal clearance in order to revolutionize cancer therapy. Recently, nanomedicine has emerged as key area of research combining the knowledge of medicine, chemistry, pharmaceutical technology, engineering and material science. This shall led the foundation of global nanomedicine market, which is projected to reach US$ 177.6 billion in 2019 with an estimated healthy compound annual growth rate (CAGR) of 12.3%. Moreover, the drug delivery sector in nanomedicine itself holds 70% of total sales along with 59% patent and 76% of published articles (http://www.transparencymarketresearch.com/pressrelease/nanomedicine-market.htm). Thus nanoparticles based medicine would herald a new age of advanced health care, proficient health economics and personalized medicine (Ranganathan et al., 2012, Venkatraman et al., 2014, Cherian et al., 2014).

In general, nanomedicine has been defined as complex nanoscale system that retains the cargo molecules throughout its circulation in the body without affecting the nearby tissues. Unlike normal tissues where these nanoparticles don’t cross the endothelial barrier, in tumor they easily accumulate at the tumor site by penetrating through the leaky blood vessels formed as a result of aberrant angiogenesis in tumor. Moreover, tumor specific accumulation of these nanoparticles can be further enhanced by active targeting. The surface of the nanoparticles is functionalized by tumor specific ligands that specifically bind to the receptor present abundantly on the surface of tumor cells, are internalized and release cargo molecules into the target cells. A large variety of nano-carrier systems has been investigated so far for their biomedical applications including polymeric nanoparticles, magnetic nanoparticles, solid lipid nanoparticles, dendrimers, nanowires polymeric micelles, etc. but various drawbacks like high

cost, toxicity, immunogenicity due to its foreign origin and insolubility in physiological conditions associated with these nanoparticles hamper their future clinical role.

Amongst several biodegradable nanoparticles, protein based nanoparticles earn wide concern as they are biodegradable, easy to produce with controllable size distribution (Langer et al., 2003), lack toxicity and immunogenicity due to its biological origin, biocompatible, ability to hold a variety of drugs in its hydrophobic pockets, improve the solubility of drugs and enhanced bioavailability by their controlled release, low cost, enhanced circulation time *in vivo* and inherent property of preferential uptake in tumor and inflamed tissue (Bhushan et al., 2014, Uday Kumar et al, 2013). With the success of food and drug administration (FDA) approved Abraxane (albumin based drug nano-formulation), albumin based nanoparticles emerged as a potential candidate in the field of nanotechnology and cancer therapy (Ibrahim et al., 2002, Miele et al., 2009, Green et al., 2006). Moreover, the presence of charged functional groups including amino and carboxylic groups offer albumin with various possibilities for surface modification and interaction with various nanoparticles and drug molecules (Gopinath et al. 2015). These properties make albumin an ideal candidate for drug delivery.

The hydrophobic nature of most of the anticancer drugs including niclosamide possesses a major hurdle for their use in cancer therapy. Moreover, the organic solvents used to augment the solubility of these drugs results in severe complications. Like many other drugs numerous efforts have been made to increase the solubility of niclosamide, but a proper delivery system has not yet designed to exploit the clinical aspect of this drug. With the implication of nanotechnological tools, the therapeutic index of nearly all drugs has been enhanced by improving their solubility and bioavailability to cells (Sahoo et al., 2003, Vasir et al., 2005). Apart from this, those therapeutic molecules that previously failed in their clinical trials or have not been yet utilized due to their solubility and toxicity concerns are now being investigated by preparing their nanoparticulate formulations (Kipp, 2004). Another major problem need to be addressed in cancer therapy is non-specific distribution and rapid clearance of most of the therapeutic molecules from the body, which results in the application of high drug dose that cause severe side effects. With the nanotechnological advancements, the cytotoxicity and genotoxicity concerns associated with these therapeutic molecules are further reduced by their efficient targeted delivery which results in the induction of apoptosis at lowest possible concentrations and thereby providing an alternative mode of cancer therapy.

In the plethora of nanomaterials, nanoceria emerged as a potential candidate for antioxidant therapy, due to its superoxide dismutase (SOD) and catalase mimetic activity, high biocompatibility and auto-regenerative properties. However, short residence time in body, poor cellular uptake and poor bioavailability to the cells may narrow down the therapeutic index of nanoceria. This provokes a need to explore a potential delivery system for nanoceria that remain stable inside the cells and provide desired steady state level of therapeutic dose that helps in defending the cells against actively generated ROS over a period of time. Other major problems associated with such antioxidant system that hamper their future clinical role are poor water solubility and use of toxic solvents in the synthesis processes. To address these problems, a variety of systems has been developed, but several drawbacks associated with them such as toxicity, non degradability, immune response etc. hinder their future clinical applications. Moreover, the accountability of all such systems remains questionable as antioxidant potential of these nanoparticles was not tested against *in vitro* or *in vivo* models. This provokes a need for the development of more suitable delivery system for nanoceria in order to endorse its clinical role.

Objectives

The main objective of the present work is as follows:

- To develop a biocompatible albumin based nanoformulation for delivery of hydrophobic anticancer drug niclosamide.
- To develop a folic acid conjugated albumin stabilized Ag NPs for tumor-targeted delivery of Ag NPs.
- To develop albumin based nanoparticles as delivery system for the sustained release of nanoceria.
- To develop albumin based artificial enzymatic system and to investigate its antioxidant potential against ROS both *in vitro* and *in vivo*.

1.2 Experimental approaches

In order to achieve the above objectives the following investigations were carried out:

- Synthesis of niclosamide and nanoceria encapsulated albumin nanoparticles by desolvation method.
- Synthesis of albumin coated nanoceria by wet precipitation method.
- Synthesis of albumin stabilized Ag NPs by sodium borohydride ($NaBH_4$) reduction method, followed by folic acid conjugation to albumin *via* carboiimide reaction.
- Nanoceria particle synthesized by hydrothermal method.

- Determination of concentration of prepared Ag NPs and nanoceria, their release and uptake by the cells by inductively coupled plasma mass spectroscopy (ICP-MS).
- Physicochemical characterization of prepared nanoparticles by UV-visible spectrometer, fourier transform infrared spectroscopy (FTIR), X-ray diffraction (XRD), Fluorescence spectrometer, dynamic light scattering (DLS), transmission electron microscope (TEM), field emission scanning electron microscopy (FE-SEM), atomic force microscopy (AFM), thermogravimetric/ differential thermal analyzer (TG/DTA).
- Determination of drug entrapment efficiency and its release by UV visible spectrometer.
- Determination of *in vitro* stability of nanoparticles by DLS.
- Examination of antioxidant potential of nanoceria by SOD assay and photometric study.
- Assessment of biocompatibility and therapeutic efficacy by 3-[4,5-dimethylthiozol- 2-yl]-2,5 diphenyltetrazolium bromide (MTT assay).
- Observation of apoptotic cell morphology by FE-SEM, acridine orange/ethidium bromide (AO/EB) and Rhodamine B (Rho B)/ Hoechst 33342 staining.
- Qualitative assessment of nanoparticles uptake by fluorescence microscopy, TEM and FE-SEM equipped with energy dispersive X-ray detector (EDX).
- Intracellular ROS assessment and cell cycle analysis by flow cytometer.
- Involvement of various apoptotic and antioxidant signaling genes by semi-quantitative reverse transcriptase-polymerase chain reaction (RT-PCR).

1.3 Significance and salient features of the present study

The significance and salient features of the present study are summarized below:

- A water soluble formulation of hydrophobic anti-cancer drug, niclosamide has been synthesized in order to facilitate its uptake by cancer cells.
- A protein based system has been realized for the first time to deliver niclosamide for cancer therapy; such protein based drug delivery system renders a scope for future clinical application.
- Formation of spherical, highly monodispersed and stable nanoparticles with improved sustained release of niclosamide in aqueous environment.
- BSA stabilized Ag NPs (BSA-Ag NPs) was synthesized and further conjugated with folic acid (FA) to aid its uptake by FR (+) cancer cells such as MCF-7 cells.
- A folate conjugated albumin stabilized Ag NPs overcomes various cytotoxicity and genotoxicity associated with Ag NPs by reducing the effective therapeutic concentration by enhancing their uptake.

- An antioxidant enzyme mimetic highly biocompatible water redispered albumin coated nanoceria particles has been synthesized in order to ease its uptake by the cells, as assessed quantitatively and qualitatively by various techniques.
- A water soluble formulation of artificial redox enzyme, nanoceria encapsulated albumin nanoparticles has been synthesized in order to facilitate its sustained release over a period of time.
- A protein based system has been realized for the first time for the synthesis and controlled delivery of nanoceria for intracellular ROS abatement.
- The antioxidant potential of albumin based nanoceria system has been confirmed by antioxidant and SOD assay.
- The therapeutic efficacy of BSA-Nic NPs and FA-BSA-Ag NPs has been validated against A549 and MCF-7 cells.
- Efficient induction of apoptosis was corroborated by ROS determination, cell cycle, morphological and nuclear analysis followed by gene expression analysis.
- The ROS scavenging potential of ANC was assessed *in vitro* against human lung epithelial cells and *in vivo* on zebrafish (*Danio rerio*). Further, the efficient preservation of the cell's antioxidant defense system and protection against the oxidant-mediated apoptosis was corroborated by gene expression analysis.

1.4 Organization of thesis

This thesis is organized into eight chapters. The literature review on cancer, albumin nanoparticles, anticancer drug niclosamide and their mode of action, metal based nanoparticles mainly Ag NPs and nanoceria are discussed in Chapter 2. The experimental techniques followed in the present study are elaborated in Chapter 3. The synthesis and characterization of niclosamide encapsulated albumin nanoparticles and their therapeutic potential is presented in Chapter 4. Chapter 5 elaborates the preparation of folate modified albumin stabilized Ag NPs and their ability to induce apoptosis at much lower concentration. The ROS scavenging potential of nanoceria encapsulated albumin nanoparticles are investigated in Chapter 6. While, Chapter 7 demonstrates the antioxidant potential of albumin coated nanoparticles to protect the human lung epithelial cells (L-132) and zebrafish embryos from oxidative stress. Finally, the conclusions and scope of future work of present study is mentioned in Chapter 8.

CHAPTER 2

LITERATURE REVIEW

This Chapter gives a brief introduction on the pro and cons associated with cancer and antioxidant therapy. The potential of protein based nanoparticles in particular albumin nanoparticles, anticancer drug niclosamide, silver nanoparticles and nanoceria have been discussed in detailed.

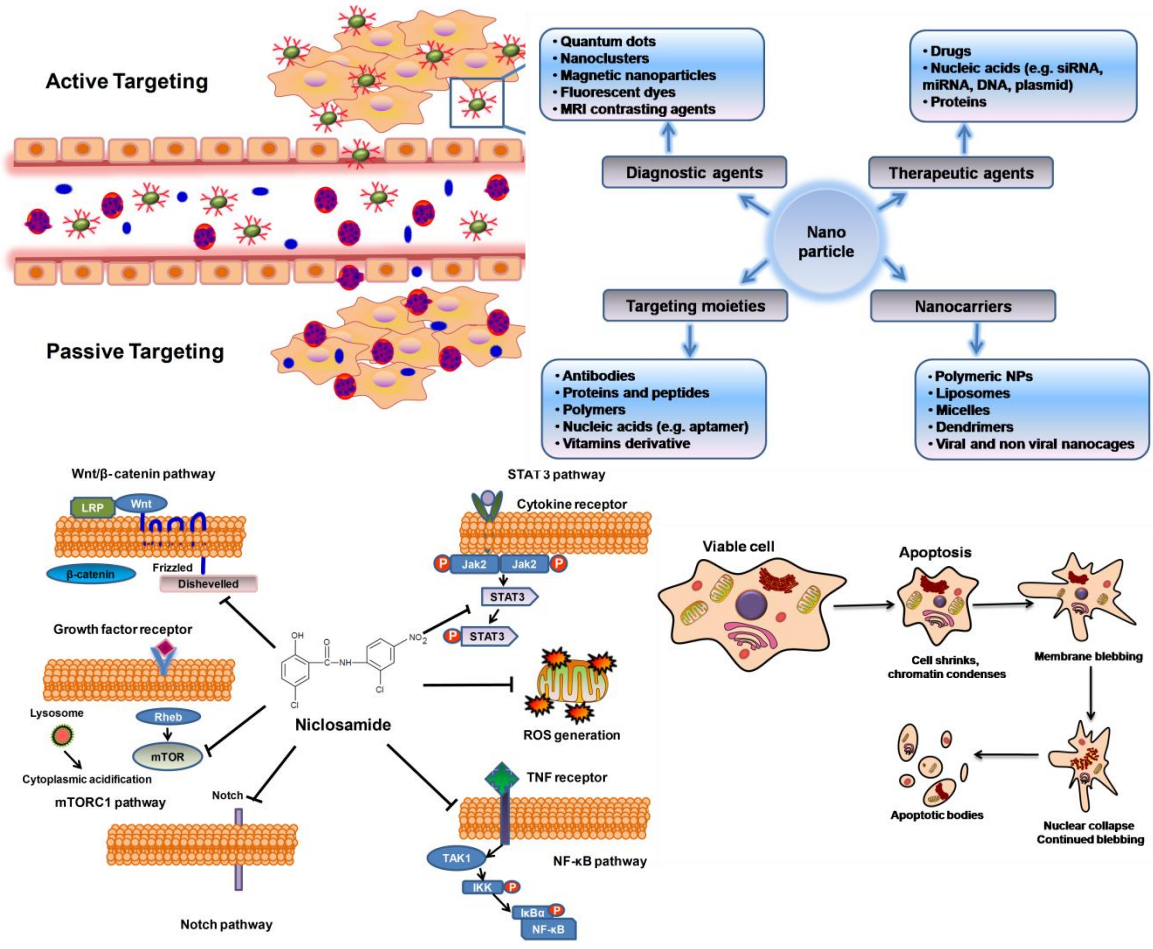

CHAPTER 2

LITERATURE REVIEW

2.1 Cancer

Cancer is a group of diseases responsible for millions of deaths, typified by the uncontrolled growth and spread of abnormal cells. Cancer is mainly caused by external factors including unhealthy diet, tobacco and infectious organism, and internal factors including hormones, immune conditions and inherited genetic mutations. Present major treatments include chemotherapy, radiation, surgery, immune therapy, hormone therapy.

In current scenario, there is rapid surge in number of cancer cases as result of growth and aging of the population, overweight, changing reproductive patterns associated changing life style, smoking and physical inactivity is putting an enormous burden on under developed and developing countries like India. According to GLOBOCAN estimates around 14.1 million new cases and 8.2 million deaths happens worldwide in 2012 as shown in Figure 2.1. Lung and breast cancer are among the four most common cancers occurring worldwide including bowel and prostate cancer. Lung cancer is responsible for more deaths as compared to other cancer in both male and female. Among males lung cancer is the most frequently diagnosed cancer, which account for 13 % of total diagnosed cancers and is leading cause of cancer death in 2012, around 221,200 new lung cancer cases and 158,040 deaths are expected in 2015. In female, lung cancer is leading cause of cancer deaths in developed countries, while in less developed countries it is the second most leading cause of cancer death. Breast cancer among females is the most recurrently diagnosed cancer and the leading cause of cancer death worldwide with 1.7 million cases and 521,900 deaths in 2012. Among females breast cancer alone account for 25 % of all cases and 15 % of all cancer deaths. (Torre et al., 2015, Siegel et al., 2015, www.cancerresearchuk.org, http://globocan.iarc.fr/Pages/fact_sheets_cancer.aspx,).

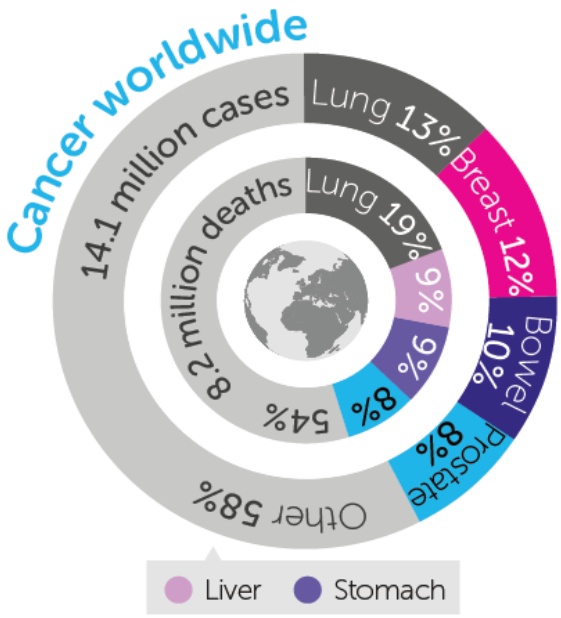

Figure 2.1 Global cancer statistics according to GLOBOCAN estimates. (www.cruk.org/cancerstats)

2.2 Conventional therapies for cancer

The conventional strategies employed for cancer treatment includes chemotherapy, radiation, surgery or combination of these strategies. Apart from them hormone therapy and immunotherapy has been also applied for some type of tumor (Miller et al., 1981). Surgery is one of the best tools to fight against cancer especially in case of non metastasized solid tumors, followed by radiation therapy which utilized the high energy waves (radiation) or particles beams such as gamma rays, X-rays, neutrons or pi-mesons for cancer therapy (Israel, 1978). These radiation ionize the major component of the cell such as DNA/RNA, protein etc. and hamper its biological activity, thus results in cell cycle arrest or cell death. These radiations are found to be more lethal for cancer cells as compare to normal cells because cancer cell are more unstable and their cellular repair mechanism is not efficient like normal cells which make it more vulnerable to radiation. However, the major drawback associated with radiotherapy is its inability to treat only cancer cells without affecting the surrounding normal tissues.

Chemotherapy is utilized for metastasized cancer, where surgery and radiation therapy is found to be ineffective. The therapeutic molecules utilized in chemotherapy act by hindering the process of cell division. However, they face the same challenge like radiation therapy due to its unspecific nature and inability to differentiate between normal and cancer cells.

Apart from them hormone therapy or androgen suppression therapy or androgen deprivation therapy are also utilized for the prevention of hormone dependent cancers such as prostrate or

breast cancer by lowering androgen level that results in tumor growth suppression and reduction of tumor volume (Vrbanec et al., 1998, Torri et al., 2005). While photodynamic therapy (PDT) act by the activation of photosensitizer by the non-toxic infrared light, which result in the formation of highly reactive singlet oxygen that cause the cancer cells to undergo apoptosis or necrosis (Chen et al., 1996 and 1997, D'Cruz et al., 2004, Dolmans et al., 2003). However, such therapy is applicable for superficial tumors such as head and neck cancer, melanomas because of the limited penetration ability of light source.

Recently, immunotherapy or biologic therapy has been emerged as a promising tool for the treatment of cancer that affects immune system such as lymphoma and leukemia. Immunotherapy aim to arouse the immune system of the body by the administration of monoclonal antibodies or cytokines such as colony-stimulating factor (CSFs), Interferon-alfa (INF-α) and interleukin-2 (IL-2) (Rosenberg, 1999). Cytokine conjugate with the cancer cell and facilitate its removal by making it recognizable to other immune cells, while monoclonal antibodies covalently conjugated with radioactive chemical specifically target the cancer cell and inhibit their growth (Weiner, 1999).

2.3 Nanoparticles in cancer therapy

A variety of nanomaterials has been extensively explored for their role in various biomedical applications such as drug delivery, bio-imaging, tissue engineering, bio-sensing, antibacterial materials etc. (Maehashi et al., 2007, Uday kumar et al., 2014, Kerman et al., 2008, Sachdev et al., 2013, Kadam et al., 2013, Matai et al., 2014, Randall et al., 2011, Dubey et al., 2015a, Okuno et al., 2008). Among them, field of drug delivery has been revolutionized with the advent of nanoparticles based carrier systems as outlined in Figure 2.2. These nanocarriers provide protection of cargo molecule from degradation; enhance the absorption of cargo molecule by facilitating cellular uptake, altering the drug distribution and pharmacokinetic profile of drug. Moreover, by amending the composition and surface properties of these nanocarriers a better therapeutic efficacy could be achieved. (Suri et al., 2007, Roco 2003, Torchilin 2008, Natarajan et at., 2014). Moreover, the enhanced physiological stability and ability of these nanoparticles to withstand physiological stress make them a potential candidate as compared to other delivery system (Sahoo et al., 2008, Couvreur et al., 2006). A large variety of nanoparticulate systems has been designed and investigated so far by utilizing the traditional synthetic polymer such as poly(cyano acrylate) (Diepold et al., 1989), poly(lactic-coglycolic acid) (PLGA) and poly(lactid acid) (PLA) (Park et al., 2009b) for drug delivery and cellular uptake studies (Couvreur et al., 1979). Moreover, polyelectrolytes such as

poly(ethylenimine) (PEI) revealed their tremendous potential in the field of gene delivery (Gharwan et al., 2003). Apart from them, a vast variety of nanoparticulate system based on natural polysaccharides such as chitosan, starch, dextran, β-cyclodextrin, Pullulan etc. has been investigated for their role in the delivery of cytotoxic agent, gene, imaging probe etc. (Liu et al., 2008, Snima et al., 2012 and 2014, Anitha et al., 2013, Lakshmanan et al., 2011). Metal nanoparticles represent another class of nanocarriers that have been screened in this campaign due to their potential in cancer diagnosis and therapy (Brown et al., 2010, Smith et al., 2010, Choi et al., 2008, Konwarh et al., 2009, Snima et at., 2013). Similarly, lipid based nanoparticles has been utilized mostly for gene delivery as lipoplexes and for various parental applications as solid lipid nanoparticles (SLP) (Koh et al., 2010, Joshi et al., 2009). But these nanoparticles come out with their own limitation which restricts their further use in biomedical applications. This provokes the researchers to develop nanostructured materials that overcome these hurdles.

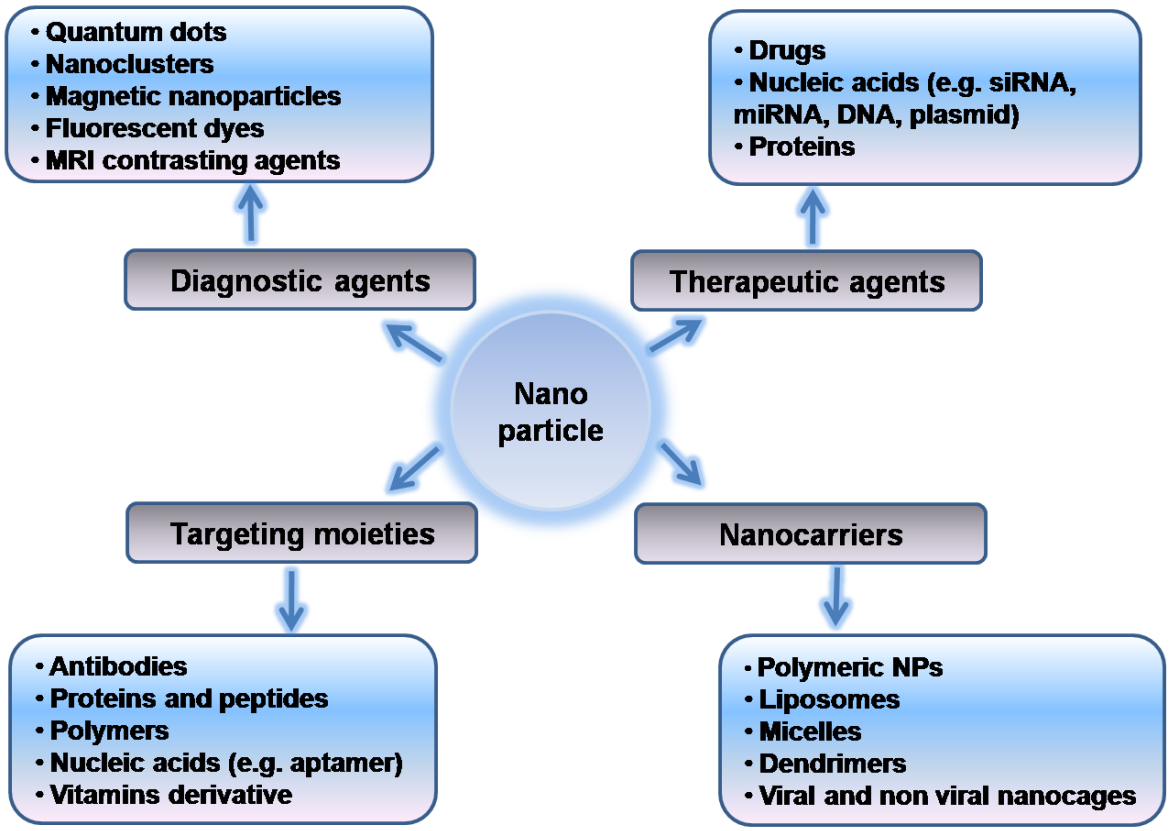

Figure 2.2 Nanoparticle based systems for biomedical applications.

2.4 Protein based nanoparticles

In recent years, protein based nanoparticles have gain remarkable interest due to its unique functionalities and probable applications in the field of nanotechnology and nanomedicine. A vast variety of nanoparticulate systems have been developed based on proteins such as Albumin (e.g. bovine serum albumin (BSA), human serum albumin (HSA) and ovalbumin), Gelatin, apotransferrin, lactoferrin, fibrinogen, ferritin, heat shock protein (Hsp), viral nanoparticles such as cowpea chlorotic mottle virus (CCMV), cowpea mosaic virus (CPMV), sendai viral envelopes, Lectin, Collagen, Milk Proteins (e.g. casein, whey proteins), Silk Proteins, Elastin, Zein, Gliadin, Soy proteins etc. (Gopinath et al. 2015, Bhushan et al. 2014, Elzoghby et al. 2011, 2012 a and b, 2013, Khan et al., 2013, Rejinold et al., 2010, 2013, 2014 and 2015, Kumar et al., 2015, Jana et al., 2002, Ramani et al., 1997 and 1998, Tiwari et al., 2012, Qi et al., 2012). Biomacromolecule protein overcomes various limitations of conventional therapy such as poor solubility of drug, greater storage stability, poor bioavailability and therapeutic efficacy of drug. These protein based system have inherent property of preferential uptake in tumor and inflamed tissue, lack of toxicity and immunogenicity and biodegradability. The amphiphilic nature of the proteins allows them to interact with both the nanoparticles and the surrounding solvent system. The presence of functionally charged groups including amino and carboxylic groups offer albumin with various possibilities for surface modification and interaction with various nanoparticles and drug molecules. These properties make protein an ideal delivery system (Bhushan et al., 2014, Uday Kumar et al., 2013, Gopinath et al., 2015)

2.5 Albumin nanoparticles

During last few decade albumin based nanoparticles have been explored for their clinical applications because of its low cost, high availability, easy purification, better drug-loading capacity and its implication in medicine but major breakthrough came with the development of FDA approved paclitaxel–albumin nanoparticles (Abraxane, an example of nanometer albumin-bound technology (nab^{TM})) for the treatment of metastatic breast cancer and advanced non-small-cell lung cancer (Ibrahim et al., 2002, Miele et al., 2009, Green et al., 2006). Since then there are around seven albumin based drugs or imaging agents in market and around ten such products are under clinical trials for various applications including oncology, diabetes, hepatitis C and rheumatoid arthritis (Ren et al., 2013).That augmented the interest in the use of BSA as nanocarrier for biomedical applications (Rahimnejad et al., 2006).

Characteristics	BSA-EGCG	BSA-ATV	BSA-PTX	BSA-VBLS	BSA-LTB-5-FU	BSA-Cur	BSA-BEX	BSA-ETX	BSA-MX	BSA-DOX
Morphology	spherical	spherical	spherical	spherical	spherical	NS	spherical	spherical	spherical	spherical
Size (nm)	186-300	97–125	210	93-282	254	223.5-228.7	171.4±4.7	215.8±3.2	100.5-111.4	214
Entrapment efficiency (%)	NS	71-94	95.3	84.83-94.78	80.1	74.76-91.01	78.12 ± 0.45	72 ± 1.3	NS	98.6
Zeta potential (mV)	-11.5--42.9	-36.3	-30	NS	-19.95	-30.1--32.2	-25.51 ± 1.42	7.8	NS	-36
Cell line	Caco-2	MiaPaCa-2	PC-3	In silico	SMMC-7721	MDAMB231	A549, MCF-7	Activated macrophages	MCF-7	QGY-7703, Hepli
Reference	Zheng et al., 2014	Sripriyalakshmi et al., 2014	Zhao et al., 2010	Zu et al., 2009	Zhao et al., 2014	Jithan et al., 2011	Qi, et al., 2014	Bilthariya, et al., 2015	Li, et al., 2012	Xie, et al., 2012

Vinblastine sulfate (VBLS), Niclosamide (Nic), Paclitaxel (PTX), Epigallocatechin gallate (EGCG), Heat-labile enterotoxin subunit B (LTB), 5-fluorouracil (5-FU), Atorvastatin (ATV), Curcumin (Cur), Bexarotene (BEX), Etoricoxib (ETX), Mitoxantrone (MX), Not specify (NS)

Table 2.1 List of previously prepared drug encapsulated BSA based NPs by desolvation method.

Albumin is the most copious plasma protein constituting more than half of the human plasma protein with a molecular weight of 66.5 kDa, which is stable over a wide range of pH from 4–9, and remain thermally stable when heated at 60 ^{o}C for up to 10 h without deleterious effects (Neumann et al., 2010, Kratz, 2008). These plasma proteins constitute a crucial components in various biological processes such as maintaining colloidal osmotic pressure, delivery of nutrients to cells, balancing plasma pH and solubilizing long chain fatty acids. Moreover, the unique ligand-delivery property of serum albumin impart enhanced solubility for serum albumin conjugated hydrophobic drugs in plasma and help in improving pharmacokinetic property of drug molecules in biological environment.

Until now, a large number of techniques are implied for the preparation of albumin nanoparticles, some of the notable techniques are mentioned here:

Desolvation or coacervation method: It is one of the most widely used methods for the preparation of albumin nanoparticles by continuous drop wise addition of desolvating agent i.e. ethanol under continuous stirring to the aqueous solution of albumin until solution appears turbid. With increase in ethanol content albumin particles get phase separated as a result of decrease in their water solubility. The particles formed are not stable and readily redissolve in water. (Langer et al., 2003, Weber et al., 2000, Li et al., 2001). In order to increase their stability cross-linking agent i.e. glutaraldehyde is added, which results in the crosslinking between the amino groups in albumin and aldehyde group of glutaraldehyde (Meziani et al., 2003, Merodio et al., 2001). A large number of drug encapsulated albumin nanoparticles have been prepared so far as listed in Table 2.1. Apart from this Lin et al. use methyl polyethylene glycol modified oxidized dextran (Dextranox-MPEG) as crosslinking agent instead of glutaraldehyde (Lin et al., 1994).

Emulsification method: In emulsification method thermal and chemical treatment are used for albumin stabilization. (Patil et al., 2003, Sundar et al., 2010) Thermal treatment are used to stabilize albumin nanoparticles prepared by homogenizing the albumin droplets containing oil phase (e.g. cotton seed oil, castor oil) by heating at high speed magnetic stirring (Jahanshahi et al., 2008, Yang et al., 2007). The cooled mixture was then mixed with ethyl ether to facilitate their separation through centrifugation by reducing the oil viscosity. While in chemical treatment, emulsified aqueous albumin solution in oil phase was denatured by adding an organic (e.g. ether, cyclohexane) solution containing crosslinking agent such as formaldehyde, glutaraldehyde or 2,3-butadiene (Sundar et al., 2010, Jahanshahi et al., 2008, Reis et al., 2006, Crisante et al., 2009).

Thermal gelation: In thermal gelation method, heat induced unfolding of protein took place followed by protein-protein interaction such as hydrophobic, electrostatic, disulphide-sulfydryl interaction and hydrogen bonding (Yu et al., 2006, Qi et al., 2010, Bronich et al., 2005).

Nano spray drying method: A vibrating mesh technology was used containing a spray cap that has thin spray mesh (perforated membrane with micron size holes) incorporated with piezoelectric crystal driven spray head. The mesh starts vibrating up and down at ultrasonic frequency by the piezoelectric actuator resulting in the formation of aerosol containing millions of precise sized droplets. (Lee et al., 2011). An electrostatic particle collector is used to collect the oppositely charged particles.

Nab-technology (nanoparticle albumin-bound technology): This novel technique was developed by American Bioscience, Inc. for preparing a hydrophobic drugs loaded albumin nanoparticles by passing through the mixture of albumin and drug molecules under high pressure through a jet. (Desai, 2007, Cortes et al., 2010). FDA approved Abraxane® (nab-paclitaxel;paclitaxel-albumin nanoparticle) is a landmark of this technology. Currently many other nab drugs are under investigation including ABI-009 (nabrapamycin) and ABI-008 (nab-docetaxel) (Desai, 2007).

2.6 Anticancer drug – niclosamide and its modes of actions

Around 50 years, niclosamide ((5-chloro-*N*-2-chloro-4-nitrophenyl)-2 hydroxy benzamide) has been used as an oral antihelminthic drug against various tapeworm infections. Apart from this niclosamide has also been utilized as molluscicide for schistosomiasis control in water treatment programs. The niclosamide acts by inhibiting the anaerobic adenosine triphosphate (ATP) production and mitochondrial oxidative phosphorylation (Weinbach et al., 1969). In last decade, niclosamide emerged as a potential candidate for cancer therapy, demonstrating its antiproliferative activity against a various cancer cells including solid tumor cells (such as prostate cancer, brain cancer, breast cancer, colon cancer and lung cancer) and hematologic cancer cells (such a acute myeloid leukemia, (AML)) (Wieland et al., 2013, Jin et al., 2010, Sack et al., 2011, Wang et al., 2013, Ren et al., 2010, Lu et al., 2011). Moreover, it also demonstrates an effective antitumor activity in xenograft nude mouse models (Jin et al., 2010, Osada et al., 2011). The mechanism of action of niclosamide is not fully understood, but recent study suggests that its acts on multiple signalling pathways as shown in Figure 2.3, thus helps in overcoming the challenges associated with conventional chemotherapy such as drug

resistance and relapse, providing it an edge over other anticancer drug molecules. Further, niclosamide appear as an impressive agent for combination therapy, it shows both synergistic effect and additive antiproliferative activity in combination with other chemotherapeutic agents such as daunorubicin, cytarabine, oxaliplatin, and etoposide against AML and colorectal cancer cell lines (Jin et al., 2010, Osada et al., 2011). Apart from this, niclosamide demonstrate minimal effect against normal cells such as peripheral blood mononuclear cells and mammary epithelial cells (MCF10A) (Osada et al., 2011).

Recently, Sack et al. demonstrated that the niclosamide inhibit the cancer cell metastasis and migration in S100A4 (a 11kDa, calcium binding protein responsible for metastasis in colon cancer) over expressing cells (Sack et al., 2011, Grum-Sc hwensen et al., 2005). In colon cancer cells (HCT116), cell migration reduces to less than 50 % as compared to control cells on niclosamide treatment as measured by scratch wound healing assays and matrigel covered Boyden chamber. Similarly, S100A4 induced metastasis inhibition was also found in colon cancer xenograft mouse model.

Modes of actions of niclosamide:

NF-κB pathway- NF-κB, a transcriptional factor responsible for the tumorigenesis, angiogenesis and cancer growth. Niclosamide inhibit translocation of p65, TNFα-induce IκBα phosphorylation and expression of NF-κB regulated genes responsible for the antileukemic activity (Jin et al., 2010).

ROS generation- Like many other chemotherapeutic agents, niclosamide was also found to induce ~ 20 fold ROS elevation in AML cells. Thus, suggesting their ROS mediated killing of tumor (Jin et al., 2010).

Wnt/β- catenin pathway- This signalling pathway plays an important role in maintaining tissue homeostasis, embryonic development and tumorigenesis (Kumar et al., 2010). Recently, reported that niclosamide inhibit β-catenin/ TCF transcription activating complex, β-catenin stabilization, upregulated endorsed Frizzled1 internalization, and down-regulated Dishevelled 2 protein expression (Osada et al., 2011).

Notch pathway- This signalling pathway takes part in various cellular processes such as apoptosis, differentiation, proliferation, maintenance and cell fate decision. Wang et al.

demonstrate that niclosamide acts by suppressing the luciferase activity of CBF1dependent reporter gene in K562 leukemia cells (Wang et al., 2009).

Stat 3 pathway- signal transducers and activators of transcription (STATs), a class of transcriptional factors that play key role in cell proliferation, angiogenesis, immune responses and cell survival (Pakala et al., 2013). Ren et al. demonstrated that the niclosamide specifically inhibit activation, transactivation, nuclear translocation and transcriptional activity of Stat 3 as compare to Stat 1 and Stat 5 (Ren et al., 2010).

mTORC1 pathway – mTORC1, a protein complex made up of serine/ threonine kinase mTOR, which play significant role in protein synthesis. Balgi et al. reported that niclosamide inhibit the mTORC1 signaling, protein ubiquitination and increase the autophagosome formation and thus induce autophagy (Balgi et al., 2009).

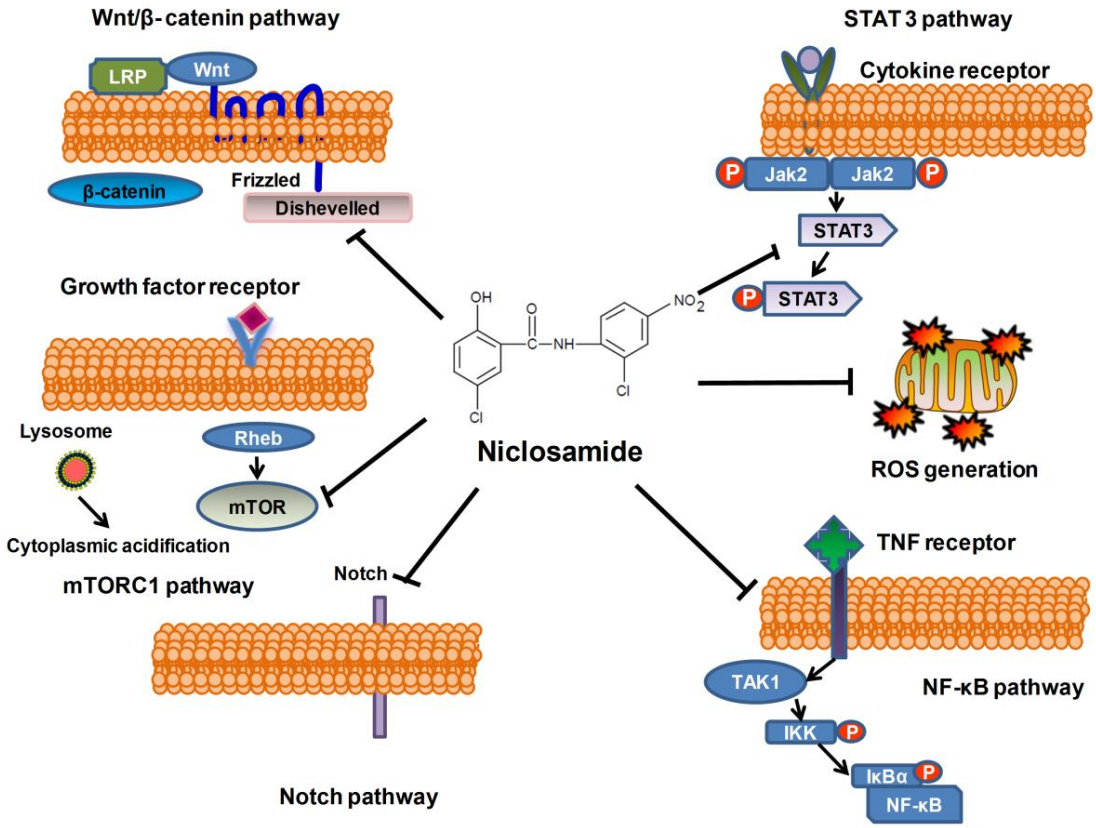

Figure 2.3 Molecular targets of anticancer drug niclosamide.

However, despite its promising anti-cancer properties like many other drugs niclosamide suffer serious drawback due to its extremely low solubility in water (solubility as low as 230 ng/mL in water) (O' Neil et al., 2001) and most organic solvent leading to their reduced bioavailability to cell that limits its clinical efficacy. To address these problems, efforts have been made in

recent past for mounting the aqueous dispersion or solubility of niclosamide (Dai et al., 2008, Yang et al., 2005, Kenawy et al., 2004, Devarakonda et al., 2005). But such systems were not designed keeping in mind their clinical aspects; therefore the biocompatibility and biotoxicity of such systems remained questionable. So far, for *in vitro* or *in vivo* studies, niclosamide was dissolved in organic solvents such as dimethyl sulfoxide (DMSO) or cremophore and later mixed with phosphate buffer saline (PBS) but implication of such organic solvent on biological systems lead to severe complications (Sack et al., 2011, Hanslick et al., 2009).

2.7 Artificial nanozyme

The term "artificial enzyme" was coined by Ronald Breslow for the materials that have enzyme mimetic properties (Breslow et al., 1970). A variety of materials including metal complexes, polymers, porphyrins, cyclodextrin and biological macromolecules such as catalytic antibodies, nucleic acid etc had been extensively studied for their enzyme mimetic properties (Wei et al., 2013, Lu et al., 2009, Pollack et al., 1986). In last few decades, nanomaterials including fullerene derivatives, rare earth nanoparticles, gold nanoparticles and ferromagnetic nanoparticles (Wang et al., 2012, Fan et al., 2012, Vernekar et al., 2014, Wei et al., 2008, Dugan et al., 1997, Ali et al., 2004, Chen et al., 2006) showed exceptional enzyme mimetic activity. Thus, results in the development of nanozymes, nanomaterials based enzyme mimetic system for various applications such as biosensing, cancer therapy, immunoassay, pollutant removal etc. The term "nanozyme" was first coined by Scrimin and co-worker for ribonuclease mimetic gold nanocluster (Manea et al., 2004). The various advantages and limitations associated with these nanozyme are shown in Figure 2.4.

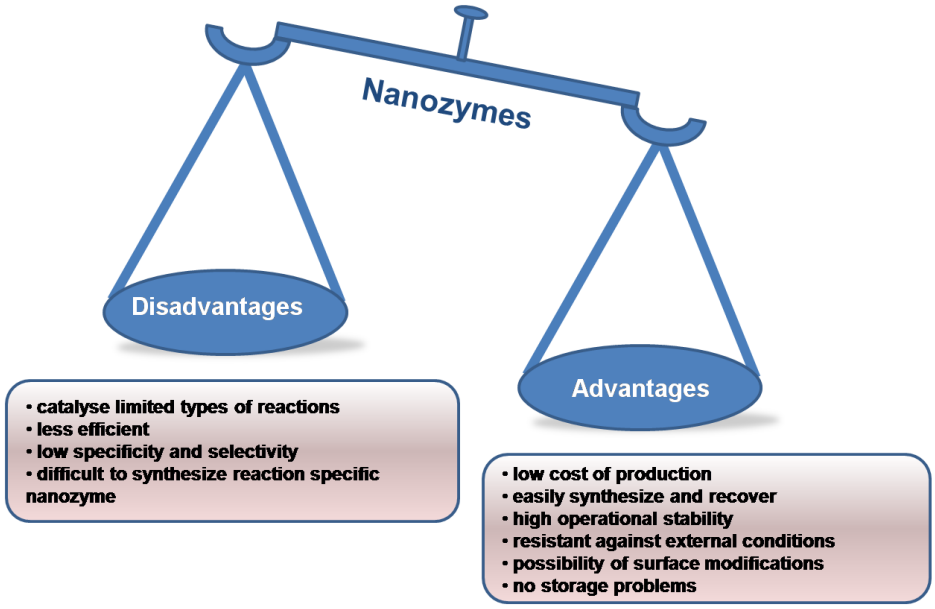

Figure 2.4 Advantages and disadvantages associated with nanozymes.

2.7.1 Nanoceria

In recent years, catalytic nanoparticles emerged as a promising candidate overruling the drawbacks associated with natural enzymes including high cost of production, easy denaturation and storage problems. Among them nanoceria shows tremendous potential to be used as artificial enzymatic system due to its antioxidant enzyme mimetic activity, high biocompatibility, regenerative or autocatalytic property, high stability, low cost of production and no storage problems (Pagliari et al., 2012, Jiao et al., 2012, Das et al., 2007, Wei et al., 2013, Korsvik et al., 2007). The therapeutic potential of nanoceria has been corroborated in a surfeit of human cell lines and animal models to defend the cells against oxidative stress, radiation induced damage, laser induced retinal damage, spinal injury, cardiovascular myopathy and other inflammatory diseases (Das et al., 2007, Wei et al., 2013, Korsvik et al., 2007, Tarnuzzer et al., 2005, Heckert et al., 2008, Niu et al., 2007, Silva, 2006, Colon et al., 2010, Park et al., 2000, McGinnis et al., 1999, Yu et al., 2009, Baran, 2008, Hirst et al., 2009). The antioxidant activity or free radical scavenging capabilities of nanoceria lies in the ability to have oxygen defect and mixed valency i.e. oxidized (+4) and reduced (+3) oxidation state imparting them with SOD (catalyzes the superoxide radical anion dismutation in living cells (Wei et al., 2013, Korsvik et al., 2007, Tarnuzzer et al., 2005)) and catalase (capability to decompose H_2O_2 to O_2 and H_2O (Wei et al., 2013, Heckert et al., 2008)) enzyme mimetic activity (Korsvik et al., 2007, Heckert et al., 2008). Seal and co-workers depicts that higher the Ce^{3+}/Ce^{4+} ratio in nanoceria better will be its SOD like activity, while Self and co-workers found that lower the Ce^{3+}/Ce^{4+} ratio in nanoceria better will be its catalase like activity (Heckert et al., 2008, Pirmohamed et al., 2010, Korsvik et al., 2007) Further, the kinetic measurement reveals that the nanoceria having a size range from 3-5 nm showed efficent SOD mimetic activity, even better than native CuZn SOD (Korsvik et al., 2007). Moreover, Seal and co-workers demonstrated the protective role of vacancy engineered nanoceria for normal cells from radiation induced damage. However, nanoceria does not protect the tumor cells, which might be due to the more loosely packed chromatin in tumor as compared to normal cells which resulted in the exposure of more bases for free radical attack (Tarnuzzer et al., 2005). Recent Pagliari et al., 2012 demonstrate that the nanoceria protect the cardiac progenitor cells (CPCs) from H_2O_2 induced ROS for one week. Apart from them the presence of mixed valency and oxygen defect in nanoceria also impart them with the ability to be utilized in other redox active processes for instance promote stem cell growth, anti-inflammatory effect and neuro-protection.

But still a lot of unresolved challenges are required to be addressed including poor solubility, short retention time and use of harmful chemicals in production, for the complete exploitation of nanoceria in the field of antioxidant therapies. In order to address these problems nanoceria has been coated with variety of materials including dextran, starch, chitosan, polyethylene glycol (PEG) and glucose (Perez et al., 2008, Zhai et al., 2013, Darroudi et al., 2014, Karakoti et al., 2009, Karakoti et al., 2007). However, there still a long way ahead to explore the antioxidant potential of nanoceria in clinical applications.

2.8 Metal based nanoparticles

In the recent years, metal based nanoparticles have shown their tremendous potential for biomedical applications. In particular, gold, silver, silica rare earth metal, and iron oxide based nanoparticles are widely used for cancer therapeutic and bio-imaging applications (Uday Kumar et al., 2013).

2.8.1 Silver nanoparticles

In recent years, silver nanoparticles found tremendous applications in the household and consumer products such as antiseptic spray, food packaging (Edwards-Jones, 2009), water purification (Gangadharan et al., 2010), and in sunscreen cream and other cosmetic items (www.nanotechproject.org) etc. due to its broad spectrum antibacterial activity. The broad spectrum antimicrobial activity of silver ions lies in their ability to obstruct the respiratory enzyme pathways, alter microbial cell wall and DNA, inhibit protein synthesis and elevate ROS as shown in Figure 2.5 (Dubey et al., 2015 b). With the development of FDA approved Acticoat (Ag NPs based wound dressing bandage) similar composites are of tremendous interest among the scientific community (Mazurak et al., 2007). Since then Ag NPs have been extensively studied either alone or in composites form for their antibacterial potential (Biswas et al., 2014, Nair et al., 2011, Sudheesh kumar et al., 2010). In order to investigate the antimicrobial activities of Ag NPs, Gogoi et al., 2006 used green fluorescent protein (GFP) expressing recombinant *Escherichia coli* (rGFP E. coli) bacteria as a model system. Recently, our group developed a porous and stable nanofiber scaffold composed of polymeric blend poly(ethylene oxide) (PEO) and polycaprolactone (PCL) incorporated with silver nanoparticle (Ag NPs) for antibacterial wound dressings applications. The prepared nanofiber scaffold demonstrates a potential antibacterial activity against rGFP expressing antibiotic-resistant *E.coli* (Dubey et al., 2015a). Moreover, Matai et al., 2014 synthesized microwave assisted silver–zinc oxide (Ag–ZnO) nanocomposites which demonstrated broad-spectrum antibacterial

activity against both Gram-negative (rGFP *E.coli*) and Gram-positive bacteria (*Staphylococcus aureus*).

The therapeutic potential of these nanoparticles was also investigated *in vitro* and *in vivo* model system. The cytotoxicity of these nanoparticles depends on their shape, size, surface chemistry, etc., as spherical silver nanoparticles and microparticles are almost non-toxic to human alveolar epithelial cells, while silver wires shows strong cytotoxicity against it (Stoehr et al., 2011).

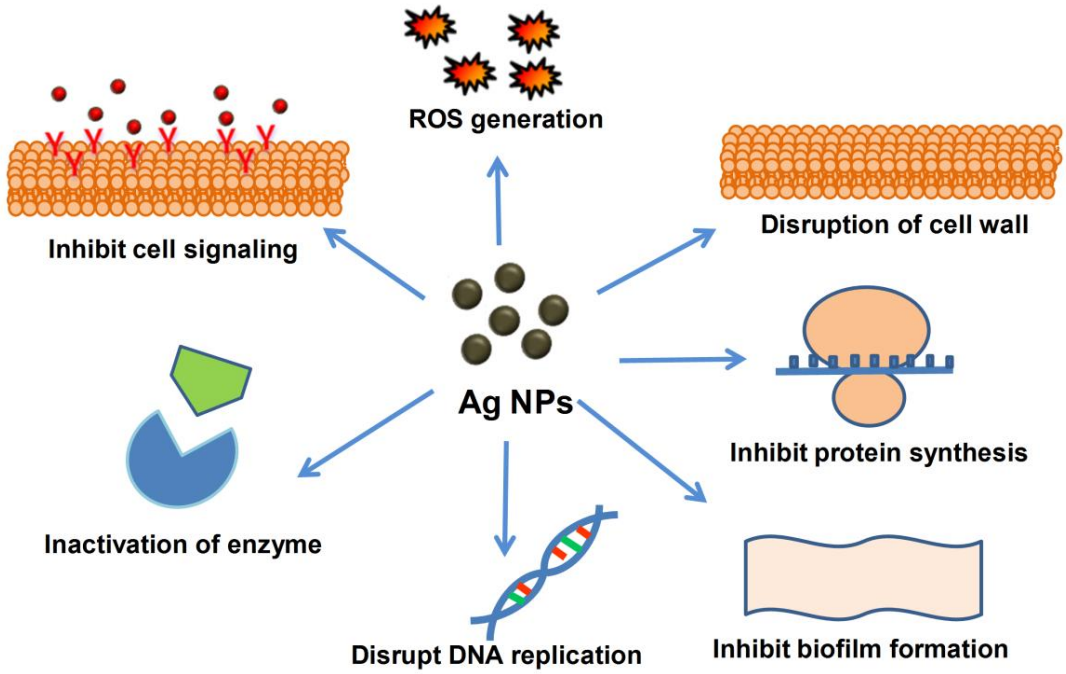

Figure 2.5 Bactericidal action of silver nanoparticles.

Gopinath et al., 2010 studied the effect of silver nanoparticles on cellular gene expression in baby hamster kidney cells (BHK21) and human colon adenocarcinoma cells (HT29). The results depict that like most of other chemotherapeutic drugs, Ag NPs also induced p53-mediated apoptotic pathway, thus suggesting their future role for biomedical and pharmaceutical applications. Moreover, Gopinath et al., 2008 also studied the role of Ag NPs in combination therapy. The Ag NPs in combination with gene therapy demonstrate a synergistic effect. A uracil phosphoribosyl transferase (UPRT) expression system and non UPRT expressing cell was used that depict a synergistic effect on apoptosis on treating the cells with Ag NPs in combination with 5 FU. Later, Matai et al., 2015 developed a poly(amidoamine) (PAMAM) dendrimer based multicomponent delivery system for cancer therapy. A Generation 5 (G5) PAMAM dendrimer stabilized Ag NPs were co-delivered with anticancer drug 5-FU,

results showed their synergistic antiproliferative effect and also induce p53 and caspase signalling gene cascade mediated apoptosis in A549 and MCF-7 cells.

Thus, previous studies by our group corroborates that apart from disturbing the membrane integrity and normal function of the cells, Ag NPs by themselves or in combination with other therapeutic agents successfully induce apoptosis in various human cancer cells. The therapeutic potential of Ag NPs lies in their ability to augment the ROS generation and activate mitochondria dependent apoptosis (Hsin et al., 2008). However, major drawbacks associated with Ag NPs such as genotoxicity and DNA damaging capability hindered their therapeutic applications (Asharani et al., 2008 and 2009). This provokes a need to develop a safe and effective system for efficient delivery of Ag NPs with enhanced therapeutic efficacy at lowest possible Ag NPs concentrations and thereby provide an alternative mode of cancer therapy.

2.9 Tumour targeting

One of the major problems associated with most of the anticancer drugs and other therapeutic molecules is widespread distribution and rapid elimination of drug from the patient's body that lead to implication of higher drug dose, which results in severe side effects (Luo et al., 2012). In order to overcome such complications and to enhance the tumor selectivity, a nanoparticle relies on two strategies namely (Figure 2.6):

Passive targeting: In passive targeting nanoparticles exploits the physical properties of tumor tissues mainly enhanced permeability and retention (EPR) effect and rely on the natural distribution pattern of nanoparticles such as passive diffusion and phagocytosis processes in order to achieve selective accumulation of nanoparticles at the targeted tumor site (Poste et al., 1983). In EPR effect hyperpermeability is created as a result of disorganized angiogenic vasculature with leaky membrane for circulating nanoparticles and macromolecules. Due to which, tumor tissue gets more nutrient as compare to normal tissue resulted in the rapid growth of tumor (Konan et al., 2002). Moreover, large molecular weight drugs (more than 40 kDa) get retained in the interstitium owing to lack of intratumoral lymphatic drainage, thus results in enhanced tumor targeting (10-100 folds) as compared to small molecular weight drug (Duncan et al., 2005). The advantages associated with passive targeting include low cost and ease of manufacturing. However, in case of metastatic carcinoma or early stage tumor where size of the tumor is too small, the passive targeting is found to be inappropriate. Moreover, it is found to be less selective than active targeting.

Active targeting: In certain tumor cells which have special gene expression, the active targeting is found to be more specific. The active targeting is achieved by attaching a biorecognition moiety to the nanoparticles such as aptamers (Farokhzad et al., 2004), small molecule (Weissleder et al., 2005), proteins (Chan, et al., 1998), antibody fragments (Qian et al., 2008), peptides (Cai et al., 2006), antibodies (Bose et al., 2005, 2006 a and b, Jiang et al., 2008) etc. But high cost and tedious conjugation process associated with these targeting moieties, promote the use of nutrients such as folic acid and glucose coated nanoparticles, which are easily taken up by the growing cancer cells in order to support their heightened metabolism.

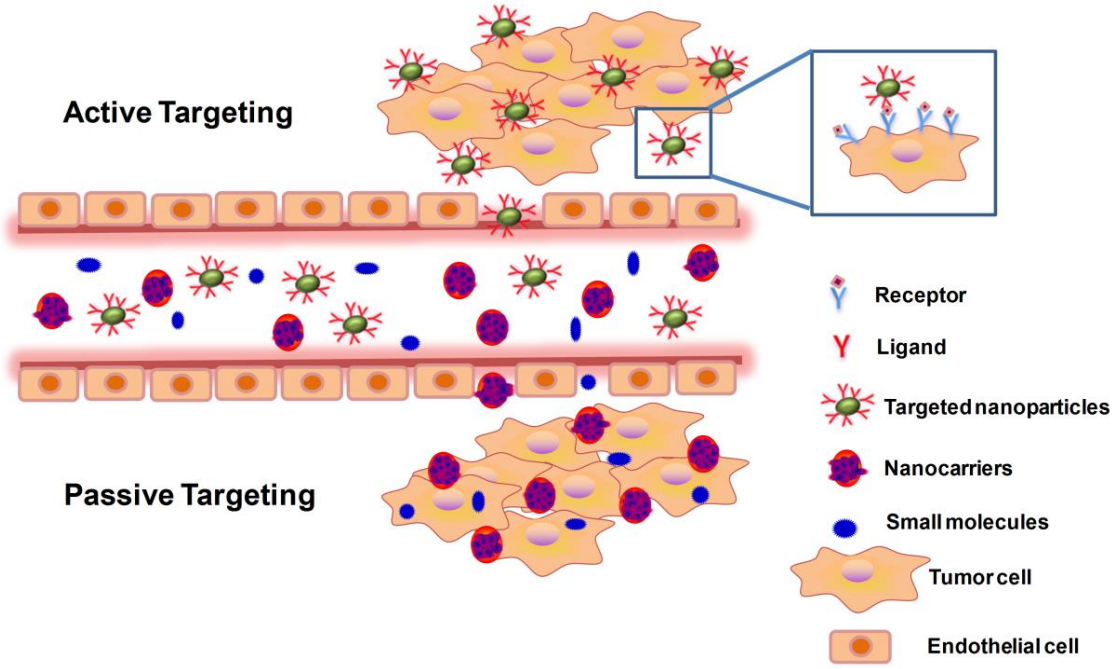

Figure 2.6 Passive and active targeting strategies of nanoparticles for cancer therapy.

2.9.1 Folate receptor mediated targeting

The current conventional therapies have many unresolved challenges including non specific accumulation of the therapeutic molecules which results in reduce therapeutic efficacy, higher toxicity to neighbouring tissues and limits the maximum dose availability (Wang et al., 2011). These drawbacks need to be addressed in order to develop an efficient tumor targeted therapeutic system for cancer therapy. Until now, researchers have exploited the natural endocytosis pathways for the efficient delivery of therapeutic agents into the cells (Gabizon et al., 1999). A vast variety of cancer specific ligands have been explored so far for the enhanced delivery and retention of therapeutic molecules inside the tumor tissue (Lu et al., 2002). Among them folate and their conjugates shows tremendous affinity towards the folate binding protein

i.e. folate receptor became a confirmed target for non-destructive cancer specific delivery of therapeutic molecules (Leamon et al., 1991, Sudimack et al., 2000). Folic acid, a natural ligand for FR is a vital dietary vitamin (vitamin B9) required for the DNA biosynthesis, cell proliferation and metabolism (Lu et al., 2002). The FR is present specifically in abundance on the surface of variety of cancer cells including ovary, breast, kidney, myeloid and brain cells as compared to normal tissues (Lee et al., 1995, Paulos et al., 2004). Moreover, the high binding affinity towards FR, small size (441.39 g/mol), non immunogenic, high stability, ease of attachment, low cost, high availability, high compatibility with organic solvents used in the synthesis process and high tumor specificity make it an ideal candidate for drug delivery (Leamon et al., 2004, Shen et al., 2011). To date a large number of macromolecules including albumin have been successfully conjugated with the carboxylic group of FA without altering its targeting capability and thereby enhancing the drug delivery in FR-positive cancer cells (Lee et al., 2003, Wang et al., 2011, Lee et al., 1994, Zhao et al., 2010, Rollett et al., 2012, Martinez et al., 2014).

The carboxylic group of folic acid is covalently conjugated with the amino group of albumin nanoparticles by using 1-ethyl-3-(3-dimethylaminopropyl) carbodiimide (EDC)/ N-hydroxy succinimide (NHS) coupling technique (Shen et al., 2011). The uptake of fluorescein isothiocyanate (FITC) labeled folate-conjugated BSA nanoparticles by SKOV3 cells (human ovarian cancer cell line) was inhibited in presence of excess free folic acid, suggesting the folate receptor mediated binding and uptake of albumin nanoparticles (Zhang et al., 2004, Leamon, 2008, Parker et al., 2005). Further, Turek et al., 1993 demonstrated that the folic acid conjugated protein bind to the folate binding protein (FBP) present on the cell membrane and were later internalized via endocytosis, with no change in the catalytic activity of protein. Further, sub cellular localization of protein folic acid conjugates was studied by using folic acid-bovine serum albumin-colloidal gold (F-BSA-CG) as a tracer in human nasopharyngeal carcinoma cells (KB cells). During initial 15-60 min, these conjugates stayed in multivesicular bodies (MVBs) and other tubular endosomes after being taken up through caveolae or uncoated pits. After 6 h, some of the conjugates were found free in the cytoplasm and in the secondary lysosomes, while rest of the conjugates remain in the MVBs.

A large number of drugs including paclitaxel (Zhao et al., 2010), mitoxantrone (Zhang et al., 2010), doxorubicin (Shen et al., 2011), epigallocatechin-3-gallate (Zu et al., 2009), cisplatin (Chen et al., 2010), vinblastine sulfate (Zu et al., 2009) and bexarotene (Qi et al., 2014) loaded folate modified albumin nanoparticles has been successfully developed so far. Recently, many

folic acid modified BSA conjugated nanoparticles were developed for cancer imaging and therapy. Lin et al., 2013 demonstrated a biomimetic synthesis of BSA-conjugated gold nanocomplexes, which on conjugation with folic acid showed specific targeting dual-modality dark-field and fluorescence imaging on MGC803 gastric cancer cells. Similarly, Meng et al., 2011 developed a folic acid conjugated BSA-coated CdTe/ ZnS quantum dots (BSA–QDs) for cancer diagnosis. About three times higher cellular uptake than BSA–QDs was observed in FR-positive KB cells, which was suppressed on pre-treating the cells with excess folic acid, confirming the FA mediated uptake enhancement.

Recently, tumor targeted multifunctional supermagnetic Fe_3O_4 nanocrystals loaded folic acid conjugated dextran BSA nanoparticles (Fe_3O_4/BSA–DEX–FA) was prepared by thermal gelation method for tumor diagnosis and therapy. Later, doxorubicin was loaded in Fe_3O_4/BSA–DEX–FA by diffusion process, resulted in the formation of highly biocompatible, stable nanoparticles with enhanced tumor inhibition efficiency in H22 tumor-bearing mice and enhanced tumor MRI in KB tumor-bearing mice (Hao et al., 2014). Similarly, multifunctional nanoparticles were prepared by protecting the surface of the doxorubicin loading a highly fluorescent carbon dots (C-dots) with BSA, followed by the FA conjugation for tumor targeted imaging and therapy in HeLa cells (Mewada et al., 2014).

Moreover, a hybrid nanocluster with magnetofluorescence property is prepared by simultaneous clustering of $MnFe_2O_4$ magnetic nanoparticles (MNPs) and $AgInS_2$–ZnS quantum dots in the presence of BSA under ultrasonication imparting them with yellow fluorescence and enhanced T2 contrasting properties in HeLa cells. The prepared hybrid nanocluster is then conjugated with folic acid and doxorubicin for tumor targeted drug delivery (Fahmi et al., 2014). Similarly, Yang et al., 2014 developed folic acid-conjugated, doxorubicin-loaded, magnetic iron oxide bovine serum albumin nanospheres (FA-DOX-BSA MNPs) with enhanced therapeutic efficacy as a result of targeted combination therapy by the anticancer drug and hyperthermia by heating of magnetic nanospheres nasopharyngeal carcinoma.

2. 10 Reactive oxygen species

ROS are ions, molecules or radicals having unpaired electron in their outermost shell, which imparts high reactivity. ROS is categorized into two groups:

(1) Free oxygen radicals including hydroxyl radical ($^{\bullet}OH$), peroxyl radicals ($ROO^{\bullet}$), nitric oxide ($NO^{\bullet}$), thiyl radicals ($RS^{\bullet}$), superoxide ($O_2^{\bullet-}$), alkoxyl radicals ($RO^{\bullet}$), thiyl peroxyl radicals ($RSOO^{\bullet}$), organic radicals ($R^{\bullet}$), sulfonyl radicals ($ROS^{\bullet}$), and disulfides (RSSR).

(2) Non-radicals including ozone/trioxygen (O_3), hydrogen peroxide (H_2O_2), nitrosoperoxy carbonate anion ($O=NOOCO2^{-}$), nitronium (NO_2^{+}), nitrocarbonate anion ($O_2NOCO_2^{-}$), dinitrogen dioxide (N_2O_2), singlet oxygen ($^1O_2$), peroxynitrite (ONO^{-}), hypochloride (HOCl), organic hydroperoxides (ROOH), and highly reactive carbohydrate or lipid derived carbonyl compounds.

Hydrogen peroxide, hydroxyl radicals and superoxide are most investigated ROS for their role in cancer. High levels of ROS production in cancer cells is attributed to the mitochondrial dysfunction, increased cellular receptor signaling, increased metabolic activity, oncogene activity, peroxisome activity, increased activity of lipoxigenases, oxidases, thymidine phosphorylase and cyclooxygenases (Storz, 2005, Szatrowski et al., 1991, Babio, 1999). In mitochondria, ROS generated as a byproduct due to incomplete reduction of oxygen in aerobic metabolism, which could be involved in cell signaling including induction of apoptosis and protection against pathogen. However, the excess level of ROS in the body leads to cell damage that endorse a variety of disorders and diseases such as Alzheimer, Parkinson, cardiovascular dysfunctions, inflammatory conditions, aging and cancer (Kumar et al., 2008, Emerit et al., 2004, Misra et al., 2009, Finkel et al., 2000). The c-Jun N-terminal kinases (JNKs) activated in response to ROS (H_2O_2 and NO release from mitochondria), catalyzed the phosphorylation and downregulation of B-cell lymphoma 2 (Bcl-2) and basal cell lymphoma-extra large (Bcl-XL), altered Bax/Bcl-2 complex composition by increasing the expression of Bcl-2-associated X protein (Bax) and subsequent induction of apoptosis (Cadenas, 2004, Storz, 2007, Lee et al., 2008, Qanungo et al., 2005, Shim et al., 2007, Zhang et al., 2008). Moreover, there are many other signaling proteins including p53, forkhead transcription factors (i.e. FOXO3a) and p66Shc that induce ROS mediated apoptosis (You et al., 2006, Brunet et al., 1999).

In normal condition, non-enzymatic molecules (i.e. vitamins A, E and C, flavenoids and glutathione) or antioxidant enzymes mainly SOD, catalase, and glutathione peroxidase generated by the cells in response to ROS and defend the body from its detrimental effects as shown in Figure 2.7 (Harris, 1992). SODs are metalloenzymes ubiquitously found in prokaryotes and eukaryotes catalyzed the superoxide dismutation into hydrogen peroxide and

oxygen by utilizing the metal ions e.g. manganese (Mn^{2+}), copper (Cu^{2+}), iron (Fe^{2+}) or zinc (Zn^{2+}) as cofactors (Copin et al., 2000). Catalase found mostly in peroxisomes and cytosol of most of the eukaryotes assist the decomposition of H_2O_2 into H_2O and O_2 (Bendayan et al., 1982, Hashimoto et al., 1990, Litwin et al., 1987). While glutathione system consist of glutathione peroxidases (GPX), glutathione (GSH), glutathione S-transferases (GST) and glutathione reductase responsible for the reduction of cytoplasmic proteins disulfide bonds in cysteines. Moreover, the GPX catalyze the organic hydroperoxides and hydrogen peroxide degradation (Brigelius-Flohe, 1999, Ursini et al., 1995). While GST act as detoxifying enzyme and catalyses conjugation of variety of endogenous and exogenous compounds with GSH (Townsend et al., 2003, Sharma et al., 2004, Hayes et al., 2005). However, in case of sudden oxidative damage such enzymes are found to be insufficient to protect the cells. This provokes a need to develop an artificial antioxidant enzyme mimetic system that has high ROS scavenging potential, biocompatible, remain stable inside the cells and provide high therapeutic index.

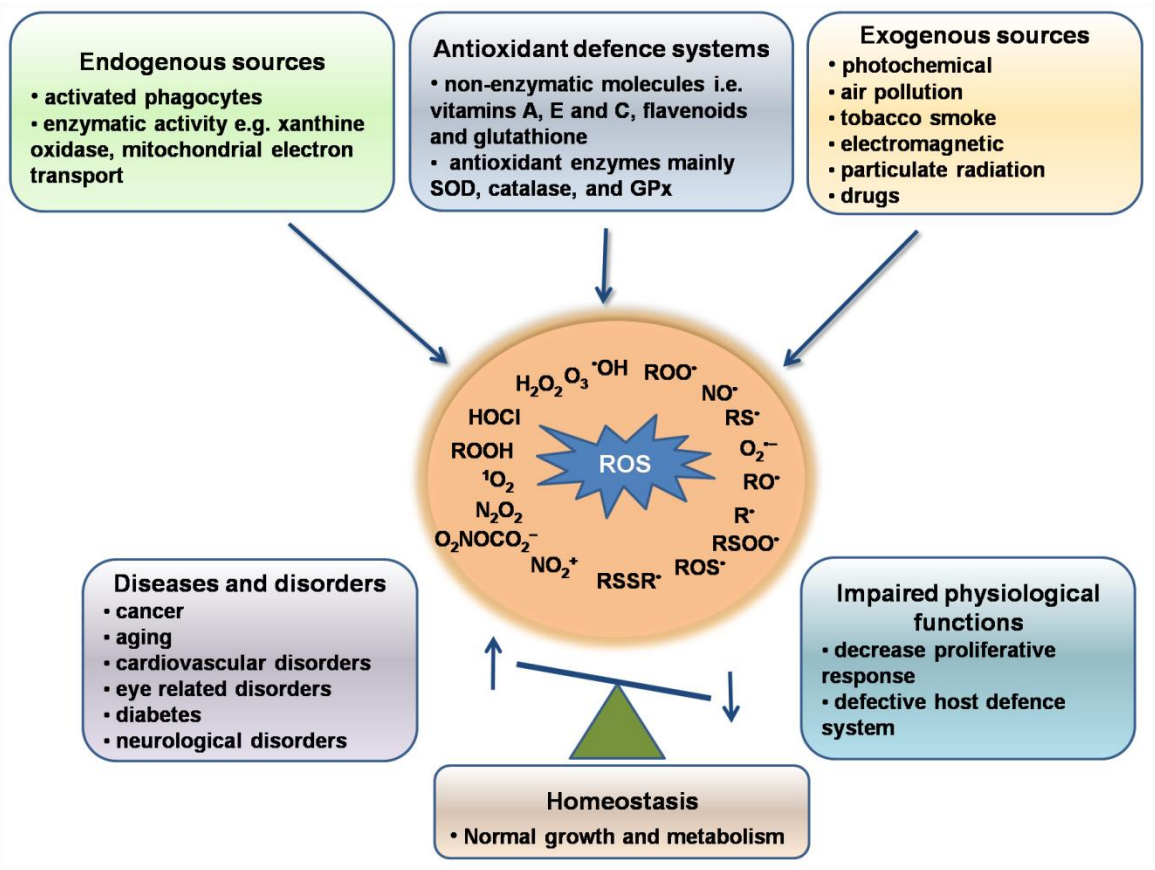

Figure 2.7 Sources, cellular responses, diseases and disorders related to ROS.

2.11 Apoptosis

The term apoptosis was first introduced in 1972 by Kerr, Wyllie and Currie. In 90's with the investigation to understand the processes of cell death that took place during the development of *Caenorhabditis elegans,* apoptosis is distinguished as genetically determined removal of cell by "programmed cell death" (Horvitz, 1999). It is a homeostatic phenomenon that occurs mainly during development and aging in order to maintain the required cell populations in tissue (Figure 2.8). Moreover, apoptosis is also induced when cells undergo damage by the harmful drugs or diseases and at times also during the immune reactions (Norbury et al., 2001). A vast variety of pathological and physiological conditions and stimuli's are responsible for the induction of apoptosis. In case of anticancer drugs and irradiation cells undergo DNA damage, which results in the trigger of p53-dependent apoptotic pathway. Apart from this there is another process which occurs simultaneously, sequentially or independently with apoptosis, which is termed as "necrosis" (Hirsch et al., 1997; Zeiss, 2003). It's the type and degree of stimuli which decide whether cells will undergo apoptosis or necrosis. In most cases, low concentration of chemotherapeutic drug and other stimuli such as radiation, heat, hypoxia induce apoptosis, but the higher doses of these stimuli leads to necrosis.

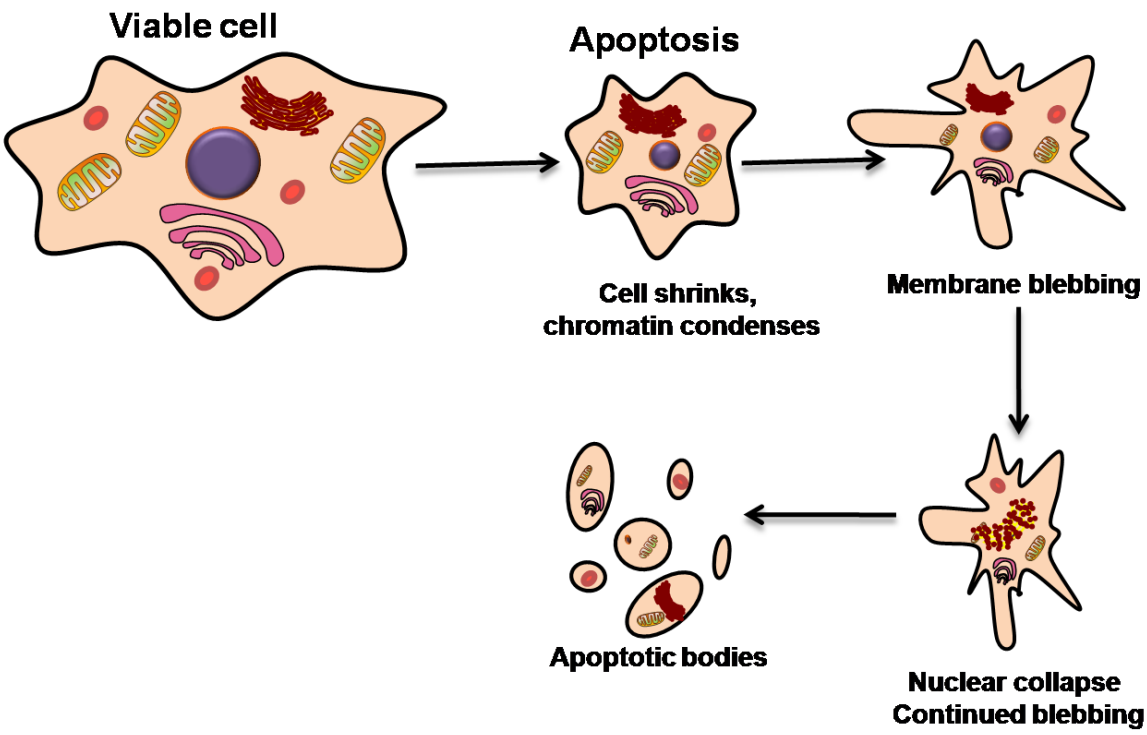

Figure 2.8 Features of the apoptotic cell death.

Recently, Ye et al., 2014 demonstrated the therapeutic potential of niclosamide *in vitro* and *in vivo* on breast cancer. A concentration dependent growth inhibition and induction of apoptosis was observed in mouse breast cancer cells (4T1cells). The induction of apoptosis was correlated with the down regulation of Bcl-2, Survivin, Mcl-1 and activation of cleaved caspases-3. In addition, niclosamide inhibit the migration and invasion of breast cancer cells along with reduction of phosphorylated SrcTyr416, STAT3Tyr705 and FAKTyr925 was also examined. Furthermore, Park et al., 2011 reveal that niclosamide treatment disrupts mitochondrial potential, decrease ATP level and promote mitochondrial fragmentation. Thus these studies reveal that niclosamide induce apoptotic cell death.

Recently, Satapathy et al., 2013 demonstrated the anticancer potential of silver based nanoparticles in human colon cancer cells. The results depicts the apoptotic cell death of HCT116 cells characterized by cleaved caspases 3, 8 and 9, p53, p21 and poly(ADP-ribose) polymerase, increase in 4´,6-diamidino-2-phenylindole-stained apoptotic nuclei, Bax/Bcl-XL ratio, while decrease in level of NF-κB and AKT. Moreover, a decrease in G1 phase of cell population was observed. Similarly, Kim et al., 2014b further confirm the p53 mediated apoptosis in human bronchial cell on Ag NPs treatment by treating the cells with p53-specific short interfering RNA (siRNA) or p53 inhibitor (pifithrin-α), thus preventing the Ag NPs induce DNA fragmentation. Moreover, the involvement of various apoptotic signaling such as Caspase-3, Bax and Bcl-2 was also confirmed at mRNA and protein level.

2. 12 Zebrafish

In past decades, rodents has been extensively exploited for toxicological studies, but due to high cost, time consuming experiments and recent restrictions by the legal authorities their use in the field of nanomedicine is restricted. Fishes, a non mammalian vertebrate have been extensively used in risk assessment and regulation (Schirmer, 2006). Among various fish species utilized for the standard testing of environmental and chemical samples, zebrafish emerged as a potential model organism due to its special characteristics (Figure 2.9). It is a small (approximately, 3-5 cm) fresh water fish found in the rivers of northern India, Nepal, Pakistan, and Bhutan. The various advantages associated with zebrafish includes short generation time i.e. 3-5 months which enables transgenerational studies, easy to manage in laboratory space at low cost due to its small size, similar mode of embryogenesis and development like higher vertebrates except the development occur outside the female body in transparent egg, rapid embryonic development i.e. development of all major organs within 24 h and fish hatched within 3 days, while at 5dpf complete yolk is consumed and external feeding

is started (Wixon, 2000, Rubinstein, 2003). Moreover, within 3-4 months, the zebrafish get sexually matured and start generating offspring. A single female lays around 200 eggs per week, thus several thousand embryos can be easily produced daily under laboratory conditions. (Stern et al., 2003). The zebrafish embryos remain transparent during initial days of life, while pigmentation starts after 1-3 dpf, thus enable the analysis of morphological changes occur within the early-stage development. Moreover, transparency can be further maintained by preventing the pigmentation by treatment with bleach or 0.003 % phenylthiourea after fixation. Recently, complete genome of the zebrafish is sequenced (Sanger Institute, http://www.sanger.ac.uk/Projects/D_retio) and found to be more complex than human genome as it has two more pairs of chromosomes (Hill et al., 2005). Moreover, the small size of the embryos and juveniles make them a better candidate for pharmacological and toxicological studies by allowing high-throughput screenings as small amount of testing compounds are required, thus sufficient replicate data can be produce along with significantly reduce volume of potentially hazardous waste (Hill et al., 2005; Spitsbergen et al., 2003). Greater ease of genetic modification and high survival rate of mutant zebrafish embryos results in production of hundreds of zebrafish phenotypic mutants for various studies including human diseases (Stern et al., 2003).

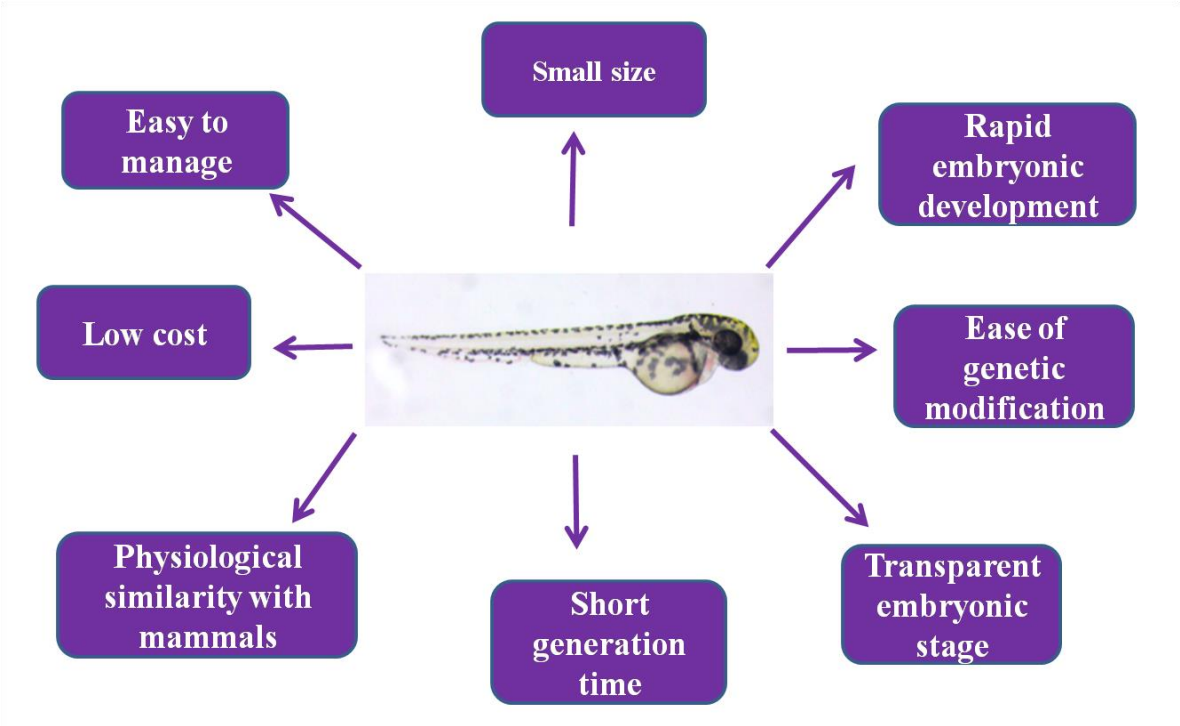

Figure 2.9 Advantages associated with zebrafish.

CHAPTER 3

MATERIALS AND METHODS

In this Chapter, the strategies involved during the preparation of albumin based nanoparticles for anticancer and antioxidant applications have been discussed. The various techniques and methodologies followed in the present study are also elaborated in this chapter.

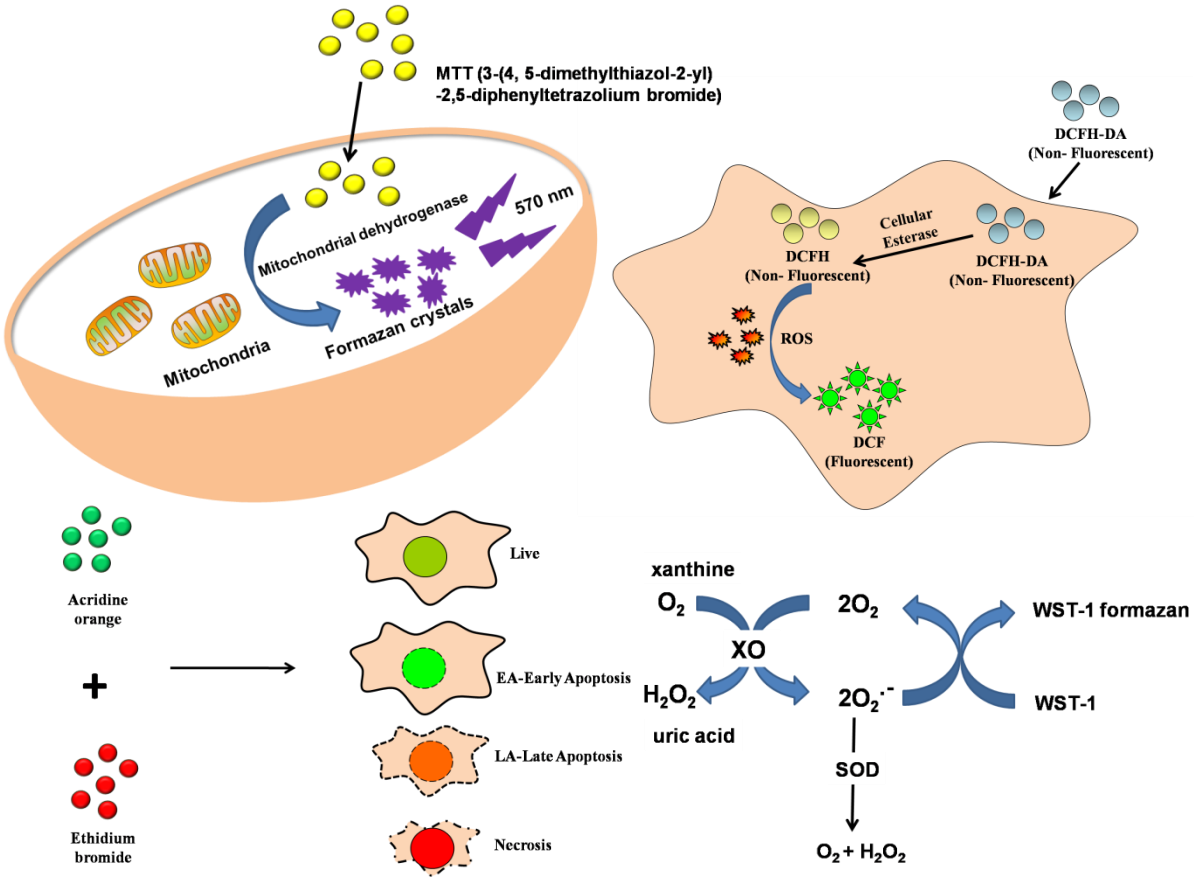

CHAPTER 3

MATERIALS AND METHODS

3.1. Materials and reagents

BSA and DMSO were purchased from HIMEDIA. Silver nitrate ($AgNO_3$), acetic acid, methyl violet (MV), iron (II) sulfate heptahydrate ($FeSO_4.7H_2O$), hydrogen peroxide (30%), ammonium hydroxide and sodium borohydride were procured from Merck (Germany). The stock solutions of MV, $FeSO_4$ and Tris-HCl buffer (pH 4.7) were prepared in ultra pure water at concentrations of $2x10^{-4}$ M, $15x10^{-3}$ M and 0.1 M, respectively. Anticancer drug niclosamide, propidium iodide (PI), EDC, NHS and 2',7'- dichlorfluorescein diacetate (DCFH-DA), $(NH_4)_2\,Ce(NO_3)_6$, CH_3COONa, SOD assay kit (Kit #19160-1KTF) and crosslinking agent glutaraldehyde (50 wt% in H_2O) were procured from Sigma–Aldrich and stored at appropriate storage conditions until used. MTT, ethanol and isopropanol was procured from Amresco, USA. The cell staining dyes rhodamine B and Hoechst 33342 were purchased from life technologies. All reagents were of analytical grade and used without further purification. All other chemicals used were molecular biology grade.

3.2 Cell culture

A549 cells, L-132 cells and MCF-7 cells were obtained from the cell repository of National Centre for Cell Science, Pune, India. They were maintained in Dulbecco's modified Eagle's medium (DMEM) with 10% calf serum and 1% Penicillin-streptomycin in the humidified incubator with 5% CO_2 at 37 °C.

3.3. Preparation of nanoparticles

3.3. 1. Preparation of niclosamide encapsulated albumin nanoparticles

BSA-Nic NPs were synthesized using a desolvation method. Briefly, 5 mL of 5 mg mL^{-1} BSA solution in water was transferred to a beaker under a continuous stirring on a magnetic stirrer at room temperature. Niclosamide (Stock concentration- 8 mg mL^{-1} in ethanol) were added drop wise at a constant rate of 0.8 ml/min into the above solution. The mixture was stirred for one hour followed by drop wise addition of pure ethanol till turbidity just appeared. The suspension was stirred for additional 10 min before glutaraldehyde was added drop-wise to the suspension.

The suspension was stirred for overnight. Afterwards, the suspension was centrifuged at 18000 x g for 10 min to remove the supernatant. The sediment was washed with ethanol to remove adsorbed glutaraldehyde and free drug from nanoparticles surface. The washed samples were resuspended in 5 mL of ultrapure water. For rhodamine loaded BSA NPs 40 µL of 10% rhodamine solution was mixed well with constant stirring and rest followed the above mentioned procedure.

3.3.2. Preparation of folate conjugated albumin stabilized silver nanoparticles

Albumin stabilized silver nanoparticles was synthesized using a $NaBH_4$ reduction method reported earlier (Gebregeorgis et al., 2013, Zhang et al., 2013). Briefly, BSA (25 mg mL^{-1}) was dissolved in 10 mL of deionized water and then $AgNO_3$ (50 mM) was added into the above solution at 25 ^oC under vigorous stirring. The pH of the solution was maintained at pH =8 with 0.1 M NaOH. After 5 min, silver ions were reduced by drop-wise addition of $NaBH_4$ (10 mM), until the colour of solution changes from colourless to brown colour. The solution was allowed to stir overnight in dark. The BSA-Ag NPs were conjugated with FA according to the standard procedure reported earlier (Qi et al., 2014, Meng et al., 2011). An active ester intermediate (NHS–folate) was prepared by the reaction of EDC/ NHS with the carboxyl groups of FA, which in turn covalently conjugates with the amine groups of BSA. Briefly, FA (27 mg) was dissolved in 2 mL DMSO, followed by addition of EDC (58.6 mg) and NHS (35.2 mg) and allowed to stir in dark for 30 min. Consequently, the pre-activated FA mixture was slowly added to the BSA-Ag NPs solution under alkaline condition (pH adjusted to 10 by 1M NaOH). The solution was allowed to stir overnight in dark at room temperature. The solution was then continuously dialyzed for 3 days and further purified by using Sephadex G-25 column to remove excess FA and other reactants. The final solution obtained was filtered and stored in amber color bottle at 4 ^oC, until further used.

3.3.3. Preparation of nanoceria

The nanoceria was synthesised *via* hydrothermal method as reported earlier (Liu et al., 2012). Briefly, $(NH_4)_2$ $Ce(NO_3)_6$ and CH_3COONa were dissolved in deionized water followed by subsequent addition of 10 mL of acetic acid to the solution and stirred for 1 h. After mixing, the solution was transferred to a Teflon-lined autoclave for hydrothermal treatment at 200 °C for 12 h. the precipitated particles were separated by centrifugation and thoroughly washed 4–6 times using deionized water and ethanol. Finally nanoparticles were dried in the hot air oven at 50 ^oC and re-suspended in water for further use.

3.3.4. Preparation of nanoceria encapsulated albumin nanoparticles

The nanoceria encapsulated albumin nanoparticles were prepared by desolvation method. In this process ceria nanoparticles were dispersed in water via sonication and then added dropwise into the 5 mL of 5 mg mL^{-1} BSA solution in water. After one hour of mixing, ethanol was added dropwise into the solution till the turbidity just appeared. The suspension was stirred for additional 10 min before glutaraldehyde was added drop-wise to the suspension. After overnight stirring, the nanoparticles were separated by centrifugation and washed thoroughly with ethanol to remove adsorbed glutaraldehyde and free nanoceria from nanoparticles surface. It was noted that some amount of free CNPs remain attached on the surface of BCNPs even after thorough washing due to the strong electrostatic interaction between the nanoceria and albumin nanoparticles as reported earlier (Patil et al., 2007), and it was not possible to complete eradicate these adsorbed CNPs. The prepared nanoparticles were lyophilized and redispersed in deionized water for further studies. The control albumin nanoparticles (BNPs) were also prepared by the above procedure without nanoceria addition. The amount of ceria nanoparticles entrapped inside the albumin nanoparticles were determined by using ICP-MS, by digesting a known amount of nanoceria encapsulated nanoparticles with concentrated nitric acid and then diluted it with deionized water. Later, the concentration was analyzed by using ICP-MS. Moreover, it should be taken into account that the concentration of nanoceria obtained by ICP-MS contained both entrapped and surface adsorbed CNPs, as it was not possible to calculate the exact amount of adsorbed CNPs. So, the entrapment efficiency obtained here is combination of both entrapped and adsorbed CNPs.

3.3.5. Preparation of albumin coated nanoceria

Albumin coated nanoceria was synthesized by alkaline precipitation method. 0.2 g bovine serum albumin was directly dissolved in 20 mL deionized water. When protein had dissolved completely, 5 mL of 1 M $(NH_4)_2$ Ce $(NO_3)_6$ was added slowly to the albumin solution with continuous stirring. The resulting solution was stirred for 30 min; subsequently, a stoichiometric amount of 1 N ammonium hydroxide was added in a dropwise manner as a precipitant and stirred for 24 h at room temperature. The yellow- colored final precipitated particles were centrifuged and thoroughly washed several times using deionized water and centrifuged to remove any adsorbed nitrate ions. Finally, the prepared nanoparticles were lyophilized and redispersed in deionized water for further studies.

3.4. Characterizations of nanoparticles

UV-visible spectroscopic measurement was done on Lasany double beam L1 2800 UV-visible spectrometer. FTIR spectra were recorded on Thermo Nicolet FTIR spectrometer in the range 4000–400 cm^{-1} using KBr pellets. Fluorescence study conducted inside a fluorescence spectrophotometer (Hitachi F- 4600, Japan) equipped with Xenon arc lamp at an excitation wavelength of 280 nm. The excitation slit width and emission slit width being 2.5 nm and 5 nm respectively. The average hydrodynamic size and surface charge for the prepared nanoparticles were determined by dynamic light scattering (DLS, Malvern). TEM (TECNAI G^2 20 S-TWIN) operating at 200 keV and FE-SEM (Carl Zeiss ULTRA PLUS) equipped with energy dispersive X-ray detector operating at an accelerating voltage of 15–20 keV were used to determine the particle size, morphology and compositional analysis of the nanoparticles. The size distribution histogram of prepared nanoparticles were analysed using ImageJ (http://rsb.info.nih.gov/ij/download.html). Morphology and average grain size of the particles were confirmed using AFM (NTEGRA PNL) operating in semi-contact mode. The images were further processed using NOVA software. XRD analysis was done by using Bruker AXS D8 advance powder X-ray diffractometer (Cu-Kα radiation, λ = 1.5406 A˚) in the range of 10–90º at a scan speed of 0.5º/min. Thermal studies were done by heating 10 mg of respective samples from 30 ºC to 1000 ºC at a constant rate of 10 ºC/ min in EXSTAR TG/DTA 6300 under controlled nitrogen atmosphere. The concentrations of nanoparticles were analyzed by ICP-MS (Perkin-Elmer ELAN DRC-e).

3.5. Entrapment efficiency (EE) of drug

The obtained nanoparticles were frozen and lyophilized at −80˚C and 0.085-mbar pressure by a freeze dryer to obtain a lyophilized nanoparticles powder for further studies. The weighed product of nanoparticles was then ultrasonicated in ethanol for 30 minutes. The released drug was centrifuged and the supernatant was collected. The supernatant solution was analyzed by UV-visible spectrophotometer and the entrapped drug was calculated by using calibration curve of niclosamide in ethanol. The EE was determined according to the formula given below.

$$EE = \frac{\text{Total amount of drug- Amount of drug in supernatant}}{\text{Total amount of drug}} \times 100\%$$

3.6. *In vitro* release studies

3.6.1. *In vitro* drug release studies of niclosamide from BSA-Nic NPs

The *in vitro* drug release studies were carried out by placing a 5 mL of BSA-Nic NPs in a dialysis tube. The dialysis tube was then placed in a Schott bottle that was filled with 15 mL

PBS (pH 7.4) solution and continuously shaken at 37 ^{o}C, 120 rpm. At the predetermined time interval, the PBS solution in the Schott bottle was removed and replaced with fresh PBS solution. The niclosamide concentration in the used PBS solution was then determined using an UV-visible spectrophotometer. Finally, the cumulative percentage of drug released at a specific time interval was calculated from the total amount of drug entrapped in BSA-Nic NPs. The drug release percent can be determined by the following equation:

Drug release [%] = c(t) /c(0) × 100

Where, c(0) and c(t) represent the amount of drug entrapped and amount of drug released at a time t, respectively. All studies were done in triplicate.

3.6.2. *In vitro* CNPs release studies

In a characteristic release experiment, 5.0 mg of BCNPs were redispersed in 5 mL of 10 mM PBS (pH = 7.4) and incubated at 37 ^{o}C with constant shaking at 150 rpm. After predefined interval the supernatant was withdrawn and replaced immediately with equivalent amount of fresh buffer in order to maintain the sink condition. The supernatant was then digested with nitric acid solution and the concentration was measured by ICP-MS.

3.7. *In vitro* stability of nanoparticles

The stability of prepared NPs in aqueous and saline solution was evaluated by detecting their mean diameter at 25 °C by DLS. Briefly, nanoparticles were reconstituted in pure water and 0.9% NaCl or PBS (pH 7.4) solutions at 25 °C. In the following 0, 12, 24, 48, 72 and 96 h, mean particle diameters were investigated by DLS.

3.8. Antioxidant and SOD assay

The antioxidant property of the as-prepared ANC was determined photometrically as reported earlier. (Zhai et al., 2013, Xue et al., 2011), Solutions used for photometric determination contained 1.2 x 10^{-5} M MV, 0.1 M Tris-HCl buffer (pH 4.7), 0.45 mM $FeSO_4$, 50 µL ANC and 0.1 M H_2O_2 (denoted as MV/$FeSO_4$/ ANC/H_2O_2), and all reagents were added as in above mentioned order. The absorbances of all solutions were obtained by using UV-Visible spectrophotometer after incubating the samples for 5 min at room temperature.

The SOD activity of ANC and released CNPs collected at different time intervals were assessed by using commercial SOD assay kit (Sigma Aldrich, USA). The superoxide radicals reduce 2-

(4-iodophenyl)-3-(4-nitrophenyl)-5-(2,4-disulfophenyl)-2H-tetrazolium monosodium salt into a water soluble formazan dye, which is inhibited by SOD. All the experiments were performed according to the instructions provided by the manufacture. Briefly, a 20 µL sample solution was added to the 200 µL of WST-1 working solution followed by the addition of 20 µL xanthine oxidase in a 96 well plate. The enzyme (xanthine oxidase) was used to produce superoxide radicals. A decrease in the color formation correlated with the inhibition activity was measured by using a Cytation 3 cell imaging multi mode plate reader (Biotek) at 450 nm. All experiments were done at room temperature.

3.9. Cell viability assay

The cell viability assay of prepared nanoparticles was evaluated by MTT assay. It is a colorimetric test based on the selective ability of viable cells to reduce the tetrazolium component of MTT into purple colored insoluble formazan crystals. Briefly, cells were seeded on a 96 well plate (Corning, Costar, NY) with a density of 10,000 cells/cm^2. Different concentrations of nanoparticles were prepared by dilution with the media. Once the cells were attached, they were treated with different concentrations of nanoparticles and incubated at 37 ºC in incubator with 5% CO_2. After 24 h incubation, the spent media was removed and cells were given a brief PBS wash. Fresh media (DMEM) (~ 90 µL) containing 10 µL of MTT (stock concentration-5 mg/mL in PBS) was added to each well. The cells were incubated at 5% CO_2 incubator for 3-4 h to form formazan crystals by mitochondrial dehydrogenases enzyme. The supernatant spent media was removed and formed crystals were solubilized in DMSO and incubated at room temperature over gyratory shaker for 15-30 minutes until the all formazon crystals get solubilized. The absorbance of the finally dissolved product was measured at 570 nm and 690 nm using a Cytation 3 cell imaging multi mode plate reader (Biotek). Triplicate samples were analyzed for each experiment. For drug alone study DMSO was used as solvent for niclosamide and equivalent amount of DMSO alone was taken as reference.

3.10. Cell morphological studies

3.10.1. Acridine orange/ethidium bromide dual staining

In order to differentiate apoptotic nuclei from necrotic nuclei, the BSA-Nic NPs and FA-BSA-Ag NPs treated A549 and MCF-7 cells were stained with AO/EB dual dye. Briefly, 2 x 10^5cells per well were seeded in a 6 well plate and allow to adhere. After overnight attachment cells were treated with desired concentrations of NPs for 24 h. The culture media were then removed and the cells were washed twice with PBS. Fresh medium containing 10 µL of AO/EB mix (10 mg mL^{-1} AO and 10 mg mL^{-1} EB stock solution in PBS) were added in each well and the cells

were incubated at 37 °C for 5-10 minutes and then given a PBS wash to remove the excess dyes (to avoid background fluorescence of free dye) before visualizing under a EVOS cell imaging system (Life technologies, USA).

3.10.2. Rhodamine B and Hoechst 33342 staining

The events of apoptosis such as nuclear chromatin compaction and cytoskeleton alteration were examined *via* Hoechst 33342 and rhodamine B fluorescent dual dyes combinations. Briefly, 2×10^5 cells per well were seeded in a 6 well plate and after attachment cells were treated with FA-BSA-Ag NPs for different time periods. After treatment spent media were removed and cells were given a brief PBS wash, followed by incubation with 2 μL Hoechst dye (stock concentration-10 mg mL^{-1}) and 5 μL Rho B (stock concentration- 1 mg mL^{-1}) at 37 °C for 10–15 min. Thereafter, overlay images were obtained under red and DAPI filters.

3.10.3. FE-SEM analysis

For FE-SEM analysis, A549 and MCF-7 cells were seeded on a sterile glass cover slip and incubate for overnight attachment. The cells were then treated with desired concentrations of BSA-Nic NPs and FA-BSA-Ag NPs for 24 h and then fixed by using 2% glutaraldehyde for 10 min followed by ethanol gradient fixation. The fixed cells were then air dried and sputtered coated with gold before examined under FE-SEM.

3.11. Cellular uptake studies

3.11.1. ICP-MS analysis

For quantitative determination of amount of nanoparticles internalized by the cells, briefly 2×10^{-5} cells were seeded in a 6 well plate and left overnight for attachment. Thereafter cells were co-incubated with different concentration of FA-BSA-Ag NPs and ANC for 3 h and 24 h respectively, while 100 μg/mL BCNPs were incubated for different time intervals. In order to remove all extra cellular nanoparticles, the cells were given extensive PBS wash and then harvested and counted. The cells were finally acid digested by using concentrated nitric acid (16 M) for 24 h. The digested sample was then diluted with deionized water and nanoparticles concentration was determined by ICP-MS.

3.11.2. FE-SEM analysis

For FE-SEM analysis cells were seeded over glass cover slips in 3.5 cm cell culture dishes. When cells get properly attached, they were co-incubated with BCNPs and ANC for 24 h. After incubation, media was removed and the cells were given thorough PBS wash. Thereafter, cells

were fixed with 2% glutaraldehyde solution followed by dehydration in graded ethanol solutions. Finally, the cells attached on cover slips were then sputter coated with gold before observation under FE-SEM.

3.11.3 TEM observation

L-132 cells were grown in 3.5 cm cell culture plate and then co-incubated with 100 μg ANC and BCNPs. After 24 h, cells were thoroughly washed with PBS and harvested through trypsinization. The collected cells were then fixed with 2% glutaraldehyde solution, followed by dehydration through graded ethanol solution. The cells were finally mounted on 300 mesh copper grid and analyzed under TEM.

3.11.4. Fluorescence microscopic analysis

Briefly, A549 and MCF-7 cells were seeded in 6 well plate with a seeding density of 2 x 10^5 cells per well and incubated at 37 ºC in incubator with 5% CO_2. Once the cells get attached, the spent media was removed and the cells were carefully washed with PBS buffer. Then the cells were incubated with rhodamine loaded BSA-Nic NPs for 8-12 h. Thereafter media was removed and cells were given a brief PBS wash. The cells were then viewed under EVOS cell imaging system (Life technologies, USA) and images were captured under green filter and transmitted mode.

3.12. Cellular ROS detection assay

Cells were seeded into six-well plates and grown to sub-confluence. Subsequently, the cells were incubated with 100 μg/mL of BCNPs for different time period. While for free nanoceria and ANC cells were incubated with different concentration of nanoparticles for 24 h. After incubation, the cells were given thrice PBS wash followed by exposure to 800 μM H_2O_2 in culture medium for 8 h at 37 °C. In case of FA-BSA-Ag NPs, cells were treated with desired concentration of FA-BSA-Ag NPs for 3 h. The DCFH-DA dye was used to measure intracellular ROS production. Inside the cell, endogenous esterases deacetylate the DCFH-DA into non-fluorescent 2', 7'-dichlorfluorescein (DCFH), which further converted into a green fluorescent dichlorofluorescein (DCF) compound in respond to ROS production that was analyzed by flow cytometry. Stock solution of DCFH-DA was prepared in DMSO. After the treatment the cells were given thorough PBS wash, followed by incubation with 20 μM DCFH-DA at 37 °C for 30 min. At the end of incubation, the cells were washed thoroughly, and then harvested. The fluorescent intensity was analyzed with a Flowsight flow cytometer (Amnis), and the data were acquired from 10,000 cells per sample. The relative fluorescence intensity

was measured as the ratio of mean intensity of the experimental cells and mean intensity of control cells. The data were analyzed by IDEAS version 6.0 software. The intracellular antioxidant activity of BCNPs and ANC was also studied by EVOS cell imaging system (life technologies, USA). L-132 cells were treated following the same procedures as mentioned above. After incubation with DCFH-DA and subsequent washing, the cells were visualized. The intracellular ROS level in each sample was reflected by the fluorescent intensity of the images.

3.13. Cell cycle analysis

The effect of FA-BSA-Ag NPs on the cell cycle of A549 and MCF-7 cells was determined by PI staining and consequent analysis by flow cytometry as described earlier (Sharma et al., 2014). Briefly, 2x 10^5 cells were seeded in a 6-wells plate and incubate overnight at 37 ^oC for attachment. The cells were then treated with desired concentration of FA-BSA-Ag NPs for 24 h. The cells were carefully harvested by trypsinization to prevent the loss of floating cells, followed by fixation with 70% alcohol for 15 min in ice. The fixed cells pellet obtained after centrifugation were then incubated with PI staining solution (50 µg/mL PI, 1 mg/mL RNase A, and 0.05% triton X-100) for 30 min at 37 ^{o} C in dark. The PI stained cells were then analysed through flow cytometer (Amnis Flowsight) to determine the cell cycle distribution. A total of 10,000 events per sample were captured and analyzed through IDEAS software in the same

3.14. Semi-quantitative RT-PCR analysis

For gene expression analysis, cells were grown in 3.5 cm plates. After overnight incubation, cells were treated with required concentration of nanoparticles. While, in case of ANC and BCNPs cells were preincubated with required concentrations of nanoparticles followed by H_2O_2 (500 µM for 24 h) treatment. Total RNA was isolated from entire cell population in each well using Tri reagent (Sigma-Aldrich, USA). cDNA was generated from total denatured RNA (1 µg) by reverse transcription performed at 42 ^oC for 50 min using Superscript II Reverse Transcriptase (Invitrogen, USA) in a total mixture of 20 µL.

Expression of antioxidant and apoptotic genes was examined using RT-PCR, where housekeeping genes β-actin (ACTB) and Glyceraldehyde-3-phosphate dehydrogenase (GAPDH) were used as internal control. Semi-quantitative PCR was carried out with 1 µL (5 times diluted stock of the above RT product) using the gene-specific upstream and downstream primers as mention in Table 3.1 in Veriti 96 well thermal cycler (Applied Biosystems). Initial denaturation (94 ^oC for 3 min) was followed by a PCR cycle of denaturation (94 ^oC for 30 s),

annealing (60 ^{o}C for 30 s), extension (72 ^{o}C for 1 min), and final extension (72 ^{o}C for 10 min). The PCR amplified products were resolved on a 1.2% agarose gel and finally visualized under UV light by ethidium bromide staining. The intensity of all bands was quantified by using Image lab 4.0 software.

3.15 *In vivo* experiments on zebrafish model

3.15.1 Origin and maintenance of zebrafish

Adult zebrafishes were procured from commercial dealer and were maintained in multi sensor-automated re-circulatory system (Aquaneering, USA). The tank temperature was between 26.8 °C to 28.0 °C, pH between 7.1 to 7.8, conductivity between 1100 µS/cm to 1400 µS/cm and with the lighting conditions of 14/10 light/dark cycle. Adult fishes were fed with micro pellet feed. Following successful pairwise breeding, the eggs were subsequently collected from the bottom of breeding tanks and the embryos were raised in embryo rearing solution (5 mM NaCl, 0.17 mM KCl, 0.4 mM $CaCl_2$ and 0.16 mM $MgSO_4$). Animal stages were recorded as hours post fertilization (hpf) or days post fertilization (dpf). All the protocols were reviewed and approved by Institutional Ethical Committee (Approval number for animal usage IBSC/2013/DBT-IDB/RRK-009) of Sathyabama University.

3.15.2 Water borne exposure of embryos to ANC and H_2O_2

Initially, H_2O_2 concentration was standardized for viability assay and the most effective concentration was opted for further experiments in 8 hpf embryos. The standardization was processed by treating the embryos (n=20) at 8 hpf with different concentrations of H_2O_2 (i.e. 30, 60, 90 and 120 mM) for 30 min. In order to evaluate the ability of ANC to protect against the H_2O_2-induced cytotoxicity, zebrafish's embryos (8 hpf) were incubated with different concentrations of ANC for 24 h and then washed 3-4 times in E3 medium. After that the embryos were treated with 120 mM H_2O_2 for 30 min and then thoroughly washed with E3 medium. Finally, embryos were incubated in fresh E3 medium and observed for deformities and mortalities for 3 days. The dead embryos were counted and removed. Moreover, embryos were also treated with different concentrations of ANC (i.e. 10, 25, 50, 100, 200 and 300 µg mL^{-1}) to evaluate their biocompatibility. Approximately, 20 embryos per well were examined for each treatment. In order to reduce variation among different batches, randomized embryos were taken from 4-5 independent pair-wise mating. All experiments were done in triplicate.

13.15.3 Heart-beat rate measurement

In order to determine the toxicity of H_2O_2 and the protective effect of ANC, the heart-beating rate of both atrium and ventricle was assessed at 32 hpf. The atrial and ventricular contraction was observed for 1 min under the microscope and results were presented in the form of average heart-beating rate per min.

3.15.4 ROS scavenging potential of ANC in zebrafish embryos

The ROS generation in zebrafish embryos were examined with the help of oxidation-sensitive fluorescent probe dye, DCFDA (Kim et al., 2014a and 2015, Ko et al, 2014, Kang et al., 2013a, 2013b and 2014). In order to investigate the protective effect of ANC against H_2O_2 induced oxidative stress, 8 hpf embryos were incubated with different concentrations of ANC. After 24 h of incubation, embryos were washed with E3 medium and treated with 120 mM H_2O_2 for 30 min. The embryo media was changed and treated embryos were then incubated with DCFDA (7 µg/mL). After, 30 min of incubation at 27 ^oC in dark, embryos were rinsed with fresh E3 medium and DCFH fluorescence values of the individual embryos were acquired using a multimode plate reader (Perkin Elmer). For fluorescence imaging, the embryos were anesthesized before visualization and images of the stained embryos were acquired by using stereo fluorescent microscope (Leica M165 FC), which was equipped with Leica DFC310 FX camera. The images were captured under GFP filter. The experiment was carried out in triplicate

13.15.5 Estimation of oxidative stress induced cell death in zebrafish embryo

Oxidative stress induced cell death in live zebrafish embryos was detected by using acridine orange, a nucleic acid specific metachromatic dye which stain the cells having disturbed plasma membrane permeability, thus stain the necrotic and late apoptotic cells (Kang et al., 2013a, 2013b and 2014). In brief, the 28 hpf embryos were incubated for 30 min, followed by treatment with 120 mM H_2O_2 for 30 min. After incubation, the embryo media was changed and the embryos were developed upto 2 dpf. The embryos were then treated with AO solution (5 µg/mL) for 30 min in dark at 28 ^oC. The embryos were then rinsed and AO fluorescence values of the individual embryos were acquired using a multimode plate reader (Perkin Elmer). For fluorescence imaging, the embryos were anesthesized before visualization and images of the stained embryos were acquired by using fluorescent microscope (Leica M165 FC), which was equipped with Leica DFC310 FX camera. The images were captured under RFP filter. The experiment was carried out in triplicate.

Genes	Primers
GAPDH	Forward: 5’ CCACCCATGGCAAATTCCATGGCA 3’ Reverse : 5’ TCTAGACGGCAGGTCAGGTCCACC 3’
SOD2	Forward: 5’ TCCACCACCGTTAGGGCTGAGG 3’ Reverse : 5’ CACCAGCAGGCAGCTGGCTCC3’
SOD1	Forward : 5’ CAATAGACACATCGGCCACAC 3’ Reverse : 5’ AAGGCCGTGTGCGTGCTGAA 3’
GPX	Forward : 5’ CCACCAGGAACTTCTCAAA 3’ Reverse : 5’ TGGCTTCTTGGACAATTGCG3’
CAT	Forward : 5’ AAGACCAGTTTACCAACTGGG 3’ Reverse : 5’ CAGATGGACATGCGCACATG3’
ACTB	Forward: 5’ CTGTCTGGCGGCACCACCAT 3’ Reverse : 5’ GCAACTAAGTCATAGTCCGC 3’
TP53	Forward: 5’ TGGCCCCTCCTCAGCATCTTAT 3’ Reverse : 5’ GTTGGGCAGTGCTCGCTTAGTG 3’
CASP3	Forward : 5’ TTCAGAGGGGATCGTTGTAGAAGTC 3’ Reverse : 5’ CAAGCTTGTCGGCATACTGTTTCAG 3’
MYC	Forward : 5’ CCAGGACTGTATGTGGAGCG 3’ Reverse : 5’ CTTGAGGACCAGTGGGCTGT 3’
BAX	Forward : 5’ AAGCTGAGCGAGTGTCTCAAGCGC 3’ Reverse : 5’ TCCCGCCACAAAGATGGTCACG 3’
BAD	Forward : 5’ CCTTTAAGAAGGGACTTCCTCGCC 3’ Reverse : 5’ACTTCCGATGGGACCAAGCCTTCC 3’
BCL2L1	Forward : 5’ATGGCAGCAGTAAAGCAAGC 3’ Reverse : 5’ CGGAAGAGTTCATTCACTACCTGT 3’

Table 3.1 List of antioxidant and apoptotic genes primers used in semi-quantitative RT-PCR analysis (PCR cycle number=28).

CHAPTER 4

PREPARATION AND CHARACTERIZATION OF NICLOSAMIDE ENCAPSULATED ALBUMIN NANOPARTICLES FOR CANCER THERAPY

In this Chapter, a water soluble formulation of hydrophobic anti-cancer drug, niclosamide has been synthesized in order to facilitate its uptake by cancer cells. The therapeutic efficacy of niclosamide encapsulated albumin nanoparticles has been validated against A549 and MCF-7 cells. Further, the efficient induction of apoptosis by these nanoparticles was corroborated by gene expression analysis.

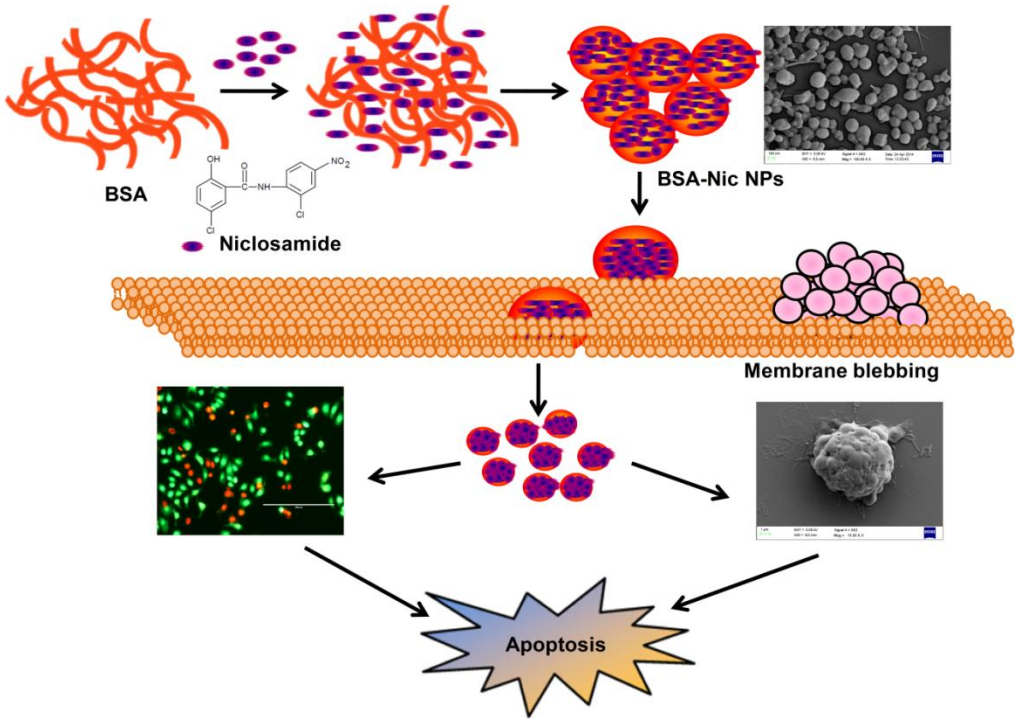

CHAPTER 4

PREPARATION AND CHARACTERIZATION OF NICLOSAMIDE ENCAPSULATED ALBUMIN NANOPARTICLES FOR CANCER THERAPY

Overview

One of the major unresolved challenges among the scientific community is to develop anticancer drugs that are safe and effective. A large number of anticancer drugs are screened so far in this campaign. Among them niclosamide has shown potent anti-cancer properties as demonstrated in a plethora of human cancer cell line and animal carcinogenesis models. But the extreme hydrophobicity and consequently, minimal systemic bioavailability associated with this drug limited its widespread clinical applications. Nanoparticle-based drug delivery approaches have the potential for realizing water soluble formulation of highly hydrophobic anticancer drugs like niclosamide, thus circumventing the pitfalls of poor solubility. In this work niclosamide was encapsulated into albumin nanoparticles through a desolvation method to improve its scope of application in cancer therapy. Physico-chemical characterization confirms that the prepared nanoparticles were spherical, highly monodispersed, and stable in aqueous system. These drug encapsulated albumin nanoparticles, unlike free drug demonstrates better *in vitro* therapeutic efficacy against a human lung and breast cancer cell lines, as assessed by cell viability assay and morphological analyses. Further, the efficient induction of apoptosis by these nanoparticles was confirmed by semi-quantitative RT-PCR. This work provides an opportunity to expand the clinical repertoire of this effectual agent by enabling ready aqueous dispersion.

Results and discussion

4.1 Preparation of BSA-Nic NPs

BSA-Nic NPs used in the present study were prepared via desolvation method (Weber et al., 2000), using ethanol as desolvating agent and glutaraldehyde as the cross linking agent as shown in schematic Figure 4.1(a). This method leads to the formation of least aggregated particles with a uniform distribution and found to be highly stable in water and cell culture medium. Glutaraldehyde, water soluble homo bifunctional reagents are capable of forming stable inter-

and intra-subunit covalent bonds. It reaction with protein leads to the formation of Schiff bases between two carbonyl ends of glutaraldehyde and positively charged amino groups of the protein. Thus, the amino moieties in lysine and arginine residues constituting around 10 percent of the total amino acids of BSA play crucial role in the formation of nanoparticles. Synthesized NPs were characterized by UV-visible spectroscopy and the absorption maximum analyzed by a spectral scan from 200 to 700 nm as shown in Figure 4.1(b). The UV-visible absorption spectrum of albumin shows a characteristic absorption peak of protein at 280 nm corresponding to the aromatic amino acids present inside the protein. The niclosamide drug alone (dissolved in ethanol) had two absorption maximum at 260 nm and 346 nm. While drug encapsulated albumin NPs in aqueous medium shows characteristic peak of drug at 346 nm. A slight change in spectra has been observed, which might be a result of chemical cross linking between the amino acids of protein and the formation of protein-drug nanoparticles complex.

4.2 Characterization: Surface morphology, particle size and zeta potential

The surface morphology of the particles was determined by the field emission-scanning electron microscopy. The images of the drug encapsulated albumin nanoparticles revealed a spherical morphology as shown in Figure 4.2(b). Majority of the particles showed uniform size distribution without any crystal precipitation. While, the micrometer size rod shaped flakes were observed for pristine niclosamide powder as shown in Figure 4.2(a). The BSA NPs and rhodamine loaded BSA NPs showed similar spherical surface morphology corresponding to BSA-Nic NPs as shown in Figure 4.3.

The stability of the nanoparticles can be attributed to the significantly higher zeta potential. The zeta potential value of the BSA-Nic NPs was found to be -34.2 mV as compared to -17.9 mV of pristine BSA. This value lies in the stable range, indicating that the nanoparticles formation lead to the formation of stable system. Moreover, the electrostatic repulsive force among the negatively charged surface of the nanoparticles affords high stability to the colloidal solution by preventing them from agglomerating in the colloid state (Sripriyalakshmi et al., 2014). Figure 4.2(d) illustrates the particle size distribution for the prepared BSA-Nic NPs. The size distribution for the nanoparticles was obtained using dynamic light scattering. The average hydrodynamic size for BSA-Nic NPs was found to be 199.9 nm. In contrast, the BSA NPs and rhodamine loaded BSA NPs (Figure 4.4) synthesized for the carrier

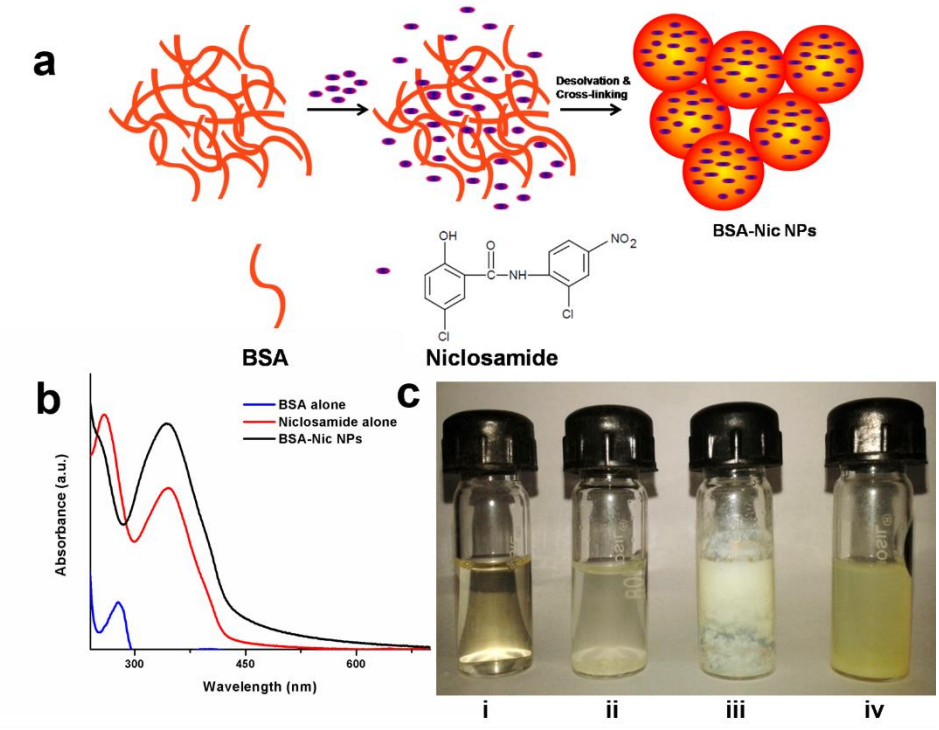

Figure 4.1 (a) Schematic outline of drug encapsulated BSA NPs fabrication by desolvation technique (b) UV–visible absorption spectra of niclosamide (in ethanol), BSA alone and BSA-Nic NPs (c) Photographs showing the insolubility of niclosamide and solubility of BSA-Nic NPs in water. (i) BSA alone (ii) Raw niclosamide powder in water (iii) Curd like precipitation on adding niclosamide solution (ethanol) in water (iv) BSA-Nic NPs.

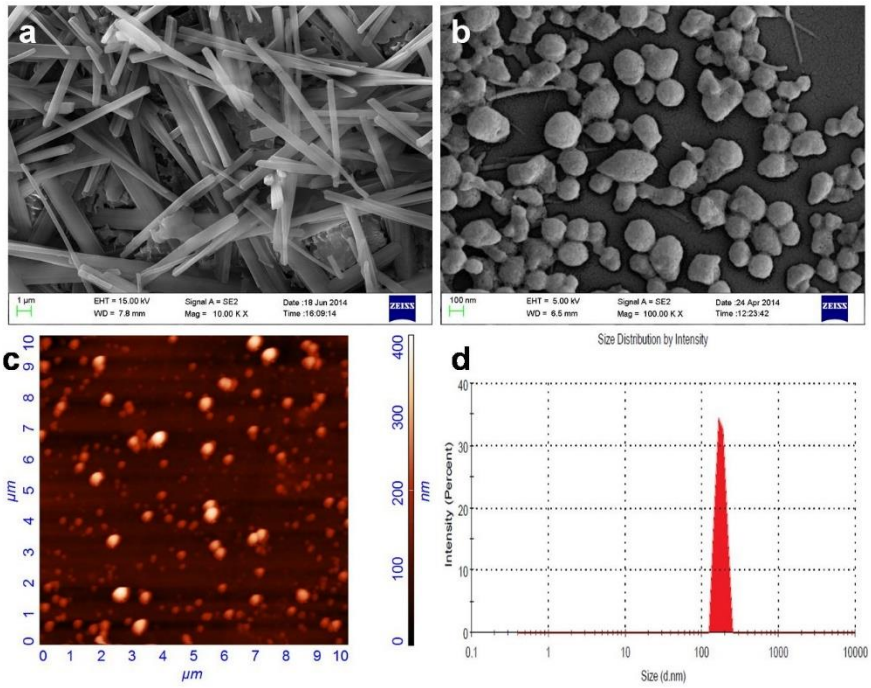

Figure 4.2 FE-SEM images of (a) raw niclosamide powder and (b) BSA-Nic NPs, showing their typical morphology (c) AFM and (d) DLS images of BSA-Nic NPs showing the distribution and size of nanoparticles.

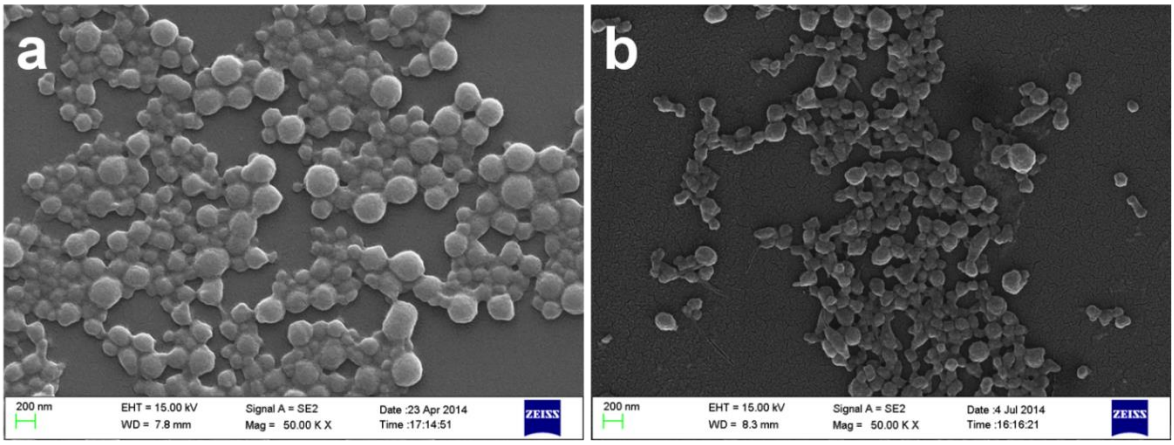

Figure 4.3 FE-SEM image of (a) BSA NPs and (b) rhodamine loaded BSA NPs, showing their typical morphology. (Scale bar- 200 nm)

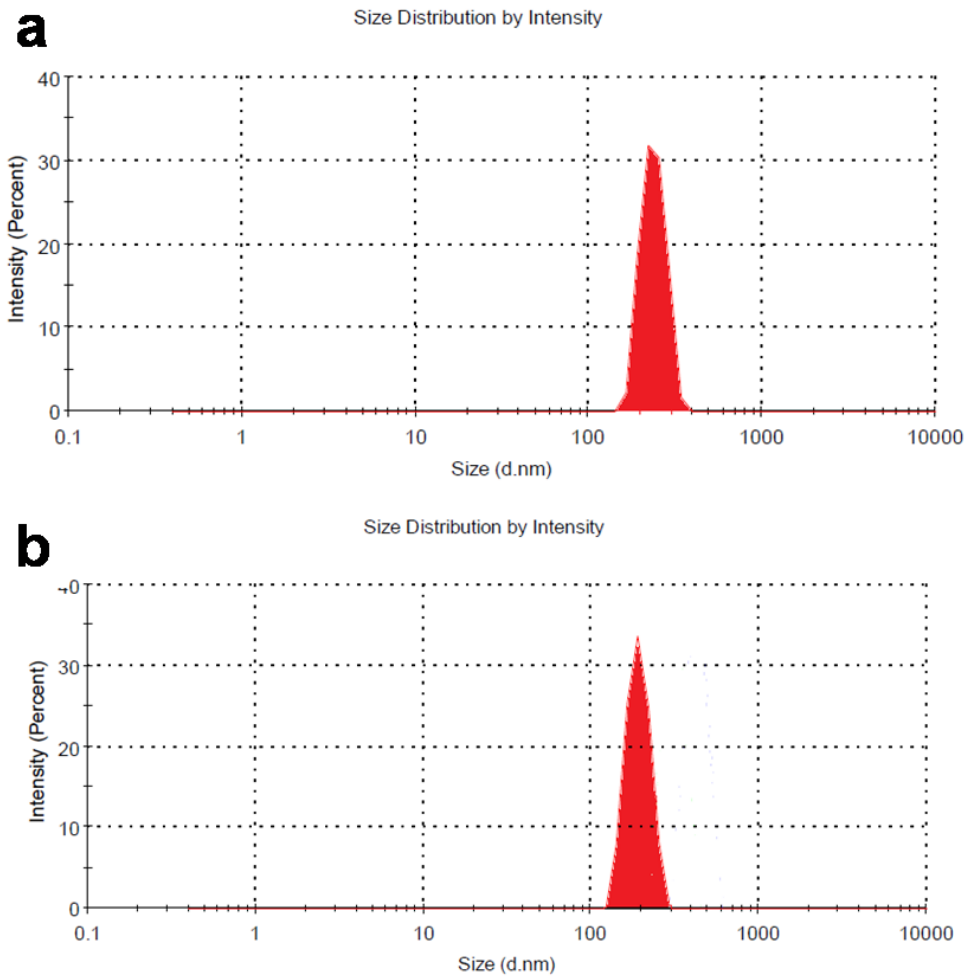

Figure 4.4 DLS images of (a) BSA nanoparticles (b) rhodamine loaded BSA nanoparticles.

cytotoxicity and cellular uptake studies were found to be 264.4 nm and 273.2 nm respectively in size. The size of the prepared BSA-Nic NPs was also estimated by AFM as shown in the Figure 4.2(c). The images were processed using NOVA software and the average grain size was found to be 188.27 nm. The size of the nanocarrier system also plays an important role in the delivery of anticancer drugs, as the nanoparticles up to 400 nm can easily extravasate through the defective vasculature system in the tumor tissues and subsequently get accumulate in the tumor microenvironment through a process known as "enhanced permeability and retention" effect and forms the basis of "passive targeting" (Peer et al., 2007). The characteristic properties of the prepared nanoparticles in the present study, hence meet the required criteria to be exploited as a drug delivery system, as compared with the previously reported drug encapsulated BSA based nanoparticles as summarized in the Table 2.1.

4.3 X-ray diffraction studies

XRD studies of the prepared nanoparticles were carried out in order to check the physical nature of the particles. On evaluating the drug encapsulated protein NPs with the control drug and observed that BSA-Nic NPs was much more amorphous in nature as compared with the niclosamide drug alone. The amorphous nature of the drug encapsulated albumin nanoparticles could be attributed to the crosslinking mechanism between the reactive residual functional groups of protein and drug molecules as well as the prominent hydrogen bonding interaction between them (Rejinold et al., 2011a and b). Figure 4.5(a) represents the XRD pattern of niclosamide and BSA-Nic NPs. Moreover, the sharp characteristic diffraction peaks of drug molecules at 25.6^{o} and 26.7^{o} of 2θ disappeared in the BSA-Nic NPs indicating that the drug were entrapped and no significant amount of free drug left in the system after interaction with protein (Li et al., 2012, Tonder et al., 2004).

4.4 FTIR and fluorescence spectroscopic studies

In FTIR spectrum of pristine BSA showed characteristic peaks at 3418.56, 3070, 1651.54, and 1539.04 cm^{-1} were assigned to the stretching vibration of –OH, amide A (mainly –NH stretching vibration), amide I (mainly C=O stretching vibrations), and amide II (the coupling of bending vibrate of N–H and stretching vibrate of C–N) bands, respectively. Near NH and OH stretching region lies amide A band (~ 3070 cm^{-1}), which is completely detectable only in lower hydrates. The major characteristic peaks of drug alone were listed in Table 4.1 (Tonder et al., 2004). On comparing the IR spectra of BSA alone, niclosamide alone and BSA-Nic NPs as shown in Figure 4.6, a major shifting of peaks were observed from 1192.09 to 1195.12, 1219.19 to 1227.90 and 1522.03 to 1511.15 cm^{-1} indicating the involvement of the C-OH, C=O, NO_2 groups of drug

molecules in the formation of protein –drug complex. Moreover, the peaks were appeared as a wide spectrum due to the potential interaction among the nanoparticles. There was a characteristic reduction in the stretching frequency in case of BSA-Nic NPs, as shown in Figure 4.5(b). The amide I peak of BSA shifted from 1651.54 to 1656.64 cm^{-1}, amide II shifted from 1539.04 to 1561.02 cm^{-1} and amide III shifted from 1395.92 to 1417.80 cm^{-1}, respectively which can be attributed to the cross-linking mechanism between the reactive residual functional groups of protein and interaction of niclosamide with the residual amide species (Rejinold et al., 2011, Kong et al., 2007, Huang et al., 2010).

Several interactions including hydrophobic force, hydrogen bonds, electrostatic interactions, and van der Waals interactions play key role in the binding process of protein with small molecules like drug. Niclosamide entered the hydrophobic microenvironment of serum proteins including human serum albumin and interacted with the hydrophobic pockets of the protein. Interaction of niclosamide with serum proteins mainly involves van der Waals interaction, hydrophobic interaction and hydrogen bonding. Like many other drug molecules, niclosamide interact with the tryptophan residues (Trp- 212) located inside the hydrophobic pocket of the BSA (Hossain et al., 2011, Maltas, 2014). To understand the effect of niclosamide on the tryptophan environment of BSA, the intrinsic fluorescence of BSA in the presence of increasing concentrations of niclosamide was studied as shown in Figure 4.7. Intrinsic fluorescence of BSA is due to two tryptophan residues: (1) Trp 134, located on the surface in the hydrophilic region of protein and characterized by a longer wavelength emission maximum (2) Trp 212, located within a hydrophobic binding pocket that is characterized by a shorter wavelength emission maximum around 340 nm. Thus, the fluorescence emission of BSA with maximum around 340 nm corresponding to the Trp residue at 212 was monitored. The fluorescence intensity of BSA decreases regularly with increasing niclosamide concentrations. This decrease in the intensity could be due to fluorescence quenching attributed to the changes in the microenvironment of the tryptophan residues suggesting interaction of niclosamide and BSA. Hence the results obtained from FTIR and fluorescence spectroscopy were in accordance with previous observation and clearly indicate the involvement of aryl groups of drug and aromatic residues of protein in the drug carrier interactions.

4.5 Thermal stability of the nanoparticles

The thermo gravimetric analysis of niclosamide, BSA-Nic NPs and BSA alone (control) were conducted, which depicted slower degradation rate of protein-drug nanoformulation

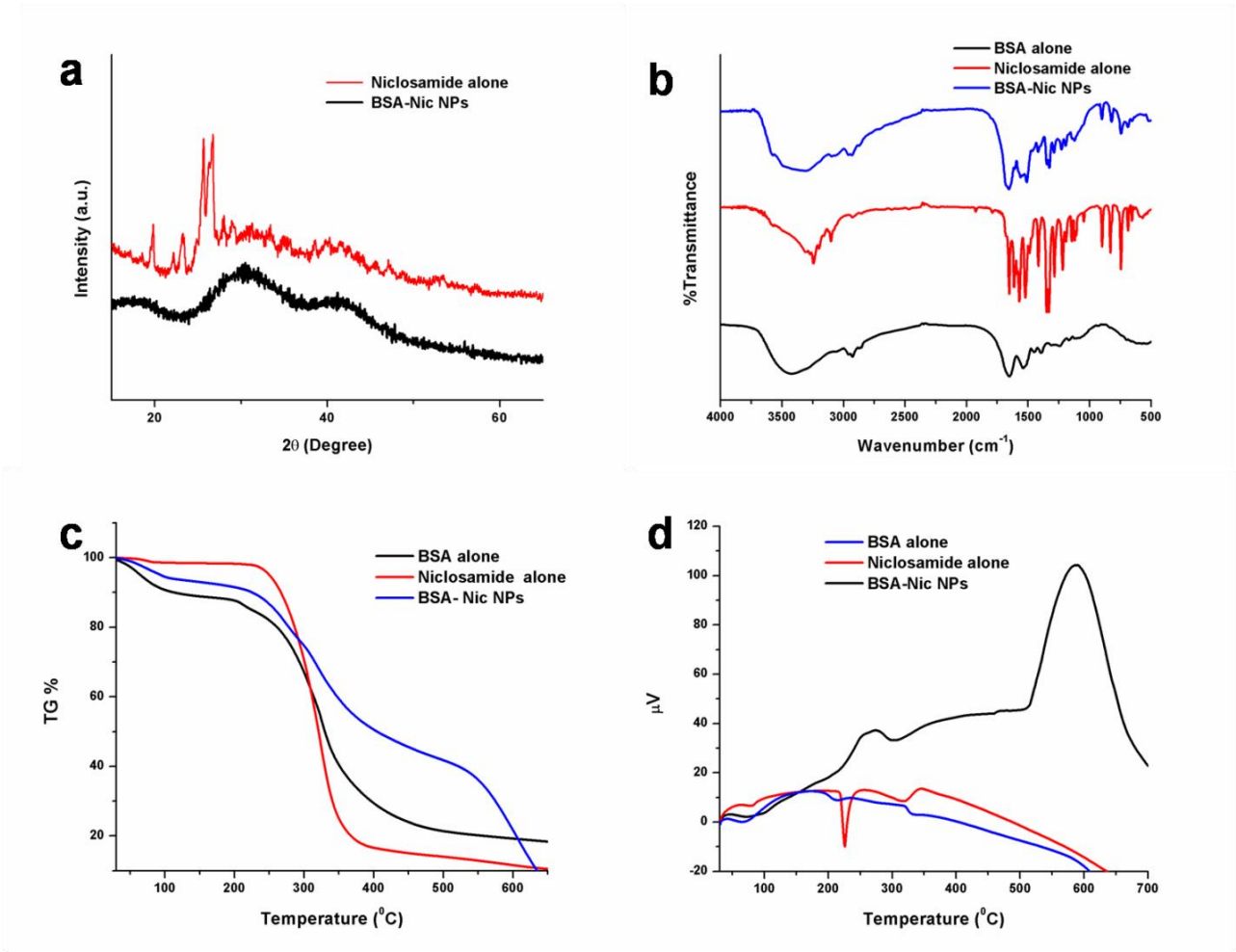

Figure 4.5 (a) XRD plot of raw niclosamide powder and BSA-Nic NPs (b) FTIR spectra (c) TG data (d) DTA curve of BSA (control), raw niclosamide powder and BSA-Nic NPs.

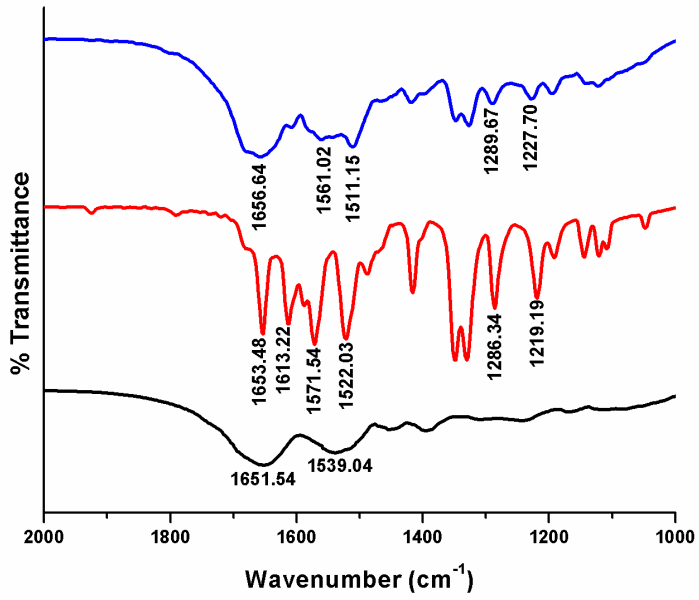

Figure 4.6 FTIR spectra of BSA (control), raw niclosamide powder and BSA Nic NPs.

Functional groups	C=C	C=O	N-H	C-N	NO2	C=O	C-OH
Wave no	1613.22	1653.48	1571.54	1286.34	1522.03	1219.19	1192.09
vibration	C=C stretch	C=O stretch	N-H bend	C-N stretch	NO2 stretch	C=O stretch	C-OH stretch

Table 4.1 Characteristic major absorption bands in the IR spectra of the raw niclosamide powder.

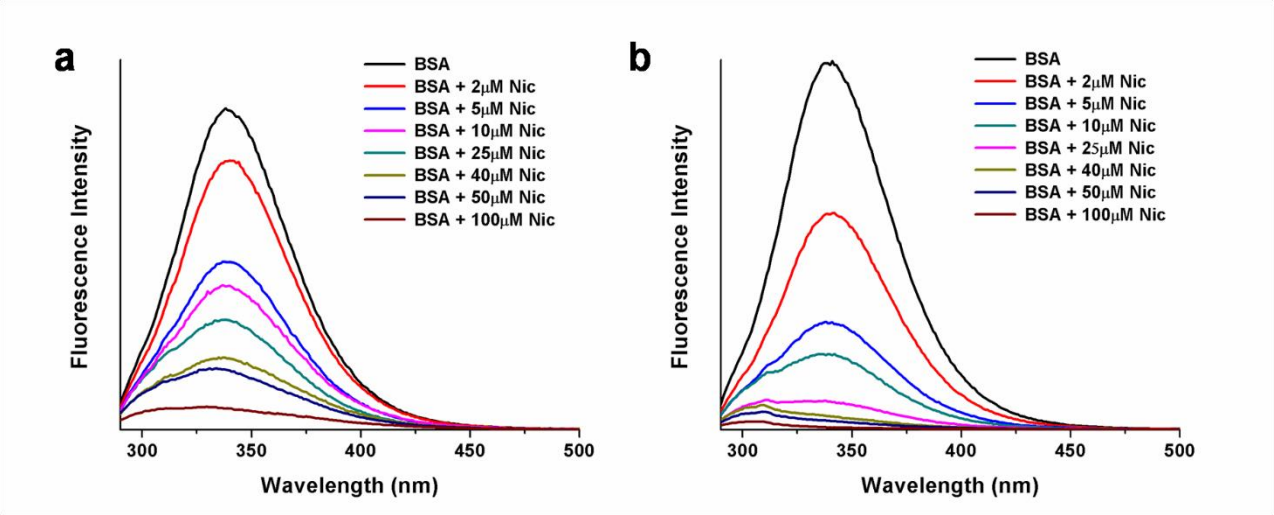

Figure 4.7 Fluorescence spectra of BSA in (a) aqueous (b) PBS with different concentration of niclosamide (0-100 µM). (T= 298 K, λex = 280 nm, λem= 295-500 nm).

a

Protein Concentration (mg)	Drug concentration (mg)	Entrapment efficiency (%)
25	5	75.96±2.206
25	10	89.66±1.868
25	12	92.36±1.552
25	15	84.72±2.218
25	20	76.85±2.272

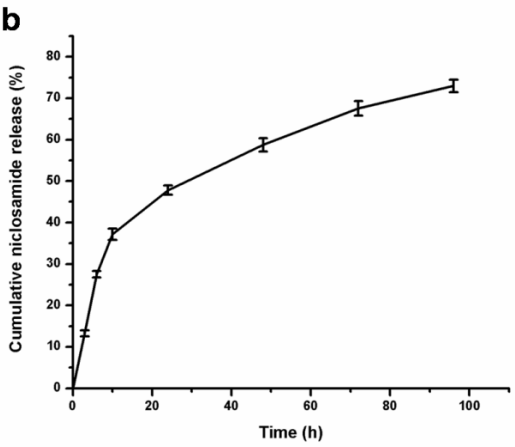

Figure 4.8 (a) Entrapment efficiency of BSA NPs with varying niclosamide concentrations (b) Niclosamide release profile from BSA NPs in PBS.

indicating their improved stability as compare to pristine BSA and niclosamide particles. From Figure 4.5(c), it was clearly visible that the degradation of particles started from 200 ^{o}C and after 250 ^{o}C, a sudden decrease in weight was observed which may be due to the loss of small molecule such as carbon dioxide, ammonia etc. At 400-500 ^{o}C there was considerable difference in weight loss was observed, as 21% was remaining for control BSA, 41% was remaining for BSA-Nic NPs, whereas only 13% was remaining for niclosamide drug alone which confirm the slower degradation rate for BSA-Nic NPs as compared to niclosamide drug alone. Beyond 500 ^{o}C, a faster rate of degradation of BSA-Nic NPs was observed as compared to BSA (control), which may be due to the crystalline nature of entrapped niclosamide drug molecules in BSA-Nic NPs. Whereas, no significant change was observed in BSA (control) due to the char formation in nitrogen atmosphere. Recently, Gebregeorgis et al., 2013 demonstrated that no char formation take place in air atmosphere as compared to nitrogen atmosphere, an additional step was required related to the combustion of the char product in air atmosphere.

The differential thermal analysis of the bare niclosamide drug showed an endothermic peak at 225 ^{o}C which was not there in case of BSA-Nic NPs depicting the high amorphous nature of the nano formulation and thereby better stability. The exothermic peak also shifted toward higher temperature range which again substantiates the high amorphous nature of protein-drug nanoformulation as evident from Figure 4.5(d). The higher amorphous nature of the therapeutic system, the more would be its delivery efficiency (Abdelwahed et al., 2006).

4.6 Encapsulation efficiency of nanoparticles

Various concentrations of the drug with the albumin nanoparticles were taken and synthesis was done by desolvation method. The encapsulation efficiency of the BSA NPs was analyzed by using different concentrations of niclosamide, while the carrier concentration was kept constant. The drug:BSA combination with the preeminent encapsulation efficiency was taken for further studies. As shown in Figure 4.8(a), 12:25 ratio of drug: BSA gave the paramount encapsulation efficiency of 92.36%.

4.7 *In vitro* drug release study

The *in vitro* drug release profiles of the BSA-Nic NPs over 96 h was studied at pre defined time intervals in PBS at pH 7.4 as shown in Figure 4.8(b). The *in vitro* drug release is a coalesced effect of diffusion of drug molecule out of the protein nanoparticles into the external environment and concurrent degradation of carrier itself. A biphasic drug release pattern was seen with an initial burst of 37.15% in the first 10 h followed by a controlled release of the drug. The initial

burst release was due to the drug attached to the surface of the BSA NPs, and the sustained release was from the entrapped drug. In the following 24 h, cumulative release reached 47.81%, in a sustained manner, making the protein based nanoparticles an effective drug carrier to fight continually against cancer cells for an effective cancer therapy. Cumulative release reached almost 73% after 4 days.

Generally, the sustained and controlled release profile of niclosamide facilitates the application of nanoparticles for the delivery of anticancer drugs. The cross linking of the BSA nano carriers using glutaraldehyde is the major reason for the enhanced stability of the particles in PBS. The results revealed that slow controlled release of the drug in the media makes it an ideal delivery system for cancer treatment. Moreover, as compared to the extremely slow release profile of raw niclosamide powder as reported earlier (Bai et al., 2013), the continuous release of niclosamide from the BSA- Nic NPs solution can be attributed to the solubilizing ability of the BSA carrier. The erosion and degradation of BSA NPs and the insolubility of niclosamide in aqueous medium were involved in the drug-release process.

4.8 *In Vitro* stability of BSA-Nic NPs

In order to evaluate the physiological stability of BSA-Nic NPs in aqueous and 0.9% saline solution, the change of particle size were monitored by DLS *in vitro* for more than 96 h. As shown in Figure 4.9, when BSA-Nic NPs were placed in aqueous and 0.9% saline solution, there was no obvious size change even after 96 h at 25°C. This phenomenon demonstrated the high stability of the BSA-Nic NPs. Since, stability always remains a crucial factor for the clinical use of drug formulation as the drug might slowly escape from the nanoparticles or may degrade with time.

4.9 Cell viability assay

The effect of BSA-Nic NPs on the viability of A549 and MCF-7 cells was assessed quantitatively by MTT assay as shown in the Figure 4.10. The results show the inhibition of cell viability by BSA-Nic NPs in a concentration-dependent manner. This might be due to the sustained release of drug molecule from the nanocarrier. The IC_{50} concentration of BSA-Nic NPs was found to be 5 μM and 2.6 μM for A549 and MCF-7 cells, respectively. On the other hand, bare niclosamide (in water) showed a nontoxic effect on both the cell lines, probably it could be due to the practical insoluble nature of the bare niclosamide drug in aqueous medium, due to which most of the drug molecules were not taken up by the cells. However, as the nanoformulation increase the niclosamide solubility in aqueous medium, it can be easily taken

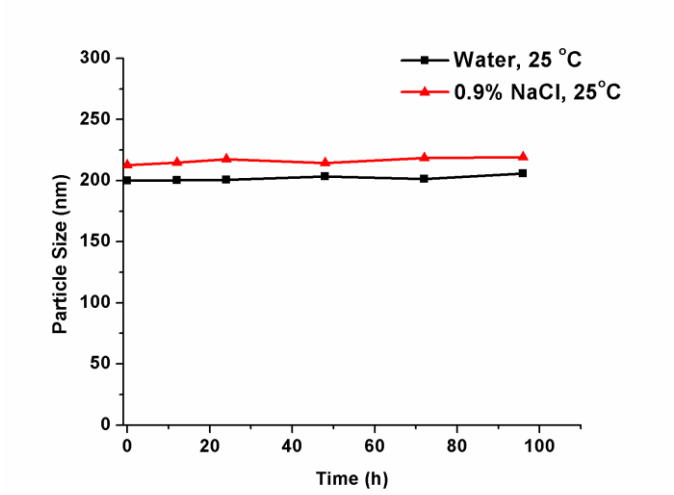

Figure 4.9 Stability studies**,** size of BSA-Nic NPs in aqueous and 0.9% saline solution.

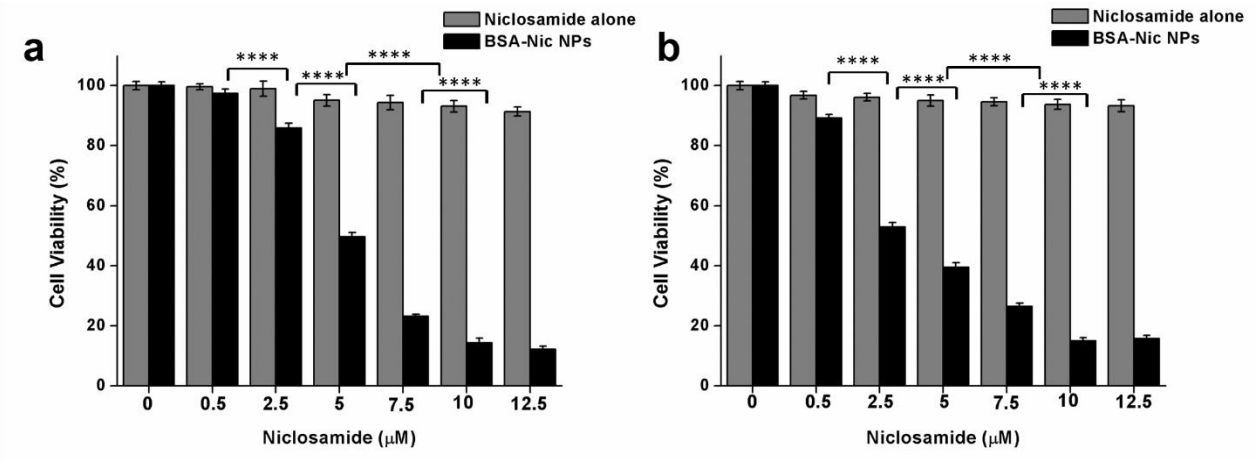

Figure 4.10 Cell viability assay (MTT assay) of raw niclosamide (in water) and BSA-Nic NPs on (a) A549 cells (b) MCF-7 cells after 24 h of treatment. The statistically significant values are denoted by *$p < 0.05$, **$p < 0.005$, ***$p < 0.001$ and ****$p < 0.0001$ (error bars denoted SD; n=3).

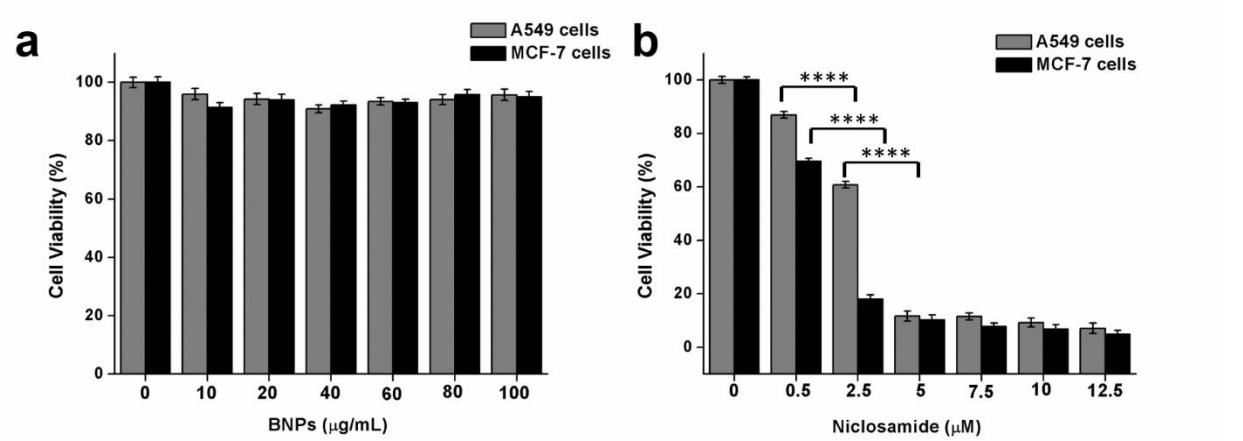

Figure 4.11 Cell viability assay (MTT assay) of (a) BSA NPs and (b) niclosamide (in DMSO) on A549 cells and MCF-7 cells after 24 h of treatment. The statistically significant values are denoted by *$p < 0.05$, **$p < 0.005$, ***$p < 0.001$ and ****$p < 0.0001$ (error bars denoted SD; n=3).

up by the cells and resulted in concentration dependent cell inhibition. Thus BSA–Nic NPs turned out to be very effective drug carrier and enhanced antiproliferative activity was observed in contrast to the free drug. However, it should be taken into account as previously reported that free niclosamide (dissolved in DMSO) also exhibited cytotoxicity against A549 and MCF-7 cell lines as shown in Figure 4.11(b). However, implication of organic solvent DMSO as a solubilizing agent lead to severe complication as it itself produce cytotoxic effect, thereby not suitable for future clinical applications. We ensured that at each concentration the drug loaded nanoparticles were taken such that the niclosamide concentration in the free drug was similar to that present in BSA-Nic NPs, making a direct comparison possible.

The bare BSA NPs were also analyzed for their cell toxicity, which showed that they were non-toxic to both the cells line as shown in the Figure 4.11(a), more than 90% cell viability was found after 24 h confirming the biocompatibility of bare nanoparticles. These results clearly indicating that the antiproliferative activity was not because of the carrier BSA NPs but due to drug encapsulated BSA NPs.

4. 10 Acridine Orange/Ethidium Bromide staining

A combination of dyes, ethidium bromide and acridine orange were used to stain the treated cells in order to investigate the mode of cell death (viz. apoptosis or necrosis) in A549 and MCF-7 cells caused by the BSA-Nic NPs treatment and observed under the fluorescence microscope. EB stain was excluded by the healthy live cell's nucleus and it appears green due to the presence of AO alone (Figure 4.12(a)). The cells treated with half the IC_{50} concentration of BSA-Nic NPs showed no significant changes in the morphology of the cell and it appears similar to untreated cells with uniformly green and normal morphology (Figure 4.12(b)). However, characteristic morphological changes associated with apoptosis (programmed cell death) including membrane blebbing, nuclear fragmentation and cytoplasmic constriction (Rello et al., 2005, Uday Kumar et al., 2014) were observed in treated cells at IC_{50} and 2x IC_{50} concentrations. Figure 4.12(c) and 4.12(d) clearly depict the presence of early apoptotic cells having condensed chromatin as well as late apoptotic cells with fragmented chromatin and apoptotic bodies. The results of AO/EB nuclear staining indicated the induction of apoptosis in A549 and MCF-7 cells by BSA-Nic NPs.

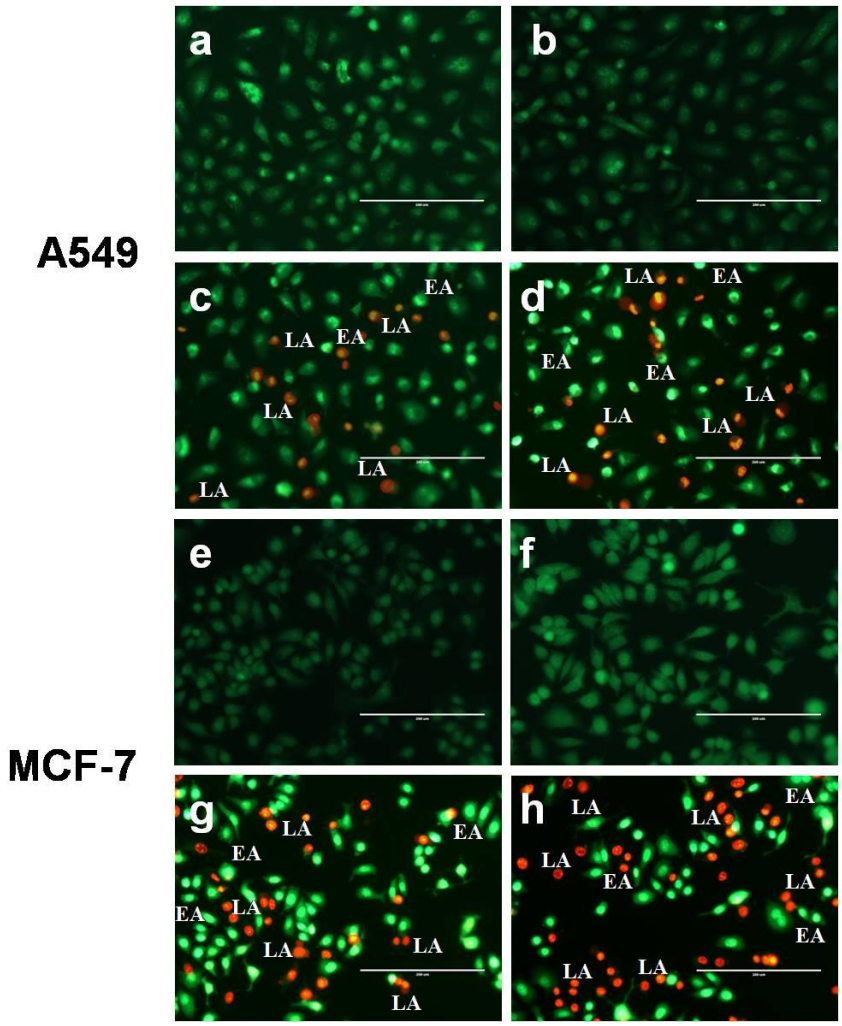

Figure 4.12 Representative images of AO/EB dual staining of (a, e) untreated (b, f) half IC_{50} (c, g) IC_{50} and (d, h) 2x IC_{50} BSA-Nic NPs treated A549 and MCF-7 cells after 24h of treatment.

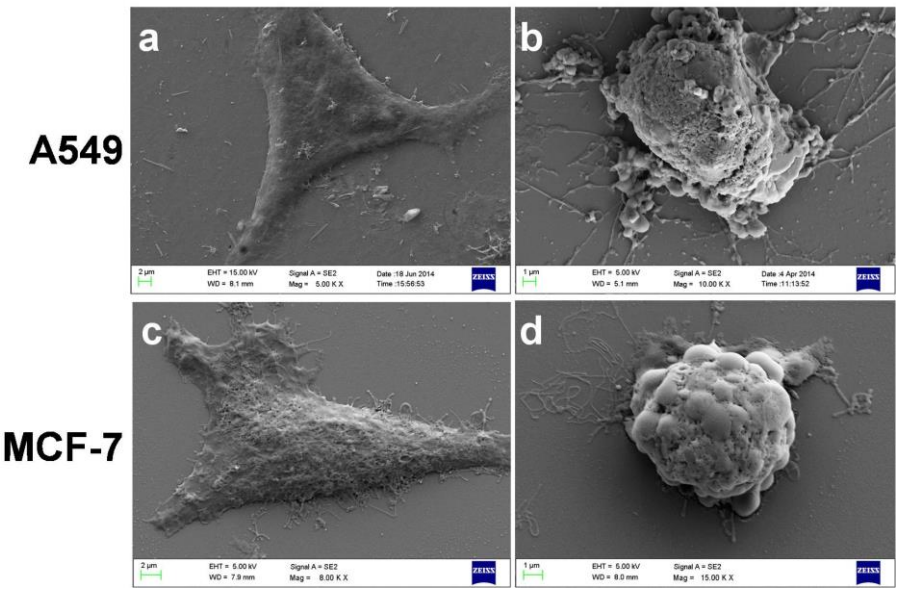

Figure 4.13 Representative FE-SEM images of (a and c) untreated and (b and d) treated A549 and MCF-7 cells.

4.11 FE-SEM analysis

In addition, to the AO/EB staining, BSA-Nic NPs treated A549 and MCF-7 cells were further examined under the FE-SEM in the pursuit of the characteristic morphological changes observed during apoptosis. Figure 4.13(a and c) shows the typical morphology of untreated A549 and MCF-7 cells that were well-attached to the surface. However, the cells treated with BSA-Nic NPs showed round-shaped and loosely attached cells (Figure 4.13(b and d)) as compared to untreated cells. In both the cells, the event of cytoplasmic constriction, membrane blebbing and formation of apoptotic bodies clearly indicate the apoptotic cell death.

4.12 Semi-quantitative RT-PCR analysis

The potency of niclosamide encapsulated BSA NPs to induce apoptosis in human breast and lung cancer was assessed *in vitro via* semi-quantitative RT-PCR analysis, which showed the involvement of various apoptotic signaling genes in BSA-Nic NPs mediated cell death as shown in Figure 4.14 (c). The NPs treated cells were analyzed for their apoptotic signaling genes expression profile such as BAD, BAX, MYC, TP53 and caspase-3 (CASP3) that indicated their up-regulation, while the expression of anti-apoptotic gene such as bcl-xl (BCL2L1) found to be down-regulated. Moreover, the expression of housekeeping gene β-actin (ACTB), which acts as an internal control remained unaltered during the process. (Figure 4.14 a and b)

It is known that anticancer drug niclosamide induces mitochondrial fragmentation and promote apoptotic cell death (Park et al., 2011). The destabilization of mitochondrial integrity precedes the release of pro-apoptotic molecules such as cytochrome- c into the cytoplasm that activate the caspases leading to apoptosis. Such phenomenon is closely regulated by a group of proteins belonging to the Bcl-2 family, namely the pro-apoptotic proteins (e.g. bcl-2-associated X protein (BAX) and bcl-2-associated death promoter (BAD)) and the anti-apoptotic protein (e.g. BCL2L1) (Wong, 2011). The anti-apoptotic proteins regulate apoptosis by blocking the mitochondrial release of cytochrome-c and also enable resistance to chemotherapeutic drugs, while the pro-apoptotic proteins act by promoting such release and play key roles in the inhibition of anti-apoptotic function of BCL2L1 (Yang et al., 1995, Boise et al., 1993). The members of the Bcl-2 family are located on the outer mitochondrial membrane and regulate the release of cytochrome c into the cytosol by controlling the membrane permeability either in the form of an ion channel or through the creation of pores (Minn et al., 1997). In the present study, a substantial increase in expression of BAD and BAX was observed, suggesting their role in the down-regulation of anti-apoptotic gene BCL2L1.

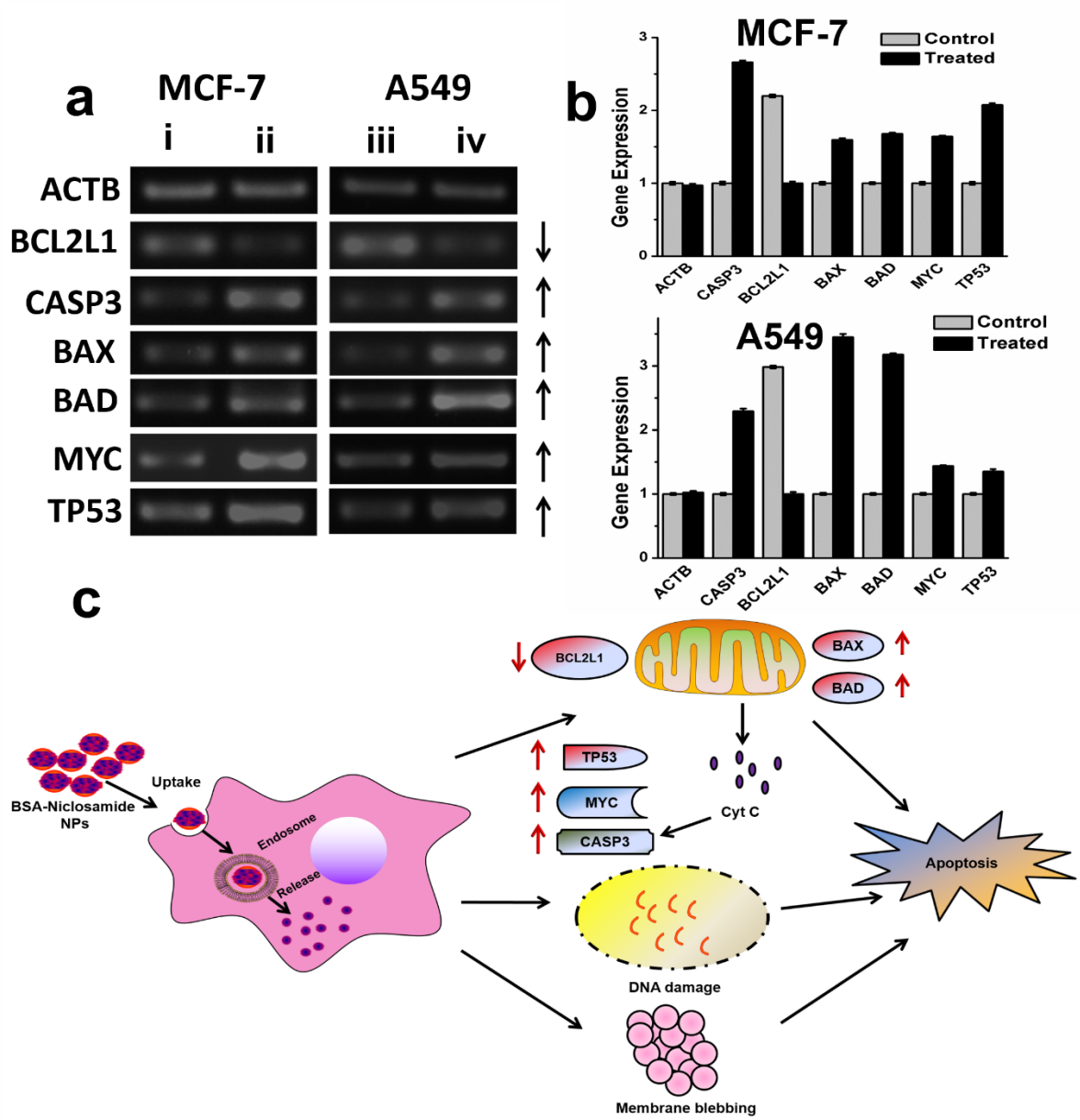

Figure 4.14 (a) Semi quantitative RT-PCR analysis of apoptotic signaling genes (i and iii) untreated control MCF-7 and A549 cells, respectively; (ii and iv) BSA-Nic NPs treated MCF-7 and A549 cells, respectively (b) Quantitative expression analysis of apoptotic signaling genes in MCF-7 and A549 cells representing the fold increment in the expression of apoptotic signaling genes in treated cancer cells as compared to the control untreated cells. (c) Schematic representation of BSA-Nic NPs induced apoptosis (error bars denoted SD; *n*=3).

p53 (TP53) gene, a key factor which play an important role in apoptosis was up regulated in the BSA-Nic NPs treated cells. It has been reported that TP53 protein up-regulates the pro-apoptotic gene BAX (Wolter et al., 1997). As, we observed an increment in the level of BAX expression suggesting the role of TP53 in their up-regulation. Similarly, c-myc (MYC) is also viewed as a promising target for anti-cancer drugs. The up-regulation of MYC, a known inducer of apoptosis, contributes further amplification of the apoptotic signals and down-regulation of anti-apoptotic genes BCL2L1.

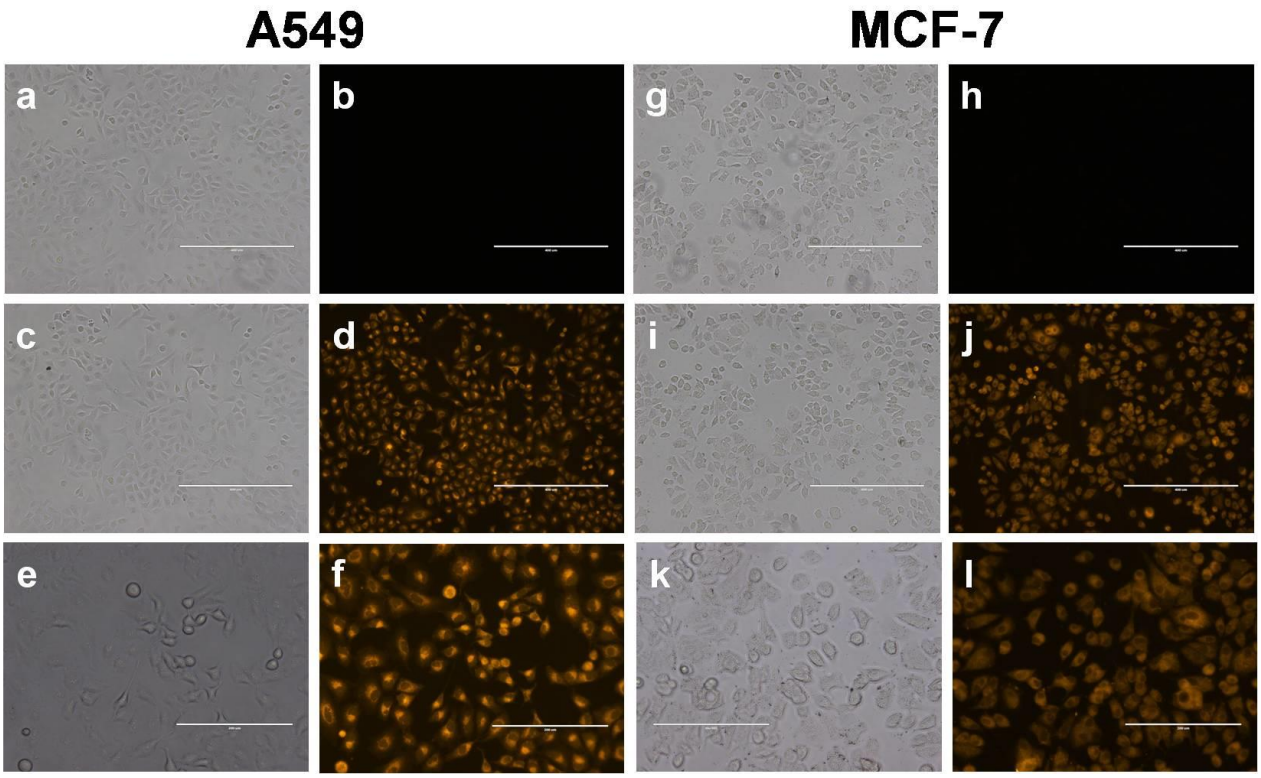

Figure 4.15 Cell uptake studies of BSA-Nic NPs on (a-f) A549 and (g-l) MCF-7 cells at different magnification. Bright field (a and g) and fluorescent images (b and h) of untreated cells did not show any fluorescence. Bright field (c, i, e and k) and fluorescent images (d, j, f and l) of rhodamine loaded BSA NPs treated cells. (c, d, I and j) at scale bar- 400 µm and (e, f, k and l) at scale bar- 200 µm.

Caspases (cysteine-aspartic acid proteases) are activated during apoptosis in many cells and are known to play a vital role in both initiation and execution of apoptosis. It was reported that caspase- 3 is accountable for the actual cleavage of cellular components during apoptosis (Fink et al., 2005). We found that in BSA-Nic NPs treated cells gene expression level of CASP3 was up-regulated, which suggested its role in BSA-Nic NPs mediated apoptosis. The gene expression profiles as mentioned above suggested that BSA-Nic NPs treatment of both the A549 and MCF-7 cells leads to programmed cell death, i.e. apoptosis and consequent cell blebbing.

4.13 Cellular uptake study

Systematic study for cellular uptake of BSA-Nic NPs by A549 and MCF-7 cells were performed by visualizing the fluorescence of rhodamine using fluorescence microscopy. As reported earlier, rhodamine loaded protein nanoparticles were used in the cell uptake studies of drug loaded protein nanoparticles (Rejinold et al., 2011). Rhodamine B is a red fluorescent dye, so the cells which uptake rhodamine loaded nanoparticles would typically appear bright red. Fluorescence microscopic images taken after 8-12 h of incubation revealed that, there was significant

internalization and retention of nanoparticles inside the cells (Figure 4.15). Images of control cells without any particles did not show any fluorescence, which further validates the study.

In summary, a novel anticancer drug loaded delivery system based on biodegradable BSA NPs was designed in the present study. This study is the first report of the enhanced solubilization and stability of niclosamide in aqueous environment by preparing a protein-drug nanoformulation via desolvation technique. It also allows us to eliminate the use of toxic organic compounds such as cremphor and DMSO. The prepared BSA-Nic NPs were characterized by DLS, FE-SEM, and AFM. Which corroborated that even after the drug incorporation, the particle size can be tuned within the optimal range for drug delivery applications. BSA-NPs showed improved sustained release of niclosamide in aqueous environment. Moreover, the MTT result revealed the non toxic nature of the nanocarrier and enhanced anti-proliferative ability of drug against breast and lung cancer cells *in vitro* than that of the free drug in aqueous medium. Morphological analysis of cells (*via* FE-SEM and AO/EB staining) and expression of apoptotic signaling genes (via semi-quantitative RT-PCR), further confirm the successful induction of apoptosis in BSA-Nic NPs treated cancer cells. The cellular uptake studies of BSA-Nic NPs using A549 and MCF-7 cells demonstrated significant internalization and retention of nanoparticles inside the cells, suggesting that these nanoparticles system can be used for delivering drug directly into the cells. Hence our studies suggest that the chemotherapeutic properties of niclosamide can be better exploited by encapsulating it in a protein based carrier for future clinical applications.

CHAPTER 5

INDUCTION OF APOPTOSIS BY FOLATE TARGETED ALBUMIN STABILIZED SILVER NANOPARTICLES

In this Chapter, a folate decorated albumin stabilized Ag NPs was synthesized to overcome various cytotoxicity and genotoxicity associated with Ag NPs. The therapeutic efficacy of FA-BSA-Ag NPs has been validated against A549 (FR (-ve)) and MCF-7 (FR (+ve)) cells. Further, the efficient induction of apoptosis by these nanoparticles was corroborated by ROS determination, cell cycle, morphological and nuclear analysis followed by gene expression analysis.

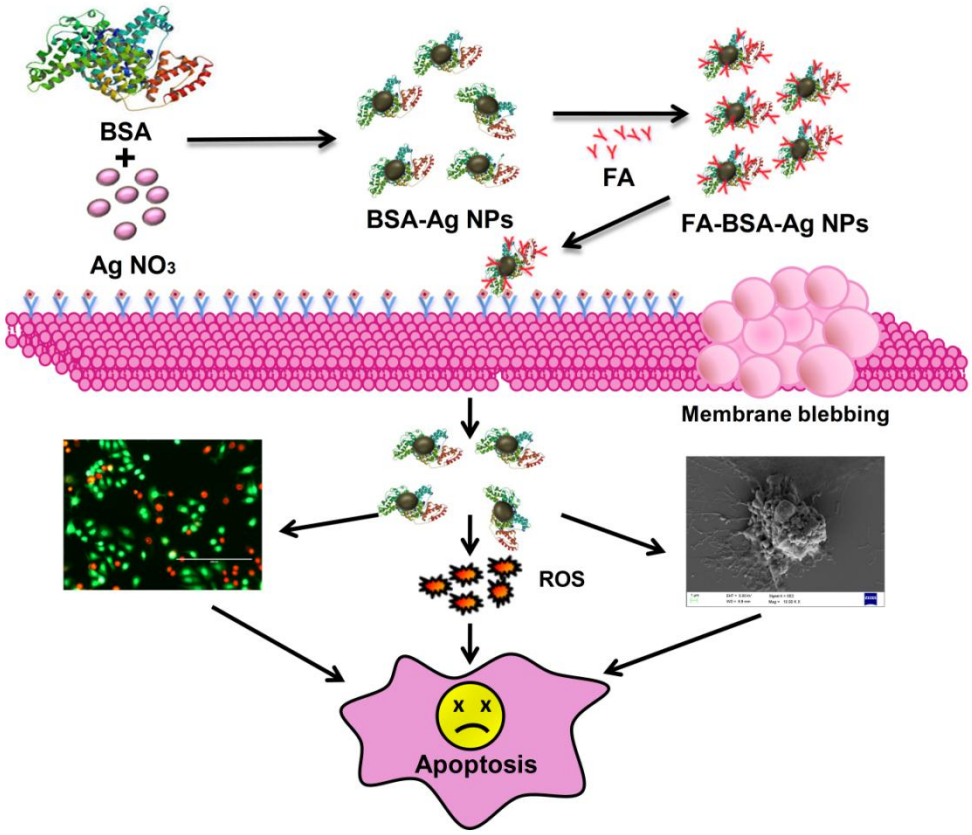

CHAPTER 5

INDUCTION OF APOPTOSIS BY FOLATE TARGETED ALBUMIN STABILIZED SILVER NANOPARTICLES

Overview

In current scenario, silver nanoparticles have been widely used in clinical and household products due to their broad spectrum antibacterial activity. But the cytotoxicity and genotoxicity associated with Ag NPs at higher concentration hindered its applications in the field of cancer therapy. The current study exploits the folate mediated delivery of bovine serum albumin stabilized Ag NPs and thereby overcoming various drawbacks associated with non specific targeting. The albumin coating enhanced the stability of Ag NPs and also provide surface for folate conjugation *via* carbodiimide reaction. Physicochemical characterization confirms the formation of folate decorated albumin stabilized Ag NPs. The prepared nanoparticles depict remarkable binding, especially in case of MCF-7 (FR-positive cells) having abundant folate receptor on its surface that leads to their enhanced cellular internalization as compared to A549 cells (FR negative cells). The cell viability assay corroborates a better therapeutic efficacy of prepared NPs against MCF-7 cells as compared to A549 cells. The flow cytometer analysis reveals reactive oxygen species increment that leads to oxidative stress induced apoptosis in both the cells. Further, cell cycle, morphological and nuclear analysis suggests characteristic apoptosis indications, which was further confirmed by gene expression analysis. Altogether, these studies implied that the tumor targeted FA-BSA Ag NPs induce apoptosis in MCF-7 cells at much lower Ag NPs concentration. In future, these targeted albumin stabilized Ag NPs could provide a more safe and effective alternative approach in the field of cancer therapy.

Results and discussion

5.1 Synthesis and characterization of FA-BSA-Ag NPs

The objective of current study is to develop an albumin based targeted therapeutic agent, where it serves the dual purpose by acting as a stabilizer of Ag NPs and provide free amino groups for the attachment of targeting moieties such as folic acid as shown in Figure 5.1. The Ag NPs were

synthesized by $NaBH_4$ reduction method in the presence of albumin as reported earlier (Gebregeorgis et al., 2013, Zhang et al., 2013). The formation of albumin stabilized Ag NPs was primarily studied by UV-visible spectroscopy showing the appearance of typical plasmonic band at 420 nm as shown in Figure 5.2. In the next step, folic acid a tumor targeting moiety was conjugated to the amines group present on the surface of BSA-Ag NPs *via* EDC/NHS coupling chemistry. The EDC and NHS activate the carboxylic acid groups of the folic acid which in turn combined with the amine groups of albumin. Figure 5.3(a) and (b) correspond to the elemental distribution and EDS pattern of FA-BSA-Ag NPs showing the existence of silver in the complex. The size and shape of the prepared NPs was determined by using TEM as shown in Figure 5.4(a) TEM image depicts that particles were spherical in shape having an average size around 8.21±2.98 nm; the size distribution histogram of FA-BSA-Ag NPs is shown in Figure 5.4(b). The bright spots in the selected area electron diffraction (SAED) pattern attributed to the crystalline nature of the Ag NPs with phases (111), (200), (220) and (311).

5.2 XRD and thermal stability studies

Figure 5.5(b) represents the XRD pattern of FA-BSA-Ag NPs. A well defined characteristic diffraction peak appeared at 38.07 ° that corresponds to (111) crystal plane of elemental silver (Gebregeorgis et al., 2013) depicting the presence of Ag NPs. In addition, broader peaks appeared around 20 ° as a result of amorphous nature of the coated albumin layer. Moreover, the thermo gravimetric analysis of BSA-Ag NPs, FA-BSA-Ag NPs and BSA alone were carried out under nitrogen atmosphere illustrating the slower rate of degradation for albumin- Ag NPs complexes i.e. BSA-Ag NPs and FA-BSA-Ag NPs as compared to pristine BSA. From Figure 5.5(a), it was clearly evident that the degradation of particles start from 200 °C and beyond 250 °C, a sudden weight loss was observed which account to the loss of small molecules i.e. ammonia, CO_2 etc. Around 400–500 °C, a substantial difference in weight loss was examined, as 21% was left for pristine BSA, 38% was left for FA-BSA–Ag NPs and 40% was remaining for BSA-Ag NPs indicating the improved stability of BSA–Ag NPs and FA-BSA-Ag NPs as compared to pristine BSA. Beyond 500 °C, a rapid rate of degradation was noticed in case of BSA-Ag NPs, which may be as a result of crystalline nature of Ag NPs. However, a slower rate of degradation was observed for FA-BSA-Ag NPs due to the presence of folic acid. Moreover, beyond 600 °C no significant change was noticed for BSA and BSA-Ag NPs due to the char formation, while in case of FA-BSA-Ag NPs a sudden weight loss was found, thus confirming the presence of folic acid (Gebregeorgis et al., 2013).

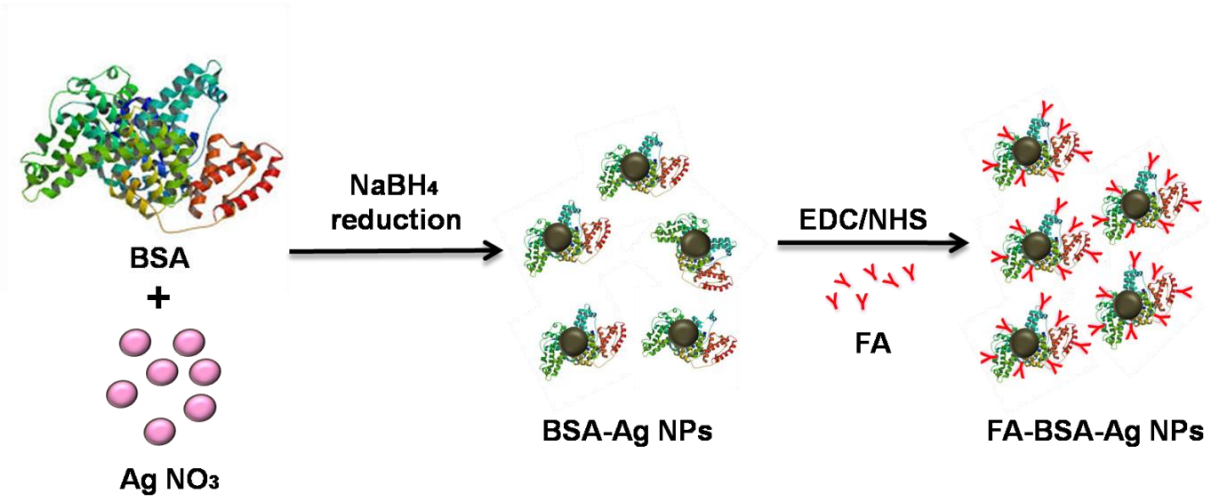

Figure 5.1 A schematic representation of preparation of FA conjugated albumin stabilized silver nanoparticles. The structure of BSA (PDB ID: 3V03) was imported from RCSB protein data bank.

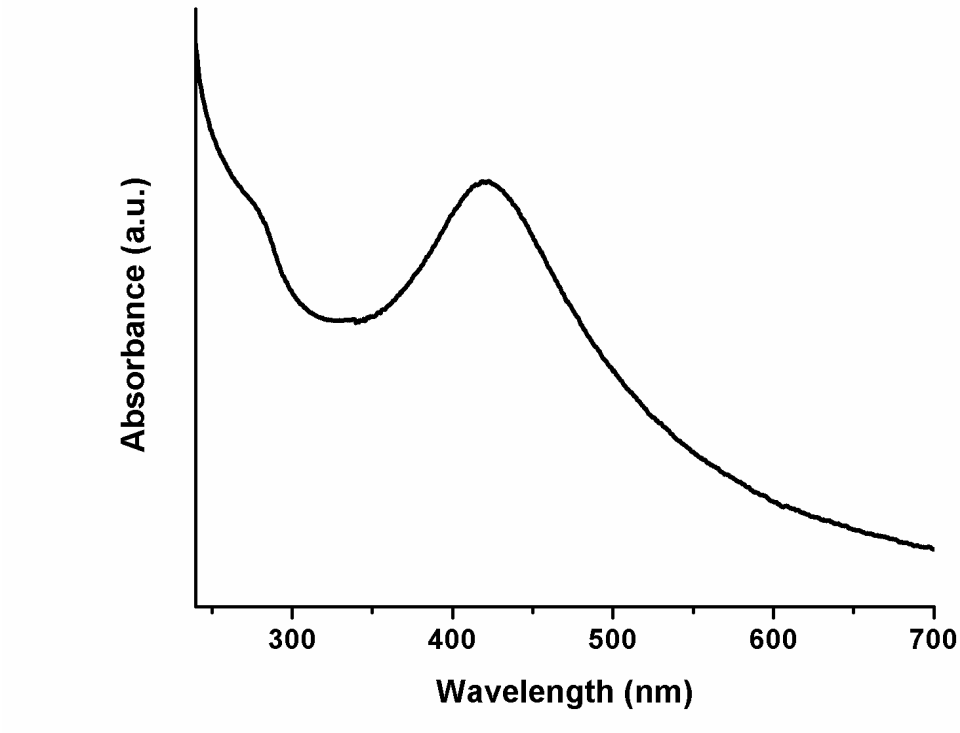

Figure 5.2 UV-visible absorption spectrum of BSA-Ag NPs.

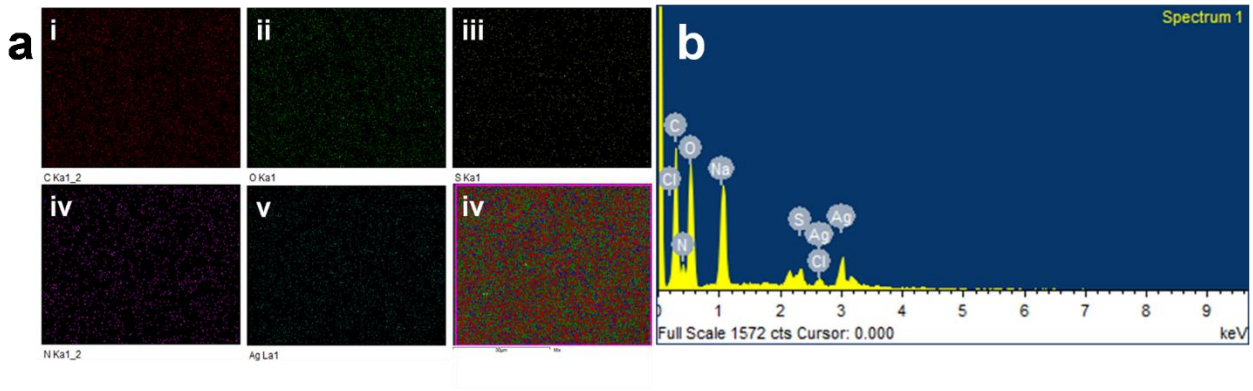

Figure 5.3 (a) Color coded SEM/EDX dot maps depicting the individual elemental distribution in FA-BSA-Ag NPs from (i-v) red for carbon, green for oxygen, yellow for sulphur, purple for nitrogen, blue for silver and (iv) overlay image. (b) Energy dispersive spectra of FA-BSA- Ag NPs.

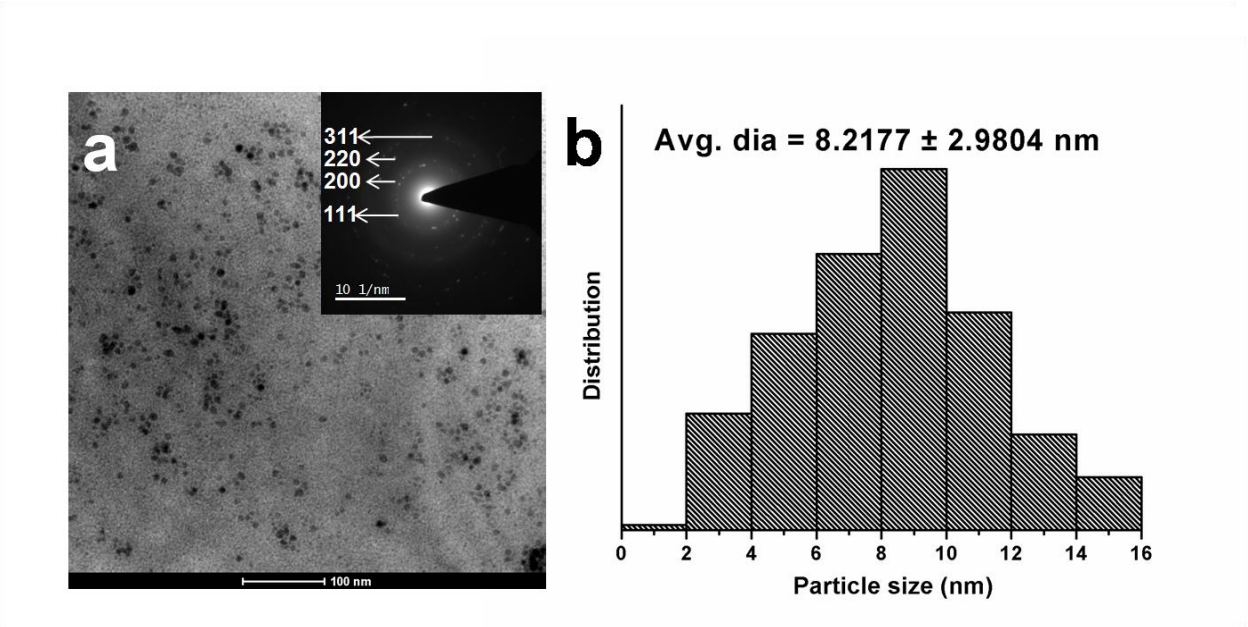

Figure 5.4 Characterization of as prepared FA-BSA-Ag NPs (a) TEM image (scale bar: 100 nm) with corresponding SAED pattern (inset) (b) Particle size distribution histogram of FA-BSA-Ag NPs.

5.3 FTIR analysis

The conjugation of BSA-Ag NPs with FA was typified by FTIR analysis. The FTIR spectrum of FA, BSA-Ag NPs and FA conjugated BSA-Ag NPs are shown in Figure 5.6. The characteristic peaks of BSA-Ag NPs and FA alone were illustrated in Table 5.1 and 5.2 (Bhushan et al., 2015b, El-Wahed et al., 2008). On comparing the BSA-Ag NPs with FA-BSA-Ag NPs, a major shift in the peaks were observed from 3306.5 to 3331.1, 2959.57 to 2931.51, 1537.43 to 1540.39, 1391.6 to 1397.52, 1242.2 to 1247.69 cm^{-1} corresponding to the stretching vibration of –OH groups, stretching vibration of N-H groups, stretching vibration of C-O groups and N-H bend respectively, along with other peaks shift confirms the interaction between the FA and BSA-Ag NPs. In case of FTIR spectrum of the FA-BSA–Ag NPs, a peak was observed at 1021.06 cm^{-1} as a result of augmented –CH bending of alkenes and a decline in anhydride C–O stretching of FA involved in the reaction. Moreover, the appearance of new peaks at 1451.39 cm^{-1}, corresponding to the phenyl ring of folic acid along with other bands confirms the successful conjugation of FA to the BSA-Ag NPs (Chowdhuri et al., 2015, Mewada et al., 2014).

5.4 *In vitro* cytotoxicity

In vitro cytotoxicity assay of BSA-Ag NPs and FA-BSA-Ag NPs was assessed *via* MTT assay on MCF-7 and A549 cells. An upregulation of folate receptor was observed in specific cancer cells such as human breast cancer cells, MCF-7 (FR-positive cells). Thus the FA-BSA-Ag NPs specifically target the breast cancer as compared to A549 (FR-negative cells). In Figure 5.7 the bare BSA was analyzed for their cytotoxicity against both the cells and found to be non toxic. After 24 h, more than 90 % cell viability was found considering the biocompatibility of BSA. Thus the results suggest that the therapeutic efficacy of FA-BSA-Ag NPs was due to Ag NPs and not because of the stabilizing agents.

Moreover, the effect of BSA-Ag NPs and FA-BSA-Ag NPs on the viability of A549 and MCF-7 cells were evaluated by MTT assay as illustrated in Figure 5.8, the results suggests a concentration dependent inhibition of cell viability by BSA-Ag NPs and FA-BSA-Ag NPs. However, the cell inhibition capability of FA-BSA-Ag NPs was enhanced significantly (around 2.59 fold) in MCF-7 as compared to BSA-Ag NPs, while a little increment was observed (around 1.36 fold) for A549 cells. The IC_{50} value of BSA-Ag NPs was found to be 14.21 and 5.97 μg mL^{-1} and of FA-BSA-Ag NPs was found to be 11 and 2.3 μg mL^{-1} on A549 and MCF-7 cells respectively, illustrating that the FA-BSA-Ag NPs exhibit excellent cytotoxicity

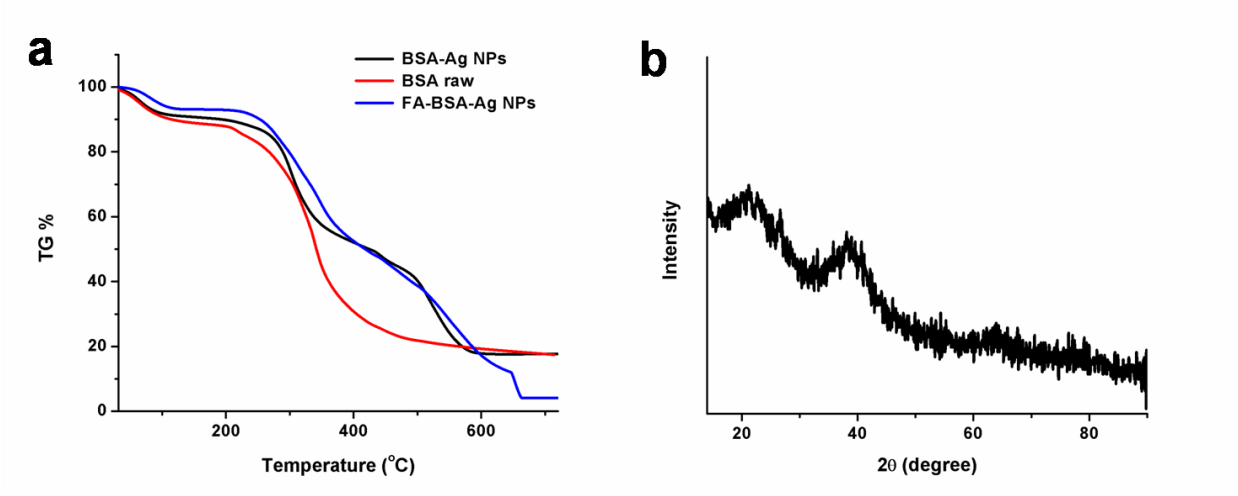

Figure 5.5 (a) TG data curve of BSA (control), BSA-Ag NPs and FA conjugated BSA-Ag NPs. (b) XRD pattern of FA-BSA-Ag NPs.

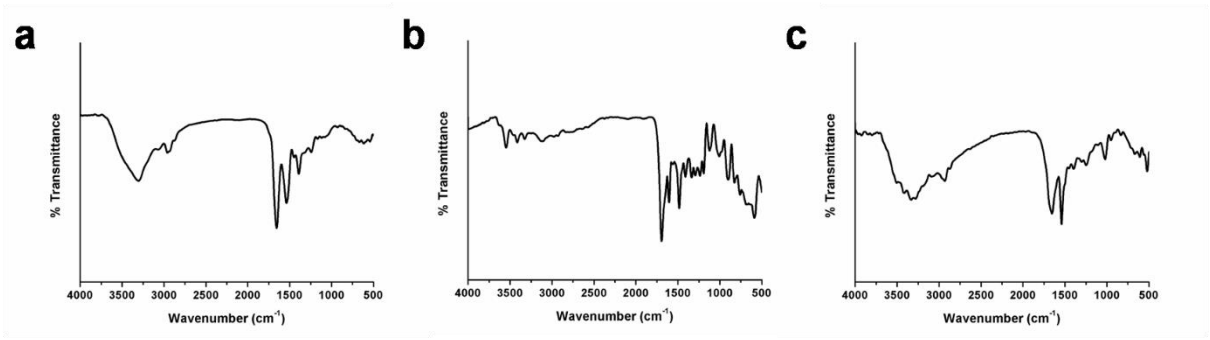

Figure 5.6 FTIR spectra of BSA-Ag NPs, FA and FA conjugated BSA-Ag NPs.

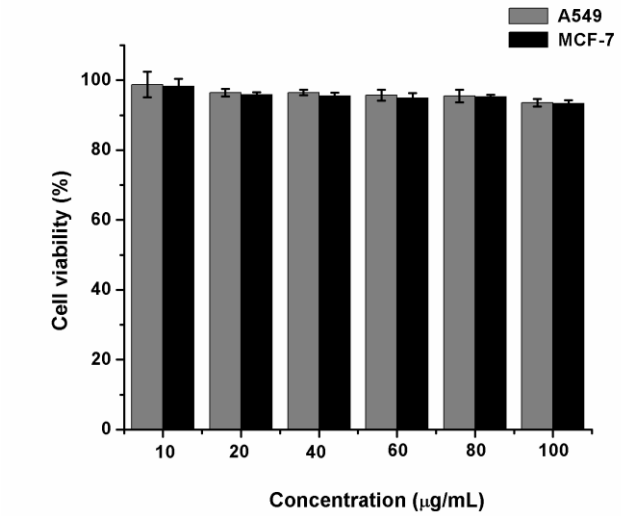

Figure 5.7 Cell viability assay (MTT assay) of BSA after 24h of treatment (error bars denoted SD; *n*=3).

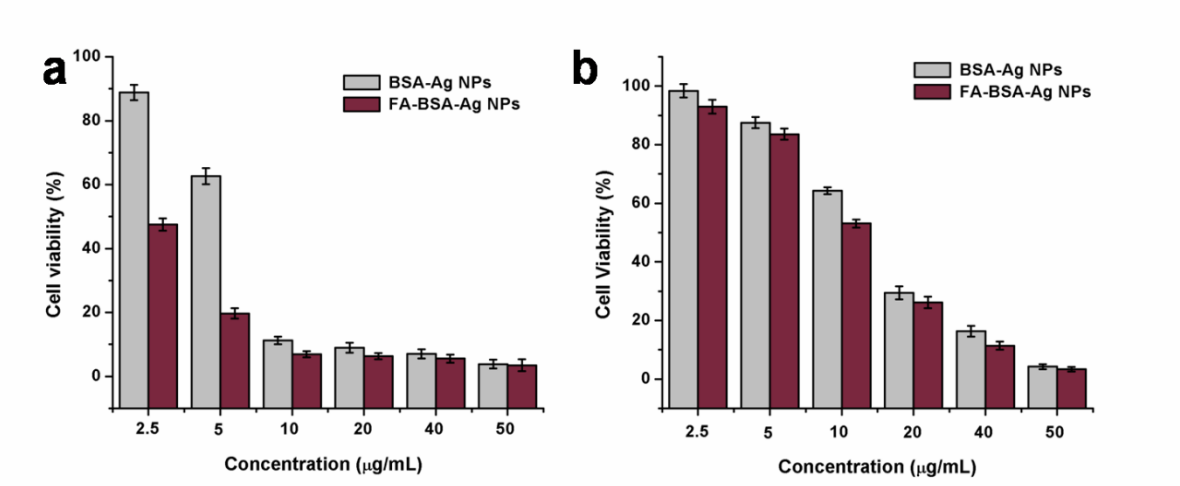

Figure 5.8 Cell viability of (a) MCF-7 cells (b) A549 cells as calculated from MTT assay. The cells were treated with BSA-Ag NPs and FA conjugated BSA-Ag NPs (having equivalent concentration of Ag) for 24h (error bars denoted SD; *n*=3).

Functional groups	-OH	N-H (amide A)	C=O (amide I)	N-H (amide II)	C-O	N-H (amide III)	C-H	C-H (aromatic)
Wave No. (cm^{-1})	3306.5	2959.57	1655.84	1537.43	1391.66	1242.24	1166.42	613.28
Vibration	-OH stretch	N-H stretch	C=O stretch	N-H bend	C-O stretch	N-H bend	C-H bend	C-H bend

Table 5.1 Characteristic major absorption bands in the IR spectra of the BSA-Ag NPs.

Functional groups	-OH	-N-H	$-CH_2$	C=O	$-CH_2$	COO-	C-C	C-N	C-O	C-H	C-O
Wave No. (cm^{-1})	3414.54	3325.76	3107.41	1694.33	1484.49	1335.35	1292.2	1236.98	1006.75	757.87	589.89
Vibration	-OH stretch	-N-H	$-CH_2$	C=O stretch	$-CH_2$	COO-	C-C	C-N	C-O stretch	C-H bend	C-O bend

Table 5.2 Characteristic major absorption bands in the IR spectra of the raw folic acid powder.

against both the cells as compared to BSA-Ag NPs. However, the enhanced therapeutic efficacy and greater suppression effect was observed on MCF-7 (FR-positive) cells treated with FA-BSA-Ag NPs. Thus the results suggests that the FA modification of BSA-Ag NPs improve therapeutic efficacy by facilitating the FR mediated cellular uptake and therefore induce apoptosis at much lower concentration of Ag NPs.

5.5 AO/EB Dual Staining

The mode of cell death in FA-BSA-Ag NPs treated A549 and MCF-7 cells was determined by staining the cells with a combination of fluorescent DNA intercalating dual dyes (i.e. AO/EB) and then examined them under fluorescent microscope. The AO dye was taken up by both viable and non viable cells and gives green fluorescence after binding with double stranded DNA. While, EB can permeate only membrane compromised cells and bind to the double stranded DNA to produce red fluorescence. The difference in the permeation capability of both dyes makes it possible to differentiate between the viable, apoptotic and necrotic cells (Uday kumar et al., 2014). The viable healthy cells effectively exclude the EB stain and it appears uniform green colored fluorescent nucleus due to the presence of AO alone as shown in Figure 5.9 (a and e). Similarly, the cells treated with half the IC_{50} concentration does not show any significant change in the cells morphology and also emit green color fluorescence as shown in Figure 5.9 (b and d). While the cells treated with IC_{50} and 2 x IC_{50} concentrations shows typical morphological changes corresponds to the apoptosis such as cytoplasmic constriction, membrane blebbing and nuclear fragmentation (Rello et al., 2005, Uday Kumar et al., 2014). Figure 5.9(c-d and g-h), clearly demonstrate the existence of early apoptosis (EA) characterized by condensed chromatin in the treated cells along with late apoptosis (LA) characterized by fragmented nuclei and apoptotic bodies. These morphological changes clearly depict the induction of apoptosis in the A549 and MCF-7 cells treated with FA-BSA-Ag NPs. Moreover, the FA modification augmented the apoptosis effect in MCF-7 cells as compared to A549, which may be due to the different expression levels of FR on the surface of two cells. The MCF-7 cells actively uptake FA-BSA-Ag NPs *via* folic acid mediated endocytic pathway. Thus, the above results are in correlation with the results obtained from MTT assay.

5.6 FE-SEM studies

Further morphological assessment of induction of apoptosis was done in FA-BSA-Ag NPs treated A549 and MCF-7 cells by using FE-SEM analysis. Fig. 5.10(a and c) clearly depict the characteristic healthy morphology of untreated cells which adhere well to the surface with no

substantiation of membrane constriction. While, in case of cells treated with FA-BSA-Ag NPs shows loosely attached rounded spherical morphology as compared to untreated cells as shown in Figure 5.10(b and d). Moreover, the events of apoptotic cell death such as membrane blebbing, formation of apoptotic bodies and cytoplasmic constriction were clearly visible in both the cell lines (Rello et al., 2005).

5.7 Hoechst-Rho B staining

In addition to AO/EB and FE-SEM analysis, further time dependent assessment of induction of apoptosis was done by using Hoechst-Rho B staining to monitor the cytoskeleton compaction and nuclear fragmentation. Hoechst 33342, a membrane permeable dye that stain nucleus and emit blue fluorescence on combining with the dsDNA. It is used to differentiate the untreated cells having normal nucleus with apoptotic cells having nucleus with condensed chromatin (pycnotic nucleus) (Allen et al., 2001). On the other hand Rho B stains the cytoplasm and mitochondria of the cells (Uday Kumar et al., 2014). Figure 5.11 clearly depict the time dependent chromatin condensation in the nucleus appearing in the form of dark spots (indicated by white arrows) accompanied with simultaneous cytoplasm constriction (as indicated by yellow arrows). Moreover, after 24 h of incubation a significant number of pycnotic nuclei were observed suggesting apoptotic mode of cell death. Altogether, all these morphological analysis suggest the role of FA-BSA-Ag NPs in inducing apoptotic cell death in A549 and MCF-7 cells.

5.8 Cellular uptake study

As reported earlier, the FA conjugates bind to the FR on the cancer cells with same affinity as that of FA alone and get internalized through plasma membrane *via* FA mediated specialized endocytosis and vesicular trafficking (Wang et al., 1998). In order to quantify the uptake of silver nanoparticles by MCF-7 and A549 cells ICP-MS analysis were conducted. Both the cells were treated with different concentration of FA-BSA-Ag NPs for 3h. As shown in Figure 5.12, a concentration dependent increase in the Ag NPs uptake was observed for both cells. However, amount of Ag NPs uptake was found to be significantly higher in case of MCF-7 as compared to A549 cells suggesting the successful FA mediated targeted delivery of Ag NPs in MCF-7 cells. This held accountable for the higher cytotoxicity in MCF-7 as compared to A549 as observed in MTT assay.

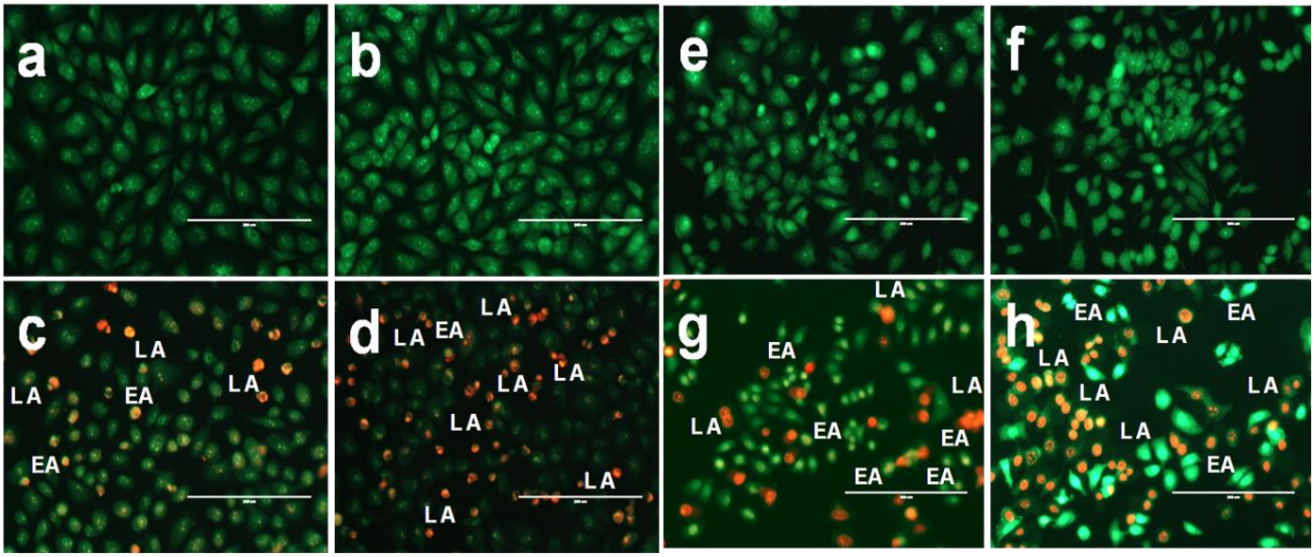

Figure 5.9 Representative images of AO/EB dual staining of (a and e) untreated (b and f) 0.5x IC_{50} (c and g) IC_{50} and (d and h) 2x IC_{50} FA- BSA–Ag NPs treated (a-d) A549 and (e-h) MCF-7 cells after 24 h of treatment.

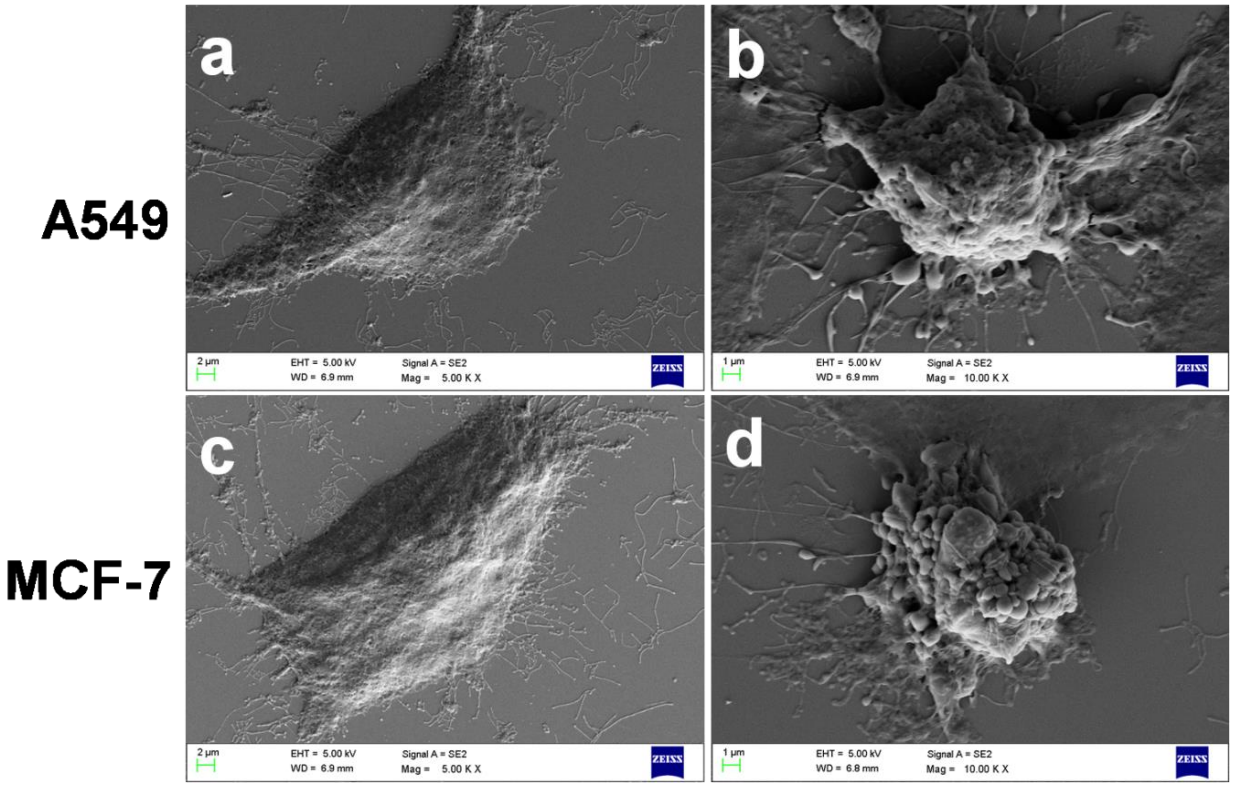

Figure 5.10 Representative FE-SEM images of (a and c) untreated and (b and d) treated A549 and MCF-7 cells.

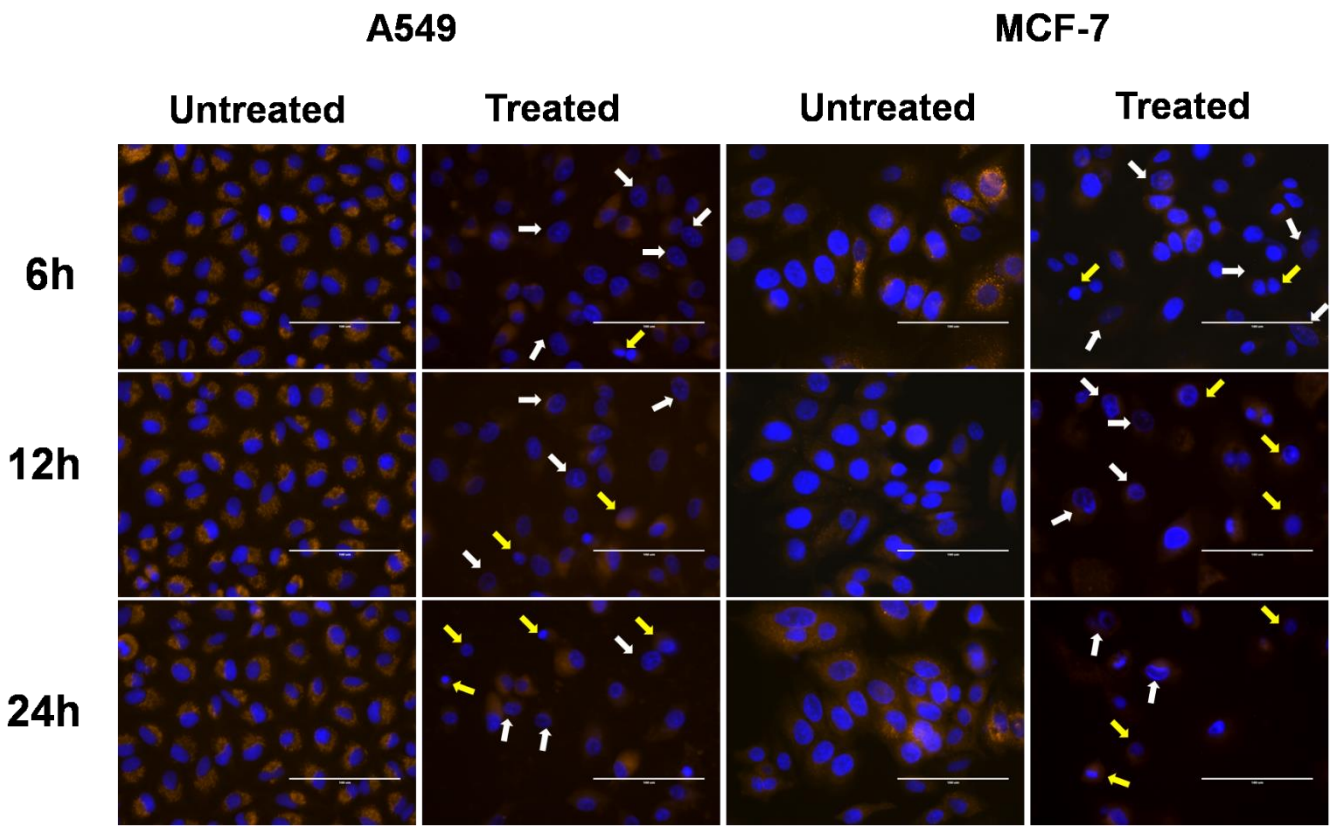

Figure 5.11 Time-dependent overlay images of untreated and FA-BSA-Ag NPs (IC_{50}) treated MCF-7 and A549 cells stained with Hoechst 33342 (blue) and co-stained with rhodamine B (red). White arrows indicate chromatin condensation (dark spots) and yellow arrows point towards cytoskeleton compaction. Scale bar: 100 μm.

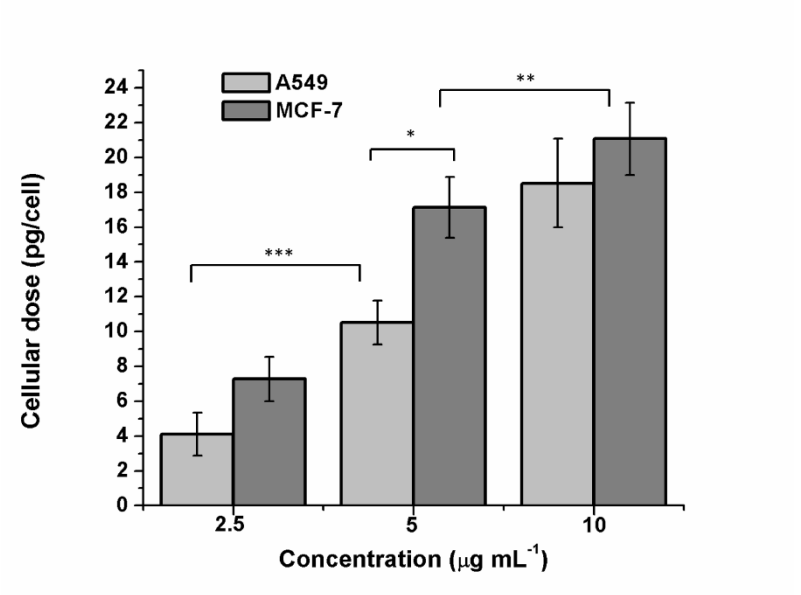

Figure 5.12 Cellular uptake of Ag in A549 and MCF-7 cells treated with different concentrations of FA-BSA-Ag NPs after 3 h. The statistically significant values are denoted by *$p < 0.05$, **$p < 0.005$ and ***$p < 0.001$ (error bars denoted SD; n=3).

5.9 Intracellular ROS determination

Reactive oxygen species induced oxidative stress is one of the crucial factors responsible for the cytotoxicity of Ag NPs as reported earlier (Lee et al., 2014, Chairuangkitti et al., 2013). Intrinsic antioxidant defence system protects the body against ROS by keeping a balance between the oxidant/antioxidant levels in the cells. However, excessive ROS generation caused due to the impaired antioxidant defence system of the body lead to the induction of oxidative stress, which finally results in the DNA damage, mitochondrial dysfunction and apoptotic cell death (Bhushan et al., 2015a, Sharma et al., 2014). The ROS levels on FA-BSA-Ag NPs treatment was investigated by using DCFH-DA assay using flow cytometer in order to assess their potential role in oxidative stress mediated cell death. Figure 5.13 depicts the level of ROS generation in FA-BSA-Ag NPs treated MCF-7 and A549 cells. The percentage of ROS producing cells were 2 % and 2.4 % in untreated MCF-7 and A549 cells respectively, which increased to 8.4% and 5 % on treating the MCF-7 and A549 cells respectively with 0.5x IC_{50} concentration. Moreover, in case of cells treated with IC_{50} and 2 x IC_{50} concentrations a significant increase in the ROS level was found. In MCF-7 the elevated ROS level at IC_{50} and 2x IC_{50} concentrations was found to be 24.1 and 41.2 % as compared to 18.1 and 26.3 % of ROS producing cell population in A549 cells respectively. These results suggest that the FA-BSA-Ag NPs induced more oxidative stress in MCF-7 as compared to A549 cells due to the FA mediated targeted delivery of Ag NPs that evokes more ROS generation in MCF-7 cells. The results are in correlation with the MTT and uptake studies.

5.10 Cell Cycle Analysis

Ag NPs is well known to induce oxidative DNA damage and chromosomal aberrations that results in the cell cycle arrest (Asharani et al., 2009, Sharma et al., 2014). The induction of apoptotic mode of cell death on FA-BSA-Ag NPs exposure was measured by PI staining, followed by flow cytometric analysis. Figure 5.14 demonstrate the effect of FA-BSA-Ag NPs on the cell cycle distribution pattern of A549 and MCF-7 cells incubated with desired concentrations FA-BSA-Ag NPs for 24 h. The results depicted that low concentration of FA-BSA-Ag NPs (i.e. 0.5x IC_{50}) did not produce any notable change in the cell cycle as compared to the untreated cells; most of the cells were found to be primarily in G0/G1 phase. However, at higher concentration (i.e. IC_{50} and 2x IC_{50}), a noticeable increase in the sub G0/G1 population accompanied by decrease in G0/G1 phase was observed with respect to untreated cells. Moreover, a marked decrease in the S phase was also monitored upon FA-BSA-Ag NPs exposure. Thus, an increase in the sub G0/G1 phase and decrease in the S phase population at

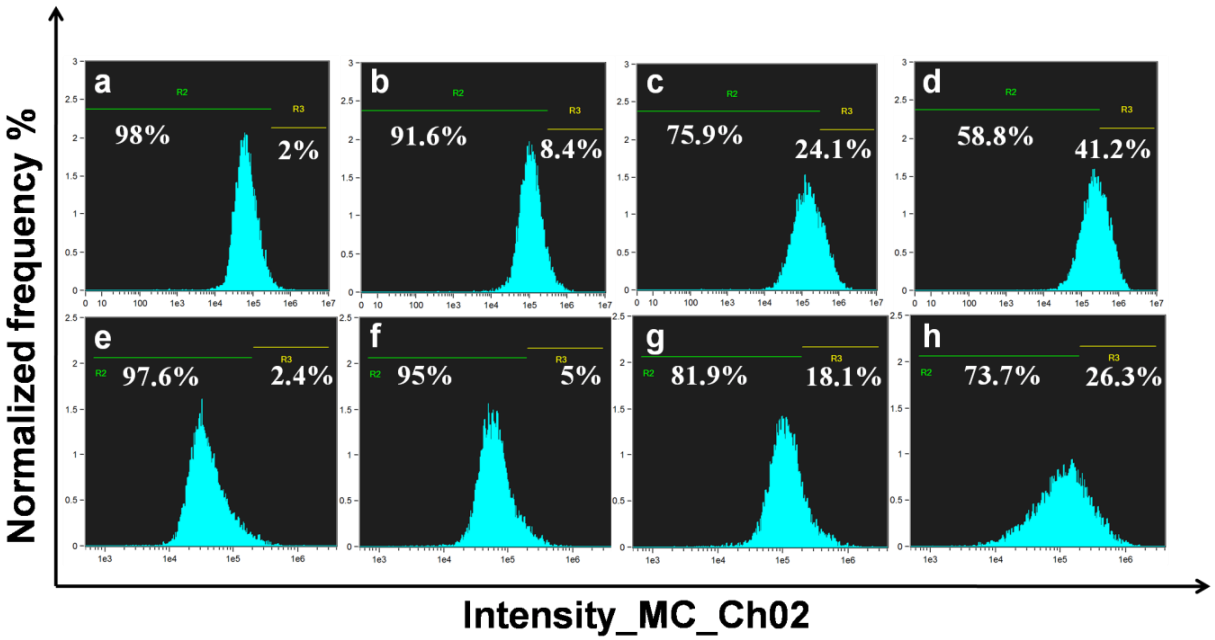

Figure 5.13 Flow cytometric analyses of ROS production in (a and e) untreated (b and f) 0.5x IC_{50} (c and g) IC_{50} and (d and h) 2x IC_{50} FA- BSA–Ag NPs treated (a-d) MCF-7 and (e-h) A549 cells.

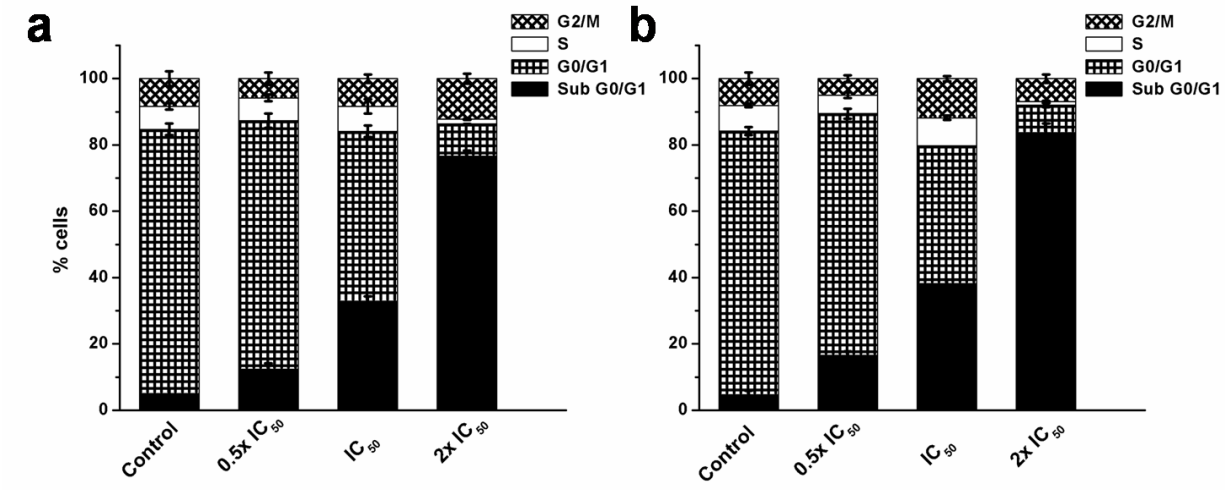

Figure 5.14 Effect of FA-BSA-Ag NPs on cell cycle in (a) A549 and (b) MCF-7 cells evaluated by calculating the percentage of cells in each phase from flow cytometric data (error bars denoted SD; *n*=3).

IC_{50} and 2x IC_{50} corresponds to the apoptotic mode of cell death (Riccardi et al., 2006, Darzynkiewicz et al., 1992).

5.11 Gene expression analysis

The potential of FA-BSA-Ag NPs to provoke apoptosis in human lung and breast cancer cells was investigated *in vitro* by means of semi-quantitative RT-PCR analysis, results suggested that the involvement of various pro-apoptotic signalling genes includes caspase 3 (CASP3), BAX, BAD, c myc (MYC), p53 (TP53) and anti-apoptotic signalling genes including bcl-xl (BCL2L1) as shown in Figure 5.15. While, β-actin (ACTB, housekeeping gene) was taken as internal control, whose expression remains unaltered during the process. As depicted in Figure 5.15(a) an upregulation was observed in the expression of pro-apoptotic genes (indicated by upward arrow), while the expression of anti-apoptotic genes was found to be down-regulated (indicated by downward arrow). Moreover, the fold change in the expression of genes was shown in Figure 5.15(b).

The apoptotic pathway involved in the FA-BSA-Ag NPs treated cells was shown in Figure 5.15(c). The FA-BSA-Ag NPs treatment leads to membrane destabilization and intracellular ROS generation, which in turn activates the intracellular signalling pathway that finally results in the activation of TP53 (Gopinath et al., 2010, Dubey et al., 2015 b). The anti-apoptotic BCL2L1 (basal cell lymphoma-extra large), a member of bcl-2 family located on the outer mitochondrial membrane prevent the cells from entering into apoptotic pathway by blocking the mitochondrial release of cytochrome-c by controlling the membrane permeability either via formation of pores or by creating an ion channel (Minn et al., 1997). While pro-apoptotic BAX and BAD promote such release and thereby endorses apoptosis by inhibiting the anti-apoptotic function of BCL2L1 (Yang et al., 1995, Boise et al., 1993). A down-regulation in the expression of BCL2L1 along with subsequent up-regulation of BAD and BAX suggests a successful initiation of apoptosis. Moreover, as reported earlier TP53 is found to be involved in the up-regulation of BAX (Wolter et al., 1997). An increase in the expression of BAX suggests the involvement of TP53 in the apoptotic cell death in FA-BSA-Ag NPs treated cells. Further, outer membrane permeabilization (MOMP) results in the translocation of BAX from cytosol to mitochondria, which leads to the release of cytochrome c, a pro-apoptotic molecule into the cytoplasm *via* pores formation (Wolter et al., 1997). Finally, the cytochrome c activate the CASP3, a key factor both in the initiation and execution of apoptosis and also accountable for the cellular DNA fragmentation during apoptosis (Liu et al., 1996, Fink et al., 2005, Hengartner, 2000).

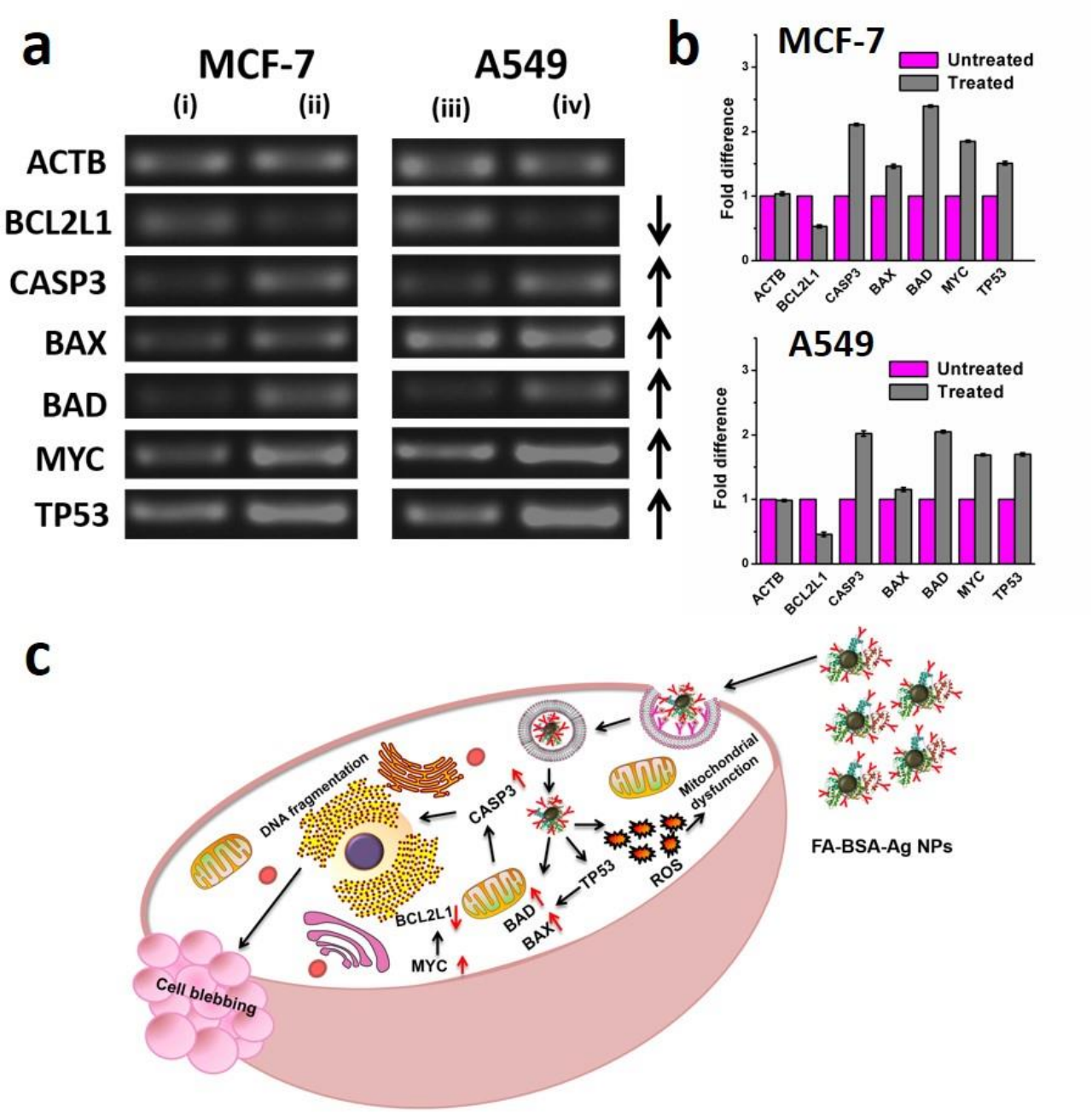

Figure 5.15 (a) Semi-quantitative RT-PCR analysis of apoptotic signaling genes (i and iii) untreated control MCF-7 and A549 cells, respectively; (ii and iv) FA- BSA–Ag NPs treated MCF-7 and A549 cells, respectively (b) quantitative expression analysis of apoptotic signaling genes in MCF-7 and A549 cells representing the fold increment in the expression of apoptotic signaling genes in treated cancer cells as compared to the control untreated cells. (c) Schematic representation of FA-BSA–Ag NPs induced apoptosis (error bars denoted SD; *n*=3).

An up-regulation in the expression of CASP3 suggests their role in the apoptosis in FA-BSA-Ag NPs treated cells. In addition to that an increased expression of MYC, a well known inducer of apoptosis was also observed, which further validate the TP53 mediated apoptotic cell death. Our results were found in correlation with the previous studies (Gopinath et al., 2010, Hsin et al., 2008). Thus the above mentioned gene expression profiles clearly demonstrated the p53 mediated apoptotic cell death along with consequent cell blebbing in the FA-BSA-Ag NPs treated A549 and MCF-7cells.

In summary, folate decorated albumin stabilized Ag NPs were synthesized. The albumin coating not only provides stability but also provide charged amino groups required for the folic acid conjugation. The physicochemical characterization demonstrates the successful folate modification of NPs necessary for their targeted delivery. The MTT assays revealed the higher therapeutic efficacy of folate modified NPs as compared to unmodified NPs against FR positive human breast cancer cells. The cellular uptake study reveals enhanced uptake in MCF-7 as compared to A549 cells due to the cancer specific targeting of Ag NPs. Moreover, the morphological and nuclear analysis suggests successful initiation of apoptosis in both the cancer cells. Further, flow cytometer and gene expression analysis corroborates the efficient induction of apoptosis by two separate mechanistic ways including: ROS production and induction of apoptotic signalling pathway in both the cancer cells. Thus, the current studies proposed that the folate modified albumin stabilized Ag NPs elicit anti-proliferative response and induce apoptosis in FR positive cells at much lower concentration and thereby reduce the complications that hinders their role in the future nanomedicine and cancer therapeutic applications.

CHAPTER 6

NANOCERIA ENCAPSULATED ALBUMIN NANOPARTICLES AS A POTENTIAL ROS SCAVENGER

In this Chapter, an albumin nanoparticles based potential delivery system for nanoceria is reported that remains stable inside the cells and provide desired steady state level of therapeutic dose that helps in defending the cells against actively generating ROS over a period of time.

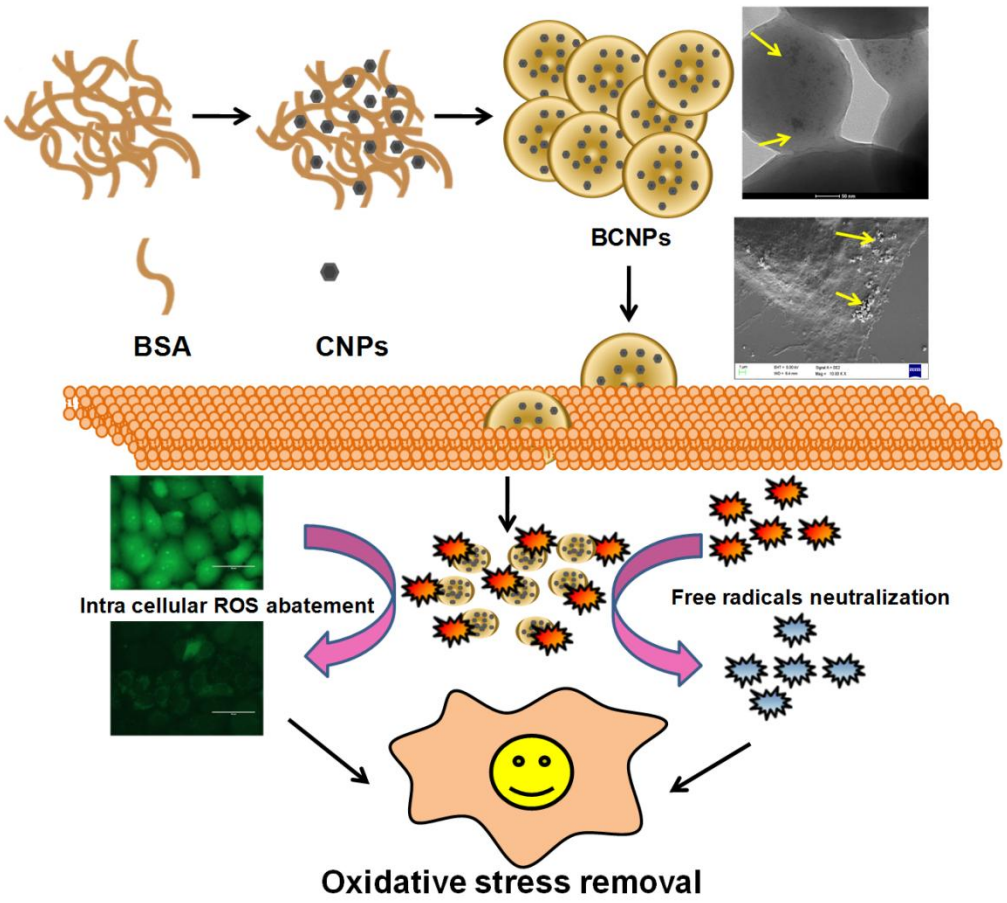

CHAPTER 6

NANOCERIA ENCAPSULATED ALBUMIN NANOPARTICLES AS A POTENTIAL ROS SCAVENGER

Overview

Several diseases and disorders including cancer are endorsed by the excessive oxidative stress caused due to incomplete removal of ROS by the antioxidant defense system of the body. Therefore present interest among the scientific community lies in the development of highly stable, biocompatible artificial enzymatic system that possesses a high ROS scavenging activity over a period of time. In recent years catalytic nanoparticles emerged as a potential candidate in the field of nanomedicine. Due to their inherent catalytic properties they are exploited as an artificial enzyme (nanozyme), to reinstate or correct aberrant enzymatic activities in patients. Among them cerium oxide nanoparticles/nanoceria emerged as a potent artificial redox enzyme, mimicking the activity of SOD and catalase and endure a tremendous ROS scavenging potential as depicted in a surfeit of human cell lines and animal models. In the present article, a facile synthesis of biocompatible nanoceria encapsulated albumin nanoparticles *via* desolvation technique that lead to the abatement of intracellular ROS is reported. Physico-chemical characterizations of as-prepared BCNPs corroborate the formation of highly monodispersed, spherical and aqueous stable delivery system. Interestingly, such entrapment does not affect the enzyme mimetic activity of CNPs as demonstrated by SOD assay. The biocompatibility and ROS scavenging potential of BCNPs were further assessed *in vitro* against human lung epithelial cells by cell viability assay and flow cytometric analysis, respectively. The quantitative and qualitative assessments of cellular uptake of BCNPs were done by ICP-MS, TEM and FE-SEM analysis. Furthermore, the BCNPs preserve the cell's antioxidant defense system and protect them from oxidant-mediated apoptosis as confirmed by semi-quantitative RT-PCR analysis. Thus, the as-prepared BCNPs could provide an opportunity to be utilized as a potential candidate against ROS induced diseases and disorders.

Results and discussion

6.1 Encapsulation of CNPs in albumin nanoparticles

CNPs were prepared by the hydrothermal method as described earlier (Liu et al., 2012). The prepared CNPs were evaluated by UV-visible spectrophotometer showing a characteristic broad absorption peak around 330 nm as shown in Figure 6.1. Figure 6.2 (a) indicates the TEM micrograph of the as-prepared CNPs. The TEM image implies that the average size of the uniformly distributed prepared CNPs was 4.35 ± 1.07 nm as shown in Figure 6.2(b) and Fig. S2 (c) depict the corresponding EDX pattern. The prepared CNPs were encapsulated inside the albumin nanoparticles *via* desolvation technique (Bhushan et al., 2015b), using ethanol as desolvating agent and glutaraldehyde as cross linking agent as shown in Figure 6.3. The bifunctional reagent glutaraldehyde endorses to the creation of Schiff bases among the two carbonyl groups of glutaraldehyde and the positively charged amino groups of protein resulted in the formation of least aggregated spherical BCNPs with uniform distribution.

6.2 Characterizations: Surface morphology and particle size

The surface morphology of the prepared BCNPs was determined by FE-SEM as shown in Figure 6.4(a). The FE-SEM micrograph of BCNPs depicts a spherical morphology with uniform distribution. Moreover, the TEM image of BCNPs as shown in Figure 6.4(c), clearly illustrated the distribution of CNPs inside the albumin nanoparticles, which confirmed the formation of CNPs encapsulated albumin nanoparticles.

The particle size distribution of prepared BCNPs was obtained by using DLS as shown in Figure 6.4(d). The average hydrodynamic size of the prepared BCNPs was found to be 278.4 nm. Further, the size of the BCNPs was also analyzed by AFM as shown in Figure 6.4(b). The average grain size of BCNPs was found to be 231.05 nm after processing the image through NOVA software. The size of the prepared nanoparticles lies within the optimal range comparable to the already prepared albumin based nanoparticles.

6.3 XRD analysis

Physical nature of the prepared BCNPs was assessed by XRD analysis. Figure 6.5(a) showed the XRD pattern of CNPs and BCNPs. The prepared CNPs have a cubic, fluorite type structure

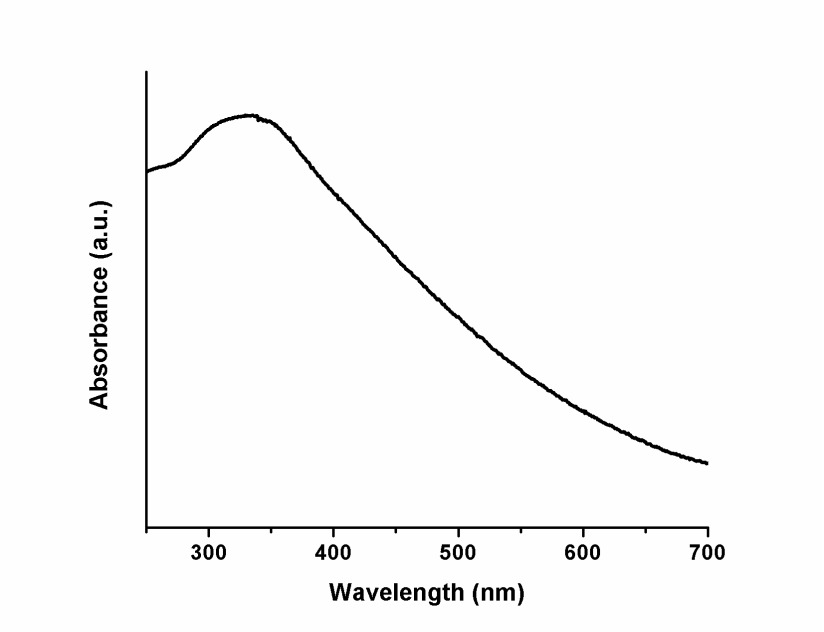

Figure 6.1 UV–visible absorption spectrum of prepared CNPs.

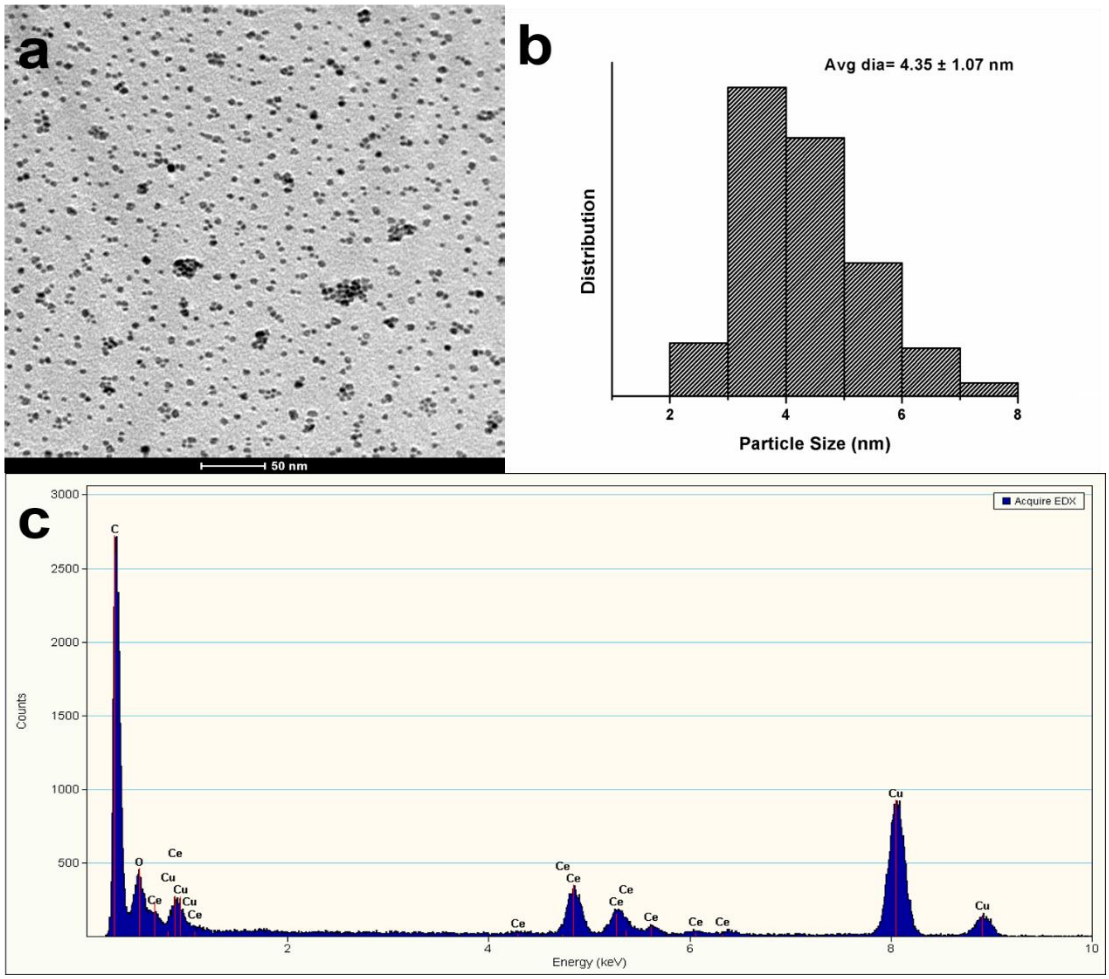

Figure 6.2 (a) TEM image of prepared CNPs. (scale bar: 50 nm) (b) Particle size distribution histogram of prepared CNPs. (c) Energy dispersive spectra of CNPs.

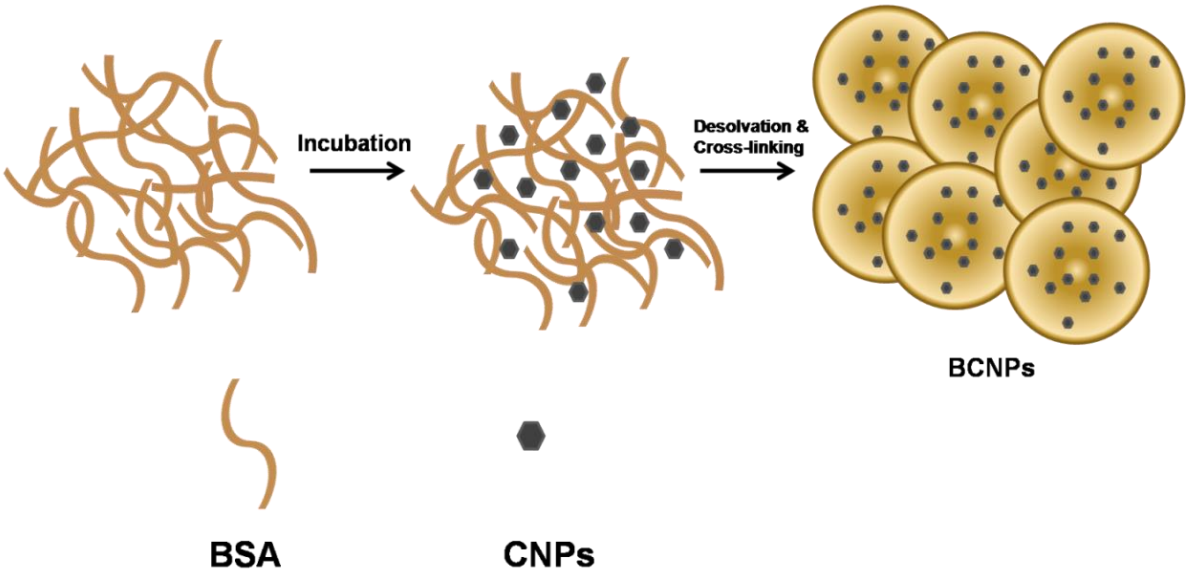

Figure 6.3 Schematic outline of nanoceria encapsulated albumin NPs fabrication by desolvation technique.

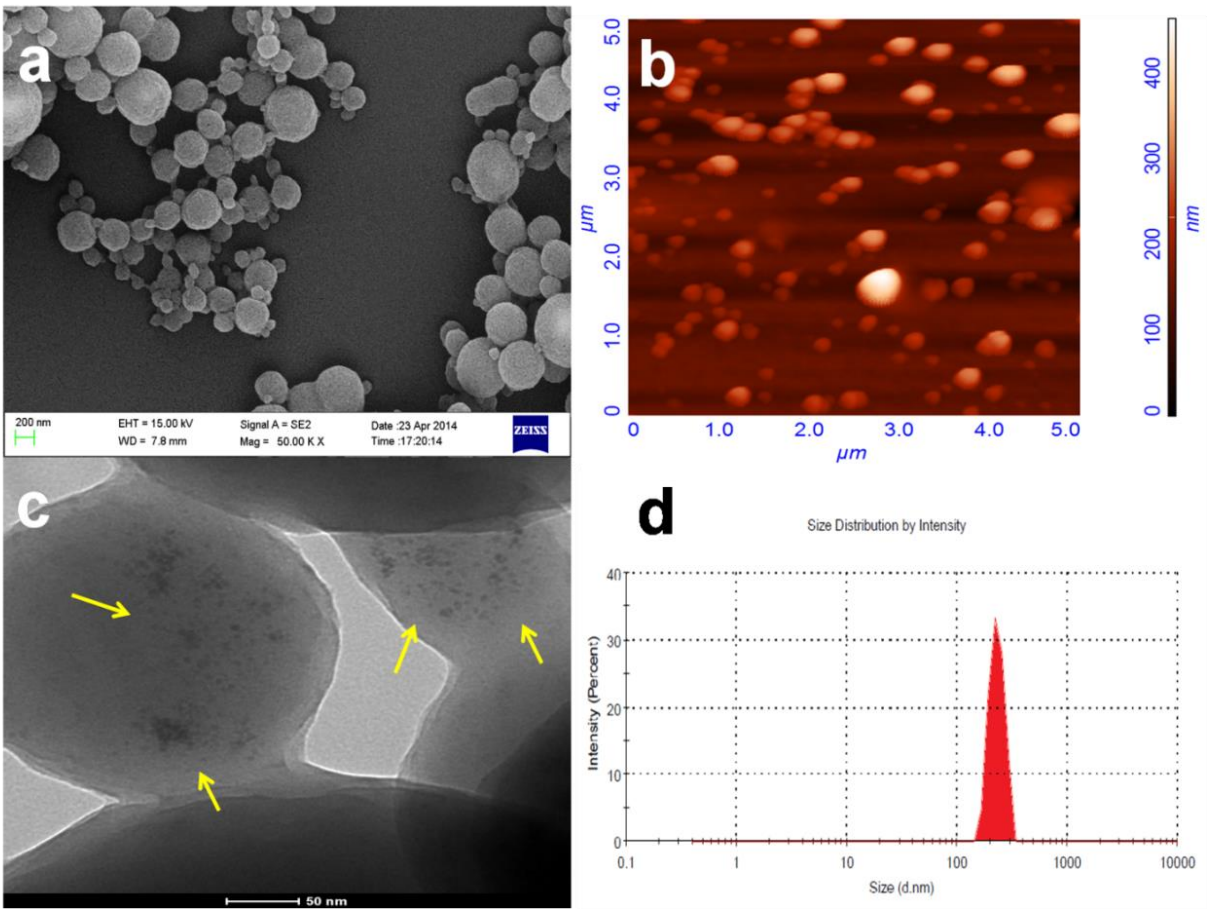

Figure 6.4 (a) FE-SEM and (b) AFM images of BCNPs showing their typical morphology (c) TEM image of BCNPs showing the encapsulated CNPs (indicated by yellow arrows) and (d) DLS image of BCNPs showing the distribution and size of nanoparticles.

showing a characteristic diffraction peaks at 28.5, 33.1, 47.4 and 56.3 corresponding to 111, 200, 220, 311 crystal planes that resembled with CeO_2 (JCPDS 78-0694). However, no such peaks were observed in case of BCNPs depicting the encapsulation of CNPs and no significant amount of CNPs were left in the system after interaction with protein. On comparing the prepared BCNPs with free CNPs, BCNPs were found to be more amorphous in nature, which might be due to the cross linking mechanism happening between the reactive functional groups of protein and CNPs along with the prominent electrostatic interaction between them may perhaps ascribe to the amorphous nature of the BCNPs (Rejinold et al., 2011).

6.4 FTIR analysis

Surface chemistry of the nanoparticles play crucial role in their interaction with protein. Several factors including hydrophobic interactions, electrostatic interaction and chemical interaction are among the leading factor responsible for protein-nanoparticle complex formation. As reported earlier electrostatic interaction was the major factor responsible for the CNPs interaction with BSA. Moreover, higher the positive zeta potential more will be the interaction. As in our case CNPs also have high value of zeta potential around 36.3 mV, while BSA have net negative charge in water (pH=7), suggesting that electrostatic interaction were mainly responsible for CNPs interaction with BSA (Patil et al., 2007, Yuan et al., 2011).

In Figure 6.5(b) major peaks were observed around 1652, 1540, 3070 and 3420 cm^{-1} for pristine BSA corresponding to the amide I (C=O stretching vibration), amide II (N–H bending vibration and C-N stretching vibration), amide A (-NH stretching vibration) and –OH stretching vibration respectively, as discussed previously (Bhushan et al., 2015b). While the FTIR spectrum of CNPs showing major characteristic peaks are listed in Table 6.1. Peaks around 3431.12, 1630.32 cm^{-1} corresponded to the physically adsorbed water on the surface of the CNPs, while the major peak around 439.51 cm^{-1} corresponding to the Ce-O stretching band confirms the formation of CNPs (Jiao et al., 2012, Kumar et al., 2013). The absorption peak around 2925.38 cm^{-1} could be assigned to a stretching vibration of the C-H group. Moreover, a strong peaks were observed at 1538.41 and 1455.76 cm^{-1} corresponds to the symmetric and asymmetric stretching vibration of carboxylic group of acetic acid. The spectra suggests that carboxyl group of acetic acid get chemically bound to the surface of synthesized CNPs imparting them high colloidal stability and zeta potential (Kumar et al., 2013, Pahari et al., 2011, Masui et al., 2002, Goharshadi et al., 2011, Girija et al., 2011). The chemical species on surfaces of CNPs were further indentified by TG analysis of CNPs depicting a slight weight loss in the temperature range between 25 and 900 ^oC. In Figure 6.6, upto 200 ^oC slight weight

loss was observed which corresponds to the desorption of the adsorbed water but beyond 200 ^{o}C a sudden loss in weight was observed as a result of carboxyl groups on the surface of CNPs confirming the FTIR outcomes (Jiao et al., 2012).

On comparing the IR spectra of CNPs, BSA alone and BCNPs as shown in Figure 6.5(b), a major shift in the peaks were observed from 3431.12 to 3298.27, 1455.76 to 1448.92 suggesting the involvement of –OH and C=O groups of CNPs in their interaction with protein. Moreover, in case of BCNPs, a characteristic suppression in the stretching frequency was observed and the peaks were appeared as a wide spectrum on account of possible interaction between the nanoparticles. A slight shift in the amide I, amide II and amide III peaks were observed, which may be attributed to the cross-linking mechanism amongst the protein amino groups and the possible interaction of protein with CNPs (Rejinold et al., 2011, Kong et al., 2007, Huang et al., 2010).

6.5 Thermal stability of the nanoparticles

The TG analysis was conducted for BCNPs and pristine BSA (control), results demonstrated the slower rate of degradation for BCNPs as compared to pristine BSA suggesting the enhanced stability of BCNPs. Figure 6.5(c) clearly depicts that degradation of pristine BSA start from 200 ^{o}C but no such change was observed for BCNPs. However, beyond 250 ^{o}C, a sudden weight loss was observed for both particles which could be due to the loss of small molecules such as ammonia, CO_2 etc. At 400-450 ^{o}C a substantial distinction in weight loss was observed, as 24 % was left for control BSA whereas 42 % was remained for BCNPs which validate the slower degradation rate for BCNPs as compared to BSA alone. Beyond 450 ^{o}C, degradation rate of BCNPs became faster as compared to pristine BSA, which could be attributed to the crystalline nature of encapsulated CNPs in BCNPs. While, no noteworthy change was detected in BSA (control) owing to the char formation in nitrogen atmosphere as recently reported (Gebregeorgis et al., 2013).

6.6 *In Vitro* Stability of BCNPs

Stability of the carrier molecule always play a crucial role for their future clinical applications, as the cargo molecules slowly escape from the carrier and form secondary aggregates that might leads to severe complications. Further, the higher stability is also correlated with the long circulation time *in vivo* and sustained release of cargo molecules. To evaluate the physiological stability of BCNPs in aqueous and PBS (pH= 7.4) solutions, the variation in particle size distribution of BCNPs were examined by DLS *in vitro* for more than 96 h.

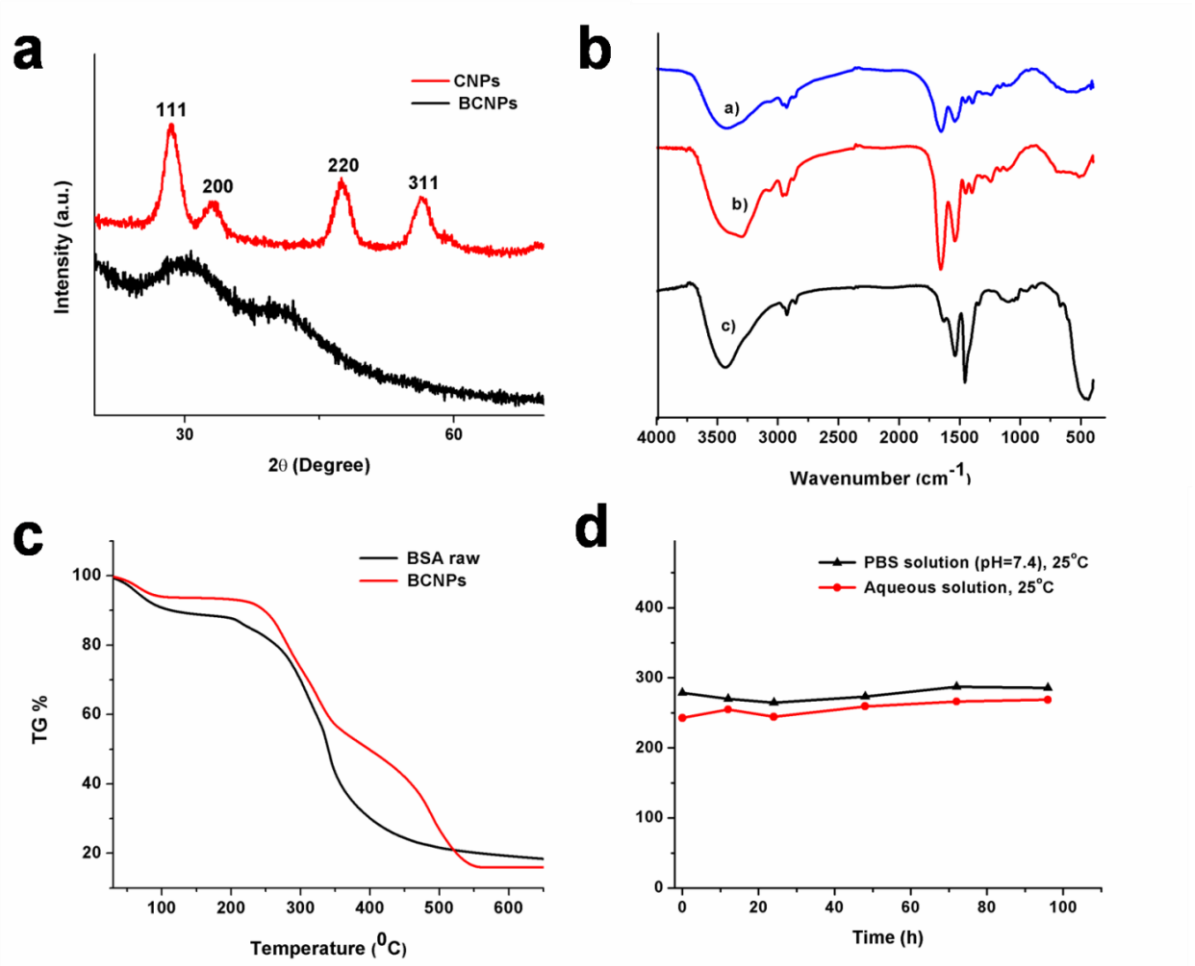

Figure 6.5 (a) XRD plot of CNPs and BCNPs (b) FTIR spectra of BSA (control), CNPs and BCNPs (c) TG data curve of BSA (control) and BCNPs (d) *In vitro* stability of BCNPs in aqueous and PBS (pH =7.4) solutions.

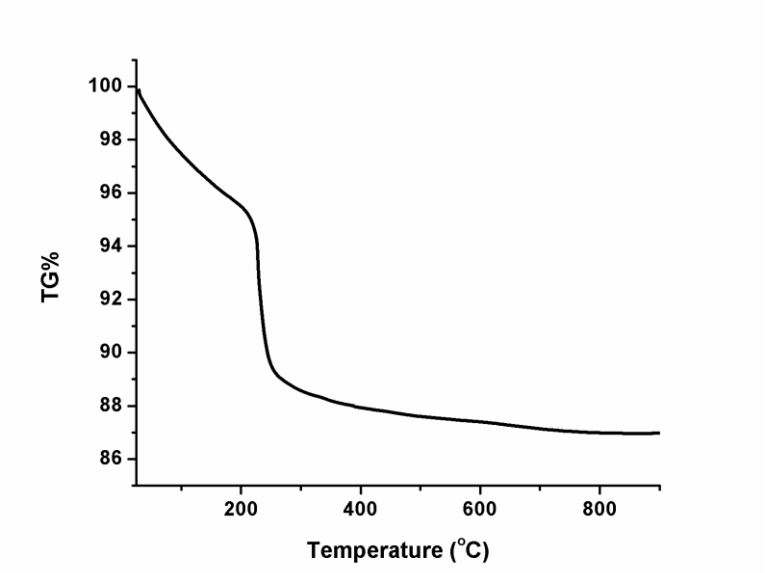

Figure 6.6 TG spectrum of CNPs.

Functional groups	-OH	-OH	C-H	C=O	C=O	N-O	Ce-O	Ce-O
Wave No. (cm^{-1})	3431.12	1630.32	2925.38	1455.76	1538.41	1338.93	873.88	439.51
Vibration	-OH stretch	-OH bend	C-H stretch	C=O stretch	C=O stretch	N-O stretch	Ce-O stretch	Ce-O stretch

Table 6.1 Characteristic major absorption bands in the IR spectra of the CNPs.

As shown in Figure 6.5(d), in aqueous and PBS solution mean particle size of the BCNPs remain constant for 96 h at 25 ^{o}C. Thus, confirmed the higher stability of BCNPs under *in vitro* physiological conditions supporting their future clinical applications.

6.7 Encapsulation efficiency of nanoparticles

A range of concentrations of the CNPs with albumin nanoparticles were taken and the BCNPs were prepared *via* desolvation technique. The encapsulation efficiency of the albumin nanoparticles was examined by using various concentrations of CNPs, whilst the carrier concentration was remains same. The protein-CNPs complex with the paramount encapsulation efficiency was opted for remaining studies. As shown in Figure 6.7(a), 5:25 ratio of CNPs: BSA provides the maximum encapsulation efficiency of 82.34 %.

6.8 *In vitro* release study

The *in vitro* release kinetic pattern of CNPs from BCNPs was studied for over 96 h at pre defined time intervals in PBS at pH 7.4 as shown in Figure 6.7(b). The *in vitro* release is a combined outcome of diffusion of nanoparticles out of the nanocarrier into the exterior environment and simultaneous degradation of carrier molecules. A biphasic release kinetic pattern was found having an initial burst release of 31.79 % in the first 10 h followed by a controlled release of the CNPs. The initial burst release was attributed to the simultaneous release of the surface bound CNPs and encapsulated CNPs from the BCNPs, while the later sustained release was corresponded to the encapsulated CNPs. In the following 24 h, the cumulative release reached 40.88 % in a sustained manner, making albumin nanoparticles as a potential nanoplatform for the sustained release of CNPs in order to protect the cells from ROS over a period of time. It is noteworthy that as expected the overall release of CNPs from

a

Protein Concentration (mg)	CNPs concentration (mg)	Entrapment efficiency (%)
25	1	67.70±1.155
25	3	74.80±2.413
25	5	82.34±1.481
25	10	76.81±2.478

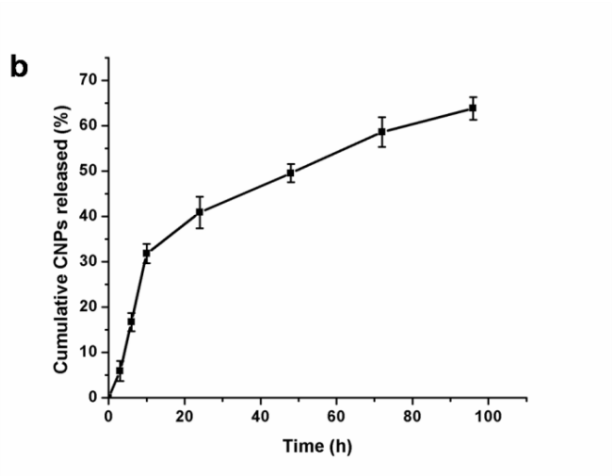

Figure 6.7 (a) Entrapment efficiency of BCNPs with varying CNPs concentrations (b) CNPs release profile from BCNPs in PBS (error bars denoted SD; *n*=3).

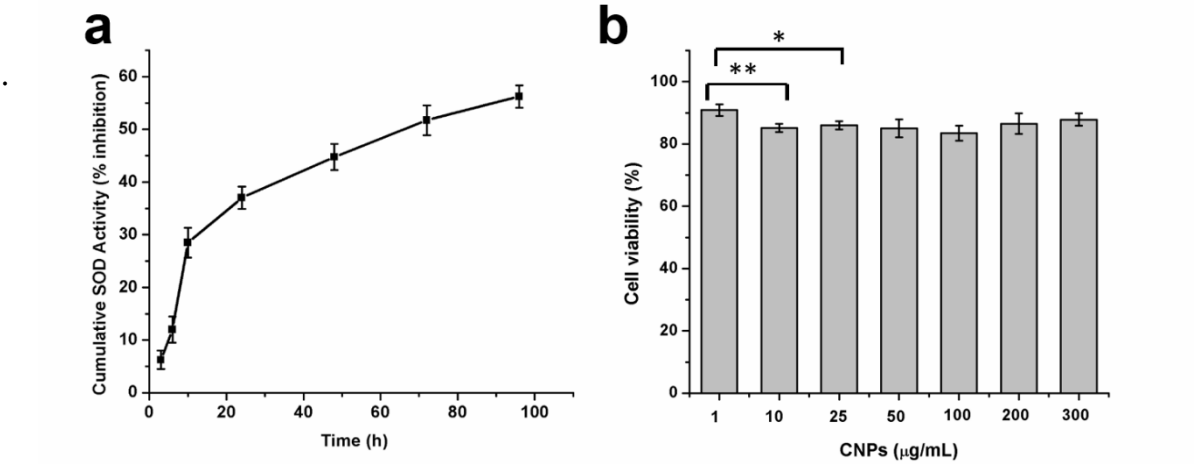

Figure 6.8 SOD activity (% inhibition) of the released CNPs from BCNPs showing the increase in SOD activity as a function of time. (b) Biocompatibility and cell viability assay (MTT assay) of CNPs on L-132 cells after 24h of treatment. The statistically significant values are denoted by *$p < 0.05$ and **$p < 0.005$ (error bars denoted SD; *n*=3).

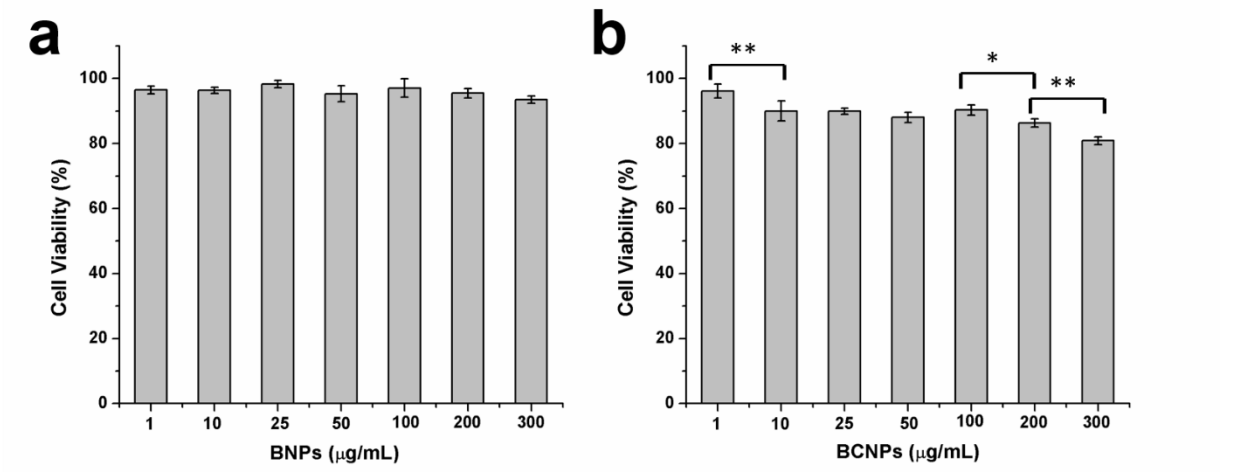

Figure 6.9 Biocompatibility and cell viability assay (MTT assay) of (a) BNPs and (b) BCNPs on L-132 cells after 24h of treatment. The statistically significant values are denoted by *$p < 0.05$ and **$p < 0.005$ (error bars denoted SD; *n*=3).

BCNPs were found to be slower unlike the release profile of other encapsulated drugs in the albumin nanoparticles, which might be due to the limited solubility of oxide nanoparticles. Moreover, the improved stability of BCNPs and their sustained release profile in the physiological buffer was attributed to the glutaraldehyde mediated cross linking mechanism of protein nanoparticles. The results suggested that the sustained release of CNPs from BCNPs in the media not only protect the cells from sudden exposure to higher concentration of CNPs but also help in fighting against the intracellular ROS for a considerable period of time making albumin nanoparticles a better delivery system for future applications in the field of nanomedicine.

6.9 SOD activity of CNPs

The SOD mimetic activity of released CNPs from BCNPs was examined as shown in Figure 6.8. A time dependent increase in the SOD mimetic activity of the CNPs was observed which correlates with the increase in the concentration of CNPs in the surrounding medium as a result of its release from the BCNPs. During the first 10 h, due to the initial burst release of CNPs from BCNPs a significant increment in the SOD activity was observed as a result of higher concentration of CNPs in the surrounding medium. While a steady increment in the SOD activity was observed from 24 to 96 h due to the sustained release of CNPs from the BCNPs. Thus the retention of antioxidant potential of released CNPs ensures that the BCNPs can be used for further therapeutic applications.

6.10 Cell viability assay

The cytotoxicity of CNPs, BCNPs and nanocarrier i.e. BSA NPs was evaluated quantitatively on the L-132 cells by MTT dye reduction method as shown in the Figure 6.8(b) and Figure 6.9. The results demonstrated that alike BSA NPs alone CNPs and BCNPs were found to be non-toxic to L-132 cells up to a concentration of 300 μg mL^{-1}. More than 80 % cell viability was observed after 24 h confirming the biocompatibility of CNPs, BCNPs and non-toxic nature of bare BSA nanoparticles.

6.11 Cellular uptake studies

Cellular uptake play a crucial role in the development of successful nanocarrier platform as it contributes to the uptake of the cargo molecule by the cells and their sustained release from the nanocarrier. In the present study, the uptake of CNPs encapsulated albumin nanoparticles was investigated *in vitro* by incubating the L-132 cells with BCNPs and then followed by their qualitative analysis by FE-SEM, TEM and quantitative analysis by ICP-MS.

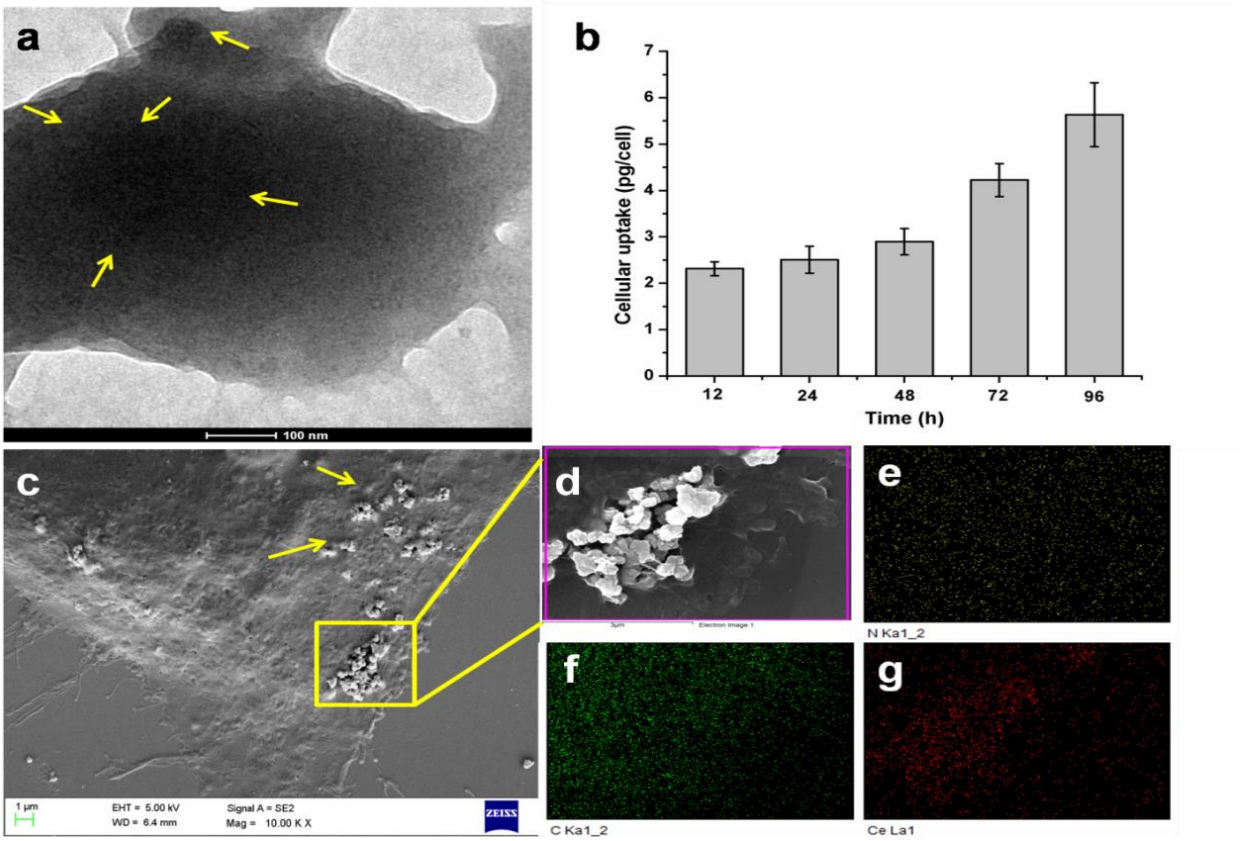

Figure 6.10 (a) TEM image of L-132 cells with internalized BCNPs indicated by yellow arrow (b) Quantification of BCNPs internalized by L-132 cells with increase in preincubation time.(c) Representative FE-SEM image of L-132 cells with BCNPs, arrows indicates the BCNPs attached on the surface of cell. (d) Magnified FE-SEM image of L-132 cell with internalized BCNPs and (e-f) color coded SEM/EDX dot maps depicting the individual elemental distribution. (yellow for nitrogen, green for carbon and red for cerium). The scale bars in (a) 100 nm and (c) 1 µm

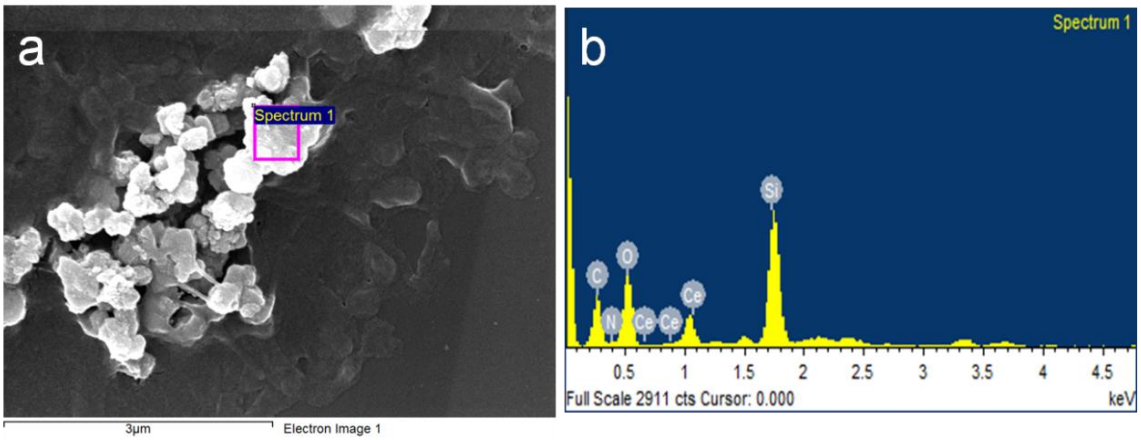

Figure 6.11 (a) Magnified FE-SEM image of internalizing BCNPs and corresponding (b) Energy dispersive spectra of selected proportion of cell.

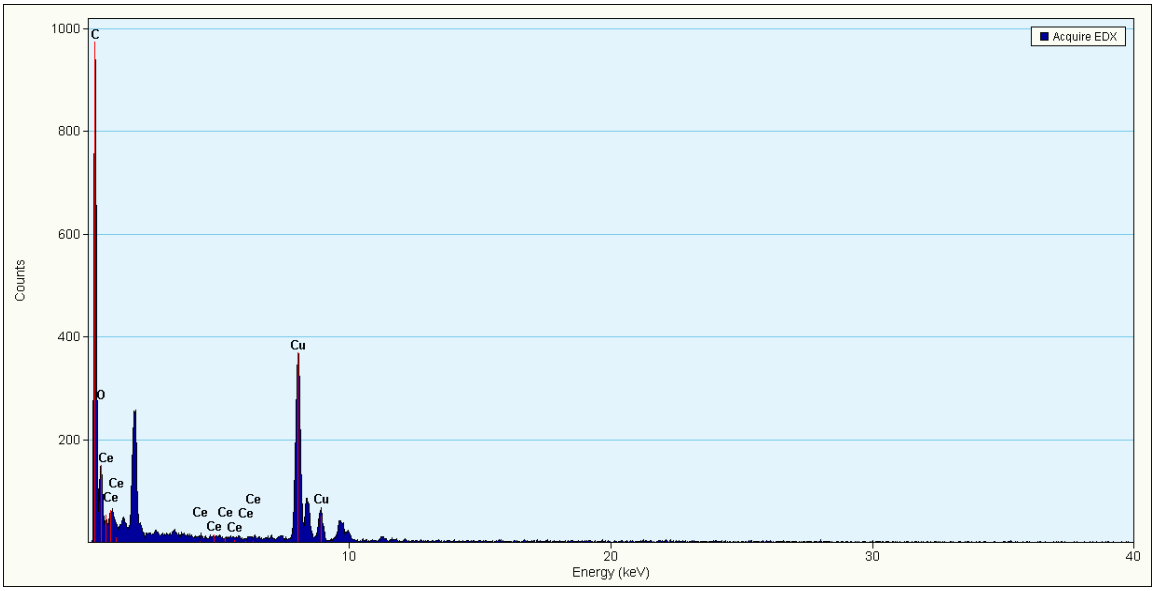

Figure 6.12 EDS analysis of internalized BCNPs on the TEM.

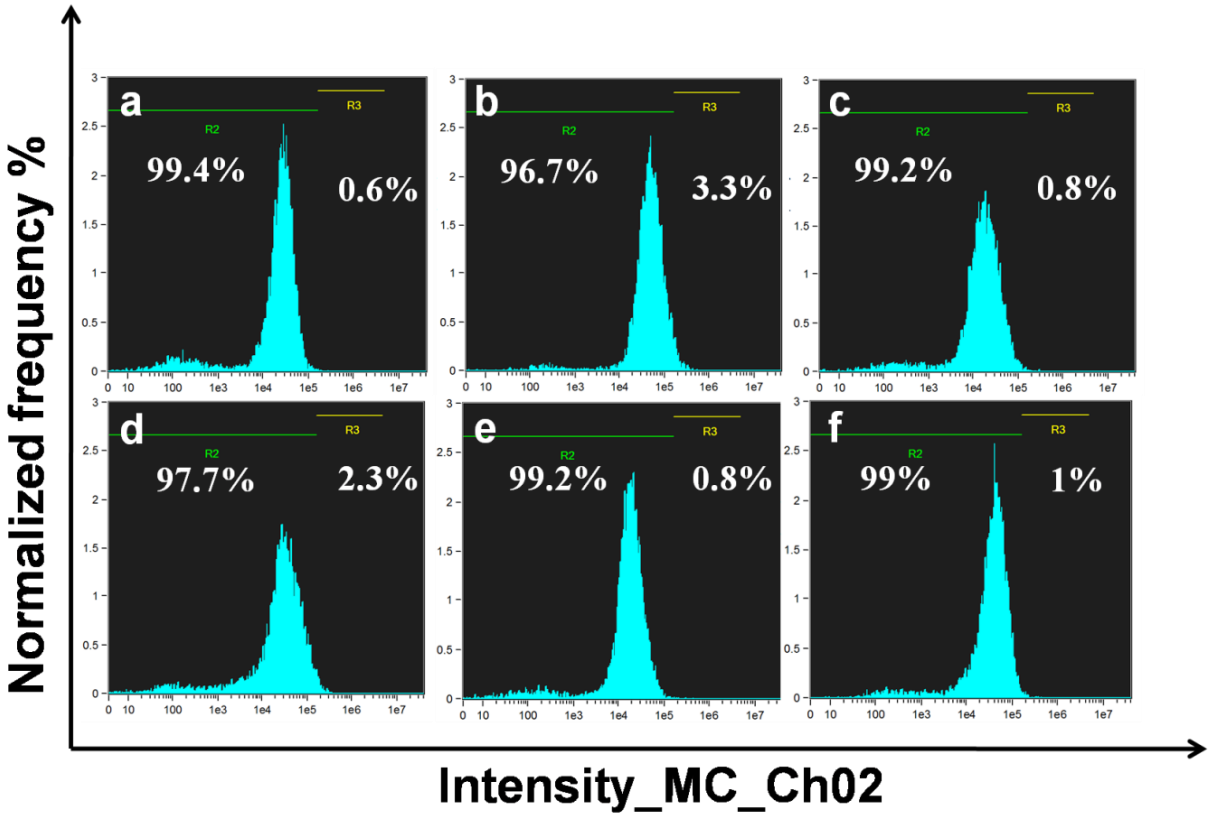

Figure 6.13 Flow cytometric analyses of ROS production in L-132 cells treated with BCNPs for different time intervals. (a) Control (b) 12 h (c) 24 h (d) 48 h (e) 72 h (f) 96 h.

The FE-SEM images of L-132 cells treated with BCNPs (Figure 6.10(c)) clearly demonstrated that the treatment of cells with BCNPs did not affect the cells as showed by the healthy morphology of the cells. Moreover, the encapsulation of CNPs in albumin enhanced the biological acceptability of the nanoparticles. The BCNPs get easily attached on the surface of the cells as indicated by the arrows in Figure 6.10(c) and gets internalized by the cells as highlighted in the box. The elemental mapping of the highlighted area as shown in Figure 6.10(d) clearly depicts the defined distribution profiles of elements Ce (red colour corresponds to CNPs), N (nitrogen) and C (carbon) (N and C denoted by yellow and green color, respectively). Moreover, the EDX analysis of highlighted area further confirms the study as shown in Figure 6.11. Thus, the results clearly signify the uptake of BCNPs by the cells. The TEM image of treated L-132 cells showed healthy morphology, while the arrow indicates the successful delivery of CNPs inside the cells by the albumin nanocarriers as showed in Figure 6.10(a). The EDX analysis as showed in Figure 6.12 further confirmed the presence of CNPs within the cells. Moreover, ICP-MS analysis conducted to quantify the cellular uptake of CNPs in L-132 cells treated with BCNPs for different time interval. The results demonstrated that the cellular uptake of CNPs was found to be increased in a time dependent manner as showed in Figure 6.10(b), which further confirmed the potential uptake of the CNPs encapsulated albumin nanoparticles and the sustained release of CNPs from it.

6.12 ROS scavenging potential of BCNPs

The ROS scavenging potential of BCNPs was assessed in L-132 cells exposed to H_2O_2 mediated oxidative stress and ROS generation. As depicted in Figure 6.13, no considerable changes in the level of ROS production took place on incubating the cells with BCNPs for different time interval as compared to untreated control. The results suggested that the BCNPs did not endorse ROS generation. In spite of that a major decrease in the DCF fluorescence intensity corresponding to the ROS content was observed when L-132 cells were exposed to H_2O_2, after preincubating the cells with BCNPs for different time intervals. As shown in Figure 6.14, a time dependent decrease in the level of ROS generation was observed as a result of sustained release of the CNPs from the BCNPs in combination with the increased intracellular level of CNPs. Initially, a significant intracellular ROS generation was detected as a result of low intracellular concentration of CNPs but with the increase in the duration of incubation significant amount of CNPs gets internalized in the cells that lead to the reduction in the intracellular ROS level, when L-132 cells were challenged to H_2O_2. In case of L-132 cells preincubated with BCNPs for 96 h, a fivefold decrease in the intracellular ROS production was observed as compared to BCNPs untreated cells.

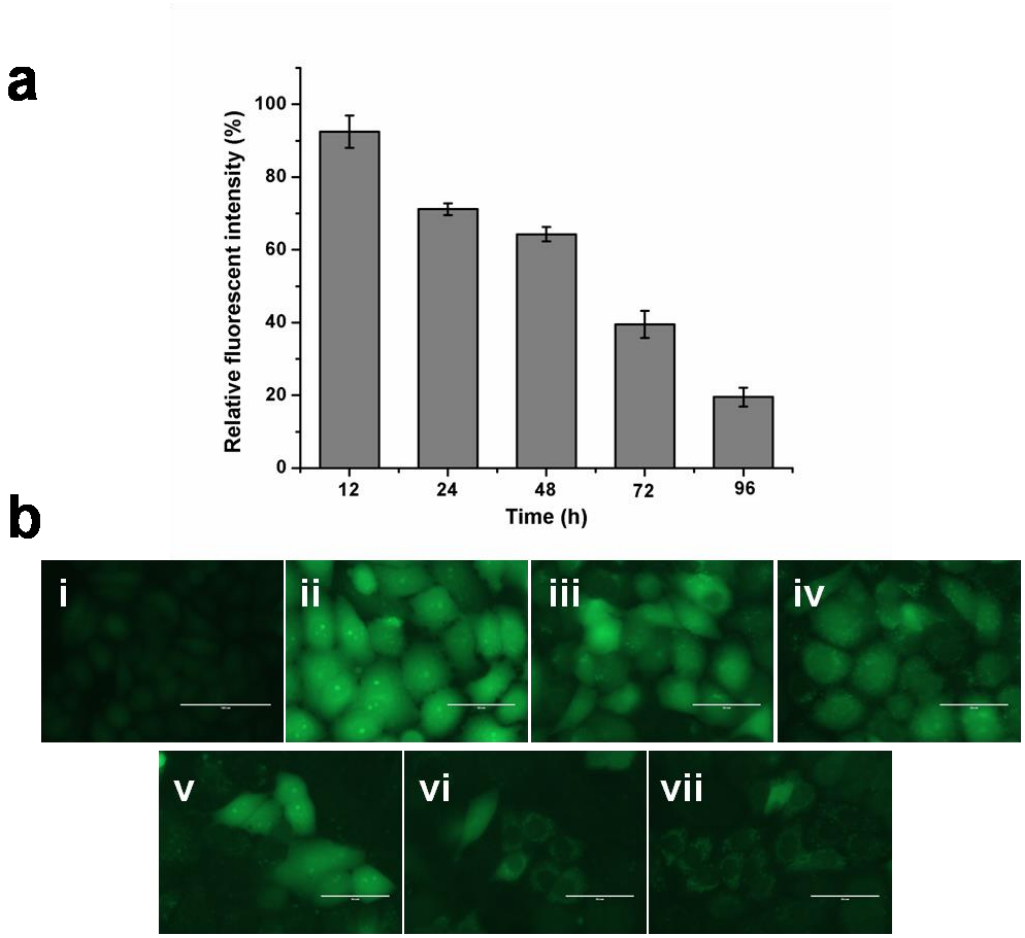

Figure 6.14 (a) Scavenging of ROS by BCNPs in L-132 cells. (b) Representative fluorescence images of H_2O_2-treated L-132 cells after staining with DCFH-DA. (i) Untreated cells (ii) H_2O_2 treated cells without BCNPs preincubation and (iii-vii) H_2O_2 treated cells with increase in BCNPs (100 µg/mL) preincubation time. All the scale bars represent 50 µm (error bars denoted SD; *n*=3).

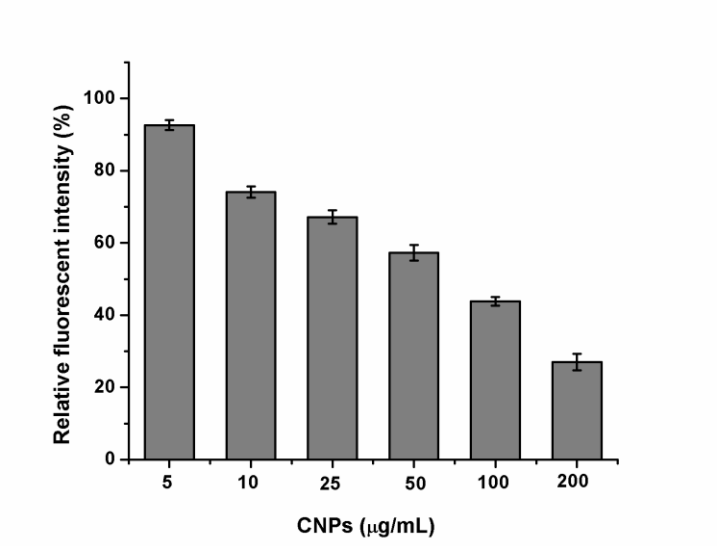

Figure 6.15 (a) Scavenging of ROS in L-132 cells preincubated with different concentration of CNPs (error bars denoted SD; *n*=3).

Similarly, on pre-incubating the cells with different concentration of free nanoceria depicts a concentration dependent ROS scavenging property of CNPs as shown in Figure 6.15. Initial low concentration of CNPs was found to be ineffective and high concentrations of free CNPs were required for effective intracellular ROS abatement. The inadequate intracellular ROS scavenging potential of free nanoceria might be correlates with the high positive zeta potential value of CNPs. As reported in previous literature (Patil et al., 2007), higher the positive zeta potential of the CNPs lower will be the cellular uptake. The encapsulation of CNPs inside the albumin nanoparticles enhanced the cellular uptake of CNPs and thereby augmented the therapeutic efficacy of CNPs.

Such abatement of intracellular ROS was also confirmed by corresponding fluorescent images of L-132 cells preincubated with BCNPs for different time period as shown in Figure 6.14(b). In H_2O_2 treated cells strong fluorescence was observed due to high level of ROS production as compared to BCNPs and H_2O_2 untreated cells. Moreover, the fluorescent signal of BCNPs pretreated L-132 cells decrease with increase in BCNPs pre incubation time suggesting an efficient removal of ROS. Thus the present study clearly revealed that the uptaken BCNPs are effective antioxidant agent and BCNPs pretreatment significantly attenuates ROS production over a period of time comparable to the H_2O_2 untreated cells. Moreover, long term ROS scavenging action of CNPs, suggests their unprecedented role for future conventional antioxidant drugs.

6.13 Gene expression studies

The antioxidant potential of CNPs encapsulated BSA NPs was assessed *in vitro* in L-132 cells *via* semi-quantitative RT-PCR analysis. The gene expression studies implied that BCNPs effectively defend the cells against oxidative stress and prevent the cells from entering into oxidative stress induced apoptosis as shown in Figure 6.16. In all such experiments the expression of housekeeping gene GAPDH was taken as internal control, which remains unchanged during the process. Oxidative stress arises as results of overproduction of ROS or incomplete removal of ROS because of decrease in the antioxidant levels. Antioxidant enzymes protect the cells from oxidative stress by comprising the primary defense system. Among them catalase, glutathione peroxidase and SOD are major enzymes, which are present in all the cells and plays a decisive role to fight against the H_2O_2 and the superoxide radical induced oxidative stress, respectively, and thereby maintain the integrity of the cell membrane (Ando et al., 2008, Halliwell et al., 2001). It was observed that the activity of antioxidant enzymes including catalase, glutathione peroxidase and SOD was found to be down-regulated

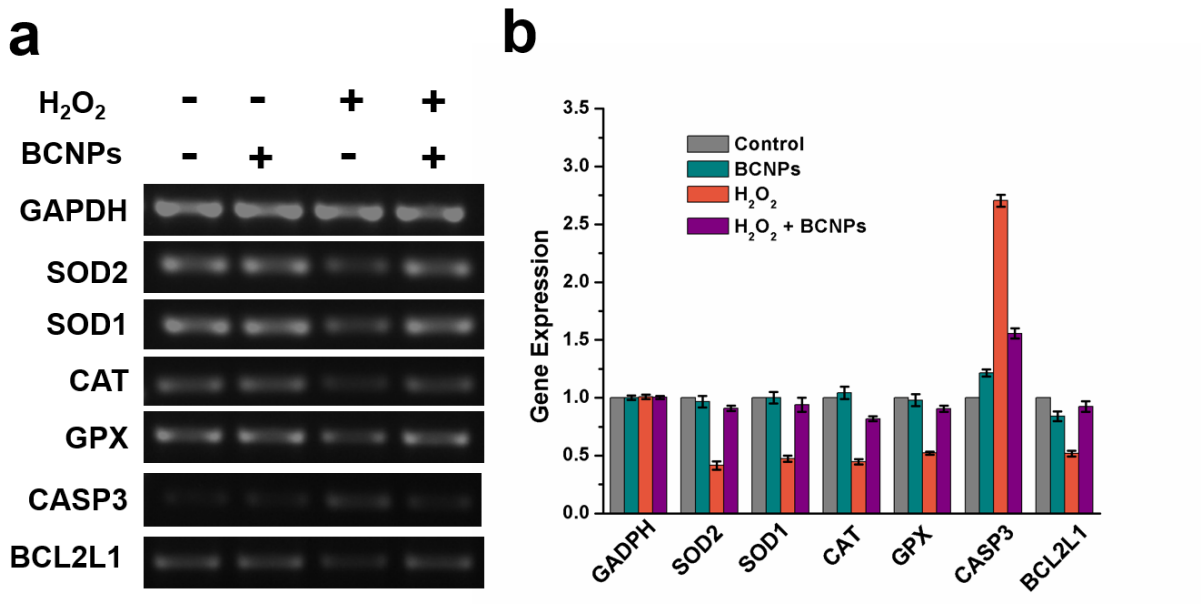

Figure 6.16 (a) Semi-quantitative RT-PCR analysis of antioxidant and apoptotic genes. (b) Fold difference in gene expression in treated L-132 cells compared to untreated L-132 cells (error bars denoted SD; *n*=3).

when L-132 cells were exposed to H_2O_2 as compared to the control. Such perturbation makes the cells more vulnerable to oxidative damage. However, no changes were found in the level of gene expression in case of BCNPs treated cells. But when the cells pre-incubated with BCNPs got exposed to H_2O_2, the level of antioxidant enzymes was found to be higher as compared to H_2O_2 treated cells. The increase in the level of gene expression in case of BCNPs preincubated cells may be correlated with the ROS scavenging activity of the BCNPs. Thus the present results confirm the antioxidant potential of the BCNPs and are supported by previous studies (Niu et al., 2011, Pandareesh et al., 2014, Zhou et al., 2014).

Moreover, BCNPs also protect the cells from entering the oxidative stress induced apoptosis. The exposure of cells with H_2O_2 leads to the induction of apoptotic gene expression. An increase in the expression of caspase-3 (CASP3), a major factor that is responsible for initiation and execution of apoptosis (Fink et al., 2005) was observed in H_2O_2 treated cells. In case of BCNPs treatment the level of caspase-3 was down-regulated which suggest that the antioxidant property of BCNPs helps in protecting the cells by removing the free radicals. Similarly, the level of anti-apoptotic gene (e.g. BCL2L1) (Wong et al., 2011) was found to be down regulated in H_2O_2 treated cells, while an increase in the level of expression was observed on BCNPs pretreatment before the addition of hydrogen peroxide.

In summary, a novel artificial antioxidant encapsulated delivery system based on biodegradable albumin nanoparticles was developed. Alike any other drugs CNPs were encapsulated inside BSA NPs using desolvation method. The delivery and sustained release of CNPs *via* biocompatible protein nanocarriers had not been addressed so far with this perspective. The physicochemical characterization of as-prepared BCNPs were done by AFM, FE-SEM and DLS depicting that even after CNPs entrapment the size of BCNPs lies within optimal range required for drug delivery applications. The MTT results revealed the biocompatibility of BNPs and BCNPs. Further, SOD and flow cytometric analysis revealed that the encapsulation of CNPs did not alter its antioxidant activity essential for their therapeutic applications. The cellular uptake studies of BCNPs conducted via TEM, FE-SEM and ICP-MS in L-132 cells depicted considerable internalization of CNPs inside the cells, implying the usefulness of these NPs for therapeutic applications. Gene expression analysis demonstrated the successful defense of cells against free radical and oxidative insults. Thus our studies propose that the therapeutic potential of CNPs could be better utilized by encapsulating it in biocompatible protein based nanocarrier for various biomedical applications.

CHAPTER 7

A FACILE SYNTHESIS AND EVALUATION OF ANTIOXIDANT POTENTIAL OF ALBUMIN COATED NANOCERIA

In this Chapter, a biocompatible albumin coated nanoceria particles with antioxidant activity has been synthesized in order to facilitate its uptake by the cells to restore the aberrant antioxidant system. The biocompatibility and ROS scavenging potential of ANC was assessed in vitro and in vivo against human lung epithelial cells and zebrafish, respectively.

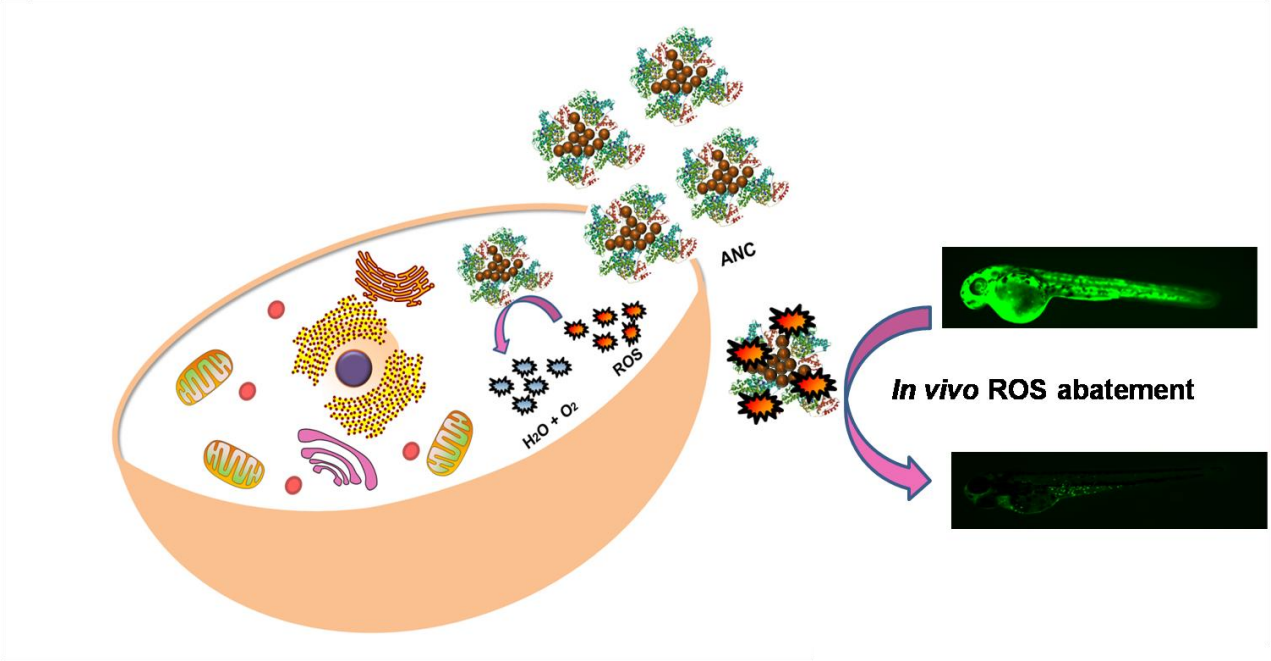

CHAPTER 7

A FACILE SYNTHESIS AND EVALUATION OF ANTIOXIDANT POTENTIAL OF ALBUMIN COATED NANOCERIA

Overview

Reactive oxygen species induced oxidative stress is one of the major factors responsible for initiation of several intracellular toxic events that leads to cell death. Antioxidant enzymes defence system of the body is responsible for maintaining the oxidative balance and cellular homeostasis. Several diseases are promoted by the excessive oxidative stress caused by the impaired antioxidant defence system that leads to oxidant/antioxidant imbalance in the body. In order to restore or precise the aberrant antioxidant system, a large number of catalytic nanoparticles has been screened so far. Exceptional antioxidative activity of nanoceria made it as a potential antioxidative nano-agent for the effective scavenging of toxic ROS. In this work albumin coated nanoceria was synthesized by alkaline based precipitation method and further characterized by TEM, UV-visible spectroscopy, XRD, TG and FTIR analysis. The antioxidant and SOD assay confirm that the albumin coating do not alter the antioxidant potential of ANC. The biocompatibility and protective efficacy of ANC against oxidative stress was investigated both *in vitro* and *in vivo* in L-132 cells and zebrafish embryos, respectively. The ICP-MS, TEM and FE-SEM analysis corroborates the uptake of ANC by the cells. Furthermore, the semi-quantitative gene expression studies confirmed that the ANC successfully defend the cells against oxidative stress by preserving the antioxidant system of the cells. Thus, the current work open up a new avenue for the development of improved antioxidant nano-drug therapies.

Results and discussion

7.1 Synthesis and characterization of albumin coated nanoceria

The ANC was synthesized by using alkaline based precipitation of nanoceria in a solution containing albumin and cerium salt. Briefly, an aqueous solution of albumin and cerium nitrate was added continuously to an ammonia solution under vigorous stirring leading to the formation of albumin coated nanoceria (Figure 7.1). The as-prepared ANC showed good resuspension in water and PBS. The UV-visible absorption spectrum of ANC depicted a characteristic peak at

318 nm as shown in Figure 7.2. The albumin coating restricts the further growth of nanoceria which result in the formation of small size ANC particles (Perez et al., 2008). In Figure 7.3(a), TEM image clearly depicts the formation of nanoceria coated with amorphous albumin layer (indicated by arrows), having a single average particle size around 2.113±0.728 nm as depicted in Figure 7.3(c). Moreover, Figure 7.3(d) and Figure 7.4 illustrate the corresponding EDS pattern and elemental distribution in ANC, respectively. In addition, the DLS studies showed that the average hydrodynamic size of the protein coated nanoceria was around 45.82 nm (Figure 7.5).

The lattice planes obtained from selected area electron diffraction pattern as shown in Figure 7.3(b) reveals the fluorite typed structure of as-prepared nanoparticles, which were in good agreement with those obtained from an XRD pattern (Figure 7.6(a)) (Sathyamurthy et al., 2005). Broader peaks were obtained as a result of smaller particle size of the as prepared nanoparticles and amorphous nature of the coated albumin layer (Korsvik et al., 2007, Bhushan et al., 2015c). Moreover, the ANC showed a considerably higher zeta potential value around 41.8 mV as compared to pristine BSA as shown in Figure 7.6(b), which confirms the stability of nanoparticles in aqueous system. Further, the FTIR analysis was done to illustrate the presence of albumin layer as shown in Figure 7.6(c). The characteristic protein peaks were found in the FTIR spectra of ANC along with corresponding nanoceria peaks confirming the association of albumin with the nanoparticles as shown in Table 7.1 (Perez et al., 2008, Bhushan et al., 2015c).

On comparing the peaks of ANC and albumin a slight shifting in the peaks were observed corroborating the interaction of albumin with nanoceria as reported earlier (Bhushan et al., 2015c, Patil et al., 2007, Yuan et al., 2011). The albumin coating on the surface of CNPs was further confirmed by TG analysis of ANC showing a minor weight loss in the temperature range between 30 to 900 ^{o}C as shown in Figure 7.6(d). Initially, up to 200 ^{o}C a minute weight loss was found which account to the desorption of adsorbed water but beyond 200 ^{o}C a sudden weight loss was observed as a result of albumin layer on the surface of CNPs confirming the FTIR outcomes. The sudden weight loss depicts the degradation of albumin coating due to the loss of small molecules such as carbon dioxide, ammonia etc.

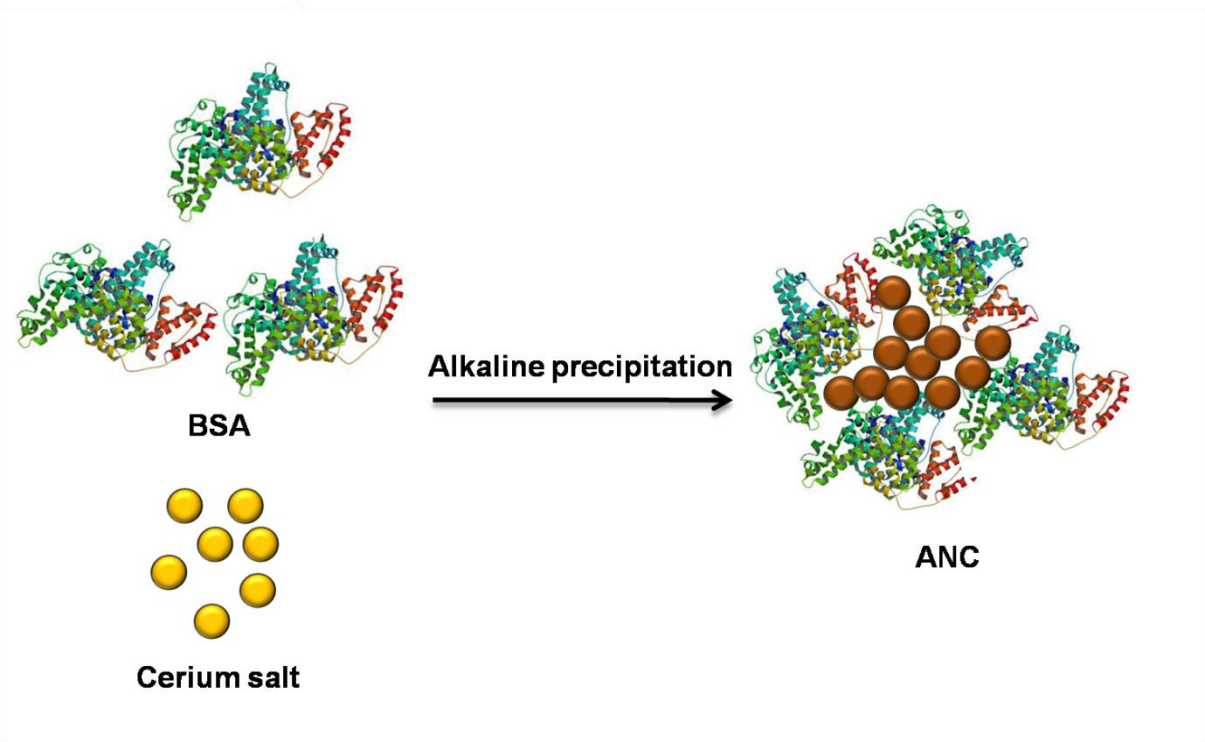

Figure 7.1 A schematic representation of preparation of albumin coated nanoceria. The structure of BSA (PDB ID: 3V03) was imported from RCSB protein data bank.

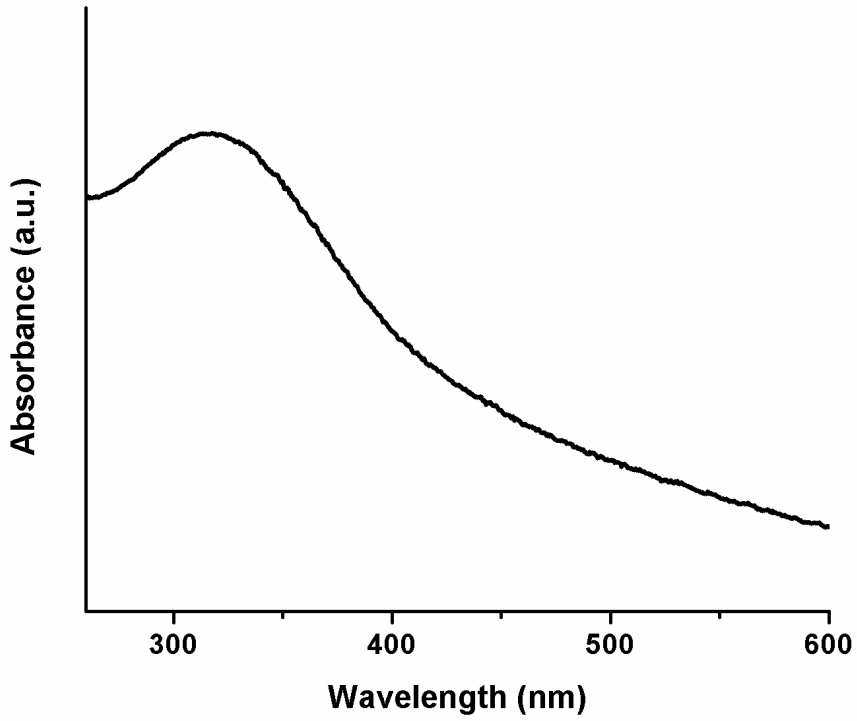

Figure 7.2 UV–visible absorption spectrum of prepared ANC.

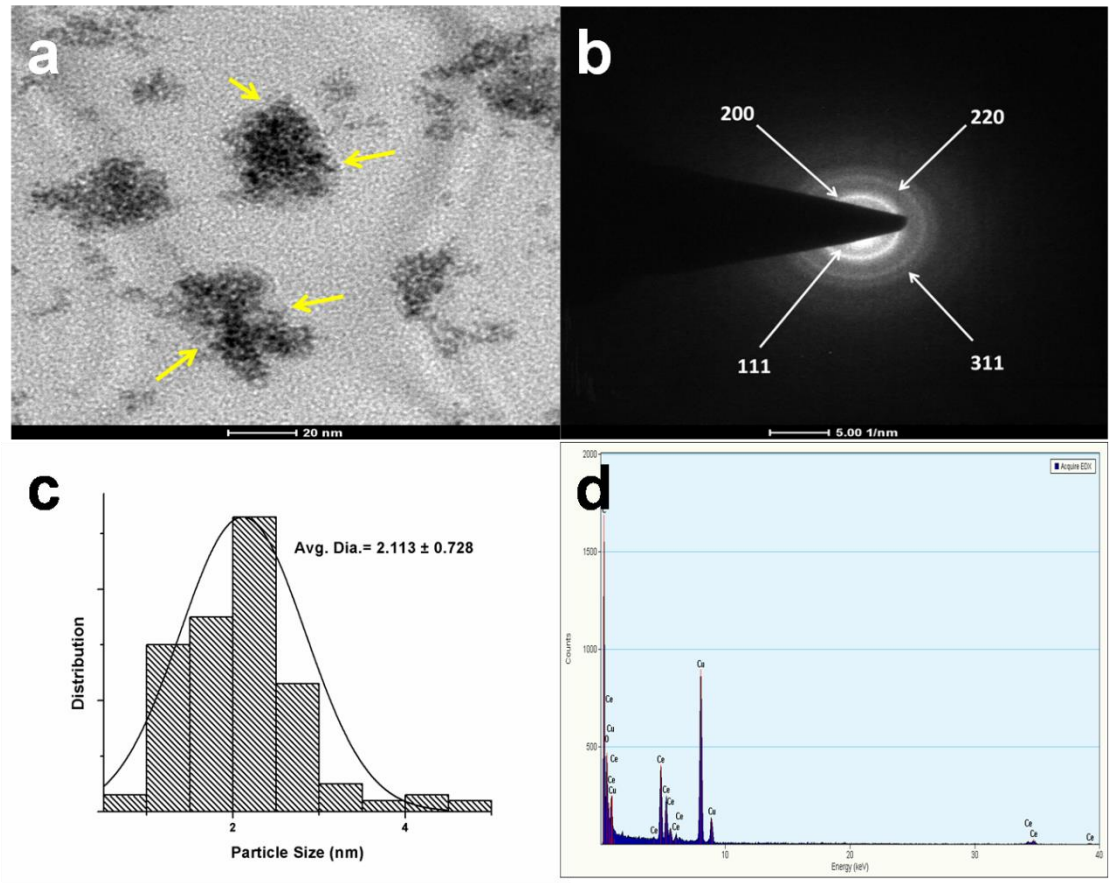

Figure 7.3 Characterization of as-prepared ANC (a) TEM image (scale bar: 20 nm) with corresponding (b) SAED pattern (c) Particle size distribution histogram and (c) Energy dispersive spectra of ANC.

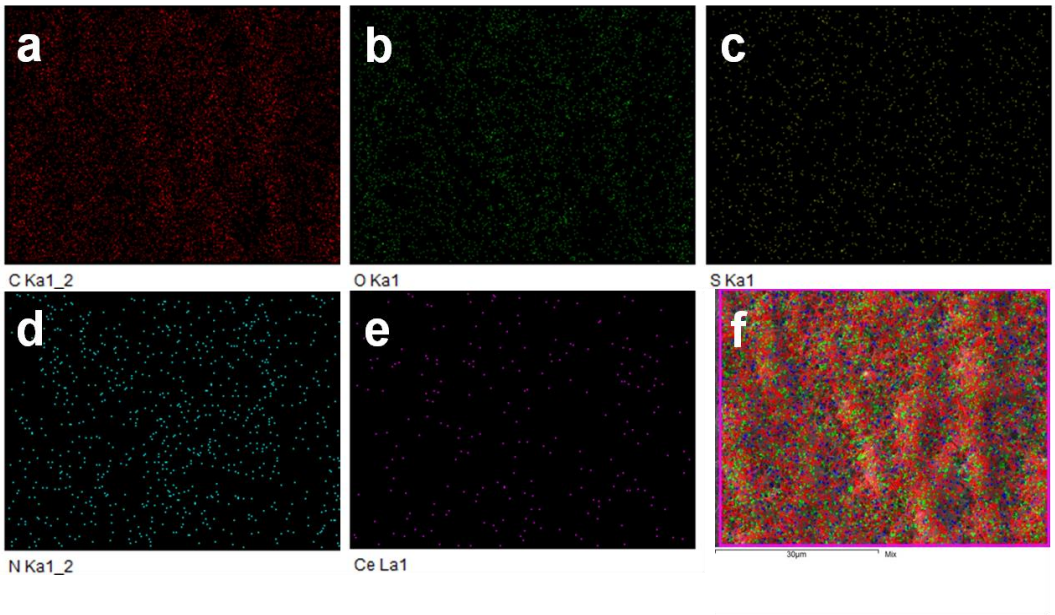

Figure 7.4 Color coded SEM/EDX dot maps depicting the individual elemental distribution in ANC from (a-e) red for carbon, green for oxygen, yellow for sulphur, blue for nitrogen, purple for cerium) and (f) overlay image.

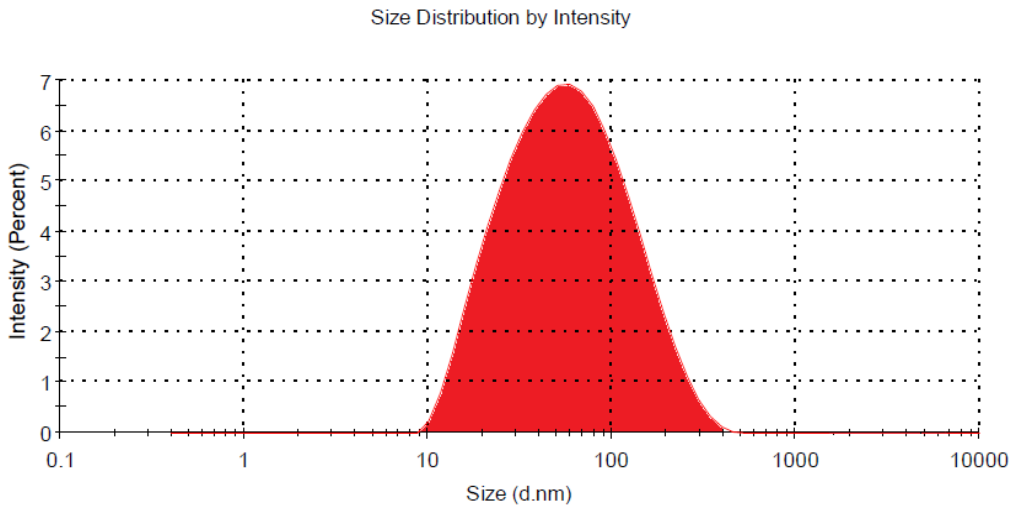

Figure 7.5 DLS images of ANC agglomerates.

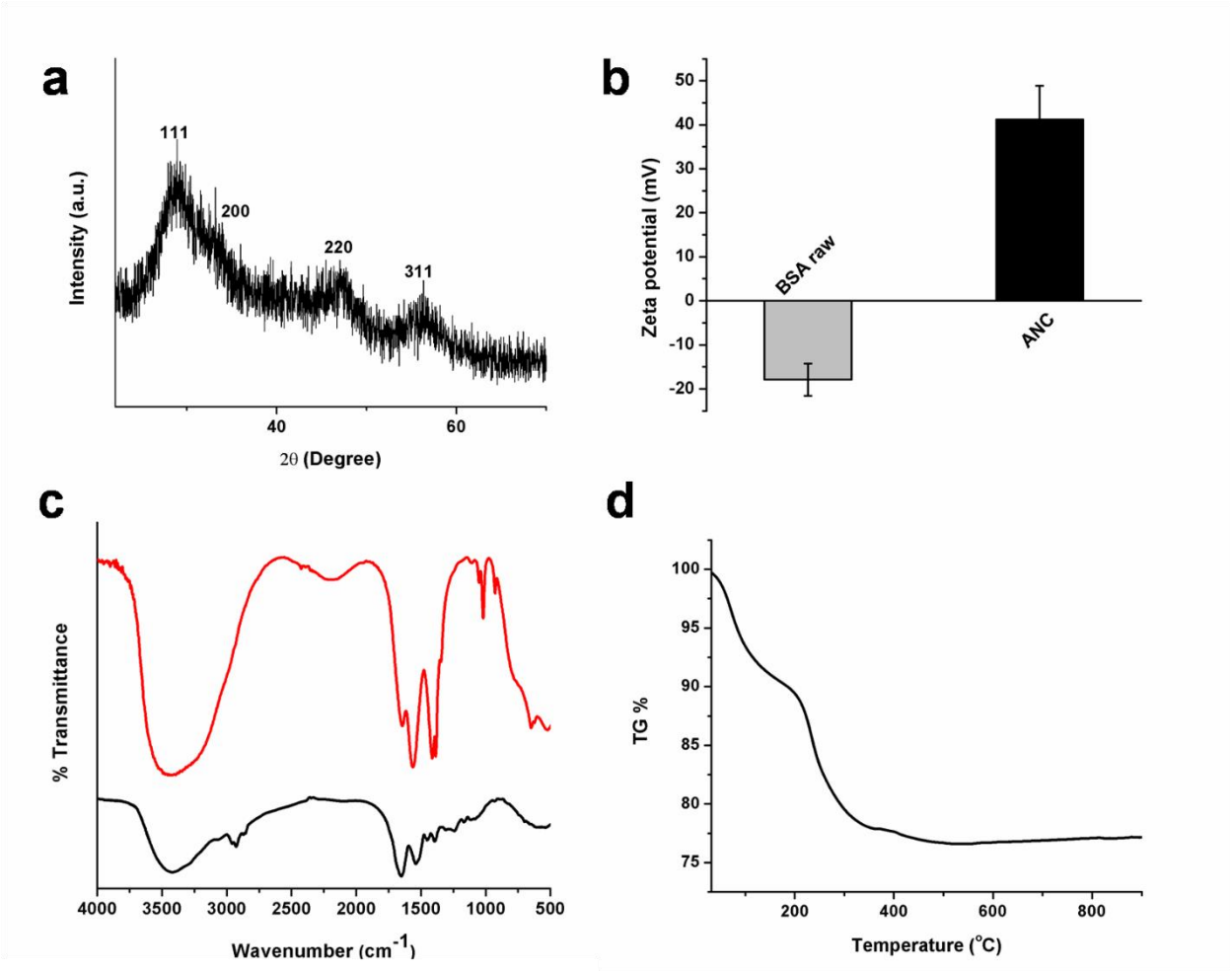

Figure 7.6 (a) XRD pattern of as prepared ANC (b) Zeta potential of aqueous solution of BSA (control), and ANC at pH=7 (c) FTIR spectra of BSA (in black) and ANC (in red) (d) TG spectrum of ANC

Functional groups	-OH	-OH	C-H	C=O	C=O	N-O	Ce-O	Ce-O
Wave No. (cm^{-1})	3431.12	1630.32	2925.38	1455.76	1538.41	1338.93	873.88	439.51
Vibration	-OH stretch	-OH bend	C-H stretch	C=O stretch	C=O stretch	N-O stretch	Ce-O stretch	Ce-O stretch

Table 7.1 Characteristic major absorption bands in the IR spectra of the ANC.

7.2 Antioxidative and SOD mimetic activity of ANC

The antioxidative activity of the as-prepared ANC was studied by a facile UV-visible spectroscopic method using a reaction with hydroxyl radicals (·OH) as described earlier (Xue et al., 2011). The methyl violet was used as chromogenic reagent having a maximum absorbance at 582 nm (curve A of Figure 7.7(a)). Addition of Fenton reagents resulted in the generation of considerable amount of ·OH, which in turn convert the MV into a colorless product. The color of MV was faded in a slower fashion and consequently leads to decrease in the maximum absorbance value (curve F of Figure 7.7(a)). On the other hand an increase in the maximum absorbance has been found in the presence of ANC (curve D of Figure 7.7(a)), which depicts the antioxidant potential of as-prepared nanoparticles by protecting the MV from degradation by effectively removing the ·OH. Thus, the albumin coating not only provides a better stability to the nanoparticles but also retain its antioxidative property. Moreover, a number of control experiments were also carried out simultaneously depicting that the presence of H_2O_2, albumin, Fe^{2+} and ANC do not alter the maximum absorbance of MV (curves B, C, E of Figure 7.7(a)).

Similarly, the SOD mimetic activity of ANC was analyzed with the help of SOD assay kit. A concentration dependent increase in the SOD mimetic activity of ANC was observed as shown in Figure 7.7(b). The superoxide produced by the xanthine oxidase reduces the WST-1 into a water soluble formazan, which have a maximum absorbance at 450 nm. Moreover, in the presence of ANC superoxide was removed which resulted in decrease in the absorbance value. Around 150 μg/mL concentrations, the SOD activity reaches half of its maximum value, while at 400 μg/mL the SOD activity reached up to 90%. Thus, the

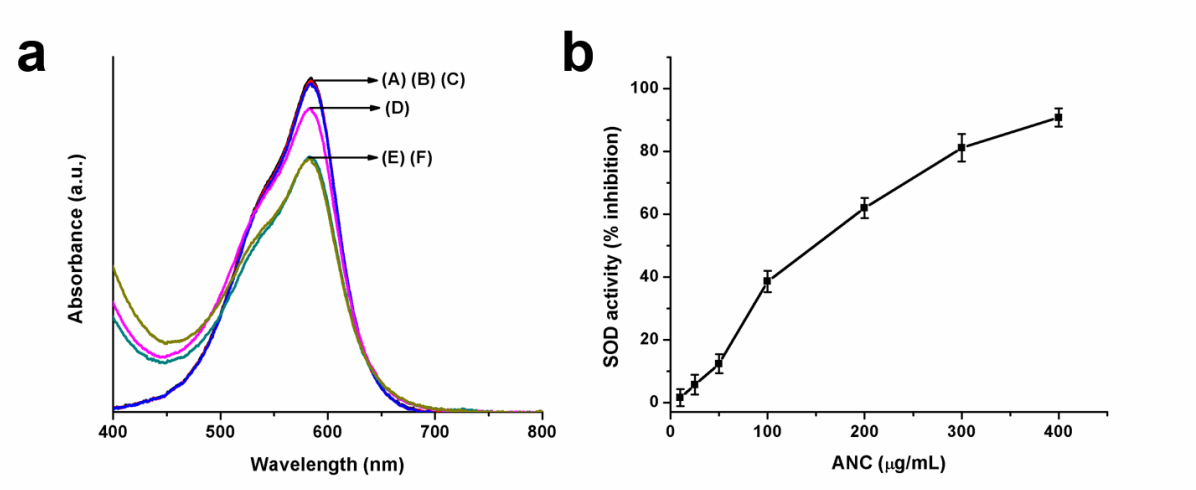

Figure 7.7 (a) UV-Vis absorption spectrum of (A) MV, (B) MV/$FeSO_4$/ANC, (C) MV/ANC/H_2O_2, (D) MV/$FeSO_4$/ANC/H_2O_2, (E) MV/$FeSO_4$/BSA/H_2O_2 and (F) MV/$FeSO_4$/H_2O_2 solutions. (b) SOD activity (% inhibition) of the ANC showing the increase in SOD activity as a function of concentration.

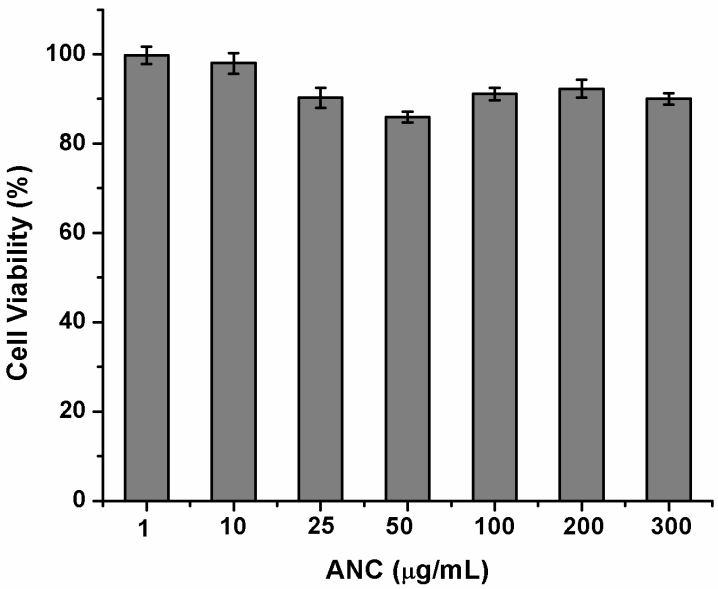

Figure 7.8 Biocompatibility and cell viability assay (MTT assay) of ANC on L-132 cells after 24 h of treatment (error bars denoted SD; *n*=3).

current results depicted the antioxidant potential of ANC, which could be further exploited for their therapeutic role.

7.3 Biocompatibility of ANC

The biocompatility of the as-prepared ANC was assessed quantitatively on the human lung epithelial cells by using standard MTT assay as shown in the Figure 7.8. The results revealed that as-prepared albumin coated nanoceria particles were found to be non- toxic to L-132 cells. More than 80% cell viability was found up to a concentration of 300 μg mL^{-1} after 24 h, which confirm the biocompatibility of ANC particles.

7.4 Cellular uptake studies

An efficient cellular internalization of the ANC particles is required in order to exploit the antioxidant potential of these nanoparticles inside the cells. The qualitative and quantitative assessments of uptake of ANC by the L-132 cells were done by using ICP-MS, TEM and FE-SEM. The L-132 cells treated with different concentration of ANC for 24 h depicted, that the uptake of ANC was increased in a concentration dependent manner as shown in Figure 7.9(a). Moreover, the qualitative assessment of uptake of ANC was confirmed by FE-SEM analysis (Figure 7.10). The FE-SEM image of ANC treated cells corroborate healthy morphology, which was in correlation with the biocompatibility results confirming the biocompatibility of ANC toward L-132 cells. Moreover, the elemental mapping of the cells clearly demonstrated the distribution profiles of various elements inside the cells. The blue color corresponds to the distribution of element cerium present on the surface and inside the cell, red color corresponds to the element carbon present inside the cell and the green color corresponds to the element oxygen present inside the cell.

In addition to that TEM analysis was also done for the qualitative assessment of ANC uptake by human lung epithelial cells. The TEM image of the ANC treated L-132 cells (Figure 7.9(b)) clearly demonstrated the internalization of ANC by the cells. Further, a magnified view of the ANC inside the cells (marked by arrows) depicts the successful internalization of nanoparticles, which was further confirmed by EDS analysis (Figure 7.10 (f)). Such studies confirm the successful internalization of ANC by the L-132 cells.

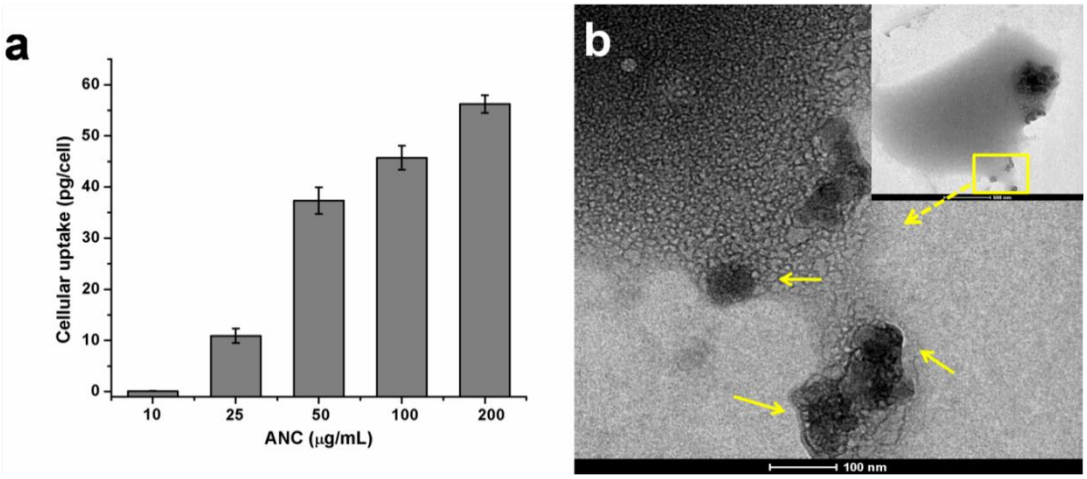

Figure 7.9 (a) Quantification of ANC internalized by L-132 cells with increase in concentration. (b) Representative TEM image of L-132 cells with ANC shown in inset (scale bar- 500 nm), and the magnified TEM image of L-132 cells with internalized ANC indicated by yellow arrows (scale bar- 100 nm).

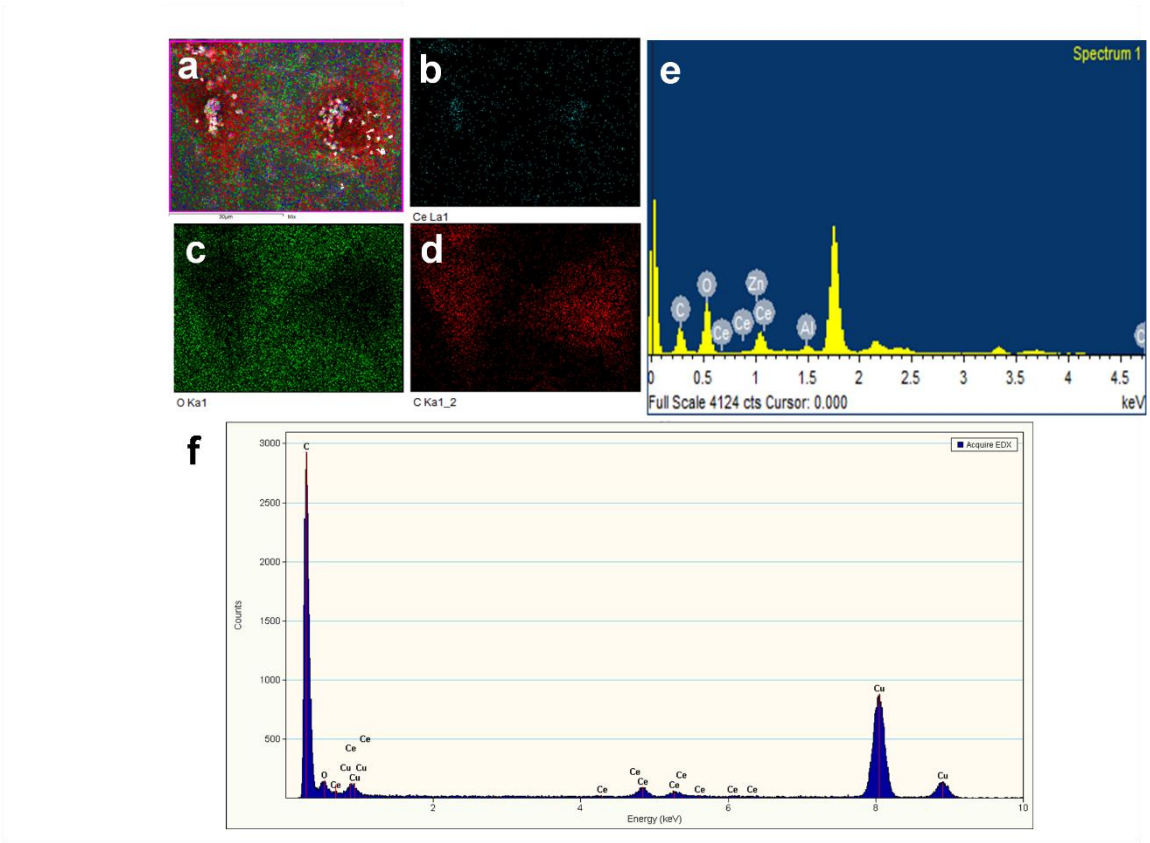

Figure 7.10 (a-d) FE-SEM image of L-132 cells with ANC and colour-coded SEM/EDX dot maps. (a) Overlay FE-SEM image showing elemental distributions in cells. (b–d) Individual elemental distribution maps (red for carbon, cyan for cerium and green for oxygen) with corresponding (e) Energy dispersive spectra of cell (f) EDS analysis of internalized ANC on the TEM.

7.5 *In vitro* antioxidant experiment

The antioxidant potential of ANC was assessed *in vitro* in L-132 cells by exposing the cells to H_2O_2 mediated oxidative stress. As illustrated in Figure 7.11(a), on exposing the L-132 cells to H_2O_2, preincubated with different concentration of ANC for 24 h, a major reduction in the DCF fluorescence intensity was observed that corresponded to the ROS content. Such concentration dependent decrease in the level of ROS content was correlated with the concentration dependent increase in the level of intracellular ANC, which converts the ROS into non-toxic products. Initially, on exposing the cells to H_2O_2, considerable amount of ROS generation was observed corresponding to the lower level of intracellular ANC, but with the increase in the concentration of ANC pretreatment, a significant amount of nanoceria particles get internalized which in turn results into an intracellular ROS abatement. In case of cells pre-treated with 300 μg/mL of ANC, the level of intracellular ROS generation was reduced to the level comparable to that of H_2O_2 untreated cells. Such intracellular ROS abatement was also corroborated by the fluorescent microscopic images of the L-132 cells pre-treated with different concentration of ANC as illustrated in Figure 7.11(b). In H_2O_2 and ANC untreated cells no ROS generation was observed, while in cells exposed to H_2O_2 without ANC pre-treatment a significant amount of ROS generation was found, corresponds to the relative high level of DCF fluorescence. However, in case of L-132 cells pretreated with different concentration of ANC, the fluorescent intensity decreased in a concentration dependent manner, suggesting the effective removal of ROS. Thus, the current study clearly signified that the ANC was effectively up taken by the L-132 cells, which in turn effectively attenuate the ROS production inside the cells on H_2O_2 exposure. Thus, the results implying the antioxidant potential of ANC, which could be utilized for future conventional antioxidant therapy.

7.6 Semi-quantitative RT-PCR analysis

The antioxidant potential of as-prepared ANC was further assessed *via* semi-quantitative RT-PCR analysis in L-132 cells. The results suggested that the ANC effectively protect the cells against oxidative stress and resist the cells from entering into the oxidative stress induced apoptosis as depicted in Figure 7.12. The expression of GAPDH, a housekeeping gene remains unaltered and was taken as internal control in all the experiments.

Incomplete removal of ROS due to the ineffective intracellular defence system of the cell results into an oxidative stress that leads to various diseases (Niu et al., 2011). Major factors responsible for such deterioration of antioxidant defence system of the lungs include cigarette smoking, aging, air pollution etc. The main antioxidant enzymes constituting the primary

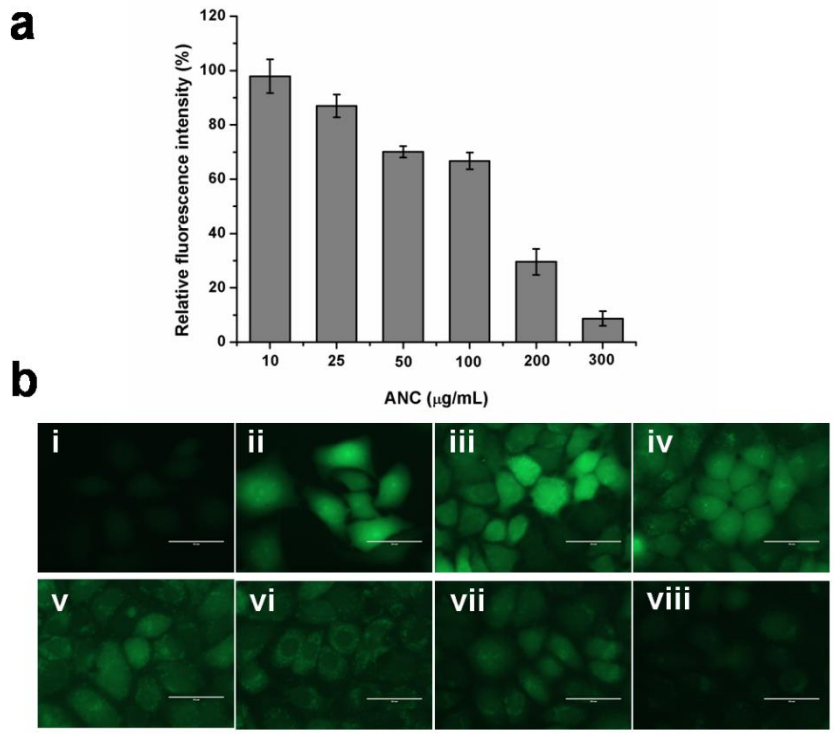

Figure 7.11 (a) Scavenging of ROS by ANC in L-132 cells. (b) Representative fluorescence images of H_2O_2-treated L-132 cells after staining with DCFH-DA. (i) Untreated cells (ii) H_2O_2 treated cells without ANC pre-incubation and (iii-viii) H_2O_2 treated cells with increase in ANC concentrations (10, 25, 50, 100, 200, 300 μg/mL), respectively. All the scale bars represent 50 μm (error bars denoted SD; *n*=3).

.

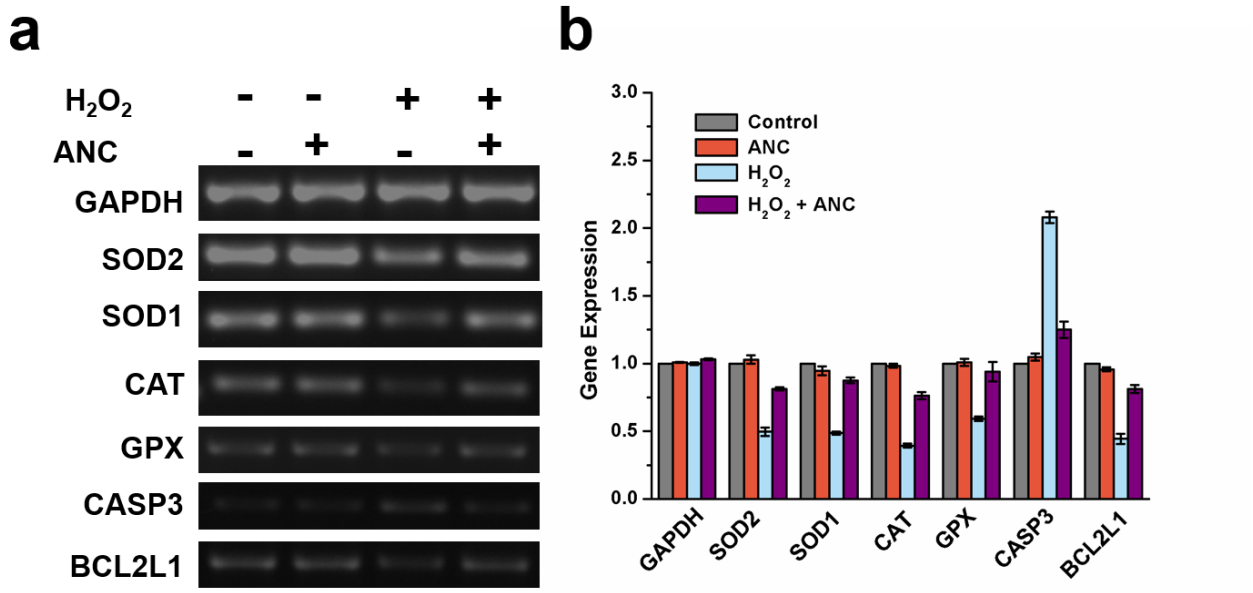

Figure 7.12 Semi-quantitative RT-PCR analysis of antioxidant and apoptotic genes illustrating the fold difference in gene expression in treated L-132 cells compared to untreated L-132 cells (error bars denoted SD; *n*=3).

defence system of the body against ROS includes glutathione peroxidise, catalase and superoxide dismutase (Ando et al., 2008, Halliwell et al., 2001). Hydrogen peroxide, is one of the major ROS inducer. Therefore H_2O_2 was taken as a source of ROS inducer to test the antioxidant potential of the ANC *in vitro* in L-132 cells. As reported earlier, on exposing the cells to H_2O_2, a down-regulation in the activity of antioxidant enzymes including glutathione peroxidase, SOD and catalase was found as compared to untreated cells as shown in Figure 7.12 (Niu et al., 2011, Pandareesh et al., 2014). Moreover, the level of antioxidant enzymes remains unaltered on ANC treatment. In contrast, when the ANC pretreated cells challenged to H_2O_2, an increase in the expression level of antioxidant enzymes was observed as compared to the untreated cells. This result clearly signifies the antioxidant potential of ANC in protecting the cells against ROS (Niu et al., 2011, Pandareesh et al., 2014, Zhou et al., 2014). As reported earlier, ROS and the resulting oxidative stress play crucial role in apoptosis (Kannan et al., 2000). An over expression of antioxidants blocks or delay apoptosis. However, perturbation of the antioxidant defence system evokes the cells to enter into apoptotic pathway. The ANC defend the cells from entering into the oxidative stress induced apoptosis by effectively scavenging the ROS. The H_2O_2 exposure to the cells resulted in the up-regulation of the apoptotic gene expression e.g. caspase-3, a key factor accountable for the initiation and execution of apoptosis was observed (Fink et al., 2005). While, the level of anti apoptotic gene e.g. bcl-xl (BCL2L1) (Wong et al., 2011) was found to be down-regulated. When ANC pretreated cells were exposed to H_2O_2, a down-regulation in the level of caspase-3 (CASP3) and up-regulation in the level of bcl-xl was observed suggesting that the ANC successfully defend the cells against oxidative stress by effectively neutralizing the ROS.

7.7 Protective effect of ANC against H_2O_2 induced embryotoxicity in zebrafish

The protective effect of ANC against the H_2O_2 induced toxicity in zebrafish embryos was determined by monitoring the embryo mortality, heart-beating disturbances and morphological malformations. Initially, the zebrafish embryos were exposed to various H_2O_2 concentrations as illustrated in Figure 7.13. Survival rate of embryos were decrease in a concentration dependent manner on H_2O_2 exposure. The survival rate of zebrafish embryos treated with H_2O_2 and co-treated with ANC is showed in Figure 7.14(b). A significant decrease in the survival rate of zebrafish embryos was found in case of only H_2O_2 treatment, in contrast co-treatment of zebrafish embryos with ANC shows a concentration dependent increase in the survival rate of embryos. Thus the results depict the protective effect of ANC against the H_2O_2 induced embryo toxicity.

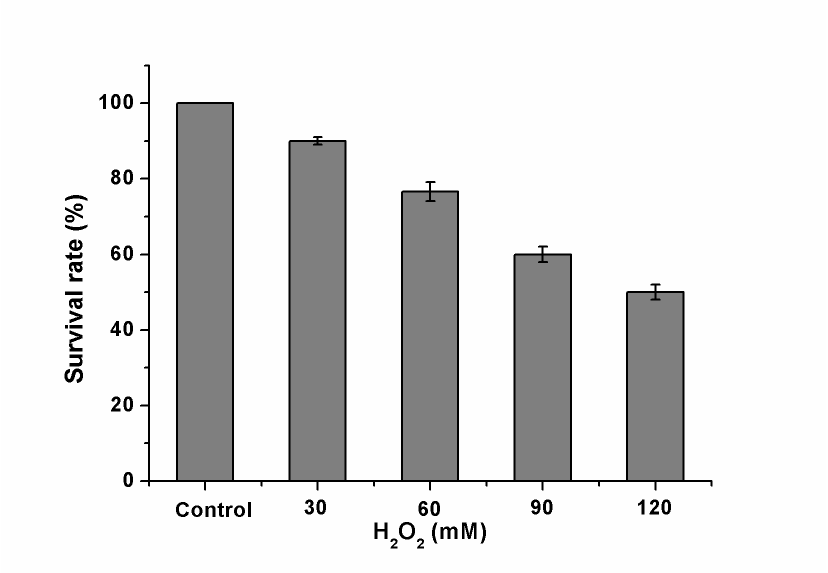

Figure 7.13 Hydrogen peroxide induced embryotoxicity in zebrafish.

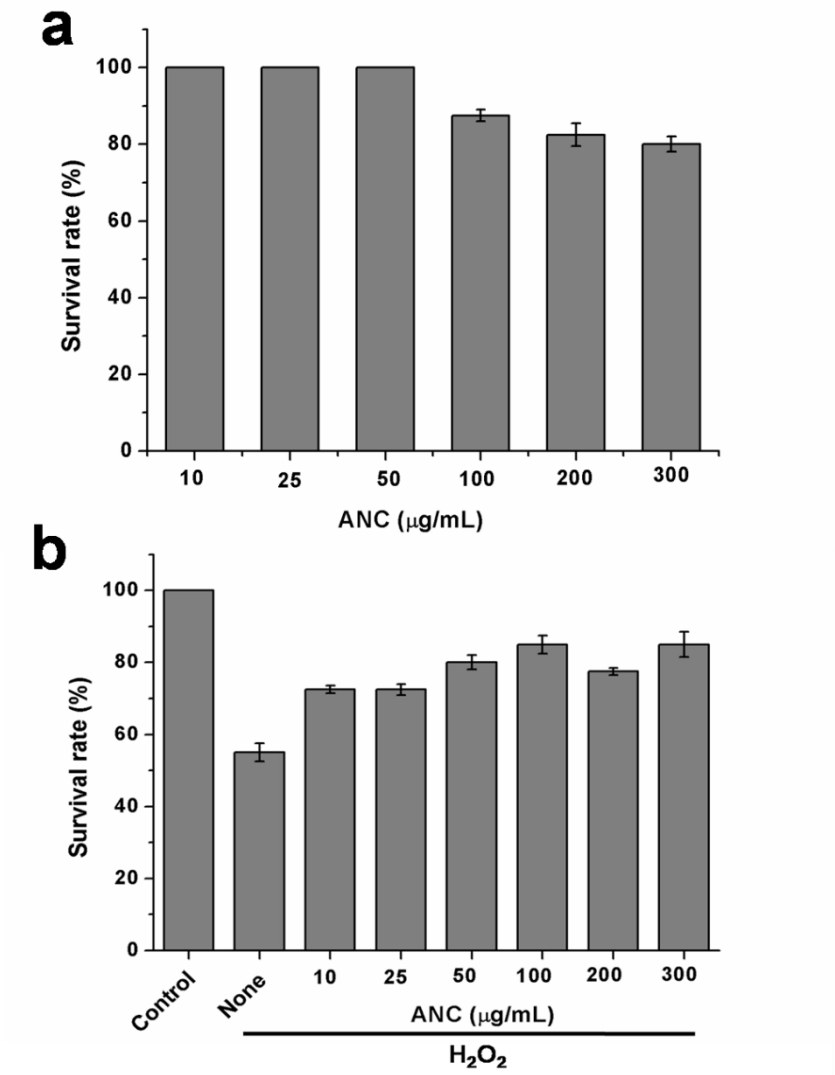

Figure 7.14 (a) Effect of ANC on the survival rate of zebrafish embryos (b) Protective effect of ANC against H_2O_2 induced embryotoxicity in zebrafish (error bars denoted SD; *n*=3).

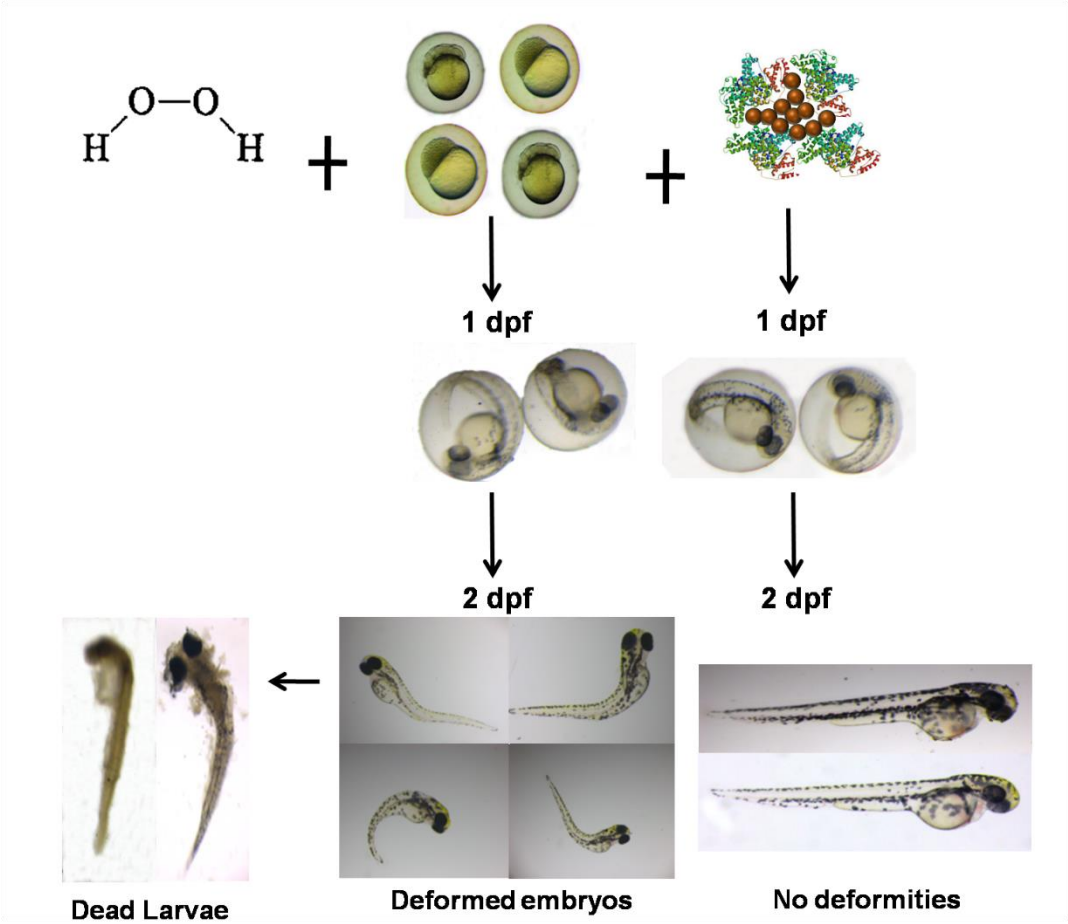

Figure 7.15 Photographs illustrating the protective effect of ANC against H_2O_2 induced morphological deformities and embryo mortality.

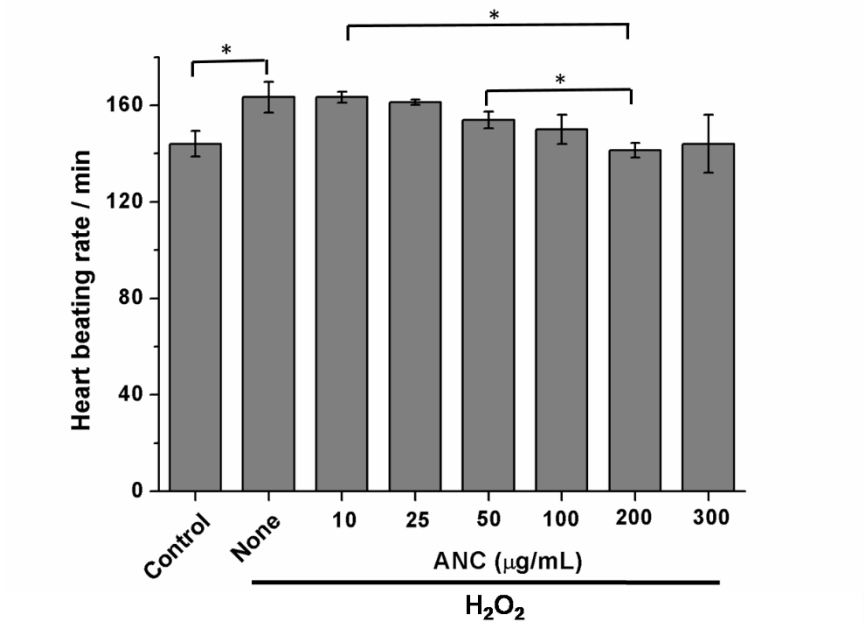

Figure 7.16 Effect of ANC on heart beat rate of zebrafish embryos. The statistically significant values are denoted by $*p < 0.05$ (error bars denoted SD; n=3).

The zebrafish embryos treated with ANC alone do not show any significant effect on the survival rate of embryos as shown in Figure 7.14(a), thus supporting their biocompatible nature. Moreover, on evaluating the morphological malformations, ANC did not evidence conspicuous adverse effects. While, several typical morphological defects were observed after H_2O_2 exposure such as contorted tail, trunk abnormalities, short body length, spinal column curving, incompletely differentiated tail ends etc. which finally resulted in the embryos mortality. However, pretreatment of the embryos with ANC successfully protect them from H_2O_2 mediated morphological deformities as shown in Figure 7.15. Apart from it, the heart-beating rate of the embryos was also examined as shown in Figure 7.16. The H_2O_2 exposure of embryos results in their enhanced heart beat rate, while in case of ANC pretreated embryos, a concentration dependent decrease in the heart beat rate was observed demonstrating the successful neutralization of free radical molecules by ANC.

7.8 Inhibitory effect of ANC on H_2O_2 induced ROS generation in zebrafish

The ROS scavenging potential of ANC was evaluated *in vivo* in zebrafish model. A concentration dependent reduction in the DCF fluorescence intensity was observed on exposing the ANC preincubated embryo to H_2O_2 mediated oxidative stress as shown in Figure 7.17(a). Such decrease in the level of ROS was corresponds to the increase in the level of intracellular ANC, which in turn results into an intracellular ROS abatement. Moreover, intracellular ROS abatement was also confirmed by corresponding fluorescent images of zebrafish embryos preincubated with different concentrations of ANC prior to H_2O_2 exposure as shown in Figure 7.17(b). In H_2O_2 treated embryo strong green fluorescence was observed as a result of high level of ROS generation as compared to ANC alone and untreated embryos. Furthermore, a significant reduction in the fluorescence was observed in ANC pretreated embryos prior to H_2O_2 exposure suggesting the effective ROS inhibition. Hence, these results demonstrate that ANC could be utilized as an efficient antioxidant agent, while zebrafish will be utilized as alternative *in vivo* model system for antioxidant material testing.

7.9 Protective effects of ANC against H_2O_2 induced cell death in live zebrafish

The protective effect of ANC against H_2O_2 induced cell death was determined by measuring the AO fluorescence intensity in the body of zebrafish (Kim et al, 2014a, Ko et al, 2014, Kang et al., 2013a, 2013b and 2014). A strong AO fluorescence intensity was observed in case of H_2O_2 treated embryos as compared to ANC and untreated embryos depicting the H_2O_2 induced cell death as shown in Figure 7.18(b). However, the cell death was reduced by the addition of ANC to the zebrafish exposed to the H_2O_2. Thus, the ANC showed protective effects against

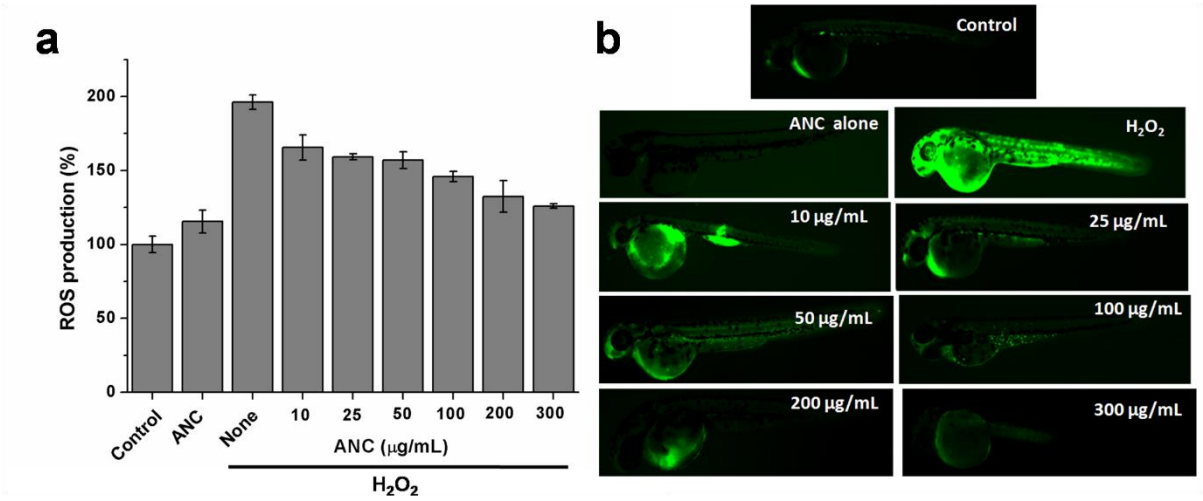

Figure 7.17 (a) ROS scavenging potential of ANC in zebrafish embryos. (b) Representative fluorescence images of H_2O_2 treated and ANC co-treated zebrafish embryos after staining with DCFH-DA (error bars denoted SD; *n*=3).

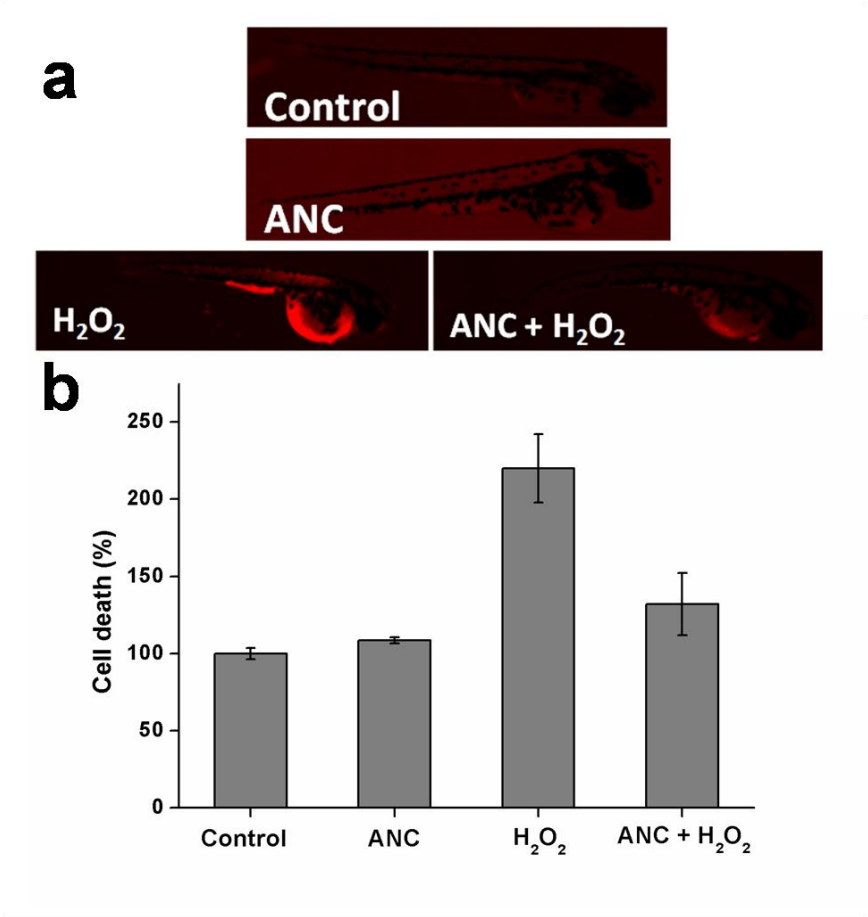

Figure 7.18 (a) Representative fluorescence images of H_2O_2 treated and ANC co-treated zebrafish embryos (b) Protective effect of ANC against H_2O_2 induced cell death in zebrafish embryos (error bars denoted SD; *n*=3).

H_2O_2. The results were further confirmed by the fluorescence images of zebrafish embryos stained with AO as shown in Figure 7.18(a). The untreated and ANC treated embryos not shown any significant fluorescence as compared to H_2O_2 treated embryos, which have strong fluorescence corresponding to the oxidative stress induced cell death. However, in case of zebrafish treated with ANC prior to H_2O_2 exposure, a significant reduction in the fluorescence intensity was observed suggesting the protective effect of ANC against oxidative stress induced cell death.

In summary, protein coated nanoceria particles were synthesized through alkaline based precipitation method. Albumin coating not only provide the aqueous stability to the system but also retain its antioxidant properties as successfully demonstrated by the antioxidant and SOD mimetic assays. The physicochemical characterization corroborates the successful coating of protein on the surface of nanoceria particles. The MTT assay further revealed the biocompatibility of the as-prepared nanoparticles towards human lung epithelial cells. Moreover, the TEM, FE-SEM and ICP-MS analysis depict the efficient uptake of ANC by the cells. Further, the flow cytometric and gene expression analysis revealed the *in vitro* antioxidant potential of as-prepared nanoparticles in defending the cells against the ROS mediated oxidative stress. Moreover, for the first time we investigated the protective effects of nanoceria against H_2O_2-induced oxidative stress and cell death in zebrafish model. Our results revealed that H_2O_2 induces toxicity in the zebrafish embryos; while ANC can protect zebrafish embryos against H_2O_2 induced oxidative stress by intracellular ROS abatement. Further, ANC demonstrated evidence in reduced morphological deformities and enhanced survival rate of embryos. Thus, the current study proposed that the albumin coated nanoceria particles could emerged as a promising antioxidant agent, while zebrafish embryos could be utilized as a valuable laboratory alternative *in vivo* model for future antioxidant experiments.

CHAPTER 8

CONCLUDING REMARKS

In this Chapter, conclusions from the present studies and the scopes for the future works are described.

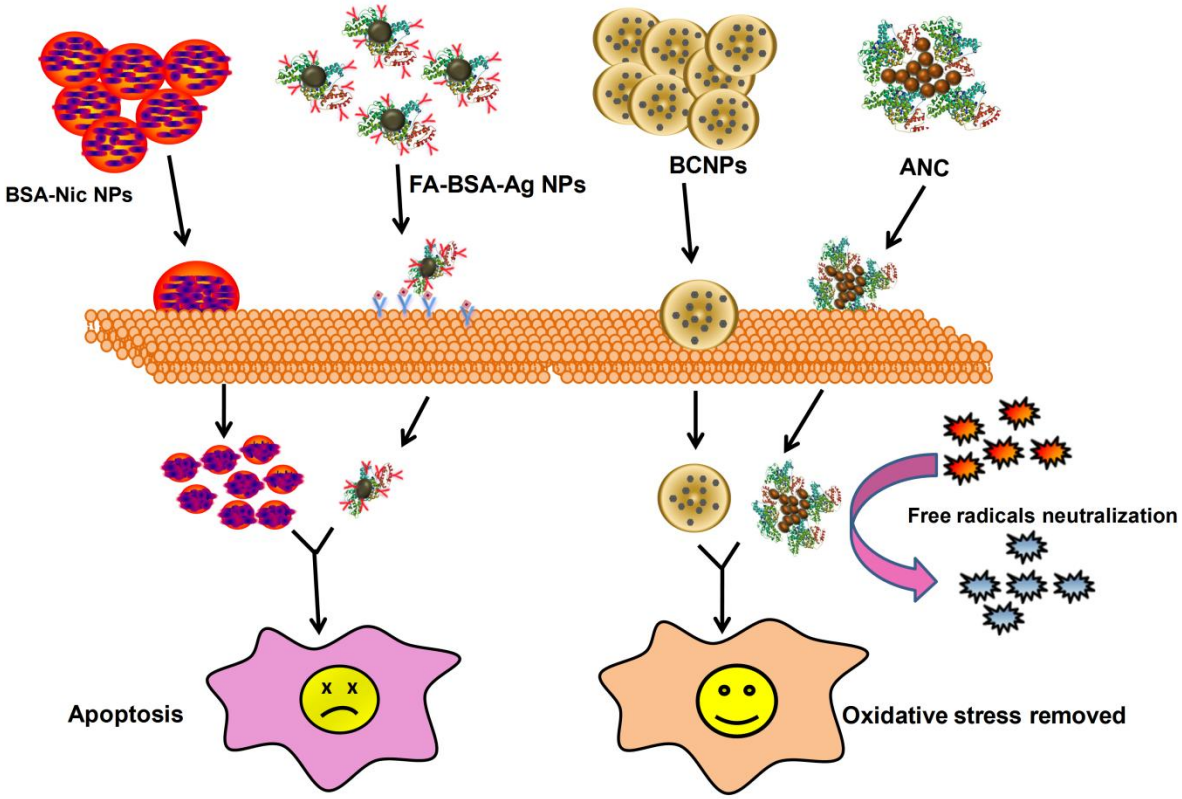

CHAPTER 8

CONCLUDING REMARKS

8.1 Conclusions

A major challenge in the field of nanomedicine is to transform laboratory innovations into commercial successful clinical products. In this campaign, a variety of nanocarrier based approaches has been designed and investigated for their role in biomedical applications. The advantages associated with the unique structure of albumin imparts it with the ability to interact with variety of molecules, while the functional groups present on their surface provide base for large number of modifications making it as an ideal nanocarrier system. This thesis illustrates the design and characterization of albumin based nanoparticles and revealed their tremendous potential to be utilized for both cancer and antioxidant therapy.

A highly feasible and reproducible method has been described to form hydrophobic anticancer drug niclosamide encapsulated albumin nanoparticles with enhanced water solubility and improved therapeutic efficacy. Such nanoformulations were further characterized and investigated *in vitro* for their role in inducing programmed cell death in human breast and lung cancer cells. Further, FR targeted folate conjugated bovine serum albumin stabilized silver nanoparticles were successfully synthesized with enhanced therapeutic efficacy, improved bioavailability, and efficient aqueous solubility by carbodiimide covalent reaction. Such system was further characterized and *in vitro* evaluated for their role in successful induction of apoptosis in human breast and lung cancer cells. The results corroborates that the FA-BSA-Ag NPs successfully induced apoptosis even at lower Ag NPs concentration as a result of improved bioavailability.

In addition, albumin nanocarrier was utilized to develop an artificial antioxidant mimetic enzyme loaded delivery system. Such artificial enzyme remain stable inside the cells and provide desired steady state level of therapeutic dose as a result of controlled release of CNPs that helps in defending the cells against actively generating ROS over a period of time. The results demonstrate the development of CNPs encapsulated albumin nanoparticles without altering their antioxidant activity. Such delivery system was further typified and examined *in vitro* for their role in protection against ROS in human lung epithelial cell line. Moreover, the

as-prepared BCNPs were also assessed for their biocompatibility and cellular uptake by L-132 cells. Finally, albumin coated nanoceria was synthesized and the antioxidant potential of such system was further investigated *in vitro* on L-132 cells and *in vivo* on zebrafish. The results demonstrated that the albumin coating provide biocompatibility to as-prepared ANC, while the antioxidant potential of such system was found to be comparable with that of CNPs. Thus, these albumin based nanostructures provides safe and effective alternative approach for biomedical applications.

8.2 Scope for Future Work

Future work could be focussed on elucidating the fundamental questions associated with their therapeutic efficacy and mechanism of action *in vivo* and to explore the hidden potential of these nanoparticles for various biomedical applications. In my view, the following are the main areas to focus on:

- The albumin based nanocarriers could be further investigated on animal models for their *in vivo* therapeutic efficacy.
- The niclosamide encapsulated albumin nanoparticles could be conjugated with tumor specific markers and imaging probe in order to develop tumor targeted theranostic system.
- The anticancer drug niclosamide shall be used in combination therapy with other therapeutic agents.
- ROS scavenging potential of albumin based nanoceria particles could be investigated for their role in other ROS induced diseases and disorders both *in vitro* and *in vivo*.
- The apoptotic and antioxidant gene expression studies could be further investigated by real time PCR and western blotting analysis.
- Nanofiber scaffold could be made from albumin based Ag NPs for wound dressing applications.
- Albumin based nanoceria particles could be further examined for their role in bio-sensing applications.
- Moreover, BSA could be substituted by HSA in future experiments in order to avoid a possible immunologic response *in vivo*.

REFERENCES

1. Abdelwahed, W., Degobert, G., Stainmesse S. and Fessi, H., Freeze-drying of nanoparticles: formulation, process and storage considerations. *Adv. Drug Delivery Rev*., 58, 1688–1713 (2006).
2. Ali, S. S., Hardt, J. I., Quick, K. L., Kim-Han, J. S., Erlanger, B. F., Huang, T. T., Epstein, C. J., Dugan, L. L., A biologically effective fullerene (C60) derivative with superoxide dismutase mimetic properties. *Free Radic. Biol. Med*., 37, 1191-1202 (2004).
3. Allen, S., Sotos, J., Sylte M. J. and Czuprynski, C. J., Use of Hoechst 33342 Staining To Detect Apoptotic Changes in Bovine Mononuclear Phagocytes Infected with *Mycobacterium avium* subsp.*paratuberculosis. Clin. Diagn. Lab. Immunol*., 8, 460–464 (2001).
4. Ando, T., Mimura, K., Johansson, C. C., Hanson, M. G., Mougiakakos, D., Larsson, C., Martins da Palma, T., Sakurai, D., Norell, H., Li, M., Nishimura M. I. and Kiessling, R., Transduction with the antioxidant enzyme catalase protects human T cells against oxidative stress. *J. Immunol.*, 181, 8382 (2008).
5. Anitha, A., Uthaman, S., Nair, S. V., Jayakumar, R. and Lakshmanan, V. K., Enhanced delivery system of flutamide loaded chitosan-dextran sulphate nanoparticles for prostate cancer. *J. Biomed. Nanotechnol.*, 9, 335-347 (2013).
6. Asharani, P. V., Mun, G. L. K., Hande, M P. and Valiyaveettil, S., Cytotoxicity and genotoxicity of silver nanoparticles in human cells. *ACS Nano*, 3, 279-290 (2009).
7. Asharani, P. V., Wu, Y.L., Gong, Z., and Valiyaveettil, S., Toxicity of silver nanoparticles in zebrafish models. *Nanotechnology*, 19, 255102 (2008).
8. Babio, B. M., NADPH oxidase: an update. *Blood*, 93, 1464–1476 (1999).
9. Bai M. Y. and Yang, H. C., Fabrication of novel niclosamide-suspension using an electrospray system to improve its therapeutic effects in ovarian cancer cells in vitro. *Colloids Surf., A*, 419, 248–256 (2013).
10. Balgi, A. D., Fonseca, B. D., Donohue, E., Tsang, T. C., Lajoie, P., Proud, C. G., Nabi, I.R. and Roberge, M., Screen for chemical modulators of autophagy reveals novel therapeutic inhibitors of mTORC1 signaling. *PLoS One*, 4, e7124 (2009).
11. Baran, E. J., Spectroscopic investigation of the VO^{2+}/chitosan interaction. *Carbohydr. Polym*., 74, 704–706 (2008).

12. Bargagli, E., Olivieri, C., Bennett, D., Prasse, A., Muller-Quernheim J. and Rottoli, P., Oxidative stress in the pathogenesis of diffuse lung diseases: A review. *Respir. Med*., 103, 1245–1256 (2009).
13. Bendayan, M., Reddy, J. K., Immunocytochemical localization of catalase and heat-labile enoyl-CoA hydratase in the livers of normal and peroxisome proliferator-treated rats. *Lab Invest*., 47, 364–369 (1982).
14. Bhushan, B. and Gopinath, P., Antioxidant nanozyme: A facile synthesis and evaluation of reactive oxygen species scavenging potential of nanoceria encapsulated albumin nanoparticles. *J. Mater. Chem. B*, 3, 4843-4852 (2015a).
15. Bhushan, B., Dubey, P., Uday Kumar, S., Sachdev, A., Matai I. and Gopinath, P., Bionanotherapeutics: Niclosamide Encapsulated Albumin Nanoparticles as a Novel Drug Delivery System for Cancer Therapy. *RSC Adv*., 5, 12078-12086 (2015b).
16. Bhushan, B. and Gopinath P., Tumor-targeted folate-decorated albumin-stabilised silver nanoparticles induce apoptosis at low concentration in human breast cancer cells. *RSC Adv*., 5, 86242-86253 (2015c).
17. Bhushan, B., Uday Kumar, S., Matai, I., Sachdev, A., Dubey P. and Gopinath, P., Ferritin Nanocages: A novel platform for biomedical applications. *J. Biomed. Nanotechnol*., 10, 2950-2976 (2014).
18. Bilthariya, U., Jain N., Rajoriya, V. and Jain, A. K., Folate-conjugated albumin nanoparticles for rheumatoid arthritis-targeted delivery of etoricoxib. *Drug Dev. Ind. Pharm.*, 41, 95-104 (2015).
19. Biswas, K., Roy, J. K., Doley, R., Mohanta, D. and Mukherjee, A. K., Imaging Bactericidal Effect of Faceted Ag Nanostructures (FAgN) on Gram Negative, Coli Form *Escherichia coli* Bacteria. *J. Bionanosci*., 8, 248-254 (2014).
20. Boise, L. H., Gonzalez-Garcia, M., Postema, C. E., Ding, L., Lindsten, T., Turka, L. A., Mao, X., Nunez G. and Thompson, C. B., bcl-x, a bcl-2-related gene that functions as a dominant regulator of apoptotic cell death. *Cell*, 74, 597–608 (1993).
21. Bose, B., Khanna, N., Acharya, S. K. and Sinha, S., Generation and characterization of a high-affinity chimaeric antibody against hepatitis B surface antigen. *Biotechnol. Appl. Biochem*., 43, 93-101 (2006a).
22. Bose, B., Khanna, N., Acharya, S. K. and Sinha, S., Generation and characterization of a single-gene mouse-human chimeric antibody against hepatitis B surface antigen. *J. Gastroenterol. Hepatol*., 9, 1439-1447 (2006b).
23. Bose, B., Khanna, N., Acharya, S. K. and Sinha, S., High affinity mouse-human chimeric Fab against hepatitis B surface antigen. *World J. Gastroenterol*., 11, 7569-7578 (2005).

24. Breslow R. and Overman, L. E., "Artificial enzyme" combining a metal catalytic group and a hydrophobic binding cavity. *J. Am. Chem. Soc*., 92, 1075–1077 (1970).
25. Brigelius-Flohe, R., Tissue-specific functions of individual glutathione peroxidases. *Free Radic. Biol. Med*., 27, 951–965 (1999).
26. Bronich, T. K., Keifer, P. A., Shlyakhtenko, L. S. and Kabanov, A. V., Polymer micelle with cross-linked ionic core. *J. Am. Chem. Soc*., 127, 8236–8237 (2005).
27. Brown, S. D., Nativo, P., Smith, J. A., Stirling, D., Edwards, P. R., Venugopal, B., Flint, D. J., Plumb, J. A., Graham, D. and Wheate, N. J., Gold Nanoparticles for the improved Anticancer Drug Delivery of the Active Component of Oxaliplatin. *J. Am. Chem. Soc*., 132, 4678-4684 (2010).
28. Brunet, A., Bonni, A., Zigmond, M. J., Lin, M. Z., Juo, P., Hu, L. S., Anderson, M. J., Arden, K. C., Blenis, J. and Greenberg, M. E., Akt promotes cell survival by phosphorylating and inhibiting a Forkhead transcription factor. *Cell*, 96, 857–868 (1999).
29. Cadenas, E., Mitochondrial free radical production and cell signaling. *Mol. Aspects Med*., 25, 17–26 (2004).
30. Cai, W., Shin, D. W., Chen, K., Gheysens, O., Cao, Q., Wang, S. X., Gambhir, S. S. and Chen, X., Peptide-labeled near-infrared quantum dots for imaging tumor vasculature in living subjects. *Nano Lett*., 6, 669-676, (2006).
31. Celardo, I., Pedersen, J. Z., Traversa E. and Ghibelli, L., Pharmacological potential of cerium oxide nanoparticles. *Nanoscale*, 3, 1411–1420 (2011).
32. Chairuangkitti, P., Lawanprasert, S., Roytrakul, S., Aueviriyavit, S., Phummiratch, D., Kulthong, K., Chanvorachote P. and Maniratanachote, R., Silver nanoparticles induce toxicity in A549 cells via ROS-dependent and ROS-independent pathways. *Toxicol. In Vitro*, 27, 330–338 (2013).
33. Chan, W.C.W. and Nie. S., Quantum dot bioconjugates for ultrasensitive nonisotopic detection. *Science*, 281, 2016-2018 (1998).
34. Chen, D., Tang, Q., Xue, W., Xiang, J., Zhang, L. and Wang, X., The preparation and characterization of folate-conjugated human serum albumin magnetic cisplatin nanoparticles. *J. Biomed. Res*., 24, 26–32 (2010).
35. Chen, J. P., Patil, S., Seal S. and McGinnis, J.F., Rare earth nanoparticles prevent retinal degeneration induced by intracellular peroxides. *Nat. Nanotechnol*., 1, 142–150 (2006).
36. Chen, W. R., Adams, R. L., Carubelli, R. and Nordquist, R. E., Laser-photosensitizer assisted immunotherapy: a novel modality for cancer treatment. *Cancer Lett*., 115, 25-30 (1997).

37. Chen, W. R., Adams, R. L., Higgins, A. K., Bartels, K. E. and Nordquist, R. E., Photothermal effects on murine mammary tumors using indocyanine green and an 808-nm diode laser: an in vivo efficacy study. *Cancer Lett*., 98, 169-173 (1996).
38. Cherian, A. M., Nair, S.V. and Lakshmanan, V. K., The role of nanotechnology in prostate cancer theranostic applications. *J. Nanosci. Nanotechnol*., 14, 841-852 (2014).
39. Choi, D. S., Park , J., Kim, S., Gracias, D. H., Cho, M. K., Kim, Y. K., Fung, A., Lee, S. E., Chen, Y., Khanal, S., Baral, S.and Kim, J. H., Hyperthermia with magnetic nanowires for inactivating living cells. *J. Nanosci. Nanotechnol.*, 8, 2323-2327 (2008).
40. Chowdhuri, A. R., Tripathy, S., Haldar, C., Chandra, S., Das, B., Roy S. and Sahu, S.K., Theoretical and experimental study of folic acid conjugated silver nanoparticles through electrostatic interaction for enhance antibacterial activity. *RSC Adv.*, 5, 21515–21524 (2015).
41. Colon, J., Hsieh, N., Ferguson, A., Kupelian, P., Seal, S., Jenkins D. W. and Baker, C. H., Cerium oxide nanoparticles protect gastrointestinal epithelium from radiation-induced damage by reduction of reactive oxygen species and upregulation of superoxide dismutase 2. *Nanomed.: Nanotechnol., Biol. Med.*, 6, 698–705 (2010).
42. Copin, J. C., Gasche, Y. and Chan, P. H., Overexpression of copper/zinc superoxide dismutase does not prevent neonatal lethality in mutant mice that lack manganese superoxide dismutase. *Free Radic. Biol. Med.*, 28, 1571–1576 (2000).
43. Cortes, J. and Saura, C., Nanoparticle albumin-bound (nab™)-paclitaxel: improving efficacy and tolerability by targeted drug delivery in metastatic breast cancer. *EJC Suppl*., 8, 1–10 (2010).
44. Couvreur, P. and Vauthier, C., Nanotechnology: intelligent design to treat complex disease. *Pharm. Res*., 23, 1417–1450 (2006).
45. Couvreur, P., Kante, B., Roland, M. and Speiser, P., Adsorption of antineoplastic drugs to poly(alkyl cyanoacrylate) nanoparticles and their release in calf serum. *J. Pharm. Sci*. 68, 1521-1524 (1979).
46. Crisante, F., Francolini, I., Bellusci, M., Martinelli, A., D'Ilario, L. and Piozzi, A., Antibiotic delivery polyurethanes containing albumin and polyallylamine nanoparticles. *Eur. J. Pharm. Sci*., 36, 555–564 (2009).
47. Dai, J., Wang, W., Liang, Y., Li, H., Guan X. and Zhu, Y., A novel molluscicidal formulation of niclosamide. *Parasitol. Res*., 103, 405–412 (2008).
48. Darroudi, M., Sarani, M., Oskuee, R. K., Zak, A. K., Hosseini H. A. and Gholami, L., Green synthesis and evaluation of metabolic activity of starch mediated nanoceria. *Ceram. Int.*, 40, 2041–2045 (2014).

49. Darzynkiewicz, Z., Bruno, S., Del, B. G., Gorczyca, W., Hotz, M. A., Lassota P. and Traganos, F., Features of apoptotic cells measured by flow cytometry. *Cytometry,* 13, 795−808 (1992).
50. Das, M., Patil, S., Bhargava, N., Kang, J. F., Riedel, L. M., Seal S. and Hickman, J. J., Auto-catalytic Ceria Nanoparticles Offer Neuroprotection to Adult Rat Spinal Cord Neurons. *Biomaterials*, 28, 1918-1925 (2007).
51. D'Cruz, A. K., Robinson, M. H. and Biel, M. A., mTHPC-mediated photodynamic therapy in patients with advanced, incurable head and neck cancer: a multicenter study of 128 patients. *Head Neck*, 26, 232-240 (2004).
52. Desai, N., Abraxis BioScience, Inc. Nanoparticle albumin bound (nab) technology: targeting tumors through the endothelial gp60 receptor and SPARC. *Nanomedicine*, 3, 337–346 (2007).
53. Devarakonda, B., Hill, R. A., Liebenberg, W., Brits M. and Villiers, M.M. D., Comparison of the aqueous solubilization of practically insoluble niclosamide by polyamidoamine (PAMAM) dendrimers and cyclodextrins. *Int. J. Pharm*., 304, 193–209 (2005).
54. Diepold, R., Kreuter, J., Guggenbuhl, P. and Robinson, J. R., Distribution of poly-hexyl- 2-cyano-[3-14C]acrylate nanoparticles in healthy and chronically inflamed rabbit eyes. *Int. J. Pharm.*, 54, 149-153 (1989).
55. Dolmans, D. E., Fukumura, D. and Jain, R. K., Photodynamic therapy for cancer. *Nat. Rev. Cancer*, 3, 380-387 (2003).
56. Dowling., J. J., Arbogast, S., Hur, J., Nelson, D. D., McEvoy, A., Waugh, T., Marty, I., Lunardi, J., Brooks, S. V., Kuwada, J. Y. and Ferreiro, A., Oxidative stress and successful antioxidant treatment in models of RYR1-related myopathy. *Brain*, 135, 1115-1127 (2012).
57. Dubey, P., Bhushan, B., Sachdev, A., Matai, I., Uday Kumar S. and Gopinath, P., Silver nanoparticles incorporated composite nanofiber for potential wound dressing applications. *J. App. Polm. Sci.*, 132, 42473 (2015a).
58. Dubey, P., Matai, I., Uday Kumar, S., Sachdev, A., Bhushan, B. and Gopinath, P., Perturbation of cellular mechanistic system by silver nanoparticles toxicity: cytotoxic, genotoxic and epigenetic potential. *Adv. Colloids Inter. Sci.*, 221, 4-21 (2015b)
59. Dugan, L. L., Turetsky, D. M., Du, C., Lobner, D., Wheeler, M., Almli, C. R., Shen, C. K., Luh, T. Y., Choi, D.W. and Lin, T. S., Carboxyfullerenes as neuroprotective agents. *Proc. Natl. Acad. Sci. U S A.*, 94, 9434-9439 (1997).

60. Duncan, R. (2005) Targeting and intracellular delivery of drugs. *In Encyclopedia of Molecular Cell Biology and Molecular Medicine*, Ed. R A Meyers. Weinheim, Germany: Wiley-VCH Verlag. 14, 163-204 (2005).
61. Edwards-Jones V., The benefits of silver in hygiene, personal care and healthcare. *Lett. Appl. Microbiol.*, 49, 147-152 (2009).
62. El-Wahed, M. G., Refat M. S. and El-Megharbel, S. M., Synthesis, spectroscopic and thermal characterization of some transition metal complexes of folic acid. *Spectrochimica. Acta Part A*, 70, 916–922 (2008).
63. Elzoghby, A. O., El-Fotoh, W. S. and Elgindy, N. A., Casein-based formulations as promising controlled release drug delivery systems. *J. Control Release*, 153, 206-216 (2011).
64. Elzoghby, A. O., Samy, W. M. and Elgindy N. A., Albumin-based nanoparticles as potential controlled release drug delivery systems. *J. Control Release*, 157, 168-182 (2012a).
65. Elzoghby, A. O., Samy, W. M. and Elgindy, N. A., Novel spray-dried genipin-crosslinked casein nanoparticles for prolonged release of alfuzosin hydrochloride. *Pharm. Res*., 30, 512-522 (2013).
66. Elzoghby, A. O., Samy, W. M. and Elgindy, N. A., Protein-based nanocarriers as promising drug and gene delivery systems. *J. Control Release*, 161, 38-49 (2012b).
67. Emerit, J., Edeas A. and Bricaire, F., Neurodegenerative diseases and oxidative stress. *Biomed. Pharmacother*., 58, 39–46 (2004).
68. Fahmi, M. Z., Ou, K. L., Chen, J. K., Ho, M. H., Tzingg, S. H. and Chang, J. Y., Development of bovine serum albumin-modified hybrid nanoclusters for magnetofluorescence imaging and drug delivery. *RSC Adv*., 4, 32762–32772 (2014).
69. Fan, K., Cao, C., Pan, Y., Lu, D., Yang, D., Feng, J., Song, L., Liang, M. and Yan, X., Magnetoferritin nanoparticles for targeting and visualizing tumour tissues. *Nat. Nanotechnol.*, 7, 459-464 (2012).
70. Farokhzad, O. C., Jon, S., Khademhosseini, A., Tran, T. N. T. LaVan, D. A. and Langer, R., Nanoparticle-aptamer bioconjugates: A new approach for targeting prostate cancer cells. *Cancer Res*., 64, 7668-7672 (2004).
71. Fink S. L. and Cookson, B. T., Apoptosis, pyroptosis, and necrosis: mechanistic description of dead and dying eukaryotic cells. *Infect. Immun*., 73, 1907–1916 (2005).
72. Finkel T. and Holbrook, N. J., Oxidants, oxidative stress and the biology of ageing. *Nature*, 408, 239–247 (2000).

73. Gabizon, A., Horowitz, A. T., Goren, D., Tzemach, D., Mandelbaum-Shavit, F., Qazen M. M. and Zalipsky, S., Targeting folate receptor with folate linked to extremities of poly(ethylene glycol)-grafted liposomes: in vitro studies. *Bioconjugate Chem*., 10, 289–298 (1999).
74. Gangadharan, D., Harshvardan, K., Gnanasekar, G., Dixit, D., Popat, K. M. and Anand, P. S., Polymeric microspheres containing silver nanoparticles as a bactericidal agent for water disinfection. *Water Res*., 44, 5481-5487 (2010).
75. Gebregeorgis, A., Bhan, C., Wilson O. and Raghavan, D., Characterization of Silver/Bovine Serum Albumin (Ag/BSA) nanoparticles structure: morphological, compositional, and interaction studies. *J. Colloid Interface Sci*., 389, 31–41 (2013).
76. Gharwan, H., Wightman, L., Kircheis, R., Wagner, E. and Zatloukal, K., Nonviral gene transfer into fetal mouse livers (a comparison between the cationic polymer PEI and naked DNA). *Gene Ther.*, 10, 810-817. (2003).
77. Girija, D., Naik, H. S. B., Sudhamani C. N. and Kumar, B. V., Cerium oxide nanoparticles - a green, reusable, and highly efficient heterogeneous catalyst for the synthesis of Polyhydroquinolines under solvent-free conditions. *Arch. Appl. Sci. Res.*, 3, 373–382 (2011).
78. Gogoi, S. K., Gopinath, P., Paul, A., Ramesh, A., Ghosh, S. S. and Chattopadhyay, A., Green fluorescent protein-expressing Escherichia coli as a model system for investigating the antimicrobial activities of silver nanoparticles. *Langmuir*, 22, 9322-9328 (2006).
79. Goharshadi, E. K., Samiee S. and Nancarrow, P., Fabrication of cerium oxide nanoparticles: Characterization and optical properties. *J. Colloid Interface Sci*., 356, 473−480 (2011).
80. Gopinath, P., Gogoi, S. K., Chattopadhyay A., and Ghosh, S. S., Implications of silver nanoparticle induced cell apoptosis for in vitro gene therapy. *Nanotechnology*, 19, 075104 (2008).
81. Gopinath, P., Gogoi, S. K., Sanpui, P., Paul, A., Chattopadhyay, A. and Ghosh, S. S., Signaling gene cascade in silver nanoparticle induced apoptosis. *Colloids Surf., B*, 77, 240–245 (2010).
82. Gopinath, P., Uday Kumar, S., Matai, I., Bhushan, B., Malwal, D., Sachdev, A. and Dubey, P., Cancer Nanotheranostics. *Springer briefs in applied science and technology*, pp. 1–93 (2015).
83. Green, M. R., Manikhas, G. M., Orlov, S., Afanasyev B. and Makhson, A. M., Abraxane, a novel Cremophor-free, albumin-bound particle form of paclitaxel for the treatment of advanced non-small-cell lung cancer. *Ann. Oncol*., 17, 1263–1268 (2006).

84. Grum-Schwensen, B., Klingelhofer, J., Berg, C. H., El-Naaman, C., Grigorian, M., Lukanidin, E. and Ambartsumian, N., Suppression of tumor development and metastasis formation in mice lacking the S100A4 (mts1) gene. *Cancer Res.*, 65, 3772-3780 (2005).
85. Halliwell, B., Role of free radicals in the neurodegenerative diseases: therapeutic implications for antioxidant treatment. *Drugs Aging*, 18, 685–716 (2001).
86. Hanslick, J. L., Lau, K., Noguchi, K. K., Olney, J. W., Zorumski, C. F., Mennerick S. and Farber, N. B., Dimethyl sulfoxide (DMSO) produces widespread apoptosis in the developing central nervous system. *Neurobiol. Dis*., 34, 1–10 (2009).
87. Harris, E. D., Regulation of antioxidant enzymes. *J. FASEB*., 6, 2675-2683 (1992).
88. Hashimoto, F. and Hayashi, H., Significance of catalase in peroxisomal fatty acyl-CoA beta-oxidation: NADH oxidation by acetoacetyl-CoA and H_2O_2. *J. Biochem*., 108, 426–431 (1990).
89. Hayes, J. D., Flanagan, J. U. and Jowsey, I. R., Glutathione transferases. *Annu. Rev. Pharmacol. Toxicol*., 45, 51–88 (2005).
90. Heckert, E. G., Karakoti, A. S., Seal S. and Self, W. T., The role of cerium redox state in the SOD mimetic activity of nanoceria. *Biomaterials*, 29, 2705–2709 (2008).
91. Hengartner, M. O., The biochemistry of apoptosis. *Nature*, 407, 770–776 (2000).
92. Hill, A. J., Teraoka, H., Heideman, W. and Peterson, R. E., Zebrafish as a model vertebrate for investigating chemical toxicity. *Toxicol. Sci*., 86, 6-19 (2005).
93. Hirsch, T., Marchetti, P., Susin, S. A., Dallaporta, B., Zamzami, N., Marzo, I., Geuskens, M. and Kroemer G., The apoptosis-necrosis paradox. Apoptogenic proteases activated after mitochondrial permeability transition determine the mode of cell death. *Oncogene*, 15, 1573–1581 (1997).
94. Hirst, S. M., Karakoti, A. S., Tyler, R.D., Sriranganathan, N., Seal S. and Reilly, C. M., Anti-inflammatory properties of cerium oxide nanoparticles. *Small*, 5, 2848–2856 (2009).
95. Horvitz, HR., Genetic control of programmed cell death in the nematode Caenorhabditis elegans. *Cancer Res*., 59, 1701s–1706s (1999).
96. Hossain, M., Khan A. Y., and Kumar, G. S., Interaction of the Anticancer Plant Alkaloid Sanguinarine with Bovine Serum Albumin. *PLoS One*, 6, e18333 (2011).
97. Hsin, Y. H., Chen, C. F., Huang, S., Shih, T. S., Lai, P. S. and Chueh, P., The apoptotic effect of nanosilver is mediated by a ROS- and JNK-dependent mechanism involving the mitochondrial pathway in NIH3T3 cells. *J. Toxicol. Lett.*, 179, 130-139 (2008).

98. Huang, P., Li, Z., Hu H. and Cui, D., Synthesis and Characterization of Bovine Serum Albumin-Conjugated Copper Sulfide Nanocomposites. *J. Nanomater*., 2010, 641545 (2010).
99. Ibrahim, N. K., Desai, N., Legha, S., Soon-Shiong, P., Theriault, R.L., Rivera, E., Esmaeli, B., Ring, S. E., Bedikian, A., Hortobagyi, G. N. and Ellerhorst, J. A., Phase I and pharmacokinetic study of ABI-007, a Cremophor-free, protein-stabilized, nanoparticle formulation of paclitaxel. *Clin. Cancer Res*., 8, 1038–1044 (2002).
100. Israel, L., editor. Conquering Cancer. *New York: Random House*, (1978).
101. Jahanshahi, M. and Babaei, Z., Protein nanoparticle: a unique system as drug delivery vehicles. *African J. Biotechnol*., 7, 4926–4934 (2008).
102. Jana, S. S., Bharali, D. J., Mani, P., Maitra, A., Gupta, C. M. and Sarkar, D. P., Targeted cytosolic delivery of hydrogel nanoparticles into HepG2 cells through engineered Sendai viral envelopes. *FEBS Lett*., 515,184-188 (2002).
103. Jiang, W., Kim, B. Y. S., Rutka, J. T. and Chan, W.C.W., Nanoparticle-mediated cellular response is size-dependent. *Nat. Nanotechnol*., 3, 145-150, (2008).
104. Jiao, X., Song, H. J., Zhao, H. H., Bai, W., Zhang L. C. and Lv, Y., Well-redispersed ceria nanoparticles: Promising peroxidase mimetics for H_2O_2 and glucose detection. *Anal. Methods*, 4, 3261–3267 (2012).
105. Jin, Y., Lu, Z., Ding, K., Li, J., Du, X., Chen, C., Sun, X., Wu, Y., Zhou J. and Pan, J., Antineoplastic mechanisms of niclosamide in acute myelogenous leukemia stem cells: inactivation of the NF-kappaB pathway and generation of reactive oxygen species. *Cancer Res*., 70, 2516–2527 (2010).
106. Jithan, A. V., Madhavi, K., Madhavi M. and Prabhakar, K., Preparation and characterization of albumin nanoparticles encapsulating curcumin intended for the treatment of breast cancer. *Int. J. Pharm. Investig.*, 2, 119–125 (2011).
107. Joshi, M. D., and Mueller, R. H. Lipid nanoparticles for parenteral delivery of actives. *Eur. J. Pharm. Biopharm*., 71, 161-172 (2009).
108. Kadam, S. and Gracias, D. H., Natural and Synthetic Nanoporous Membranes for Cell Encapsulation Therapy in *Bioengineered Nanomaterials*, *CRC Press*, 199-224 (2013).
109. Kang M. C., Cha, S. H., Wijesinghe, W. A., Kang, S. M., Lee, S. H., Kim, E. A., Song, C. B. and Jeon, Y. J., Protective effect of marine algae phlorotannins against AAPH-induced oxidative stress in zebrafish embryo. *Food Chem*., 138, 950-955 (2013a).
110. Kang, M. C., Kim, K. N., Kang, S. M., Yang, X., Kim, E. A., Song, C. B., Nah, J. W., Jang, M. K., Lee, J. S., Jung, W. K. and Jeon, Y. J., Protective effect of dieckol isolated from

Ecklonia cava against ethanol caused damage in vitro and in zebrafish model. *Environ. Toxicol. Pharmacol*., 36, 1217-1226 (2013b).

111. Kang, M. C., Kim, S. Y., Kim, Y. T., Kim, E. A., Lee, S. H., Ko, S. C., Wijesinghe, W. A., Samarakoon, K. W., Kim, Y. S., Cho, J. H., Jang, H. S. and Jeon, Y. J., In vitro and in vivo antioxidant activities of polysaccharide purified from aloe vera (Aloe barbadensis) gel. *Carbohydr. Polym.*, 99, 365-371 (2014).
112. Kannan K. and Jain, S. K., Oxidative stress and apoptosis. *Pathophysiology*, 7, 153-163 (2000).
113. Karakoti, A. S., Kuchibhatla, S. V. N. T., Babu K. S. and Seal, S., Direct synthesis of nanoceria in aqueous polyhydroxyl solutions. *J. Phys. Chem. C*, 111, 17232–17240 (2007).
114. Karakoti, A. S., Monteiro-Riviere, N. A., Aggarwal, R., Davis, J. P., Narayan, R. J., Self, W. T., McGinnis J. and Seal, S., Nanoceria as Antioxidant: Synthesis and Biomedical Applications. *JOM.*, 60, 33–37 (2008).
115. Karakoti, A. S., Singh, S., Kumar, A., Malinska, M., Kuchibhatla, S. V. N. T., Wozniak, K., Self W.T. and Seal, S., PEGylated Nanoceria as Radical Scavenger with Tunable Redox Chemistry. *J. Am. Chem. Soc*., 131, 14144–14145 (2009).
116. Kenawy E. and Rizk, E., Polymeric Controlled Release Formulations of Niclosamide for Control of*Biomphalaria Alexandrina*, the Vector Snail of Schistosomiasis. *Macromol. Biosci*., 4, 119–128 (2004).
117. Kerman, K., Saito, M., Tamiya, E., Yamamura, S. and Takamura, Y., Nanomaterial-based electrochemical biosensors for medical applications. *TrAC Trends Anal. Chem*., 2008, 27, 585−592 (2008).
118. Kerr, J. F., Wyllie, A. H. and Currie, A. R., Apoptosis: a basic biological phenomenon with wide-ranging implications in tissue kinetics. *Br. J. Cancer*, 26, 239–257 (1972).
119. Khan, J. M., Qadeer, A., Ahmad, E., Ashraf, R., Bhushan, B., Chaturvedi, S. K., Rabbani, G. and Khan, R. H., Monomeric banana lectin at acidic pH overrules conformational stability of its native dimeric form. *PLoS One*, 8, e62428 (2013).
120. Kim, E. A., Lee, S. H., Ko, C. I., Cha, S. H., Kang, M. C., Kang, S. M., Ko, S. C., Lee, W. W., Ko, J. Y., Lee, J. H., Kang, N., Oh, J. Y., Ahn, G., Jee, Y. H. and Jeon, Y. J.,. Protective effect of fucoidan against AAPH-induced oxidative stress in zebrafish model. *Carbohydr Polym*., 102, 185-191 (2014a).
121. Kim, H. R., Shin da, Y., Park, Y. J., Park, C. W., Oh, S. M. and Chung K. H., Silver nanoparticles induce p53-mediated apoptosis in human bronchial epithelial (BEAS-2B) cells. *J. Toxicol Sci*., 39, 401-412 (2014b).

122. Kim, E. A., Kang, M. C., Lee, J. H., Kang, N., Lee, W. W., Oh, J. Y., Yang, H. W., Lee, J. S. and Jeon, Y. J., Protective effect of marine brown algal polyphenols against oxidative stressed zebrafish with high glucose. *RSC Adv.*, 5, 25738-25746 (2015).
123. Kipp, J. E., The role of solid nanoparticle technology in the parenteral delivery of poorly water-soluble drugs. *Int. J. Pharm*., 284, 109-122 (2004).
124. Ko, J. Y., Kim, E. A., Lee, J. H., Kang, M. C., Lee, J. S., Kim, J. S., Jung, W. K. and Jeon, Y. J., Protective effect of aquacultured flounder fish-derived peptide against oxidative stress in zebrafish. *Fish Shellfish Immunol*., 36, 320-323 (2014).
125. Koh, C. G., Zhang, X., Liu, S., Golan, S., Yu, B., Yang, X., Guan, J., Jin, Y., Talmon, Y., Muthusamy, N., Chan, K. K., Byrd, J. C., Lee, R. J., Marcucci, G. and Lee, L. J., Delivery of antisense oligodeoxyribonucleotide lipopolyplex nanoparticles assembled by microfluidic hydrodynamic focusing. *J. Controlled Release*, 141, 2-69. (2010).
126. Konan, Y. N., Gurny, R. and Allemann, E., State of the art in the delivery of photosensitizers for photodynamic therapy. *J. Photochem. Photobiol. B: Biol.*, 66, 89-106 (2002).
127. Kong J. and Shaoning, Y. U., Fourier Transform Infrared Spectroscopic Analysis of Protein Secondary Structures. *Acta Biochim. Biophys. Sin*., 39, 549–559 (2007).
128. Konwarh, R., Karak, N., Rai, S. K. and Mukherjee, A. K., Polymer-assisted iron oxide magnetic nanoparticle immobilized keratinase. *Nanotechnology*, 20, 225107 (2009).
129. Korsvik, C., Patil, S., Seal S. and Self, W. T., Superoxide dismutase mimetic properties exhibited by vacancy engineered ceria nanoparticles. *Chem. Commun.*, 10, 1056–1058 (2007).
130. Kratz, F., Albumin as a drug carrier: design of prodrugs, drug conjugates and nanoparticles. *J. Controlled Release*, 132, 171–183 (2008).
131. Kumar, B., Koul, S., Khandrika, L., Meacham R. B. and Koul, H. K., Oxidative stress is inherent in prostate cancer cells and is required for aggressive phenotype. *Cancer Res*., 68, 1777–1785 (2008).
132. Kumar, E., Selvarajan P. and Muthuraj, D., Synthesis and characterization of CeO2 nanocrystals by solvothermal route. *Mater. Res*., 16, 269-276 (2013).
133. Kumar, M., Mani, P., Pratheesh, P., Chandra, S., Jeyakkodi, M., Chattopadhyay, P., Sarkar, D. P. and Sinha, S., Membrane Fusion Mediated Targeted Cytosolic Drug Delivery Through scFv Engineered Sendai Viral Envelopes. *Curr. Mol. Med*., 15, 386-400 (2015).
134. Kumar, R. M. N., Nano and microparticles as controlled drug delivery devices. *J. Pharm. Pharm. Sci.*, 3, 234-258 (2000).

135. Kumar, R., Balasenthil, S., Pakala, S. B., Rayala, S. K., Sahin, A. A. and Ohshiro, K., Metastasis-associated protein 1 short form stimulates Wnt1 pathway in mammary epithelial and cancer cells. *Cancer Res*., 70, 6598-6608 (2010).
136. Lakshmanan, V. K., Snima, K. S., Bumgardner, J. D., Nair S. V. and Jayakumar, R., Chitosan-based nanoparticles in cancer therapy, *Adv. Polym. Sci.*, 243, 55–92 (2011).
137. Langer, K., Balthasar, S., Vogel, V., Dinauer, N., von Briesen, H. and Schubert, D., Optimization of the preparation process for human serum albumin (HSA) nanoparticles. *Int. J. Pharm*., 257, 169–180 (2003).
138. Leamon C. P. and Low, P.S., Delivery of macromolecules into living cells: a method that exploits folate receptor endocytosis. *Proc. Natl. Acad. Sci. U. S. A*., 88, 5572–5576 (1991).
139. Leamon C.P. and Reddy, J.A., Folate-targeted chemotherapy. *Adv. Drug Delivery Rev*., 56, 1127–1141 (2004).
140. Leamon, C. P., Folate-targeted drug strategies for the treatment of cancer. *Curr. Opin. Investig. Drugs.*, 9, 1277-1286 (2008).
141. Lee R. J. and Low, P. S., Delivery of liposomes into cultured KB cells via folate receptor-mediated endocytosis. *J. Biol. Chem*., 269, 3198–3204 (1994).
142. Lee R. J. and Low, P. S., Folate-mediated tumor cell targeting of liposome-entrapped doxorubicin in vitro. *Biochim. Biophys. Acta*, 1233, 134–144 (1995).
143. Lee, C. H., Yao, C. F., Huang, S. M., Ko, S., Tan, Y. H., Lee-Chen, G. J. and Wang, Y. C., Novel 2-step synthetic indole compound 1,1,3-tri(3-indolyl)cyclohexane inhibits cancer cell growth in lung cancer cells and xenograft models. *Cancer*, 113, 815–825 (2008).
144. Lee, E. S., Na K. and Bae, Y. H., Polymeric micelle for tumor pH and folate-mediated targeting. *J. Controlled Release*, 91, 103–113 (2003).
145. Lee, S. H., Heng, D., Ng, W. K., Chan, H. K. and Tan, R. B., Nano spray drying: a novel method for preparing protein nanoparticles for protein therapy. *Int. J. Pharm.*, 403, 192–200 (2011).
146. Lee, Y. H., Cheng, F. Y., Chiu, H. W., Tsai, J. C., Fang, C. Y., Chen C. W. and Wang, Y. J., Cytotoxicity, oxidative stress, apoptosis and the autophagic effects of silver nanoparticles in mouse embryonic fibroblasts. *Biomaterials*, 35, 4706–4715 (2014).
147. Li, C., Xing L. and Che, S., Coordination bonding based pH-responsive albumin nanoparticles for anticancer drug delivery. *Dalton Trans*., 41, 3714–3719 (2012).
148. Li, F. Q., Hu, J. H., Lu, B., Yao, H. and Zhang, W. G., Ciprofloxacin-loaded bovine serum albumin microspheres: preparation and drug-release in vitro. *J. Microencapsul*., 18, 825–829 (2001).

149. Lin, J., Zhou, Z., Li, Z., Zhang, C., Wang, X., Wang, K., Gao, G., Huang, P. and Cui, D., Biomimetic one-pot synthesis of gold nanoclusters/nanoparticles for targeted tumor cellular dual-modality imaging. *Nanoscale Res. Lett*., 8, 170 (2013).
150. Lin, W. Coombes, A. G., Garnett, M.C., Davies, M. C., Schacht, E., Davis, S. S. and Illum, L., Preparation of sterically stabilized human serum albumin nanospheres using a novel Dextranox-MPEG crosslinking agent. *Pharm. Res*., 11, 1588–1592 (1994).
151. Litwin, J. A., Völkl, A., Müller-Höcker, J., Hashimoto, T. and Fahimi, H. D., Immunocytochemical localization of peroxisomal enzymes in human liver biopsies. *Am. J. Pathol*., 128, 141–150 (1987).
152. Liu, X. Y., Wei, W., Yuan, Q., Zhang, X., Li, N., Du, Y. G., Ma, G. H., Yan C. H. and Ma, D., Apoferritin–CeO_2 nano-truffle that has excellent artificial redox enzyme activity. *Chem. Commun.*, 48, 3155–3157(2012).
153. Liu, X., Kim, C. N., Yang, J., Jemmerson R. and Wang, X., Induction of apoptotic program in cell-free extracts: requirement for dATP and cytochrome c. *Cell*, 86, 147–157 (1996).
154. Liu, Z., Jiao, Y., Wang, Y., Zhou C. and Zhang, Z., Polysaccharides-based nanoparticles as drug delivery systems. *Adv. Drug Deliv. Rev*., 60, 1650–1662 (2008).
155. Lu Y. J. and Low, P. S., Folate-mediated delivery of macromolecular anticancer therapeutic agents. *Adv. Drug Delivery Rev*., 54, 675– 693 (2002).
156. Lu, W., Lin, C., Roberts, M. J., Waud, W. R., Piazza G. A. and Li, Y., Niclosamide suppresses cancer cell growth by inducing Wnt co-receptor LRP6 degradation and inhibiting the Wnt/β-catenin pathway. *PLoS One*, 6, e29290 (2011).
157. Lu, Y., Yeung, N., Sieracki, N. and Marshall, N. M., Design of functional metalloproteins. *Nature*, 460, 855-862 (2009).
158. Luo, R., Neu, B. and Venkatraman, S. S., Surface functionalization of nanoparticles to control cell interactions and drug release. *Small*, 8, 2585-2594 (2012).
159. Maehashi, K., Katsura, T., Kerman, K., Takamura, Y., Matsumoto, K. and Tamiya, E., Label-free protein biosensor based on aptamer-modified carbon nanotube field-effect transistors. *Anal. Chem.*, 79, 782-787 (2007).
160. Maltas, E., Binding interactions of niclosamide with serum proteins. *J. Food Drug Anal*., 22, 549–555 (2014).
161. Manea, F., Houillon, F. B., Pasquato L. and P. Scrimin, P., Nanozymes: Gold-Nanoparticle-Based Transphosphorylation Catalysts. *Angew. Chem., Int. Ed.*, 43, 6165–6169 (2004).
162. Martınez, A., Olmo, R., Iglesias, I., Teijon J. M. and Blanco, M. D., Folate-Targeted Nanoparticles Based on Albumin and Albumin/Alginate Mixtures as Controlled

Release Systems of Tamoxifen: Synthesis and *In Vitro* Characterization. *Pharm. Res.*, 31, 182–193 (2014).

163. Masui, T., Hirai, H., Imanaka, N., Adachi, G., Sakata T. and Mori, H., Synthesis of cerium oxide nanoparticles by hydrothermal crystallization with citric acid. *J. Mater. Sci. Lett.*, 21, 489–491 (2002).
164. Matai, I., Sachdev, A. and Gopinath, P., Multicomponent 5-fluorouracil loaded PAMAM stabilized-silver nanocomposites synergistically induce apoptosis in human cancer cells. *Biomater. Sci.*, 3, 457-468 (2015).
165. Matai, I., Sachdev, A., Dubey, P., Uday Kumar, S., Bhushan B. and P.Gopinath, P., Antibacterial activity and mechanism of Ag-ZnO nanocomposite on S.aureus and GFP-expressing antibiotic resistant E.coli. *Colloids Surf., B*, 115, 359-367 (2014).
166. Mazurak, V. C., Burrell, R. E., Tredget, E. E., Clandinin M. T. and Field, C., The effect of treating infected skin grafts with Acticoat™ on immune cells. *Burns*, 33, 52-58 (2007).
167. McGinnis, J. F., Stepanik, P. L., Chen, W., Elias, R., Cao W. and Lerious, V., Unique retina cell phenotypes revealed by immunological analysis of recoverin expression in rat retina cells. *J. Neurosci. Res*., 55, 252–260 (1999).
168. McGinnis, J., Patil, S., Wong, L., Sezate, S., Chen J. and Seal, S., Inhibition of reactive oxygen species and protection of mammalian cells. US Pat., 7727559 (2010).
169. Meng, H., Chen, J. Y., Mi, L., Wang, P. N., Ge, M. Y., Yue Y. and Dai, N., Conjugates of folic acids with BSA-coated quantum dots for cancer cell targeting and imaging by single-photon and two-photon excitation. *JBIC, J. Biol. Inorg. Chem.*, 16, 117–123 (2011).
170. Merodio, M., Arnedo, A., Renedo, M. J. and Irache, J. M., Ganciclovir-loaded albumin nanoparticles: characterization and in vitro release properties. *Eur. J. Pharm. Sci*., 12, 251–259 (2001).
171. Mewada, A., Pandey, S., Thakur, M., Jadhav D. and Sharon, M., Swarming carbon dots for folic acid mediated delivery of doxorubicin and biological imaging. *J. Mater. Chem. B*, 2, 698–705 (2014).
172. Meziani, M. J. and Sun, Y. P., Protein-conjugated nanoparticles from rapid expansion of supercritical fluid solution into aqueous solution. *J. Am. Chem. Soc*., 125, 8015–8018 (2003).
173. Miele, E., Spinelli, G. P., Miele, E., Tomao F. and Tomao, S., Albumin-bound formulation of paclitaxel (Abraxane ABI-007) in the treatment of breast cancer. *Int. J. Nanomed*., 4, 99–105 (2009).
174. Miller, A. B., Hoogstraten, B., Staquet, M. and Winkler, A., Reporting results of cancer treatment. *Cancer*, 47, 207-214 (1981).

175. Minn, A. J., V´elez, P., Schendel, S. L., Liang, H., Muchmore, S. W., Fesik, S. W., Fill M. C. and Thompson, B., Bcl-x_L forms an ion channel in synthetic lipid membranes. *Nature*, 385, 353–357 (1997).
176. Misra, M. K., Sarwat, M., Bhakuni, P., Tuteja R. and Tuteja, N., Oxidative stress and ischemic myocardial syndromes. *Med. Sci. Monit*., 15, 209–219 (2009).
177. Nair, R. G., Roy, J. K., Samdarshi, S. K. and Mukherjee, A. K., Enhanced visible light photocatalytic disinfection of gram negative, pathogenic Escherichia coli bacteria with Ag/TiV oxide nanoparticles. *Colloids Surf. B Biointerfaces*, 86, 7-13 (2011).
178. Natarajan, J. V., Nugraha, C., Ng, X. W. and Venkatraman, S. Sustained-release from nanocarriers: A review. *J. Control. Release*, 193, 122-138 (2014).
179. Neumann, E., Frei, E., Funk, D., Becker, M. D., Schrenk, H. H., Muller-Ladner U. and Fiehn, C., Native albumin for targeted drug delivery. *Expert Opin. Drug Delivery*, 7, 915–925 (2010).
180. Niu, J. L., Azfer, A., Rogers, L. M., Wang X. H. and Kolattukudy, P. E., Cardioprotective effects of cerium oxide nanoparticles in a transgenic murine model of cardiomyopathy. *Cardiovasc. Res.*, 73, 549–559 (2007).
181. Niu, J., Wang K. and Kolattukudy, P. E., Cerium oxide nanoparticles inhibit oxidative stress and nuclear factor-κB activation in H9c2 cardiomyocytes exposed to cigarette smoke extract. *J. Pharmacol. Exp. Ther.*, 338, 53–61 (2011).
182. Norbury C. J. and Hickson I. D., Cellular responses to DNA damage. *Annu. Rev. Pharmacol. Toxicol.*, 41, 367–401 (2001).
183. Okuno, J., Maehashi, K., Kerman, K., Takamura, Y., Matsumoto, K. and Tamiya, E., Label-free immunosensor for prostate-specific antigen based on single-walled carbon nanotube array-modified microelectrodes. *Biosens. Bioelectron.*, 22, 2377-2381 (2007).
184. O'Neil, M. J., Smith, A., Heckelman P. E. and Budavari, S., in The Merck Index, *Merck*, New York, 13th edn, (2001).
185. Osada, T., Chen, M., Yang, X. Y., Spasojevic, I., Vandeusen, J. B., Hsu, D., Clary, B. M., Clay, T. M., Chen, W., Morse, M. A. and Lyerly, H. K., Antihelminth compound niclosamide downregulates Wnt signaling and elicits antitumor responses in tumors with activating APC mutations. *Cancer Res.*, 71, 4172-4182 (2011).
186. Pagliari, F., Mandoli, C., Forte, G., Magnani, E., Pagliari, S., Nardone, G., Licoccia, S., Minieri, M., Di Nardo P. and Traversa, E., Cerium Oxide Nanoparticles Protect Cardiac Progenitor Cells from Oxidative Stress. *ACS Nano*, 6, 3767–3775 (2012).

187. Pahari, S. K., Sutradhar, N., Sinhamahapatra, A., Pal P. and Panda, A. B., Synthesis of nearly monodispersed metal oxide nanoparticles in water. *New J. Chem.*, 35, 1460-1465 (2011).

188. Pakala, S. B., Rayala, S. K., Wang, R. A., Ohshiro, K., Mudvari, P., Reddy, S. D., Zheng, Y., Pires, R., Casimiro, S., Pillai, M. R., Costa, L. and Kumar, R., MTA1 promotes STAT3 transcription and pulmonary metastasis in breast cancer. *Cancer Res*., 73, 3761-3770 (2013).

189. Pandareesh, M. D., Anand T. and Bhat, P. V., Cytoprotective propensity of Bacopa monniera against hydrogen peroxide induced oxidative damage in neuronal and lung epithelial cells. *Cytotechnology*, doi 10.1007/s10616-014-9767-3 (2014).

190. Park, H. S., Kim S. R. and Lee, Y. C., Impact of oxidative stress on lung diseases. *Respirology*, 14, 27–38 (2009a).

191. Park, J., Fong, P. M., Lu, J., Russell, K. S., Booth, C. J., Saltzman, W. M. and Fahmy, T. M., PEGylated PLGA nanoparticles for the improved delivery of doxorubicin. *Nanomedicine*, 5, 410-418 (2009b).

192. Park, S. D., Vohs J. M. and Gorte, R. J., Direct oxidation of hydrocarbons in a solid-oxide fuel cell. *Nature*, 404, 265–267 (2000).

193. Park, S. J., Shin, J. H., Kang, H., Hwang J. J. and Cho, D. H., Niclosamide induces mitochondria fragmentation and promotes both apoptotic and autophagic cell death. *BMB Rep*., 44, 517–522 (2011).

194. Parker, N., Turk, M. J., Westrick, E., Lewis, J. D., Low, P. S. and Leamon, C. P., Folate receptor expression in carcinomas and normal tissues determined by a quantitative radioligand binding assay. *Anal. Biochem*., 338, 284–293 (2005).

195. Patil, G. V., Biopolymer albumin for diagnosis and in drug delivery. *Drug Dev. Res.*, 58, 219–247 (2003).

196. Patil, S., Sandberg, A., Heckert, E., Self W. and Seal, S., Protein adsorption and cellular uptake of cerium oxide nanoparticles as a function of zeta potential. *Biomaterials*, 28, 4600–4607 (2007).

197. Paulos, C. M., Turk, M. J., Breur G. J. and Low, P. S., Folate receptor-mediated targeting of therapeutic and imaging agents to activated macrophages in rheumatoid arthritis. *Adv. Drug Delivery Rev*., 56, 1205–1217 (2004).

198. Peer, D., Karp, J. M., Hong, S., Farokhzad, O. C., Margalit R. and Langer, R., Nanocarriers as an emerging platform for cancer therapy**.** *Nat. Nanotechnol.*, 2, 751–760 (2007).

199. Perez, J. M., Asati, A., Nath S. and Kaittanis, C., Synthesis of Biocompatible Dextran-Coated Nanoceria with pH-Dependent Antioxidant Properties. *Small*, 4, 552–556 (2008).

200. Pirmohamed, T., Dowding, J. M., Singh, S., Wasserman, B., Heckert, E., Karakoti, A. S., King, J. E., Seal, S. and Self, W. T., Nanoceria exhibit redox state-dependent catalase mimetic activity. *Chem. Commun*., 46, 2736–2738 (2010).

201. Pollack, S. J., Jacobs, J. W. and Schultz, P. G., Selective chemical catalysis by an antibody. *Science*, 234, 1570-1573 (1986).

202. Poste, G. and Kirsh, R., Site-specific (targeted) drug delivery in cancer therapy. *Nat. Biotechnol.*, 1, 869–878 (1983).

203. Qanungo, S., Das, M., Haldar, S. and Basu, A., Epigallocatechin-3-gallate induces mitochondrial membrane depolarization and caspase-dependent apoptosis in pancreatic cancer cells. *Carcinogenesis*, 26, 958–967 (2005).

204. Qi, J., Yao, P., He, F., Yu, C. and Huang, C., Nanoparticles with dextran/chitosan shell and BSA/chitosan core—doxorubicin loading and delivery. *Int. J. Pharm*., 393, 176–184 (2010).

205. Qi, L., Guo, Y., Luan, J., Zhang, D., Zhao Z. and Luan, Y., Folate-modified bexarotene-loaded bovine serum albumin nanoparticles as a promising tumor targeting delivery system. *J. Mater. Chem. B*, 2, 8361–8371 (2014).

206. Qi, X. Y., Huang, X., Li, H., Wang, Y., Xia, Y., Natarajan, M., Wei, J. and Venkatraman, S. S., Zhang H. Vault protein-templated assembles of nanoparticles, *ACS Nano*, 7, 1250001-1250007 (2012).

207. Qian, X., Peng, X.-H., Ansari, D. O., Yin-Goen, Q., Chen, G. Z., Shin, D. M.,Yang, L., Young, A.N., Wang, M.D. and. Nie, S., In vivo tumor targeting and spectroscopic detection with surface-enhanced Raman nanoparticle tags. *Nat. Biotechnol*., 26, 83-90, (2008).

208. Rahimnejad, M., Jahanshahi M. and Najafpour, G. D., Production of biological nanoparticles from bovine serum albumin for drug delivery. *Afr. J. Biotechnol*., 5, 1918–1923 (2006).

209. Ramani, K., Bora, R.S., Kumar, M., Tyagi, S. K. and Sarkar, D. P., Novel gene delivery to liver cells using engineered virosomes. *FEBS Lett*., 404, 164-168 (1997).

210. Ramani, K., Hassan, Q., Venkaiah, B., Hasnain ,S. E. and Sarkar, D. P., Site-specific gene delivery in vivo through engineered Sendai viral envelopes. *Proc. Natl. Acad. Sci. U S A*, 95, 11886-11890 (1998).

211. Randall, C. L., Kalinin, Y. V., Jamal, M., Shah, A. and Gracias, D. H., Self-folding immunoprotective cell encapsulation devices. *Nanomedicine*, 7, 686-689 (2011).

212. Ranganathan, R., Madanmohan, S., Kesavan, A., Baskar, G., Krishnamoorthy, Y. R., Santosham, R., Ponraju, D., Rayala, S. K. and Venkatraman, G., Nanomedicine:

towards development of patient-friendly drug-delivery systems for oncological applications. *Int .J. Nanomedicine*., 7, 1043-1060 (2012).

213. Reis, C. P., Neufeld, R. J., Ribeiro, A. J. and Veiga, F., Nanoencapsulation I. Methods for preparation of drug-loaded polymeric nanoparticles. *Nanomedicine*, 2, 8–21 (2006).
214. Rejinold, N. S., Baby,T., Chennazhi, K. P. and Jayakumar R., Multi drug loaded thermo-responsive fibrinogen-graft-poly(Nvinyl caprolactam) nanogels for breast cancer drug delivery. *J. Biomed. Nanotechnol.*, 11, 392–492 (2015).
215. Rejinold, N. S., Muthunarayanan, M., Chennazhi, K. P., Nair S. V. and Jayakumar, R., Curcumin Loaded Fibrinogen Nanoparticles for Cancer Drug Delivery. *J. Biomed. Nanotechnol.*, 7, 521–534 (2011a).
216. Rejinold, N. S., Baby, T., Nair, S. V. and Jayakumar, R., Paclitaxel loaded fibrinogen coated CdTe/ZnTe core shell nanoparticles for targeted imaging and drug delivery to breast cancer cells. *J. Biomed. Nanotechnol.*, 9, 1657-1671 (2013).
217. Rejinold, N. S., Baby,T., Chennazhi, K. P. and Jayakumar, R., Dual drug encapsulated thermo-sensitive fibrinogen-graft-poly (N-isopropyl acrylamide) nanogels for breast cancer therapy. *Colloids Surf. B Biointerfaces*, 114, 209-217 (2014).
218. Rejinold, N. S., Muthunarayanan, M., Chennazhi, K. P., Nair, S. V. and Jayakumar, R., 5-fluorouracil loaded fibrinogen nanoparticles for cancer drug delivery applications. *Int. J. Biol. Macromol.*, 48, 98-105 (2011b).
219. Rejinold, N. S., Muthunarayanan, M., Deepa, N., Chennazhi, K. P., Nair, S. V. and Jayakumar, R., Development of novel fibrinogen nanoparticles by two-step co-acervation method. *Int. J. Biol. Macromol*., 47, 37-43 (2010).
220. Rello, S., Stockert, J. C., Moreno, V., G'amez, A., Pacheco, M., Juarranz, A., Canete M. and Villanueva, A., Morphological criteria to distinguish cell death induced by apoptotic and necrotic treatments. *Apoptosis*, 10, 201–208 (2005).
221. Ren, K., Dusad, A., Dong R. and Quan, L., Albumin as a Delivery Carrier for Rheumatoid Arthritis. *J. Nanomed. Nanotechnol.*, 4, 176 (2013).
222. Ren, X. M., Duan, L., He, Q., Zhang, Z., Zhou, Y., Wu, D., Pan, J., Pei D. and Ding, K., Identification of Niclosamide as a New Small-Molecule Inhibitor of the STAT3 Signaling Pathway. *ACS Med. Chem. Lett*., 1, 454–459 (2010).
223. Riccardi C. and Nicoletti, I., Analysis of apoptosis by propidium iodide staining and flow cytometry. *Nat. Protoc*., 1, 1458−1461 (2006).
224. Roco, M. C., Nanotechnology: convergence with modern biology and medicine. *Curr. Opin. Biotechnol*., 14, 337–346 (2003).

225. Rollett, A., Reiter, T., Nogueira, P., Cardinale, M., Loureiro, A., Gomes, A., Cavaco-Paulo, A., Moreira, A., Carmo A. M. and Guebitz, G. M., Folic acid-functionalized human serum albumin nanocapsules for targeted drug delivery to chronically activated macrophages. *Int. J. Pharm*., 427, 460–466 (2012).
226. Rosenberg, S. A., A new era for cancer immunotherapy based on the genes that encode cancer antigens. *Immunity*, 10, 281-287 (1999).
227. Rubinstein, A. L., Zebrafish: from disease modeling to drug discovery. *Curr. Opin. Drug Discov. Devel.*, 6, 218-223 (2003).
228. Sachdev, A., Matai, I., Uday Kumar, S., Bhushan, B., Dubey P. and Gopinath, P., A novel one-step synthesis of PEG passivated multicolour fluorescent carbon dots for potential biolabeling application. *RSC Adv.*, 3, 16958-16961 (2013).
229. Sack, U., Walther, W., Scudiero, D., Selby, M., Kobelt, D., Lemm, M., Fichtner, I., Schlag, P. M., Shoemaker R. H. and Stein, U., Novel Effect of Antihelminthic Niclosamide on S100A4-Mediated Metastatic Progression in Colon Cancer. *J. Natl. Cancer Inst*., 103, 1018–1036 (2011).
230. Sahoo, S. K. and Labhasetwar, V., Nanotech approaches to drug delivery and imaging. *Drug Discov. Today*, 8, 1112-1120 (2003).
231. Satapathy, S. R., Mohapatra, P., Preet, R., Das, D., Sarkar, B., Choudhuri, T., Wyatt, M. D. and Kundu, CN., Silver-based nanoparticles induce apoptosis in human colon cancer cells mediated through p53. *Nanomedicine (Lond)*, 8, 1307-1322 (2013).
232. Sathyamurthy, S., Leonard, K. J., Dabestani R. T. and Paranthaman, M. P., Reverse micellar synthesis of cerium oxide nanoparticles. *Nanotechnology*, 16, 1960–1964 (2005).
233. Schirmer, K., Proposal to improve vertebrate cell cultures to establish them as substitutes for the regulatory testing of chemicals and effluents using fish. *Toxicology*, 224, 163–183 (2006).
234. Schunemann, H. J., Muti, P., Freudenheim, J. L., Armstrong, D., Browne, R., Klockc R. A. and Trevisan, M., Oxidative Stress and Lung Function. *Am. J. Epidemiol*., 146, 939–948 (1997).
235. Sharma, R., Yang, Y., Sharma, A., Awasthi, S. and Awasthi, Y. C., Antioxidant role of glutathione S-transferases: protection against oxidant toxicity and regulation of stress-mediated apoptosis. *Antioxid. Redox. Signal.*, 6, 289–300 (2004).
236. Sharma, S., Chockalingam, S., Sanpui, P., Chattopadhyay A. and Ghosh, S. S., Silver nanoparticles impregnated alginate-chitosan-blended nanocarrier induces apoptosis in human glioblastoma cells. *Adv. Healthc. Mater*., 3, 106-114 (2014).

237. Shen, Z., Li, Y., Kohama, K., Oneill, B. and Bi, J., Improved drug targeting of cancer cells by utilizing actively targetable folic acid-conjugated albumin nanospheres. *Pharmacol. Res*., 63, 51–58 (2011).

238. Shim, H. Y., Park, J. H., Paik, H. D., Nah, S. Y., Kim, D. S. and Han, Y. S., Acacetin-induced apoptosis of human breast cancer MCF-7 cells involves caspase cascade, mitochondria-mediated death signaling and SAPK/JNK1/2-c-Jun activation. *Mol. Cells*, 24, 95–104 (2007).

239. Siegel, R. L., Miller, K. D. and Jemal, A., Cancer statistics, 2015. *CA Cancer J. Clin*., 65, 5-29 (2015).

240. Silva, G. A., Nanomedicine: Seeing the benefits of ceria. *Nat. Nanotechnol*., 1, 92–94 (2006).

241. Smith, C. A., de la Fuente, J., Pelaz, B., Furlani, E. P., Mullin, M. and Berry, C. C., The effect of static magnetic fields and tat peptides on cellular and nuclear uptake of magnetic nanoparticles. *Biomaterials*, 31, 4392-4400 (2010).

242. Snima, K. S., Sreelakshmi, K.V., Renu, G., Nair, S.V., Subramanian, K. R. V. and Lakshmanan, V. K., Development of Activated Carbon-Ceria Nanocomposite Materials for Prostate Cancer Therapy. *Adv. Sci. Engineer. Med*., 5, 1132-1136 (2013).

243. Snima, K. S., Jayakumar, R. and Lakshmanan, V. K., In vitro and in vivo biological evaluation of O-carboxymethyl chitosan encapsulated metformin nanoparticles for pancreatic cancer therapy. *Pharm. Res*., 31, 3361-3370 (2014).

244. Snima, K.S., Jayakumar, R., Unnikrishnan, A. G., Nair, S. V., Lakshmanan,V K., O-Carboxymethyl chitosan nanoparticles for metformin delivery to pancreatic cancer cells. *Carbohyd. Polym*., 89, 1003–1007 (2012).

245. Spitsbergen, J. M. and Kent, M. L., The state of the art of the zebrafish model for toxicology and toxicologic pathology research – Advantages and current limitations. *Toxicol. Pathol*., 31, 62-87 (2003).

246. Sripriyalakshmi, S., Anjali, C. H., Doss, C. G. P., Rajith B. and Ravindran, A., BSA nanoparticle loaded atorvastatin calcium--a new facet for an old drug. *PLoS One*, 9, e86317 (2014).

247. Stern, H. M. and Zon, L. I., Cancer genetics and drug discovery in the zebrafish. *Nat. Rev. Cancer*, 3, 533-539 (2003).

248. Stoehr, L. C., Gonzalez, E., Stampfl, A., Casals, E., Duschl, A., Puntes, V. and Oostingh, G. J., Shape matters: effects of silver nanospheres and wires on human alveolar epithelial cells. *Part. Fibre Toxicol.* 8, 36 (2011)

249. Storz, P., Mitochondrial ROS--radical detoxification, mediated by protein kinase D. *Trends Cell Biol*., 17, 13–18 (2007).
250. Storz, P., Reactive oxygen species in tumor progression. *Front Biosci*., 10, 1881–1896 (2005).
251. Sudheesh Kumar, P. T., Abhilash, S., Manzoor, K., Nair, S. V., Tamura, H. and Jayakumar, R., Preparation and characterization of novel β-chitin/nano silver composite scaffolds for wound dressing applications. *Carbohydr. Polym*., 80, 761–767 (2010).
252. Sudimack J. and Lee, R. J., Targeted drug delivery via the folate receptor. *Adv. Drug Delivery Rev*., 41, 147–162 (2000).
253. Sundar, S., Kundu, J. and Kundu, S. C., Biopolymeric nanoparticles. *Sci. Technol. Adv. Mater*., 11, 1–13 (2010).
254. Suri, S. S., Fenniri, H. and Singh, B., Nanotechnology-based drug delivery systems. *J. Occup. Med. Toxicol*., 1, 2–16 (2007).
255. Szatrowski, T. P. and Nathan, C. F., Production of large amounts of hydrogen peroxide by human tumor cells. *Cancer Res*., 51, 794–798 (1991).
256. Tarnuzzer, R. W., Colon, J., Patil S. and Seal, S., Vacancy engineered ceria nanostructures for protection from radiation-induced cellular damage. *Nano Lett*., *5*, 2573-2577 (2005).
257. Tiwari, S. K. and Venkatraman, S., Electrospinning pure protein solutions in core-shell fibers. *Polym. Int.*, 61, 1549-1555 (2012).
258. Tonder, E. C. V., Maleka, T. S. P., Liebenberg, W., Song, M., Wurster D. E. and Villiers, M. M., Preparation and physicochemical characterization of 5 niclosamide solvates and 1 hemisolvate. *Int. J. Pharm*., 269, 417–432 (2004).
259. Torchilin, V. P., Nanotechnology in Drugs, second ed. Imperial College Press, London, (2008).
260. Torre, L. A., Bray, F., Siegel, R. L., Ferlay, J., Lortet-Tieulent, J. and Jemal, A., Global Cancer Statistics 2012. *CA Cancer J. Clin.*, 65, 87–108 (2015).
261. Torri, V. and Floriani, I., Cyproterone acetate in the therapy of prostate carcinoma. *Arch. Ital. Urol. Androl*., 77, 157-163 (2005).
262. Townsend, D. M. and Tew, K. D., The role of glutathione-S-transferase in anti-cancer drug resistance. *Oncogene*, 22, 7369–7375 (2003).
263. Turek, J. J., Leamon, C. P. and Low, P. S., Endocytosis of folate-protein conjugates: ultrastructural localization in KB cells. *J. Cell Sci*., 106, 423-430 (1993).
264. Uday Kumar, S., Bhushan, B., Dubey, P., Matai, I., Sachdev A. and Gopinath P., Emerging Applications of Nanoparticles for Lung Cancer Diagnosis and Therapy. *Int. Nano Lett.*, 3, 45-53 (2013).

265. Uday Kumar, S., Matai, I., Dubey, P., Bhushan, B., Sachdev A. and Gopinath, P., Differentially cross-linkable core-shell nanofibers for tunable delivery of anticancer drugs: synthesis, characterization and its anticancer efficacy. *RSC Adv*., 4, 38263 - 38272 (2014).

266. Ursini, F., Maiorino, M., Brigelius-Flohé, R., Aumann, K. D., Roveri, A., Schomburg, D. and Flohé, L., Diversity of glutathione peroxidases. *Methods Enzymol*., 252, 38–53 (1995).

267. Vasir, J. K., Reddy, M. K. and Labhasetwar V., Nanosystems in drug targeting: opportunities and challenges. *Curr. Nanosci*., 1, 47-64 (2005).

268. Venkatraman, S., Has nanomedicine lived up to its promise? *Nanotechnology*, 25, 372501 (2014).

269. Vernekar, A. A., Sinha, D., Srivastava, S., Paramasivam, P.U., D'Silva, P. and Mugesh, G., An antioxidant nanozyme that uncovers the cytoprotective potential of vanadia nanowires. *Nat. Commun.*, 5, 5301 (2014).

270. Vrbanec, D., Belev, B., Pavlinić-Diminić, V., Pezerović, D., Dusper, B., Plestina, S. and Unusić, J., Hormonal therapy with aromatase inhibitor in advanced breast cancer. *Lijec Vjesn*, 120, 315-318 (1998).

271. Wang S. S. and Low, P. S., Folate-mediated targeting of antineoplastic drugs, imaging agents, and nucleic acids to cancer cells. *J. Controlled Release*, 53, 39–48 (1998).

272. Wang, A. M., Ku, H. H., Liang, Y. C., Chen, Y. C., Hwu, Y. M. and Yeh, T. S., The autonomous notch signal pathway is activated by baicalin and baicalein but is suppressed by niclosamide in K562 cells. *J. Cell Biochem*., 106, 682-692 (2009).

273. Wang, F. H., Zhang, D. R., Duan, C. X., Jia, L. J., Feng, F. F., Liu, Y., Wang, Y. C., Hao L.L. and Zhang, Q., Preparation and characterizations of a novel deoxycholic acid–O-carboxymethylated chitosan–folic acid conjugates and self-aggregates. *Carbohydr. Polym*., 84, 1192–1200 (2011a).

274. Wang, F. H., Zhang, D. R., Zhang, Q., Chen, Y. X., Zheng, D. D., Hao, L. L., Duan, C. X., Jia, L. J., Liu G. P. and Liu, Y., Synergistic effect of folate-mediated targeting and verapamil-mediated P-gp inhibition with paclitaxel -polymer micelles to overcome multi-drug resistance. *Biomaterials*, 32, 9444–9456 (2011b).

275. Wang, Y. C., Chao, T.K., Chang, C. C., Yo, Y. T., Yu M. H. and Lai, H. C., Drug screening identifies niclosamide as an inhibitor of breast cancer stem-like cells. *PLoS One*, 8, e74538 (2013).

276. Wang, Z. L., Liu, H. Y., Yang, S. H., Wang, T., Liu C. and Cao, Y. C., Nanoparticle-based artificial RNA silencing machinery for antiviral therapy. *Proc. Natl. Acad. Sci. U. S. A.*, 109, 12387–12392 (2012).

277. Weber, C., Coester, C., Keruter J. and Langer, K., Desolvation process and surface characterisation of protein nanoparticles. *Int. J. Pharm*., 194, 91–102 (2000).
278. Wei H. and Wang, E., Nanomaterials with enzyme-like characteristics (nanozymes): next-generation artificial enzymes. *Chem. Soc. Rev.*, 42, 6060-6093 (2013).
279. Wei, H. and Wang, E., Fe3O4 magnetic nanoparticles as peroxidase mimetics and their applications in H_2O_2 and glucose detection. *Anal Chem.*, 80, 2250-2254 (2008).
280. Weinbach, E. C. and Garbus, J., Mechanism of action of reagents that uncouple oxidative phosphorylation. *Nature*, 221, 1016 – 1018 (1969).
281. Weiner, L. M., An overview of monoclonal antibody therapy of cancer. *Semin. Oncol.*, 26, 41-50 (1999).
282. Weissleder, R., Kelly, K., Sun, E. Y., Shtatland, T. and Josephson, L., Cell-specific targeting of nanoparticles by multivalent attachment of small molecules. *Nat. Biotechnol*., 23, 1418-1423, (2005).
283. Wieland, A., Trageser, D., Gogolok, S., Reinartz, R., Hofer, H., Keller, M., Leinhaas, A., Schelle, R., Normann, S., Klaas, L., Waha, Koch, P., Fimmers, R., Pietsch, T., Yachnis, A. T., Pincus, D. W., Steindler, D. A., Brustle, O., Simon, M., Glas M. and Scheffler, B., Anticancer effects of niclosamide in human glioblastoma. *Clin. Cancer Res*., 19, 4124–4136 (2013).
284. Wixon, J., *Danio reri*o, the zebrafish. *Yeast*, 17, 225-231 (2000).
285. Wolter, K.G., Hsu, Y., Smith, C. L., Nechushtan, A., Xi X. and Youle, R. J. J., Movement of Bax from the cytosol to mitochondria during apoptosis. *Cell Biol*., 139, 1281–1292 (1997).
286. Wong, R. S. Y., Apoptosis in cancer: from pathogenesis to treatment. *J. Exp. Clin. Cancer Res*., 30, 87 (2011).
287. Xie, L., Tong, W., Yu, D., Xu, J., Li J. and Gao, C., Bovine serum albumin nanoparticles modified with multilayers and aptamers for pH-responsive and targeted anti-cancer drug delivery. *J. Mater. Chem.*, 22, 6053–6060 (2012).
288. Xue, Y., Luan, Q. F., Yang, D., Yao X. and Zhou, K. B., Direct Evidence for Hydroxyl Radical Scavenging Activity of Cerium Oxide Nanoparticles. *J. Phys. Chem. C*, 115, 4433–4438 (2011).
289. Yang W. and Villiers, M. M. D., Effect of 4-sulphonato-calix[n]arenes and cyclodextrins on the solubilization of niclosamide, a poorly water soluble anthelmintic. *AAPS J*., 7, E241–E248 (2005).

290. Yang, E. H., Zha, J., Jockel, J., Boise, L. B., Thompson C. B. and Korsmeyer, S. J., Bad, a heterodimeric partner for Bcl-XL and Bcl-2, displaces Bax and promotes cell death. *Cell*, 80, 285–291 (1995).
291. Yang, L., Cui, F., Cun, D., Tao, A., Shi, K. and Lin, W., Preparation, characterization and biodistribution of the lactone form of 10-hydroxycamptothecin (HCPT)-loaded bovine serum albumin (BSA) nanoparticles. *Int. J. Pharm*., 340, 163–172 (2007).
292. Yang, R., An, Y., Miao, F., Li, M., Liu P. and Tang, Q., Preparation of folic acid-conjugated, doxorubicin-loaded, magnetic bovine serum albumin nanospheres and their antitumor effects in vitro and in vivo. *Int. J. Nanomedicine*, 9, 4231-4243 (2014).
293. Ye, T., Xiong, Y., Yan, Y., Xia, Y., Song, X., Liu, L., Li, D., Wang, N., Zhang, L., Zhu, Y., Zeng, J., Wei, Y. and Yu, L., The Anthelmintic Drug Niclosamide Induces Apoptosis, Impairs Metastasis and Reduces Immunosuppressive Cells in Breast Cancer Model. *PLoS One*, 9, e85887 (2014).
294. You, H., Yamamoto, K. and Mak, T. W., Regulation of transactivation-independent proapoptotic activity of p53 by FOXO3a. *Proc. Natl. Acad. Sci. U S A*, 103, 9051–9056 (2006).
295. Yu, L., Lu, Y., Man, N., Yu S. H. and Wen, L. P., Rare Earth Oxide Nanocrystals Induce Autophagy in HeLa Cells. *Small*, 5, 2784–2787 (2009).
296. Yu, S., Yao, P., Jiang, M. and Zhang, G., Nanogels prepared by self-assembly of oppositely charged globular proteins. *Biopolymers*, 83, 148–158 (2006).
297. Yuan, D., Shen, Z., Liu, R., Chi Z. and Zhu, J., Study on the binding of cerium to bovine serum albumin. *J. Biochem. Mol. Toxicol*., 4, 263-268 (2011).
298. Zeiss, C. J., The apoptosis-necrosis continuum: insights from genetically altered mice. *Vet. Pathol*., 40, 481–495 (2003).
299. Zhai, Y., Zhou, K., Xue, Y., Qin, F., Yang L. and Yao, X., Synthesis of water-soluble chitosan-coated nanoceria with excellentantioxidant properties. *RSC Adv.*, 3, 6833–6838 (2013).
300. Zhang D. and Yang, H., Synthesis of biomacromolecule-stabilized silver nanoparticles and their surface-enhanced Raman scattering properties. *Appl. Phys. A*., 112, 739-745 (2013).
301. Zhang, L. K., Hou, S. X., Zhang, J. Q., Hu, W. J. and Wang, C. Y., Preparation, characterization, and in vivo evaluation of mitoxantrone-loaded, folate-conjugated albumin nanoparticles. *Arch. Pharm. Res*., 33, 1193–1198 (2010).
302. Zhang, L., Hou, S., Mao, S., Wei, D., Song, X. and Lu, Y., Uptake of folate-conjugated albumin nanoparticles to the SKOV3 cells. *Int. J. Pharm*., 287, 155–162 (2004).

303. Zhang, R., Humphreys, I., Sahu, R. P., Shi, Y. and Srivastava, S. K., In vitro and in vivo induction of apoptosis by capsaicin in pancreatic cancer cells is mediated through ROS generation and mitochondrial death pathway. *Apoptosis*, 13, 1465–1478 (2008).
304. Zhao, D. M., Zho, X. H., Zu, Y. G., Li, J. L., Zhang, Y., Jiang, R. and Zhang, Z. H., Preparation, characterization, and *in vitro* targeted delivery of folate-decorated paclitaxel-loaded bovine serum albumin nanoparticles. *Int. J. Nanomed.*, 5, 669-677 (2010).
305. Zhao, L., Su, R., Cui, W., Shi, Y., Liu L. and Su, C., Preparation of biocompatible heat-labile enterotoxin subunit B-bovine serum albumin nanoparticles for improving tumor-targeted drug delivery via heat-labile enterotoxin subunit B mediation. *Int. J. Nanomed.*, 9, 2149-2156 (2014).
306. Zheng, L., Jungheun, H., Tao Z. and Liwei, G., Fabrication of coated bovine serum albumin (BSA)–epigallocatechin gallate (EGCG) nanoparticles and their transport across monolayers of human intestinal epithelial Caco-2 cells. *Food Funct*., 6,1278-1285 (2014).
307. Zhou, G., Li, Y., Zheng, B., Wang, W., Gao, J., Wei, H., Li, S., Wang S. and Zhang, J., Cerium oxide nanoparticles protect primary osteoblasts against hydrogen peroxide induced oxidative damage. *Micro. Nano. Lett*., 9, 91-96 (2014).
308. Zu, Y. G., Yuan, S., Zhao, X. H., Zhang, Y., Zhang, X. N. and Jiang, R., Preparation, activity and targeting ability evaluation in vitro on folate mediated epigallocatechin-3-gallate albumin nanoparticles. *Yao Xue Xue Bao*, 44, 525–531 (2009).
309. Zu, Y., Zhang, Y., Zhao, X., Zhang, Q., Liu Y. and Jiang, R., Optimization of the preparation process of vinblastine sulfate (VBLS)-loaded folate conjugated bovine serum albumin (BSA) nanoparticles for tumor-targeted drug delivery using response surface methodology (RSM). *Int. J. Nanomed.*, 4, 321-333 (2009).